The Pennsylvania State University

The Graduate School

Department of Aerospace Engineering

An Experimental Study of the Effect of Tail Configuration on the Spinning Characteristics of General Aviation Aircraft

A Thesis in

Aerospace Engineering

by

Mark G. Ballin

Submitted in Partial Fulfillment
of the Requirements
for the Degree of

Master of Science

March 1982

We approve the thesis of Mark G. Ballin.

Date of Signature:	Signatories:
_____	_____ Barnes W. McCormick, Professor and Head of Aerospace Engineering Thesis Adviser
_____	_____ Joseph J. Eisenhuth, Associate Professor of Aerospace Engineering
_____	_____ Hubert C. Smith, Assistant Professor of Aerospace Engineering

ABSTRACT

Spinning characteristics of general aviation aircraft are closely related to the spin-damping properties of the tail. Previous experimental studies have concentrated on obtaining aerodynamic characteristics of a complete airplane, making dynamic testing necessary to duplicate the effects of a rotational flow field. In studies of an isolated tail, static testing may be possible. The purpose of this investigation is to determine the feasibility of using static wind tunnel tests to obtain information about spin damping characteristics of an isolated general aviation aircraft tail. A representative tail section was oriented to the tunnel free streamline at angles simulating an equilibrium spin. A full range of normally encountered spin conditions was employed. In addition, parametric studies were performed to determine the effect of spin damping on several tail design parameters. The results show satisfactory agreement with NASA rotary balance tests. Wing and body interference effects are present in the NASA studies at steep spin attitudes, but agreement improves with increasing pitch angle and spin rate, suggesting that rotational flow effects are minimal. Vertical position of the horizontal stabilizer is found to be a primary parameter affecting yaw damping, and horizontal tail chordwise position induces a substantial effect on pitching moment. A full-span rudder produces greater yawing moments than a partial-span rudder under steep spin conditions, while differences are small under flat spin conditions. Correlation of yawing moments to exposed vertical tail area is fair for steep spin conditions. For a flat spin, a three-dimensional model of the separated region above the horizontal tail is necessary for an improved correlation.

TABLE OF CONTENTS

LIST OF TABLES

LIST OF FIGURES

LIST OF SYMBOLS

A	axial force
AR	aspect ratio
b	span of wing or tail surface
C_L	lift coefficient for a finite wing or airplane, $L/\frac{1}{2} \rho V^2 S$
C_{L_α}	lift curve slope for a finite wing or airplane, $\frac{1}{1/2 \rho V^2 S} \frac{\partial L}{\partial \alpha}$
C_{l_α}	section lift curve slope, $l/\frac{1}{2} \rho V^2 c \quad \frac{\partial l}{\partial \alpha}$
C_{F_s}	side force coefficient, $F_s/\frac{1}{2} \rho V^2 S$
C_m	pitching moment coefficient, $m/\frac{1}{2} \rho V^2 Sc$
C_N	normal force coefficient, $N/\frac{1}{2} \rho V^2 S$
C_n	yawing moment coefficient, $n/\frac{1}{2} \rho V^2 Sb$
C_p	pressure coefficient, $p/\frac{1}{2} \rho V^2$
c	chord length
$\bar{c}$	mean aerodynamic chord
F_s	side force
g	acceleration of gravity
h	vertical distance from the horizontal stabilizer to the fuselage reference line
h/b_v	ratio of horizontal stabilizer height to vertical tail span
I_x	moment of inertia about the x-axis
I_y	moment of inertia about the y-axis
K	pressure distribution under the horizontal tail
K_1	constant used in spin predictive parameter

K_2	constant used in spin predictive parameter
L	lift
l_t	distance from horizontal tail 1/4-chord point to c.g.
m	pitching moment; aircraft mass
N	normal force
n	yawing moment
R_s	spin radius
S	area of wing or tail surface
V_d	descent velocity
V_T	total velocity
x, y, z	body-fixed coordinate axes; x positive forward, z positive down
α_v	angle at which flow approaches the tail in the plane parallel to the spin axis and the body-fixed y-axis
β_v	tail body-fixed sideslip angle
θ	pitch angle
μ	density coefficient, $m/\rho Sb$
ρ	density
ϕ	roll angle
Ω	spin rate, radians per second
$\bar{\Omega}$	nondimensional spin rate, $\frac{\Omega b}{2V}$

Subscripts

h	horizontal tail
v	vertical tail
w	main wing

ACKNOWLEDGEMENTS

I would like to express my appreciation to Dr. Barnes W. McCormick for his guidance in the conception and realization of this work. I am also indebted to Mr. Rex Jacobs and Mr. Leon Fetterolf for their help in designing and building the experimental apparatus.

CHAPTER I

INTRODUCTION

In a steady spin, the velocity at the tail of an airplane results from the vector sum of the vertical descent velocity and transverse velocity caused by rotation of the airplane. The resulting flow therefore approaches the tail from below and to one side, at an angle which is dependent on pitch and roll attitude, spin rate, and descent velocity. From the aircraft reference frame, the flow is rotational, making conventional wind tunnel studies inappropriate for determining aerodynamic forces on a complete airplane. The purpose of this investigation is to determine whether or not forces at the tail can be accurately obtained with static wind tunnel tests by orienting a model tail to the flow at angles duplicating an actual spin. In addition, the effectiveness of several tail configurations to damp a spin is investigated through parametric studies of horizontal and vertical stabilizer placement, planform shape, and size, using a representative general aviation aircraft tail. The effectiveness of spin recovery controls in providing pitching and yawing moment changes is also examined.

Overview of Spin Dynamics

The spin is defined as the motion of an airplane, usually at an angle of attack above stall but under 90°, descending towards the earth while rotating about a vertical axis (Neihouse et al. 1960). The motion involves rolling, pitching, and yawing as the airplane operates in the

nonlinear aerodynamic region well beyond stall. As shown in figure 1-1, the center of gravity of the spinning aircraft describes a helix. The distance from the center of gravity to the vertical axis is defined as the spin radius, R_s, and θ is defined as the pitch angle with respect to the vertical flight path.

Spinning is caused by a combination of aerodynamic and inertial forces operating simultaneously. Yawing moments are created by the autorotative effect of a stalled wing and rotation of the tail and fuselage about the flight path. Rolling and yawing moments are created by the negative lift slope of a stalled wing; in a roll, the down-going wing experiences reduced lift, thereby perpetuating the roll. A Nose-down pitching moment is created by flat plate drag of the horizontal tail operating at a high angle of attack. Gyroscopic moments created by centrifugal forces on the nose, tail, and wings tend to oppose the principal aerodynamic moments. An equilibrium spin is attained when the nose-down aerodynamic moment equals the nose-up inertial moment, and aerodynamic moments tending to rotate the aircraft about the spin axis are balanced by spin-damping aerodynamic and inertial moments. Figure 1-2 shows typical curves of equilibrium about earth-fixed y and z-axes when plotted as functions of pitch angle and spin rate. The intersection of the two curves results in an equilibrium spin.

The complexity of the spin phenomenon has made analytical studies difficult, so spin research has traditionally involved a large amount of empirical analysis. Similarly, this report is concerned primarily with experimental studies of spin dynamics. For more information on the analysis of spinning, the reader is referred to Bihrle and Barnhart or McCormick (1981). Testing techniques involve the use of spin-tunnel

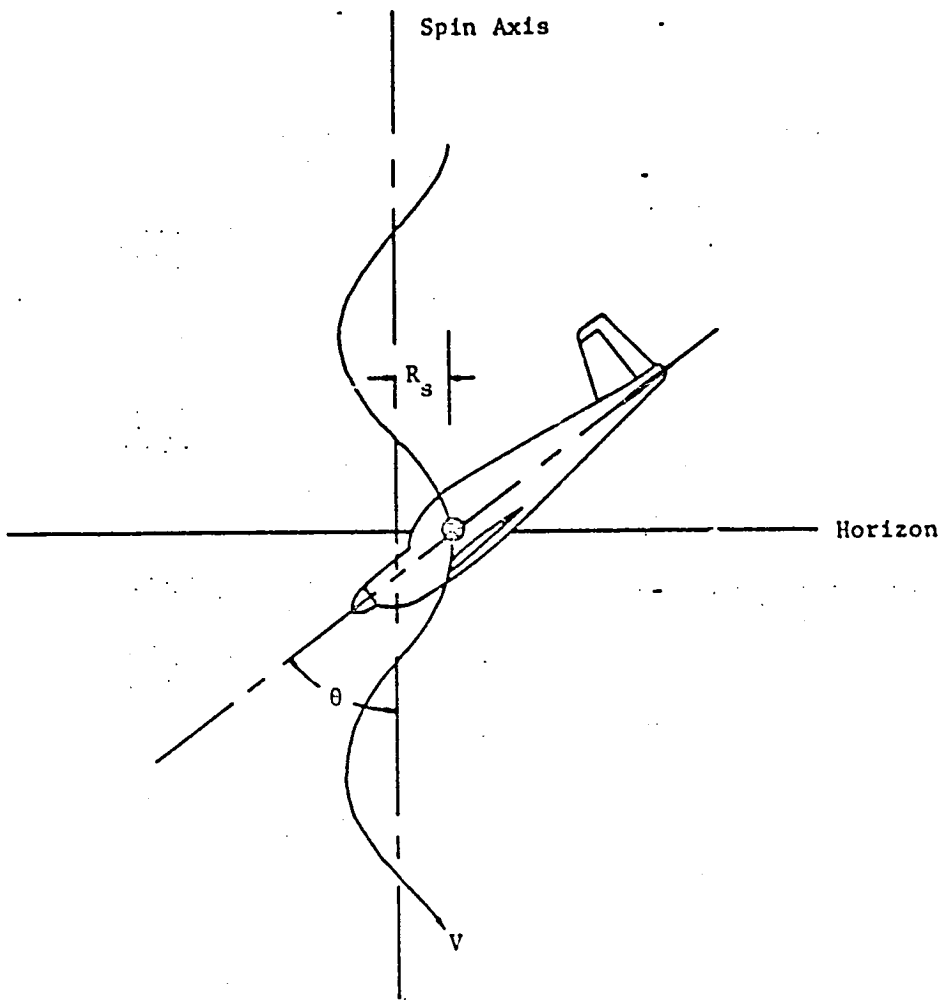

Figure 1-1. Aircraft Flight Path in an Equilibrium Spin

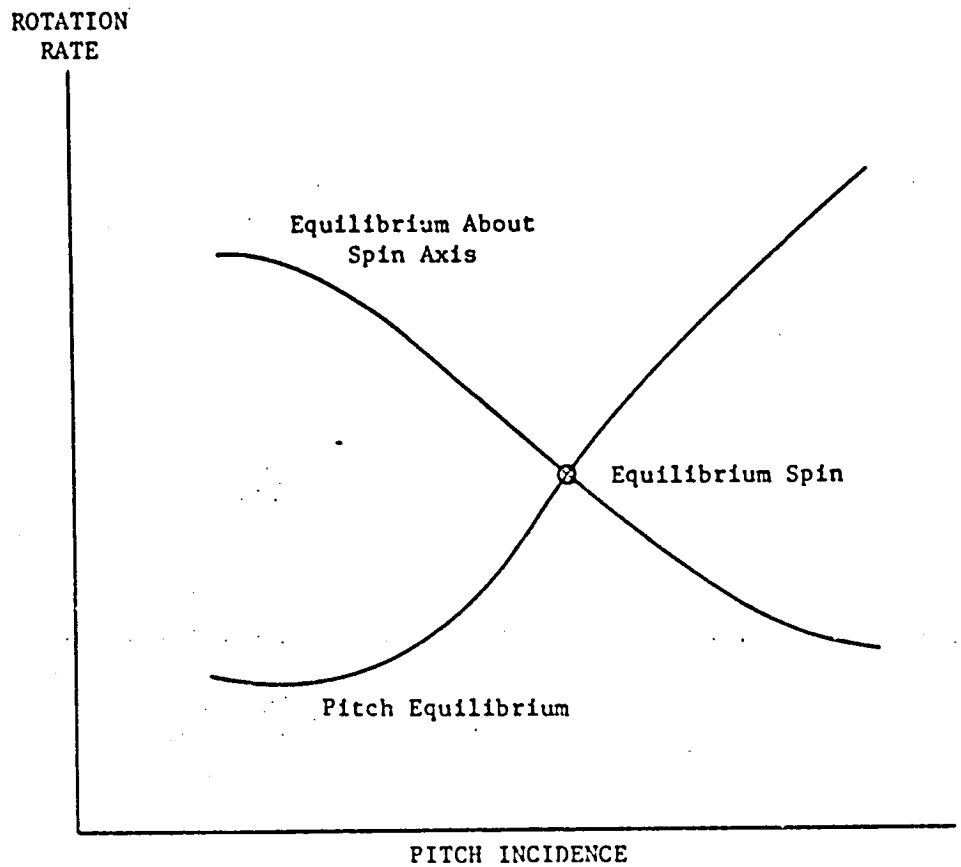

Figure 1-2. Balance of Forces Necessary for Equilibrium Spin

models in both free-flight and rotary balance studies; dynamically scaled model flight tests, and full scale flight tests. Such tests allow controlled study of the influences of configuration and mass distribution on equilibrium spin modes and recovery characteristics, and analysis of spin recovery techniques. In much of the testing, special consideration must be given to time scaling of the dynamic tests and scaled model mass distribution, as well as re-creation of the rotational flow field experienced by the spinning aircraft. These factors complicate the testing process, but are important in simulating the actual spin dynamics.

Scope of the Present Testing

Almost all past tail studies have involved an entire spinning aircraft or model in order to duplicate actual spin conditions. Many of these tests have been qualitative in nature and were concerned only with determining equilibrium spin modes and departure/recovery characteristics. The tests have not attempted to isolate airplane components to examine their separate influences.

The present study investigates the feasibility of using static testing techniques in a conventional wind tunnel to study the isolated effects of an aircraft tail in spin. The testing consisted of static wind tunnel force measurements of several tail configurations. The tails were positioned in the tunnel at extreme angles of attack as determined by the spin rate, pitch angle, and vertical descent velocity. Spin orientations covered a full range of equilibrium spin conditions typical for general aviation aircraft. A representative general aviation aircraft tail, designed to incorporate average characteristics

of several aircraft currently produced, was used for the testing. The aft fuselage shape was not a test parameter and its cross-section was therefore chosen to influence experimental results as little as possible. Configuration parameters consisted of vertical and horizontal placement of the horizontal stabilizer, vertical and horizontal tail aspect ratios, and deflection of elevator and rudder controls. Airfoil cross-section, horizontal tail dihedral angle, angles-of-sweep, and taper ratios were considered of secondary importance and were held constant for all tests.

CHAPTER II

PREVIOUS RESEARCH

Early Studies

The first theoretical description of spinning and recovery techniques was presented in Great Britain during World War I. At this time the spin was actually used as a tactical maneuver to evade combat. During the 1920's, the first rotary balance measurements were performed in conventional wind tunnels, while in the next decade, the first spin tunnels were developed and the importance of inertia and tail design became apparent (Chambers 1980).

The Inertia Yawing Moment Parameter (IYMP), defined by

$$IYMP = \frac{I_x - I_y}{mb^2}$$

was found to be an important factor in spinning characteristics and spin recovery. If the aircraft weight is distributed mainly along the wing (the case of a multi-engined airplane with wing-mounted nacelles), the moment of inertia about the roll axis is greater than the moment in pitch, and IYMP will be positive. If the pitching moment of inertia is greater than the rolling inertia, as is the case for most modern fighter aircraft, the loading is defined as negative. For most general aviation aircraft, IYMP is found to be close to zero. Spinning characteristics and recovery procedures are quite different for the

three major mass distributions. For the zero loading condition, the most effective recovery controls are found to be positive (down) elevator and a rudder deflection opposing the yaw rotation.

Early research concentrated on the importance of the tail in damping the spin. This led to the Tail Damping Power Factor (TDPF), a design criterion which later research proved to be of questionable value. The TDPF was an attempt to define satisfactory recovery characteristics of an aircraft through a methodical description of the geometry of the tail. Unfortunately, the early research failed to isolate tail effects from the rest of the airplane. This was the result of underestimating the importance of other factors which can override the anti-spin properties of the tail.

As recently as 1971, the three most influential factors were listed as relative distribution of mass between wing and fuselage; density of the aircraft relative to that of air; and tail design (Bowman). More recent research has shown definite contributions from such parameters as wing leading edge shape, aft fuselage shape, strakes and ventral fins, outboard wing leading edge droop, and wing placement.

The Tail Damping Power Factor

The Tail damping Power Factor was derived from early spin research conducted by the British Royal Aircraft Establishment in the late 1920's and early 1930's. It is actually the product of two terms, the Unshielded Rudder Volume Coefficient (URVC) and the Tail Damping Ratio (TDR). The two terms, although developed independently, were thought to be of equal importance in determination of spinning qualities, and were therefore multiplied to form the TDPF.

The URVC, developed by the Royal Aircraft Establishment, is used to provide an indication of rudder recovery effectiveness. Referring to Figure 2-1, it is determined by the equation

$$URVC = \frac{S_{R_1} L_1 + S_{R_2} L_2}{S(b/2)}$$

The TDR, defined by

$$TDR = \frac{S_\Gamma L^2}{S(b/2)^2}$$

is determined for body and/or vertical tail area beneath the horizontal tail. It was developed by NACA in 1939 from the previously used Body Damping Ratio in an effort to improve correlation with spin tunnel findings.

Because the density coefficient, μ, and the Inertia Yawing Moment Parameter were known to be significant factors affecting recovery characteristics, they were used as parameters in determining boundaries for satisfactory spin recoveries. Figure 2-2 is typical of those developed in the late 1940's by NACA, based on spin tunnel recovery studies of over 100 military and civil airplane designs.

In the studies, a spin tunnel model was considered to have satisfactory recovery characteristics if it stopped spinning within two turns of application of recovery controls. In addition, recovery tests were performed with a modified control configuration, based on the assumption that it is unrealistic to expect a pilot to apply perfect recovery controls. This relaxed recovery criterion was referred to as

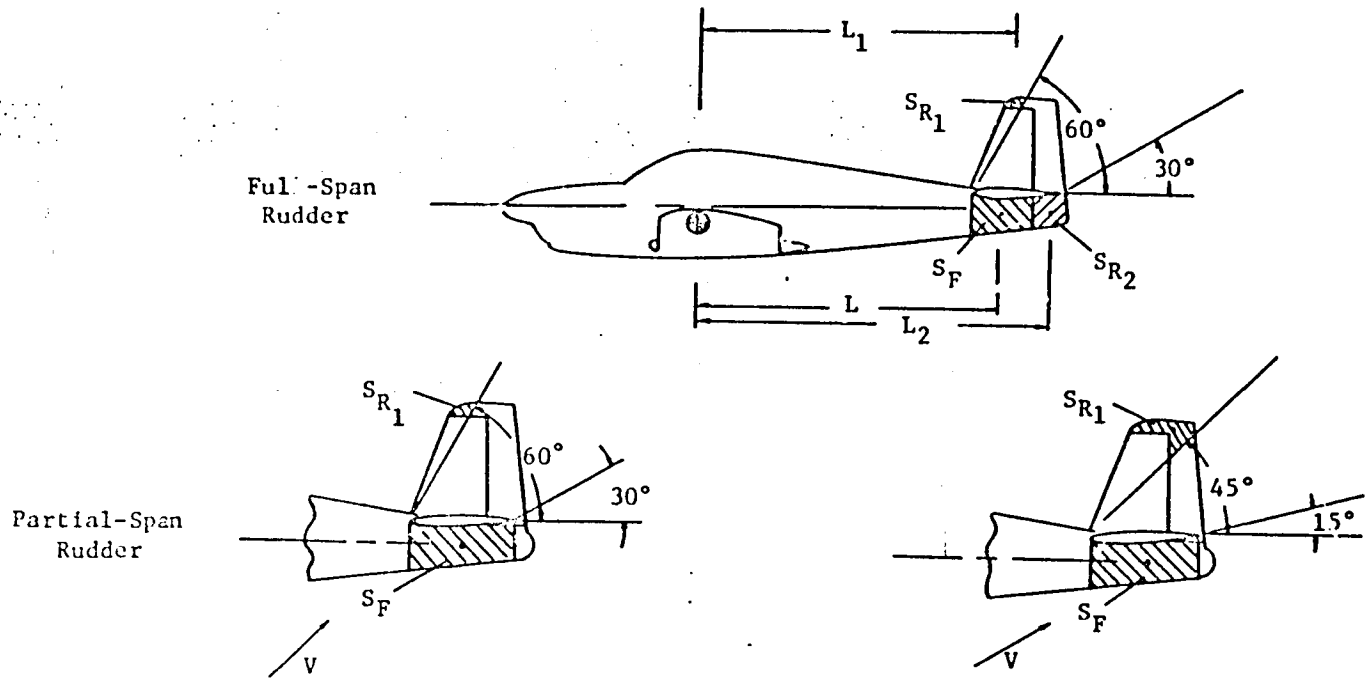

$$TDPF = URVC \times TDR$$

$$TDPF = \frac{S_{R_1} L_1 + S_{R_2} L_2}{S(b/2)} \times \frac{S_F L^2}{S(b/2)^2}$$

Figure 2-1. Computation of the Tail Damping Power Factor

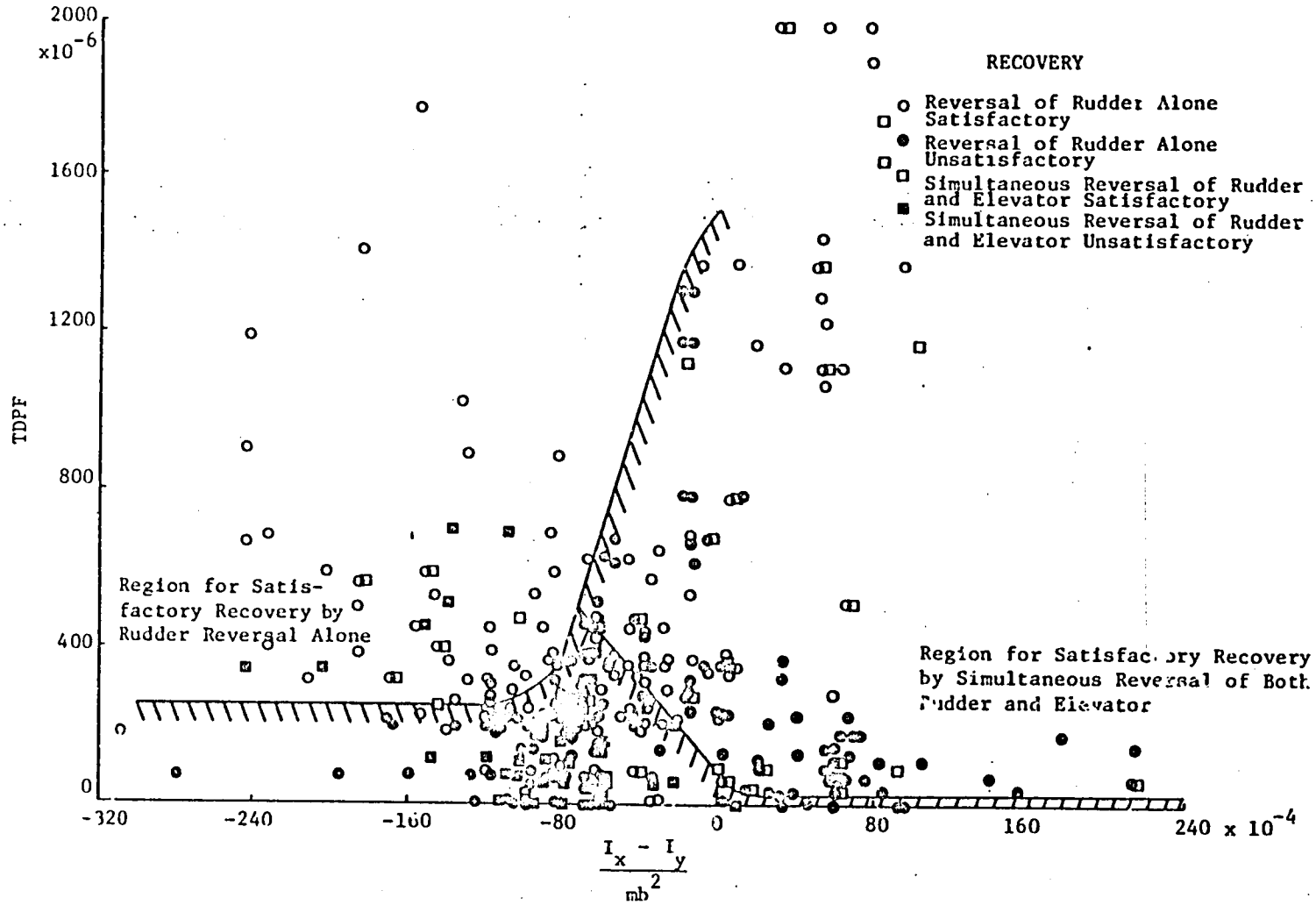

Figure 2-2. Tail Damping Power Factor as a Function of IYMP, $\mu \leq 15$

the "criterion spin." It was defined as that recovery effected by the application of one-third of full aileron deflection in the direction opposing spin recovery (usually stick-left in a right spin), two-thirds of full negative elevator deflection, and one-third of full pro-recovery rudder deflection. A model was judged satisfactory if it recovered within 2.25 turns.

The results show a significant scatter among satisfactory and unsatisfactory designs, making the determined boundaries questionable. It was concluded at the time that "...other factors (such as wing design) undoubtedly influence recovery characteristics and may account in part for some mixture of the satisfactory and unsatisfactory points shown" (Neihouse et al. 1946).

The TDPF was applied to light general aviation aircraft in a 1947 NACA study (Neihouse). The criterion devised (Figure 2-3) was developed from the previous testing, using only those configurations resembling general aviation types. Aileron control effects were not considered. The criterion is conservative in that boundaries are determined such that no unsatisfactory recoveries lie in the satisfactory region, although several satisfactory recoveries lie in the unsatisfactory region. Recovery requirements were relaxed, however, for general aviation aircraft. Recovery was considered satisfactory if the models recovered within 2.25 turns after initiation of full recovery controls.

Recent Free-Flight Spin Tunnel Tests

Similar studies have been conducted more recently using the "typical single-engine general aviation design" shown in Figure 2-4. The effects of control deflections were again studied as functions of

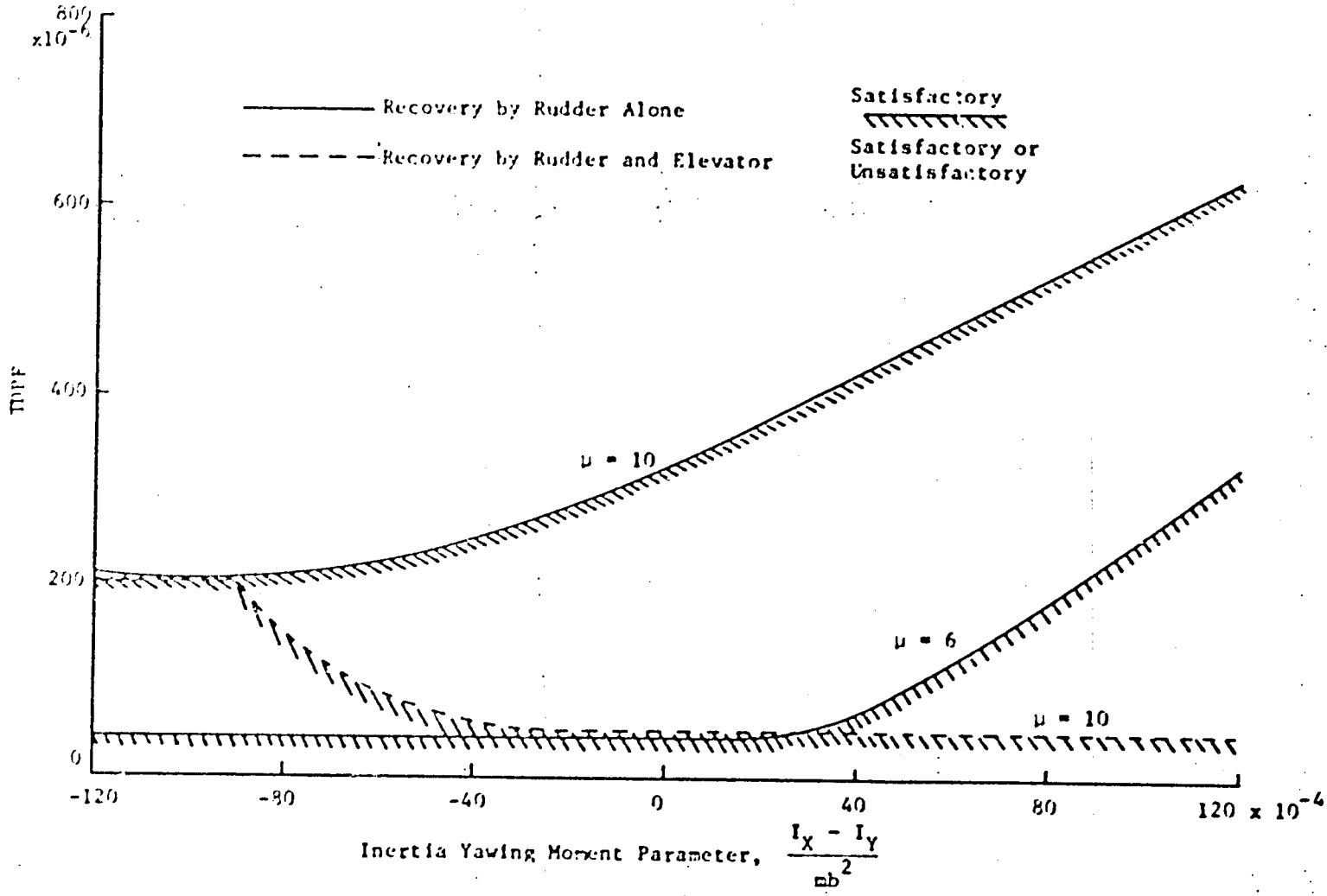

Figure 2-3. General Aviation Spin Criterion Based on the TDPF (1947)

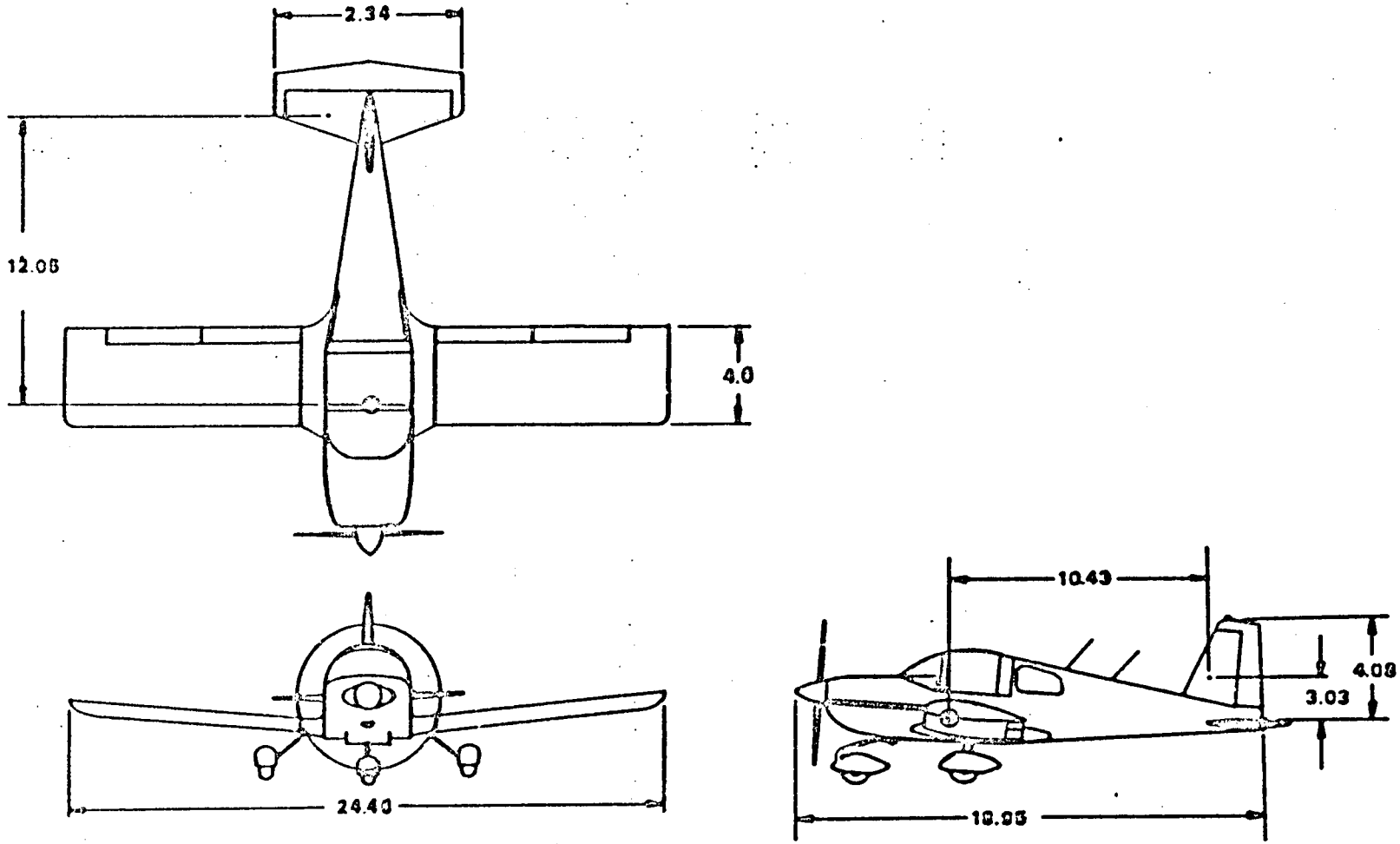

Figure 2-4. NASA Typical Single-Engine General Aviation Design

tail configuration, c.g. position, and fuselage/wing modifications. The results showed that, although tail configuration is an important parameter, other features such as rounded fuselage bottom, the addition of ventral fins, wing fillets and strakes had an appreciable effect on the equilibrium spin modes and recovery characteristics. Conclusions made about tail configuration were minimal, although several possible trends were noted. The tests also proved that the TDPF did not correctly predict spin recoveries, and it was concluded that "...the existing tail design criterion obviously cannot be used to predict recovery characteristics" (Burk et al. 1977).

Rotary Balance Tests

Spin tunnel rotary balance tests conducted by NASA have proven to be useful in analytical studies of fully developed spins. Rotary balances have been in use for several years, but the ability of a balance to obtain accurate and repeatable data has been a recent development. The rotary balance apparatus enables net forces and moments due to aerodynamic and inertia effects to be measured as functions of spin rate, orientation, and spin radius. It consists of a strain gage balance attached to a rotating rig as shown in Figure 2-5. The present balance has a pitch angle range of 0 to 90°, a roll angle range of $\pm$ 15°, and a rotation rate of 0 to 90 rpm.

Isolated aerodynamic forces may be measured by enclosing the model in a box structure, making aerodynamic forces negligibly small. The test is performed for a given condition, and isolated inertial forces are recorded. The test is then repeated without the model enclosure, and inertial forces are subtracted from the net force measurements.

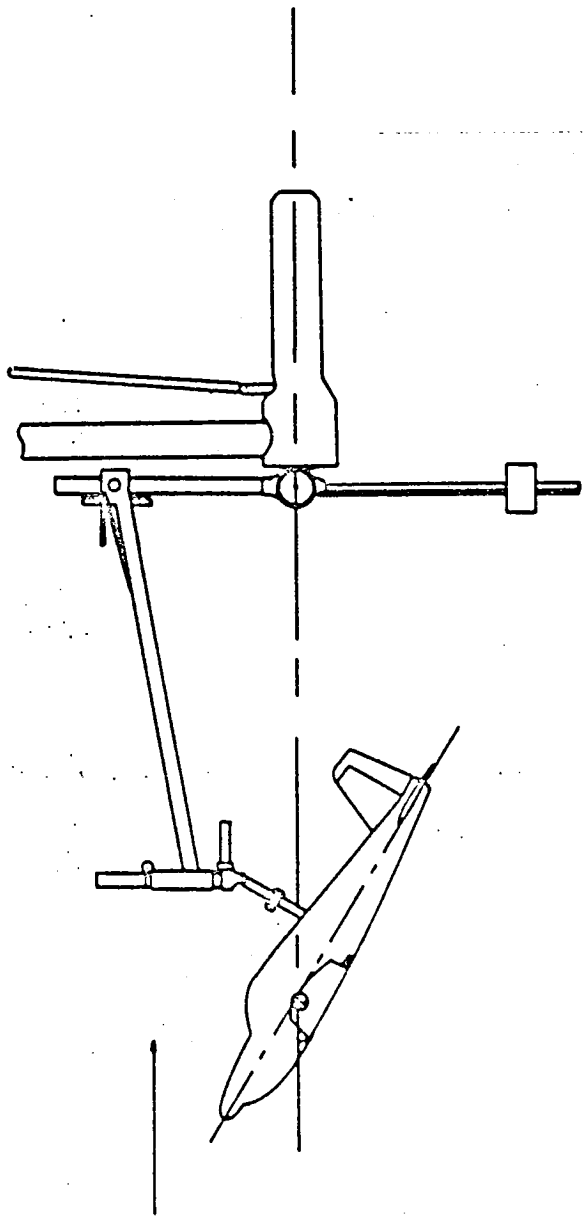

Figure 2-5. NASA-LaRC Rotary Balance Apparatus

Data presented by Bihrle et al. (1978) are the results of tests run for R_s equal to 0, θ ranging from 30 to 90°, and a roll angle, ϕ, approximately equal to 0. The present testing duplicates these conditions and a comparison of the two tests is presented in Chapter IV.

CHAPTER III

EXPERIMENTAL PROCEDURE

Spin Orientations

The major spin orientation parameters were simulated in the wind tunnel by orienting a model tail at pre-determined angles to the tunnel free streamline. Relevant angles are presented in Figures 3-1 and 3-2. As seen in the first figure, the aircraft is assumed to be spinning about a vertical axis passing through its c.g., with ϕ equal to 0. The tail experiences a net velocity containing components from the descent velocity, V_d, and the product of the spin rate and horizontal distance to the spin axis, $\Omega l_t \sin\theta$. The angle in the vertical plane at which the resultant velocity impinges the vertical tail, α_v, is a primary controller of spin damping. Note that for these static wind tunnel tests, V_d is related to the test section velocity by

$$V_d = V_T \cos \alpha_v .$$

Pitch angle also has a large influence by determining the shape of the separated region above the horizontal stabilizer. Pitch angle is related to α_v by the equation

$$\alpha_v = \tan^{-1}\left(\frac{\Omega l_t}{V_d} \sin\theta\right)$$

$$\alpha_v = \tan^{-1}\left[\frac{1}{\omega}\left(\frac{2l_t}{b}\right) \sin\theta\right]$$

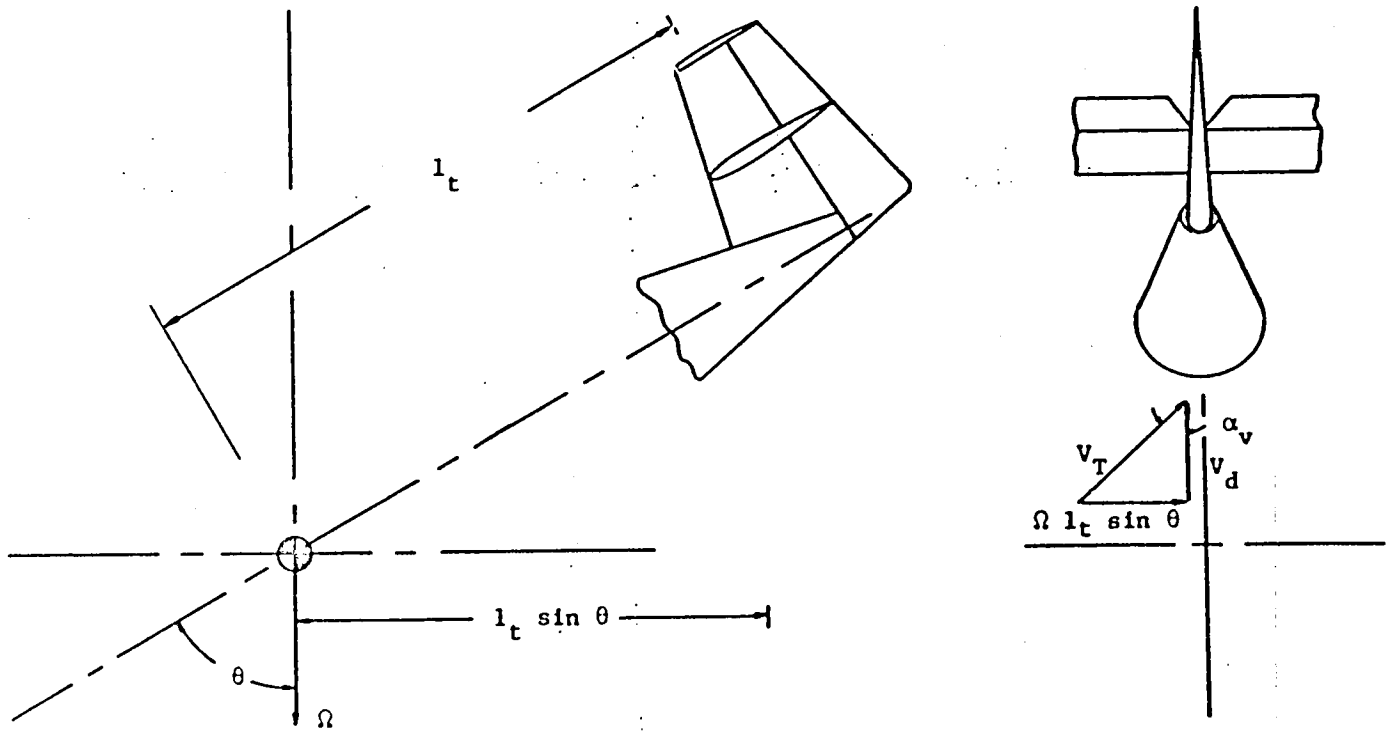

Figure 3-1. Velocities Affecting Tail in an Idealized Spin

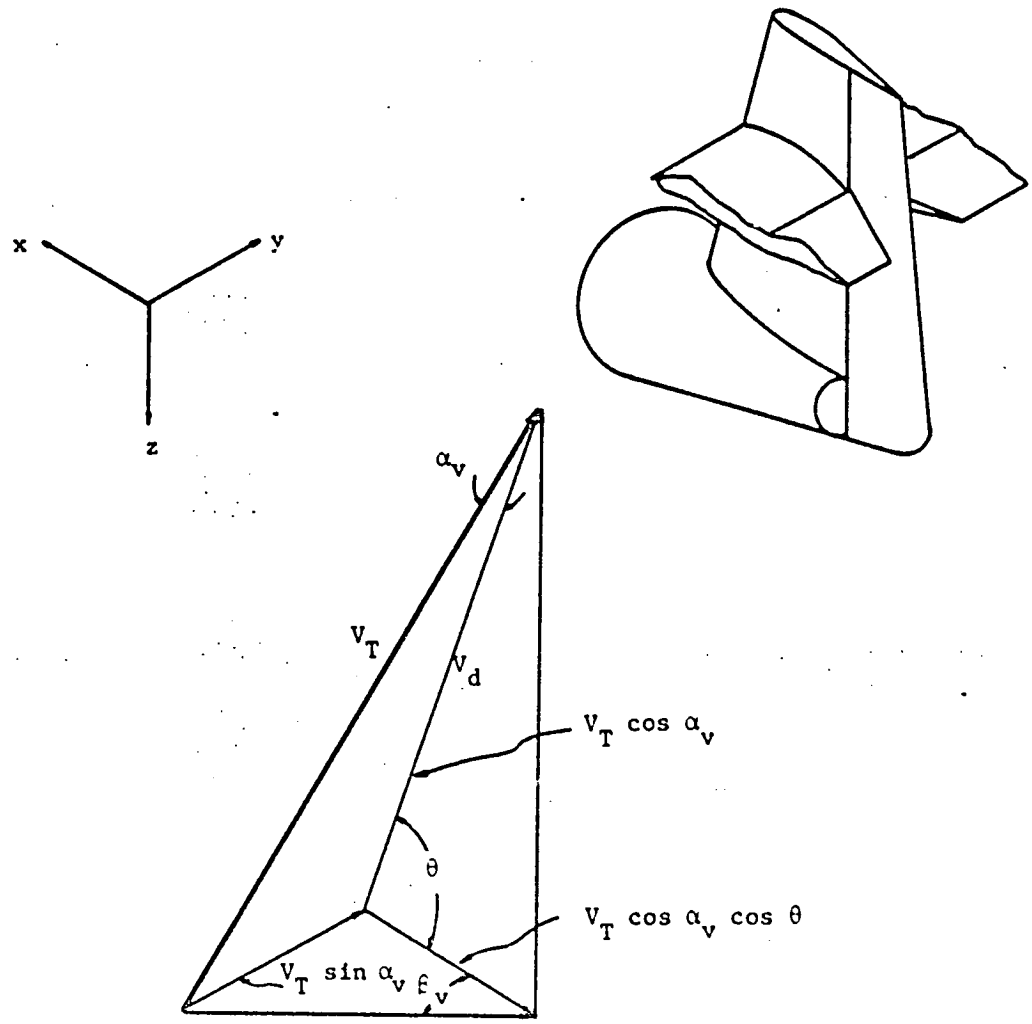

Figure 3-2. Tail Orientation with Respect to Total Velocity Vector

where

$$\bar{\omega} = \frac{\Omega b}{2V_d} .$$

The dimensionless spin rate, $\bar{\omega}$, is an important parameter in scaled spin studies. Equilibrium values of $\bar{\omega}$ for actual spins vary depending on the degree of spin. Steep spins are normally characterized by low values of θ and low spin rates, with a pitch angle of 40° and a spin rate of 0.3 being typical. Flat spins normally possess high theta values, usually above 60°, with $\bar{\omega}$ typically having a value of 0.7. Equilibrium spin states are strongly dependent on mass-inertia properties and aerodynamic characteristics of an aircraft, and therefore will vary from one configuration to another.

The present testing is concerned with a wide range of spin rates and pitch angles to obtain information about equilibrium conditions of a variety of aircraft configurations. Over the range tested, values of α_v were determined using reference values of l_t and b, and are presented in table 3-1.

The assumption that R_s is equal to 0 should not affect results greatly. Spin radius can be approximated as a function of pitch attitude by equating gyroscopic and aerodynamic forces acting on the aircraft. For an aircraft in an equilibrium spin having a negligible roll angle,

$$R_s = \frac{g}{\Omega^2 \tan\theta} . \quad \text{(derived in McCormick 1981)}$$

For a flat spin, R_s is therefore small compared to the wingspan. The

Table 3-1

Angle of Attack as a Function of Pitch Angle and Spin Rate for Test Orientations

$\bar{\omega}$	α_v (Degrees) $\theta = 40°$	60°	80°
0	0	0	-
.3	12.78	17.00	-
.5	20.71	27.00	30.08
.7	27.89	35.50	39.04
.9	-	42.52	46.20

assumption is less valid for low theta values. Because the aircraft is nosed inward toward the spin axis, the principal effect of neglecting R_s is an underestimation of yaw damping. The assumption is therefore conservative for steep spin conditions. It should be noted, however, that any analysis of spin departure should include the effects of spin radius.

The roll angle is also assumed to be zero. Full scale flight tests show this assumption to be valid for flat spins, while steep spins possess a slight roll angle, having the effect of increasing pitching moment and decreasing yawing moment tail contributions. Such effects are probably negligible because of the small magnitudes of ϕ. However, flight test results show that roll angle is oscillatory in an actual spin (Stough and Patton 1979). Roll angle should therefore be an additional parameter for a complete dynamic analysis.

Model Configurations

The tail section models were designed to be typical of general aviation aircraft tails, based on available information. The baseline model configuration (Configuration A) was designed based on average tail volume coefficients and tail planforms of several light single-engine aircraft. Because of the wide differences in planform and configuration, however, some assumptions were necessary. The vertical tail angle-of-sweep, sometimes used to increase the moment arm and stalling angle of attack of the vertical tail, was found to vary considerably between manufacturers. Angle-of-sweep was set equal to zero at mid-chord to result in a vertical tail planform resembling that of the NASA tests. Many aircraft use variable-incidence horizontal stabilizers (also known as all-moving tails) which allow greater c.g. range and better control. The fixed tail configuration is equally popular, and was used in the present testing. Most aircraft have cross-sections varying from root to tip, averaging approximately 8% thickness. Construction complexity and strength considerations necessitated a horizontal stabilizer of constant thickness with respect to span, and slightly increased thickness for extra strength. A symmetrical NACA 0012 airfoil section was used for all surfaces.

Because of its variable influence, aft fuselage cross-sectional shape should be the subject of a separate test program, and its influence was not determined in the present studies. A circular cross-section was used, preventing a propelling yawing moment under all test orientations. Although points of flow separation are not well-defined on a fuselage shape of this type, they do not change position with α_v orientation. The primary influence of the aft fuselage is therefore a

fairly constant force in the direction of V.

A scale drawing of the baseline configuration is presented in Figure 3-3. Note that the horizontal tail is placed at a mid-span position on the vertical tail. Horizontal and vertical tail tips are formed by revolving the airfoil section around the tail surface tips.

Test parameters consist of the vertical position of the horizontal tail, chordwise position of the horizontal tail, vertical tail aspect ratio, and horizontal tail aspect ratio. The effects of control deflections are also studied, for both full-span and partial-span rudder configurations.

The vertical position of the horizontal tail can have an appreciable effect on yaw damping characteristics. It is expressed in terms of the height, h, of the horizontal tail above the fuselage reference line, divided by the vertical tail span, b_v. Configurations B, A, C, and D were used in variation of h/b_v from 0 to 1.0, as indicated in Figure 3-4. Five distinct locations were used in the earlier NASA spin tunnel studies. In the present study, four locations are used because of difficulty in mating the horizontal tail to the curved upper fuselage. Also, note that construction of Configuration D, with h/b_v equal to 0, necessitated cutting approximately 3.4 square inches from the root of the horizontal tail.

The chordwise position of the horizontal tail may have an effect on pitch and yaw damping through moment variation and vertical tail blanketing. Three chordwise positions were employed: 20% of the chord forward of the neutral position; neutral; and 20% of the chord aft of neutral, represented by Configurations E, A, and F (see Figure 3-5).

The vertical tail aspect ratio, AR_v, is defined as the vertical

tail span squared divided by the vertical tail area, b_v^2/S_v. It is found to vary considerably among standard tail configurations, with a value of 1.3 being an approximate average. Aspect ratio was varied from a minimum value of 1.1 to a maximum of 1.7 in the testing, measured from the reference centerline of the fuselage. Taper ratio was held constant, resulting in varying leading and trailing edge sweep angles. As indicated in Figure 3-6, Configurations G, H, A, and J represent the variation of AR_v and its effect on vertical tail planform.

Finally, the horizontal tail aspect ratio, AR_h, was varied while maintaining constant horizontal tail lift effectiveness at low angles of attack. The three-dimensional lift curve slope can be obtained from approximate lifting surface theory by:

$$C_{L_\alpha} \approx C_{l_\alpha} \frac{AR}{AR + [2(AR + 4)/AR + 2]} .$$

Thus, in order to maintain the same lift effectiveness,

$$\frac{AR_h S_h}{AR_h + [2(AR_h + 4)/AR_h + 2]} = C$$

This, of course, assumes a constant C_{l_α} for all horizontal tail surfaces.

Four horizontal stabilizers were constructed, varying AR_h from a minimum of 3.48 to a maximum of 5.40, represented by Configurations K, A, L, and M (see Figure 3-7).

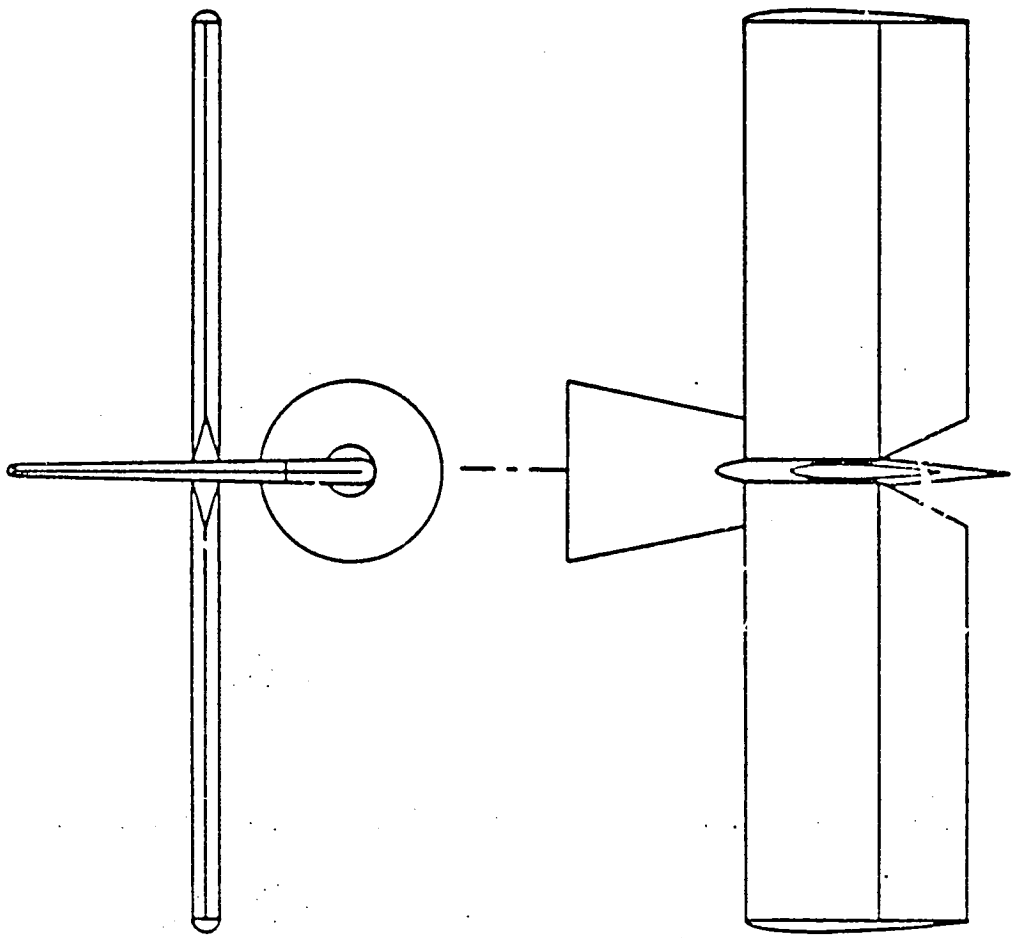

Scale 1:4

b_h = 20 in.

b_v = 7.5 in.

S_h = 100 in.^{2}

S_v = 37.5 in.^{2}

AR_h = 4.0

AR_v = 1.5

h/b_v = 0.5

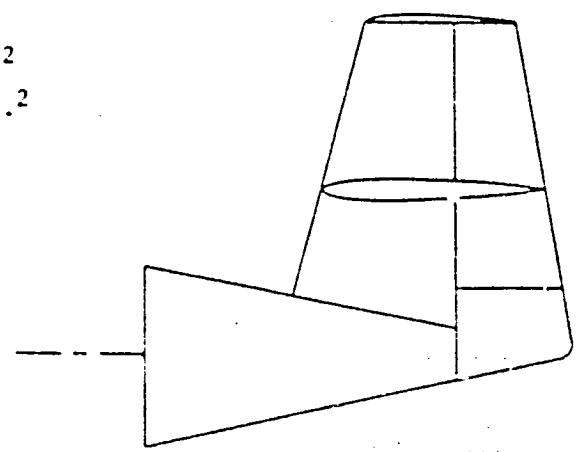

Figure 3-3. Configuration A

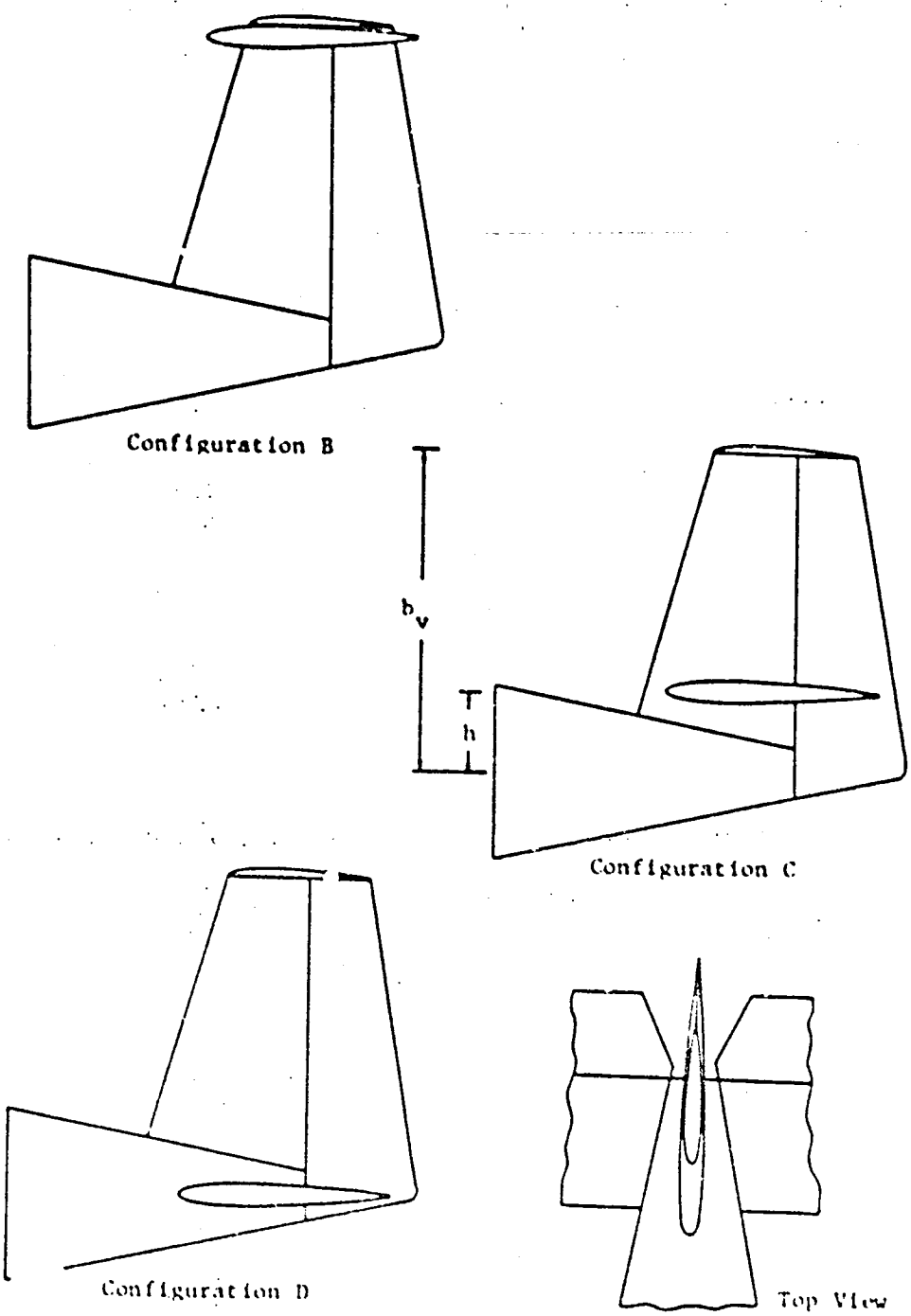

Figure 3-4. Variation of h/b_v

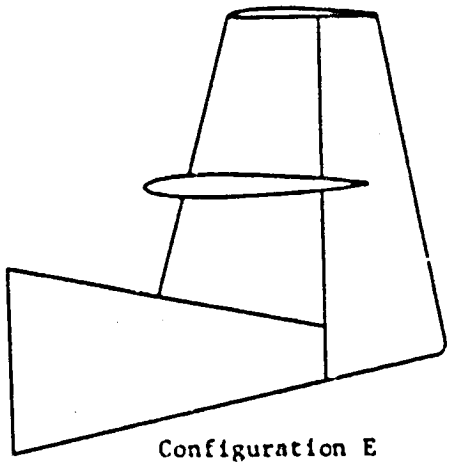

Configuration E

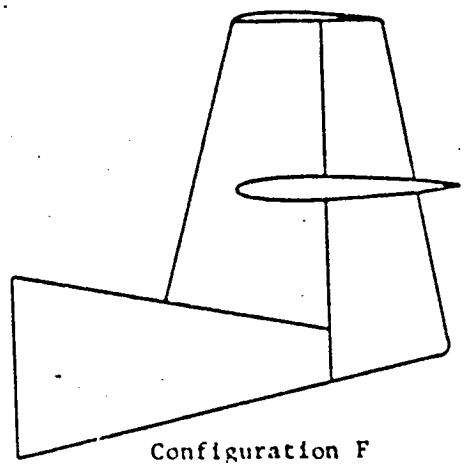

Configuration F

Figure 3-5. Variation of Tailplane Chordwise Position

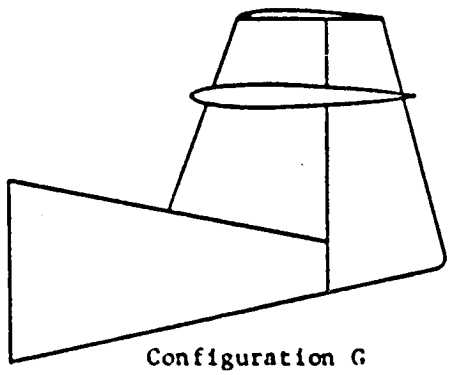

Configuration G

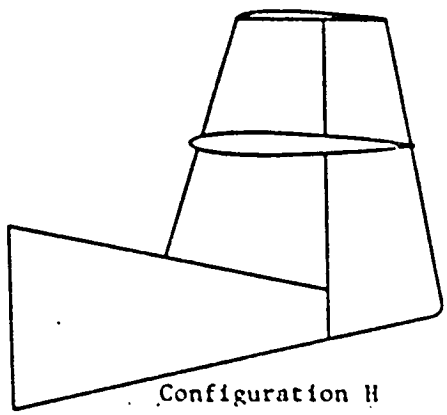

Configuration H

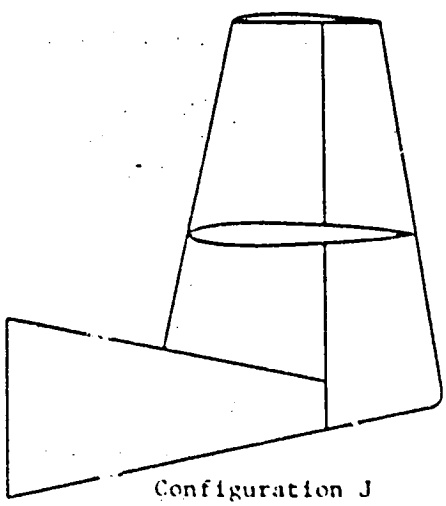

Configuration J

Figure 3-6. Variation of AR_v

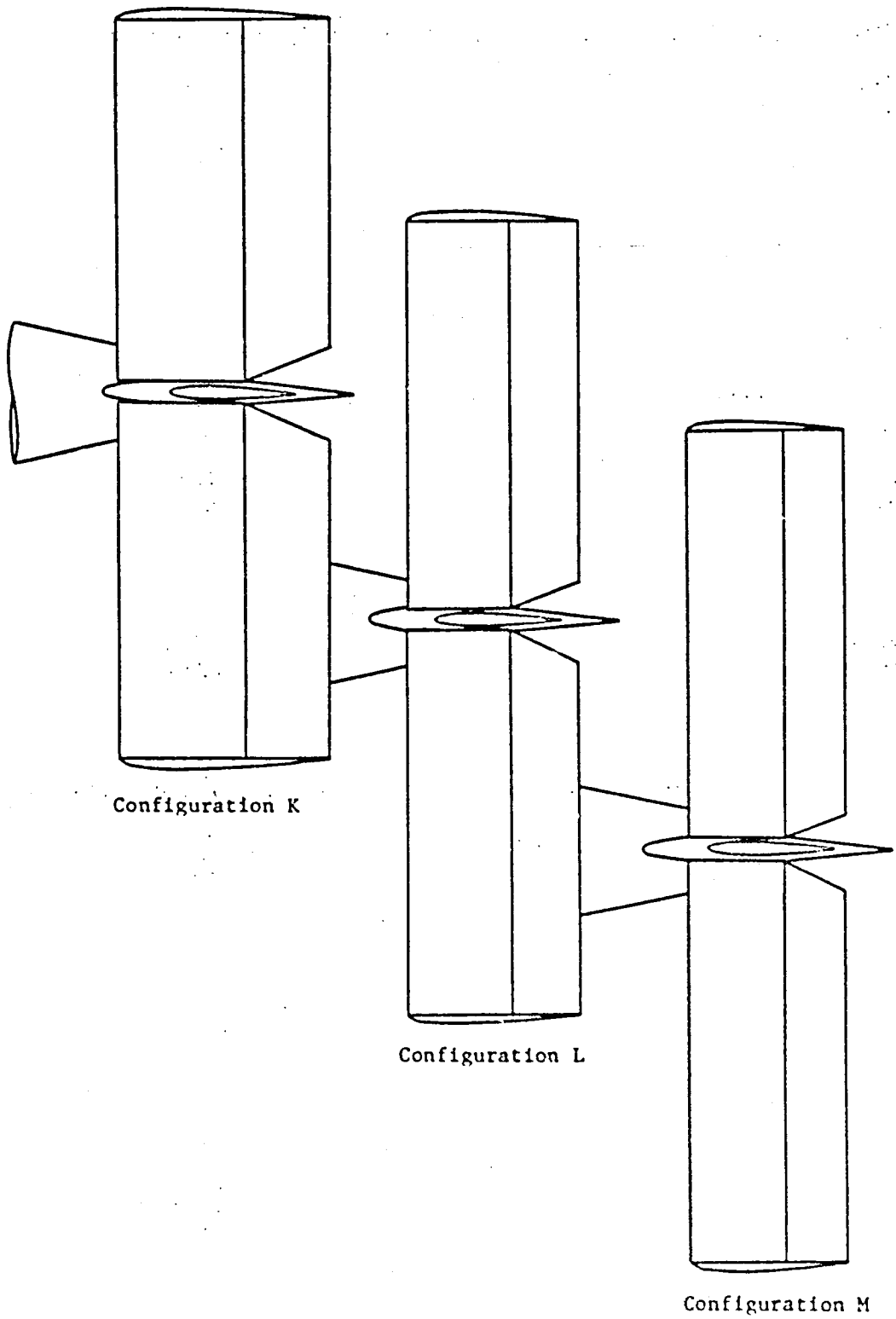

Figure 3-7. Variation of AR_h

Rudder travel is equal to $\pm$ 25° for both full-span and partial-span controls. The partial-span rudder extends from h/b_v equal to 0.2 to 1.0. Elevator travel is equal to $\pm$ 15°. Relevant dimensions and test parameters for each configuration are presented in Appendix A.

Because of the limited range of parameters feasible in an experiment of this scope, some parameters were eliminated. Horizontal tail taper ratio, angle-of-sweep, and dihedral angle were held constant for all test configurations. Vertical tail taper ratio and angle-of-sweep were also held fixed. Such parameters may influence tail damping characteristics appreciably and should be included in future studies.

General Experimental Design

The experimental set-up is shown in Figure 3-8. The tests were performed in a four-foot by five-foot atmospheric closed-return wind tunnel. All tails were mounted on a supporting structure which allowed rotation about the body-fixed y-axis and the tunnel-fixed x-axis. Orientations were maintained through a pin-locking system as shown in Figure A-1. An internally-mounted strain-gage balance, borrowed from NASA-Langley Research Center, was used for all force and moment measurements.

A forward body which abuts, but does not touch, the aft fuselage was used in order to provide a continuous fuselage surface. In addition, under steep spin conditions, interference or flow interuption from a forward fuselage may be significant, making an abutting fuselage necessary for accurate modelling of the actual flow field. Moreover, the forward fuselage eliminates flow impinging directly on the exposed part of the balance and it minimizes strut interference. The fuselage

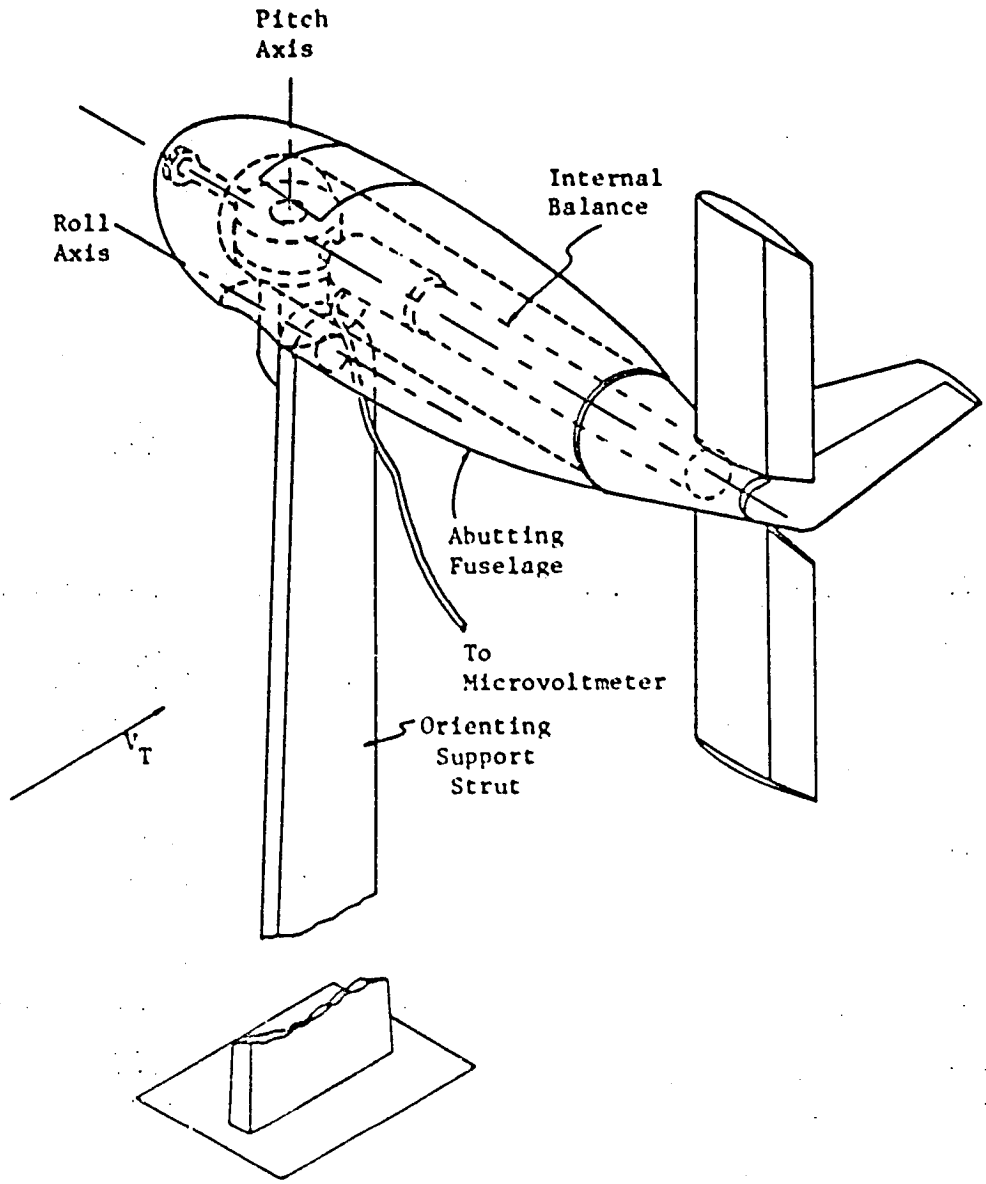

Figure 3-8. Schematic of Model and Measurement System

was attached to the forward part of the orienting support, and therefore did not directly contribute to the forces and moments which were measured on the tail. A scale drawing of the forward fuselage is presented in Figure A-2. Note that a door was cut in order to provide access to the pitch adjustment without disassembly.

The model was centered laterally in the wind tunnel for all tests, and angles were adjusted during assembly from an alignment position designed into the orienting support. This zero position corresponded to a pitch angle of 90° and an α_v equal to 0, as shown in Figure 3-11.

A 5 volt balance excitation was provided by a d.c. power supply which maintained constant voltage to $\pm$ 0.02%. Output voltage was obtained from an integrating microvoltmeter. The strain gage balance was provided with an extensive set of calibration equations containing linear and nonlinear interaction terms. A full calibration of the balance was last performed by NASA-LaRC in 1977. A rough check of the calibration showed agreement to within approximately 1%.

Model Construction Considerations

All test models were built by the author from Philippine mahogany, laminated to prevent warpage. Vertical tail surfaces were reinforced with 0.125-inch T-3 aluminum bars, and horizontal tail surfaces were reinforced with steel rods extending the entire span of each horizontal tail. Vertical tails were bolted to the aft fuselage, while horizontal tails were held in place by tension, which could be adjusted by bolts in each wingtip. Bending of the models due to wind forces was too small to be measurable. Wood outer surfaces were finished in gloss polyurethane coating, hand rubbed with rottenstone and glass polish. Outer wingtip

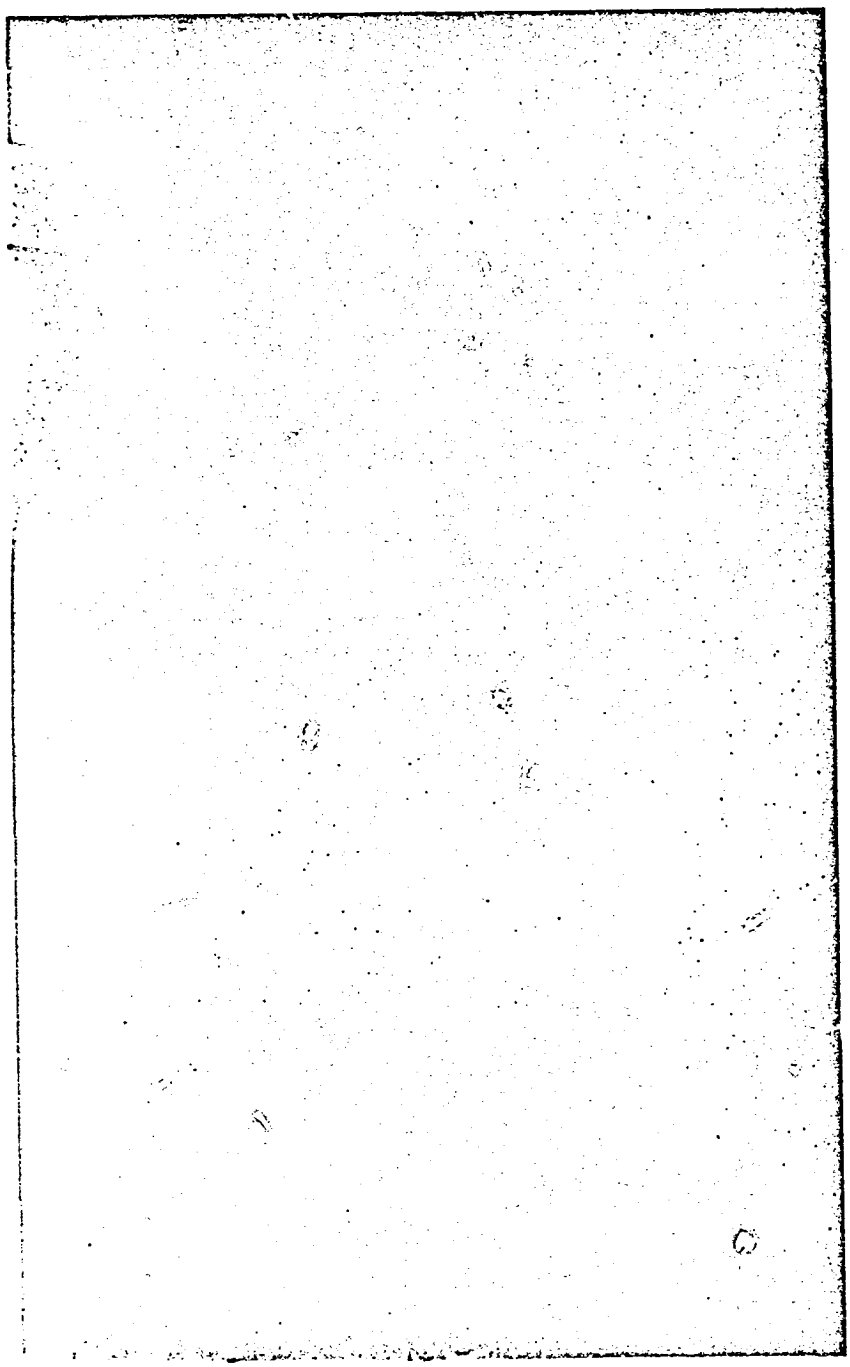

Figure 3-9. Model and Support in Test Section, Configuration A; $\delta_e = 15°$, $\delta_r = 25°$

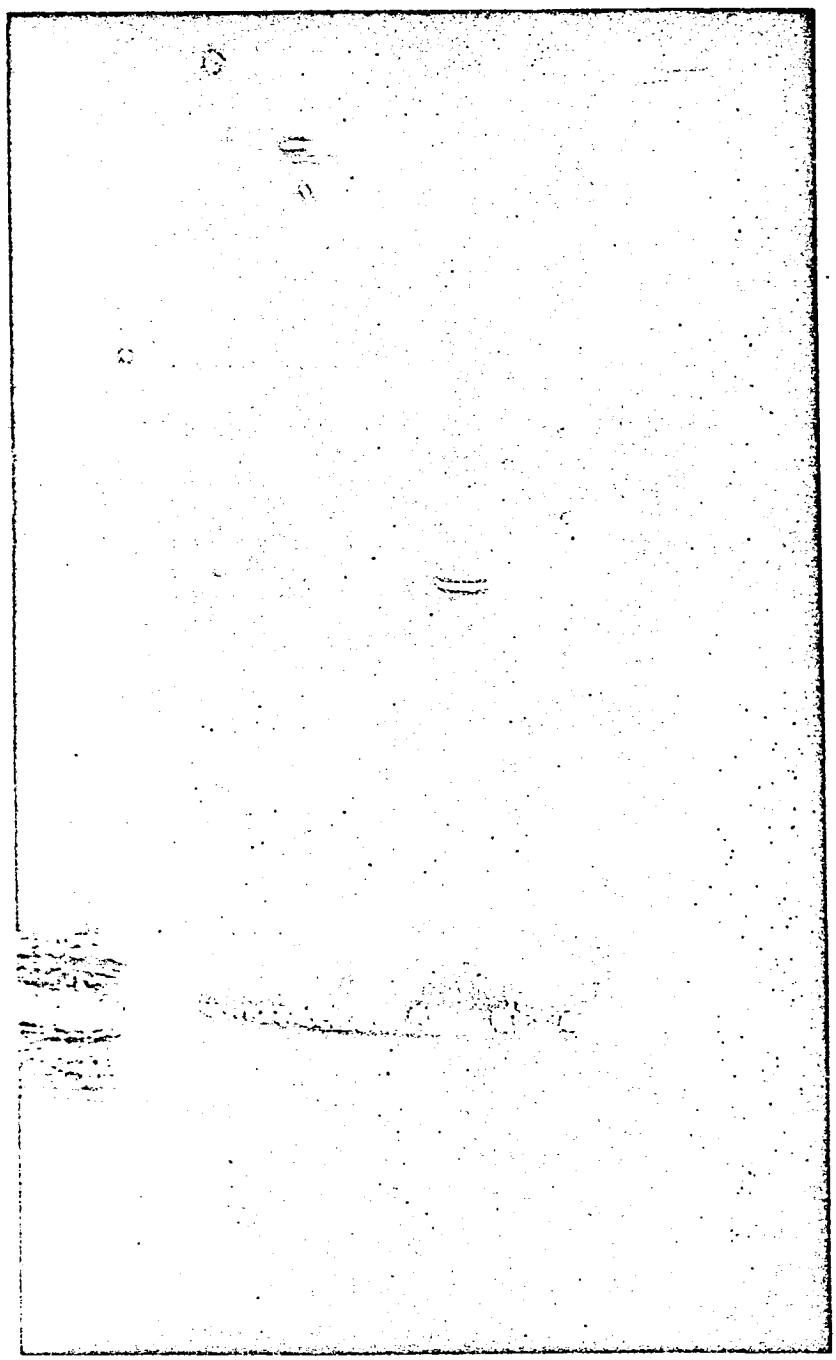

Figure 3-10. Configuration B in Test Section

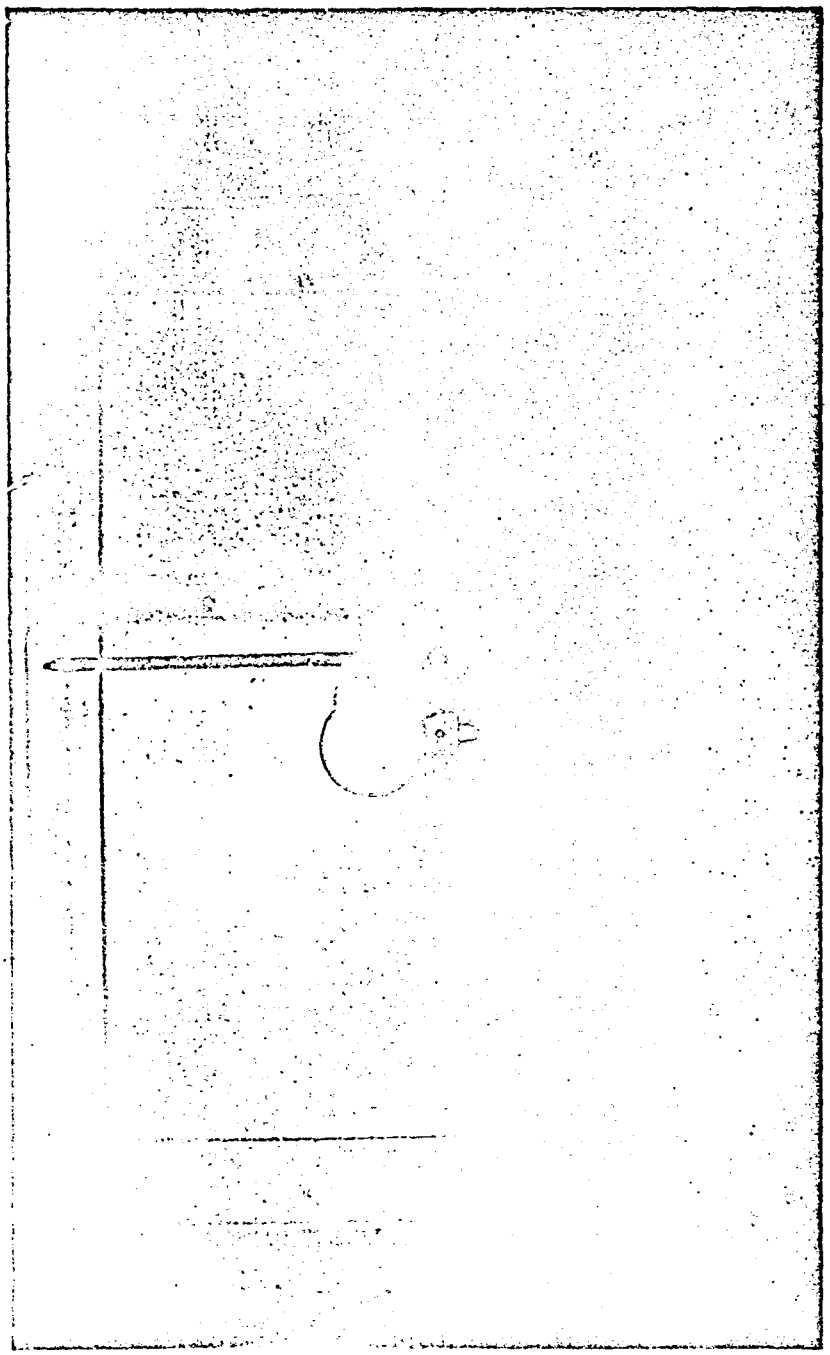

Figure 3-11. Configuration M; Alignment Position

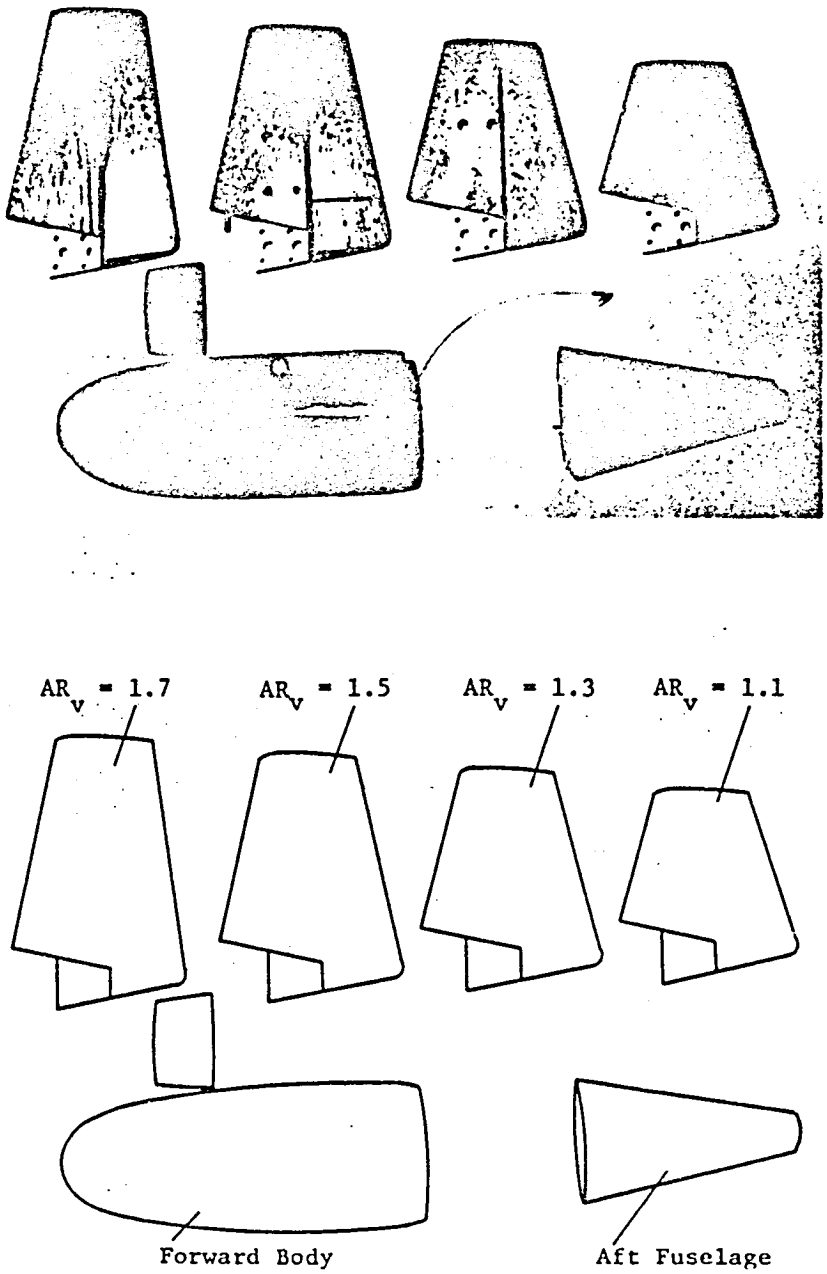

Figure 3-12. Fuselage and Vertical Tail Models

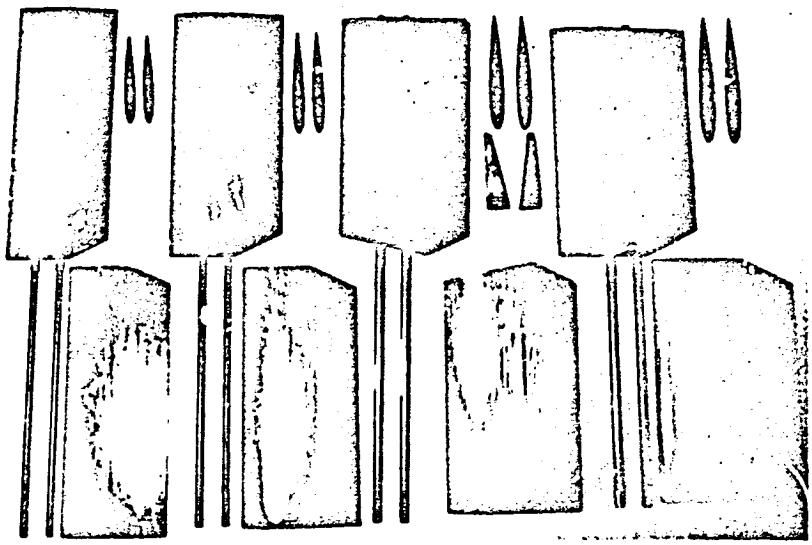

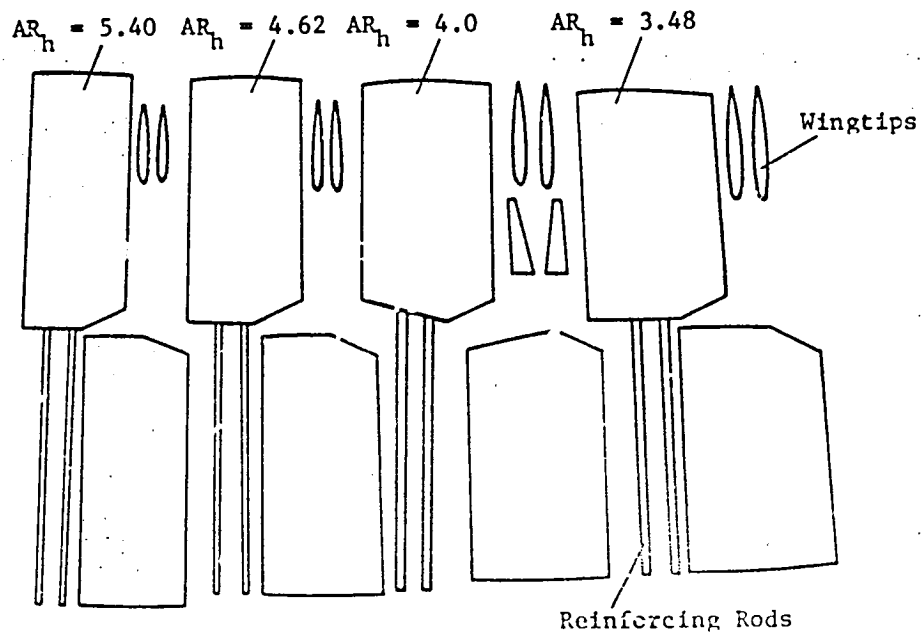

Figure 3-13. Horizontal Tail Models

fairings were cast from wood molds using a mixture of white spot putty and fiberglass resin. All final surfaces were waxed before testing.

Testing Considerations

At the angles of attack simulating the empennage in a spin, separation is well-defined at the leading and trailing edges of the tail surfaces. Reynolds number effects should therefore be small, as shown by spin tunnel tests run at Reynolds numbers as low as 6% of full-scale. The tests demonstrated that longitudinal aerodynamic characteristics are not significantly affected by R_E for pitch attitudes greater than 30^o (Bihrle et al. 1978). Preliminary tests were run to determine the effect of R_E in the present testing, and a small variation was noted in the force measurements. This variation may have been caused by a change in tunnel turbulence level with tunnel velocity. The increased turbulence may have affected the separation point on the aft fuselage enough to cause a variation in the data in some cases. Orientation changes made the use of a boundary layer trip wire impractical, and it was therefore decided to perform all tests at the relatively high tunnel speed of 100 fps. The Reynolds number, based on reference main wing MAC, was thus equal to 4.59×10^5, which was approximately 21% of full scale.

Wall interference effects were minimized by use of model wingspans which were less than 50% of the test section height. Corrections were not feasible because of the lack of applicability of current corrective methods. Heyson (1962; 1971) has developed a linearized boundary correction to account for the large wake deflections characterizing V/STOL testing. Unfortunately, large transverse velocities encountered

in most test orientations prevented its application. Solid blockage and wake blockage corrections were estimated, based on model projected area, using the approximation presented by Pope (1954). Their effects were found to be negligible.

The testing procedure was straightforward, with no unexpected difficulties occurring. Each configuration was aligned after assembly, and balance alignment was checked periodically. The balance was zeroed before each test to compensate for model weight, excitation voltage fluctuations, and temperature changes. Tunnel velocity was allowed to stabilize before readings were taken. Velocity was determined by means of a pitot-static tube connected to a water manometer, and temperature was measured with a thermometer mounted in the settling section.

Sources of Experimental Error

There are several possible sources of error, but their effects on the final results are minimal. Errors caused by voltage oscillations in the readings were reduced by the use of an integrating microvoltmeter. These fluctuations were caused by wind tunnel turbulence previously mentioned, and by vortices shedded from the forward and aft fuselages. Moreover, a large air compressor located in close proximity to the wind tunnel created a noticable low-frequency vibration. Lateral oscillations were reduced with the addition of a supporting brace, seen in Figure 3-9.

The compressor also contributed to line fluctuations, which varied periodically by approximately $\pm$ 5 μV. Excitation voltage also drifted, but the balance calibration check suggested it had a minimal effect on readings.

All support angle measurements and position measurements were limited by tolerances associated with metal work. Because of the support design, small pitch angle errors can result in angular errors at the balance center. The support was aligned and positioned in the test section manually, also resulting in possible errors.

Small sources of error are also inherent in the model design. The effect of flow on the front surface of the aft fuselage is unknown, but it probably has an insignificant effect on tail normal and side forces. Although the flow was minimized with the use of the abutting body, some test orientations may create a higher dynamic pressure inside the forward fuselage, causing bleed flow between the two fuselages. Control horns, used to maintain control surface angular position, may also have a small effect on force measurements. They were placed on the leeward side of all tail surfaces (within the stalled air cavity) to minimize their influences.

Model dimensions were accurate to within $\pm$ 0.025 inches and all surfaces were smooth. Holes and gaps between tail surfaces were filled with clay, making errors originating from model construction and configuration changes negligibly small.

Data Reduction

Three forces and three moment components were recorded for each test run. Moments were resolved about the balance center, which was located 4.05 inches forward of the 1/4-chord point of the baseline horizontal tail.

Experimental precision was satisfactory. Two baseline tests, corrected for differing tunnel velocities and performed on different

days, resulted in an average normal force error of -0.7%, an axial force error of 14.0%, and a side force error of 1.91%. The higher axial force error is somewhat misleading because extremely small forces were experienced in the axial direction.

In order to present the data in a usable form, typical reference values of l_t, S_w, c_w, and b_w were employed in converting to dimensionless moment coefficients resolved about an aircraft center of gravity. Based on a typical horizontal tail volume coefficient of 0.596 and an average value of S_h/S_w of 0.169, the following reference quantities were used.

$$S_w = 591.2 \text{ in.}^2$$

$$c_w = 9.92 \text{ in.}$$

$$b_w = 59.5 \text{ in.}$$

$$l_t = 35.0 \text{ in.}$$

All data were reduced using the above reference values and the descent velocity, V_d.

CHAPTER IV

RESULTS AND DISCUSSION

The following discussion will consider the pitching and yawing moments generated by the tail about the aircraft center of gravity. Tail force coefficients and rolling moments are not discussed because of their comparatively small effect on aircraft spin characteristics. For completeness, however, they are presented in Appendix C.

Effects of Spin Rate on Aerodynamic Moment Coefficients

Measured moments as functions of spin rate are presented in Appendix B for all tail configurations. As indicated in Figures B-1 through B-12, higher pitch angles result in larger pitching moments, caused by the greater profile drag associated with larger angles of attack. The curves also display a concave downward characteristic, with C_m increasing in magnitude with increasing spin rate. Yawing moment effects are presented in Figures B-13 through B-24. Higher spin rates result in greater y-direction velocity components, creating greater magnitudes of C_n. Interference from the horizontal tail is evident in the plots, caused primarily by blanketing effects and horizontal tail positioning.

It is interesting to note that in several yawing moment plots, curves of constant θ intersect each other in the region of $\bar{\omega}$ equal 0.3. Pitching moment curves suggest that errors caused by incorrect orientation are negligible. Possible causes for the phenomenon will be discussed.

Comparison with Rotary Balance Data

To determine the usefulness of a conventional wind tunnel in isolated tail studies, representative configurations can be compared with similar NASA test configurations used in the rotary balance studies of Bihrle et al. (1978). Configuration B was found to resemble tail 5 of the NASA tests, with the major difference being the lower horizontal tail aspect ratio and higher taper ratio of the NASA tail. Configuration C is similar to NASA tail 3 except for the above planform differences and a lower horizontal tail vertical placement, as shown in Figure 4-1.

For proper comparison, test data was adjusted to conform to NASA test conditions as closely as possible by calculating moments using reference lengths and areas based on the NASA test airplane. Scaling of these values was based on the areas of the vertical tails, which are similar in planform. The effect of changing to the NASA reference quantities is significant, as can be seen by comparison of test data in Figure B-3 with that of Figure 4-2. Because of this, moment coefficients presented in Appendix C are resolved about the balance center.

Figure 4-2 is a pitching moment comparison of Configuration C with NASA body and tail data BH3V. Results from the two tests show a high correlation, especially at low theta angles. At higher angles of pitch, Configuration C displays a pitching moment of higher magnitude, but the change of C_m with spin rate is similar for both tests. The discrepancy at high theta angles may possibly be attributed to horizontal tail area differences. Because scaling of reference values is based on vertical tail area, the scaled horizontal tail area of the NASA tests is

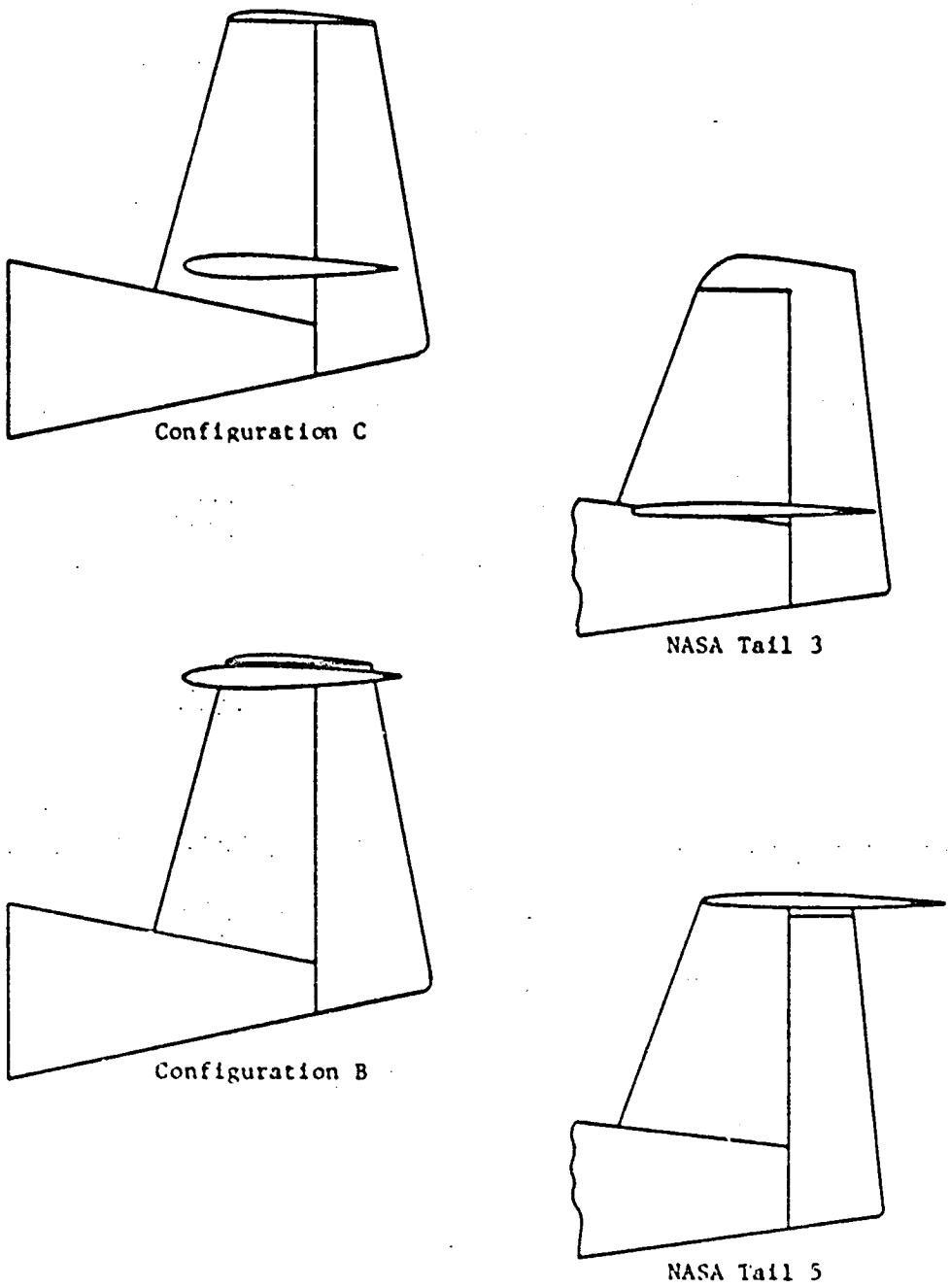

Figure 4-1. Tails Used in Comparison with NASA Rotary Balance Data

approximately 70% of that of Configuration C. This results in net C_m values of lower magnitude, notably at lower spin rates and higher pitch rates where normal force at the tail is caused almost entirely from flat-plate drag effects.

Yawing results are affected by contributions from the fuselage of the aircraft. While fuselage effects are not accounted for in the present tail studies, all rotary balance data contain body tare and interference effects. In order to obtain the correlation shown in Figure 4-3, body data were subtracted from the NASA body-tail data. Although this assumption of superposition does not account for the interference effects, it does partially account for the fuselage contribution to the net moment. The figure suggests that at higher spin rates, fuselage interference is significant. The large divergence at θ equal to 80° is probably caused by differences in h/b_v values for the two tails. As will be discussed, there is a discrepancy between NASA results and the present results concerning the effect of h/b_v at high pitch angles.

Rotary balance data for the T-tail configuration is available only for a complete wing-body-tail combination. As in the previous case, wing and body contributions were subtracted from the complete airplane data using measurements from an isolated wing-body test in order to obtain isolated tail moments. Figures 4-4 and 4-5 show that interference effects, probably from the stalled main wing, are considerable, particularly under steep spin conditions. The yawing moment comparison shows a strong correlation at the high pitch angle, lending support to the premise that wing wake interference is significant at lower pitch angles.

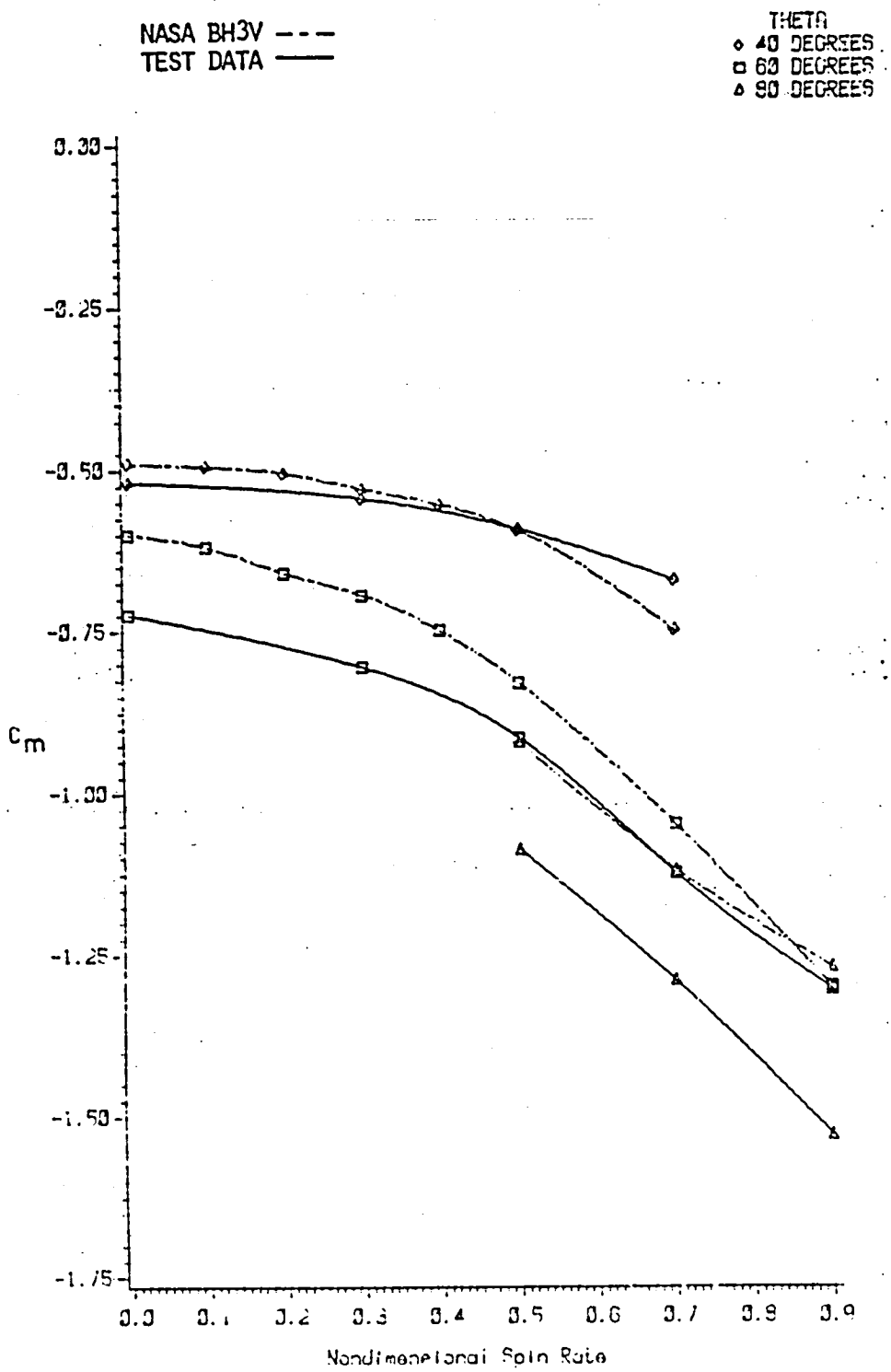

Figure 4-2. Pitching Moment as a Function of θ and $\bar{\omega}$, Configuration C

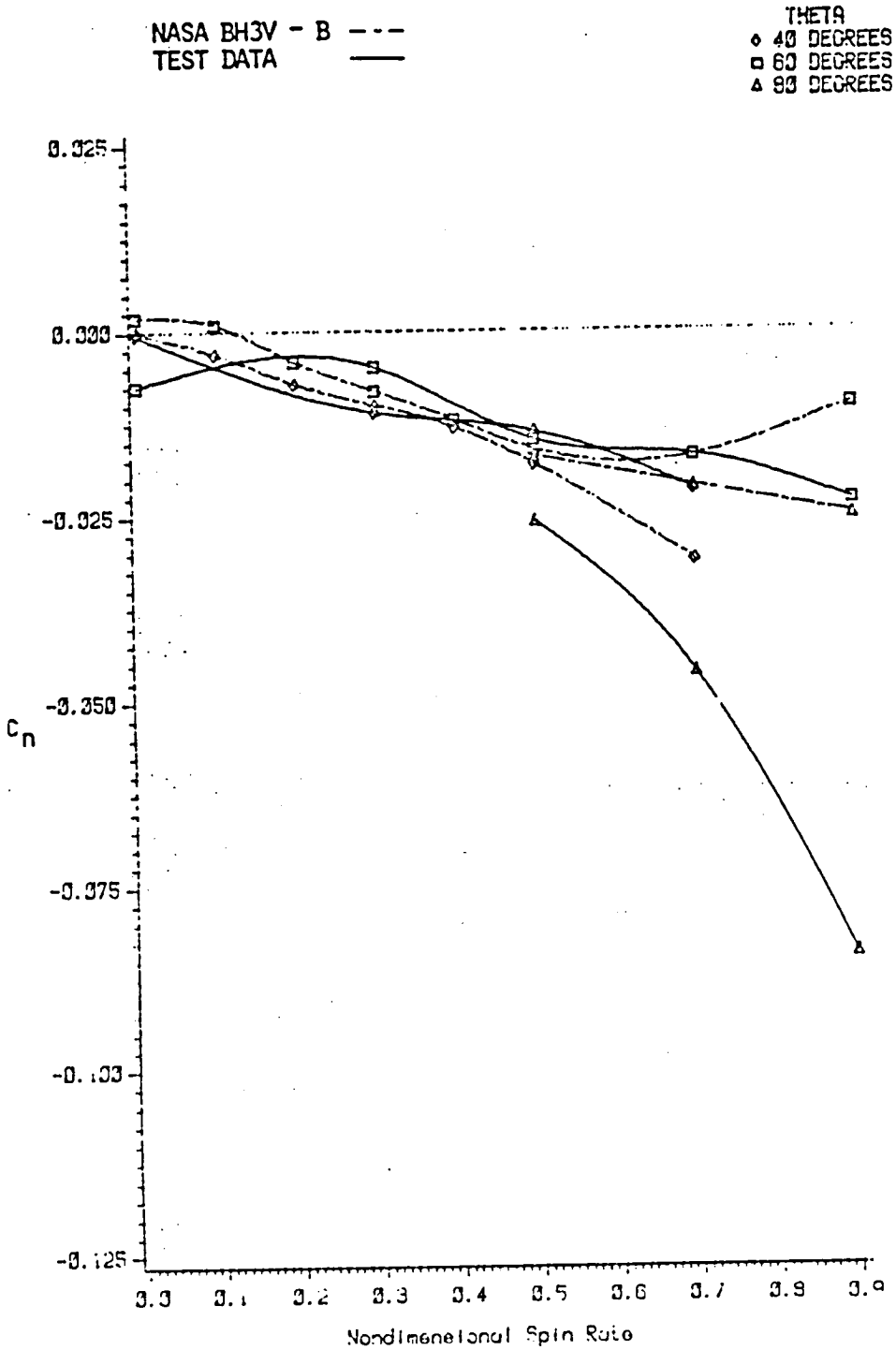

Figure 4-3. Yawing Moment as a Function of θ and $\bar{\omega}$, Configuration C

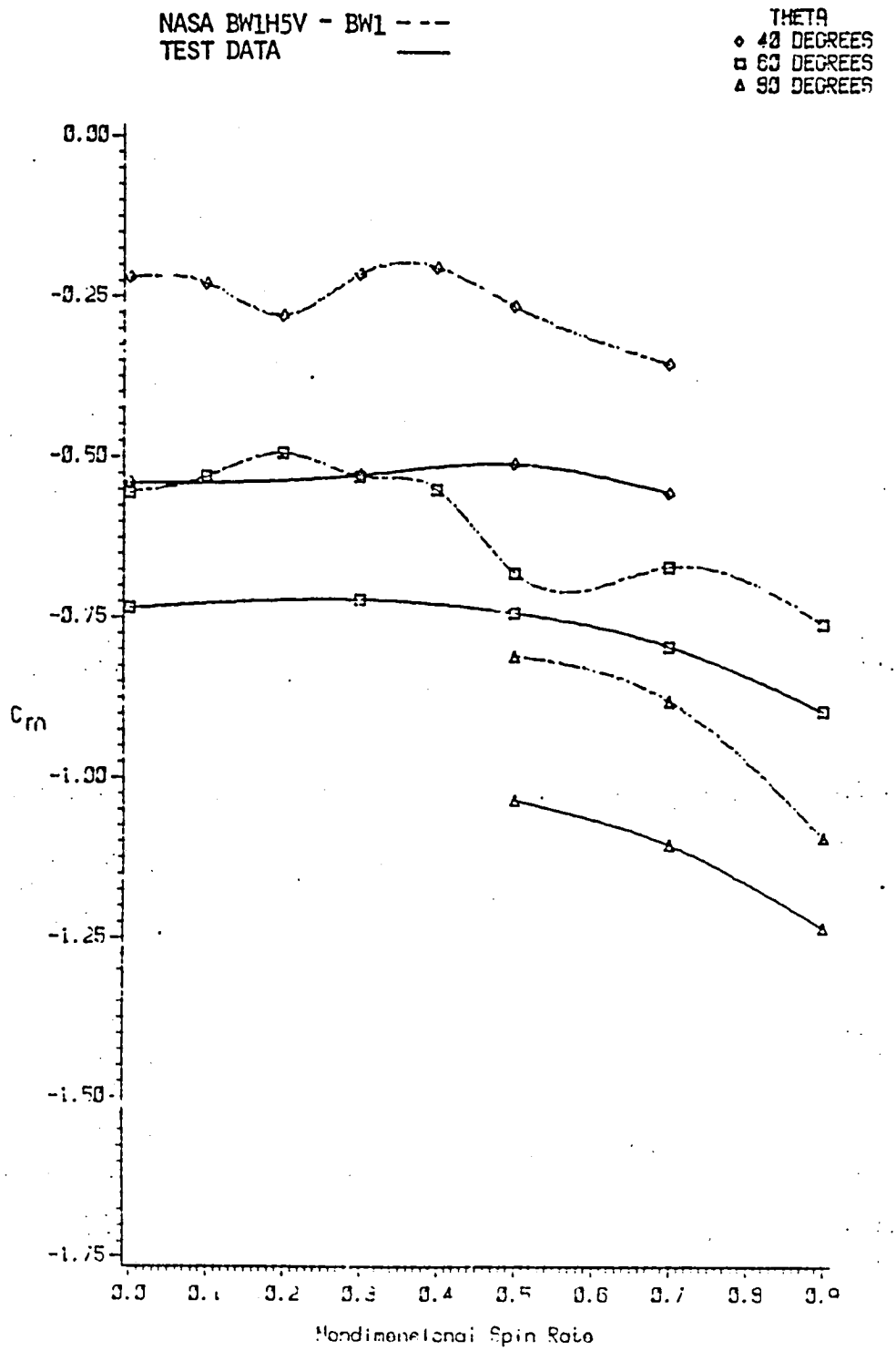

Figure 4-4. Pitching Moment as a Function of $\bar{C}$ and $\bar{\omega}$, Configuration B

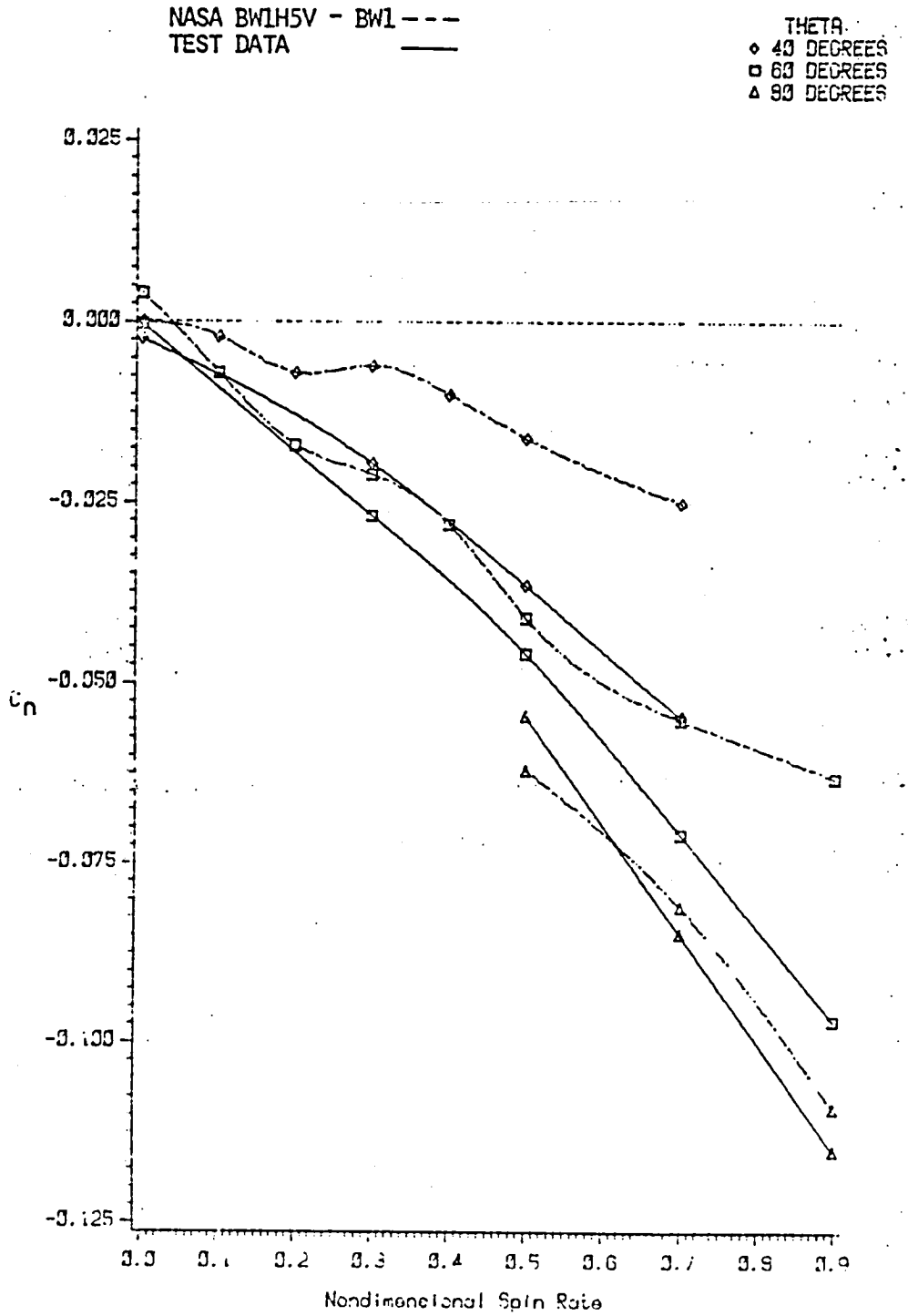

Figure 4-5. Yawing Moment as a Function of θ and $\bar{\omega}$, Configuration B

In addition to those already noted, there are several differences in the two studies which make quantitative comparison difficult. The NASA tests used a descent velocity of 25 feet per second, considerably slower than that used in the present testing. However, studies performed with the rotary balance tests showed Reynolds number effects to be small (see Bihrle et al.). The NASA aft fuselage directly under the horizontal tail has a flat bottom, which may cause interference effects which could not be accounted for by subtracting body data from body-tail data. Finally, the NASA tests were performed at non-zero roll angles. The roll angles were measured in fractions of a degree, however, and their effects are probably insignificant.

Effects of Horizontal Tail Vertical Position

Figures 4-6 through 4-10 show the effects of h/b_v on pitching moment. At low spin rates, they are minimal, with a larger effects developing with increasing $\bar{\omega}$. At moderate spin rates and higher pitch rates, a low horizontal tail appears most favorable, while at high spin rates, a mid-span horizontal tail placement results in stronger pitching moments The first effect is a direct result of fuselage and vertical tail blanketing of the leeward horizontal tail surface at high values of h/b_v. A second effect may arise from a horizontal tail-fuselage interaction as shown in Figure 4-11. Configuration C, with h/b_v equal to 0.25, may produce a larger net downwash than Configuration D, even though the leeward surface is largely blanketed. A larger increase in h/b_v destroys such a lift effect because flow is more prone to deflect around the leading and trailing edges of the vertical tail.

At θ equal to 40^o, a combination of interference effects causes an

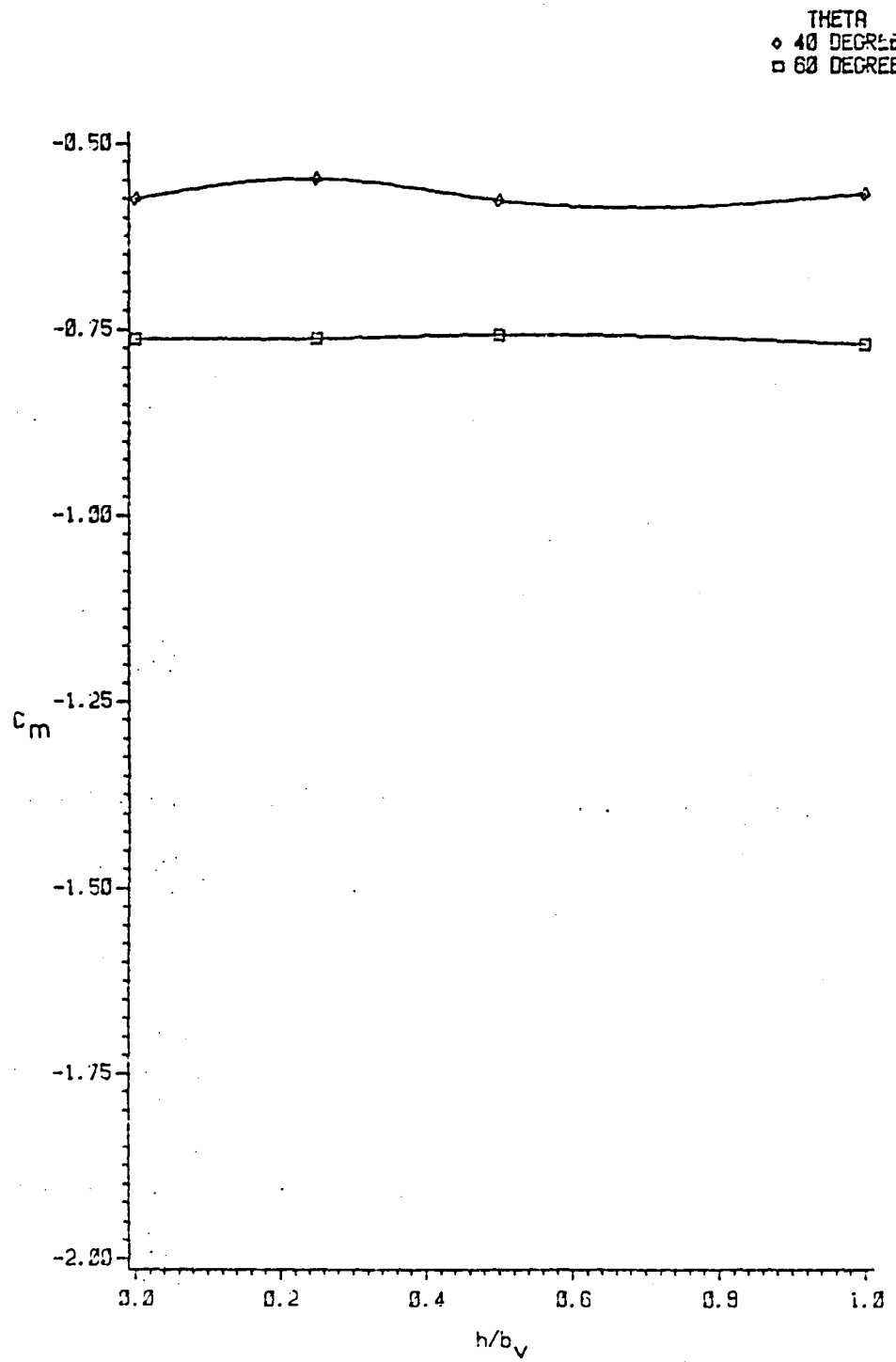

Figure 4-6. Pitching Moment as a Function of Vertical Position of Horizontal Tail, $\bar{\omega} = 0$

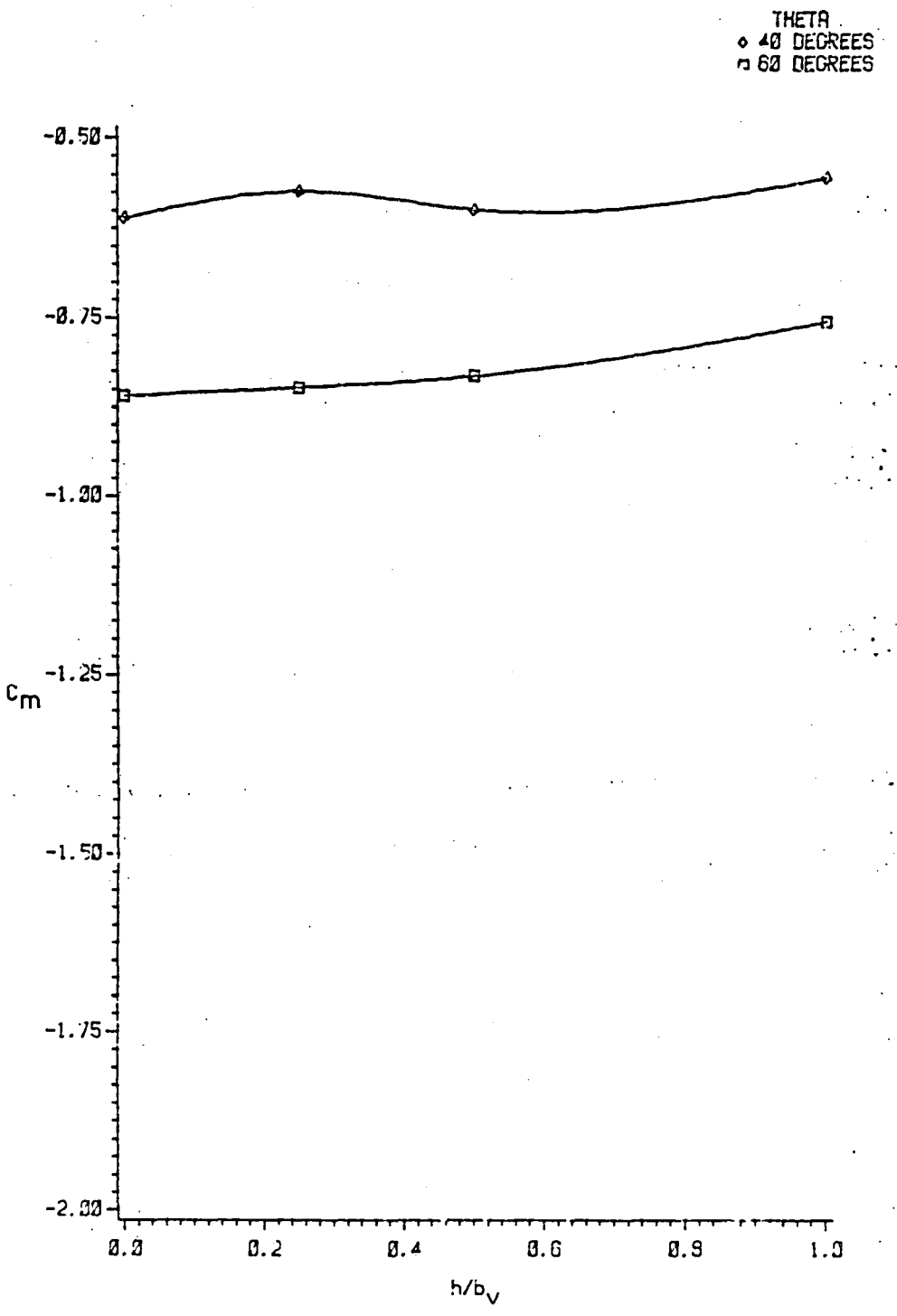

Figure 4-7. Pitching Moment as a Function of Vertical Position of Horizontal Tail, $\bar{\omega}$ = .3

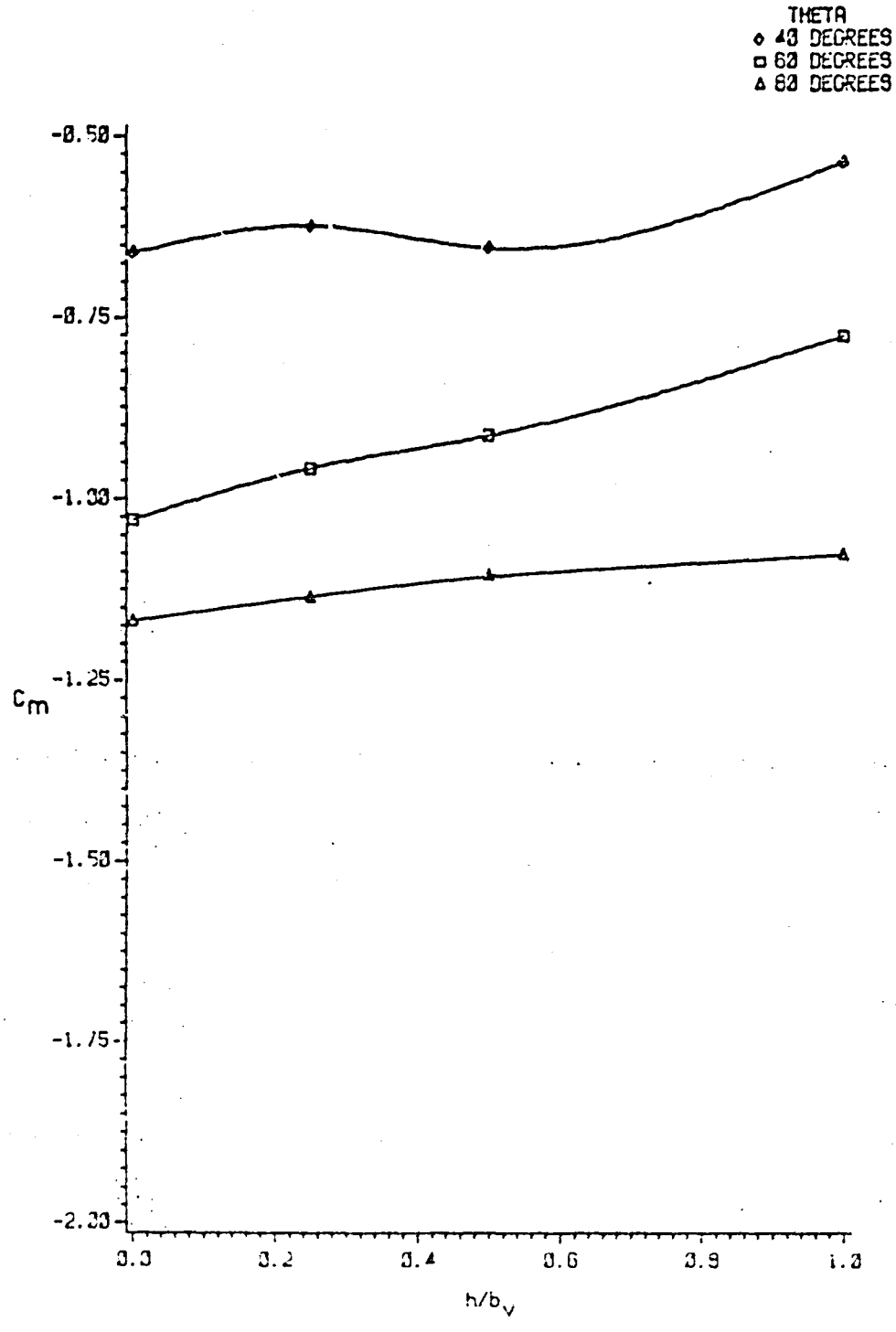

Figure 4-8. Pitching Moment as a Function of Vertical Position of Horizontal Tail, $\bar{\omega}$ = .5

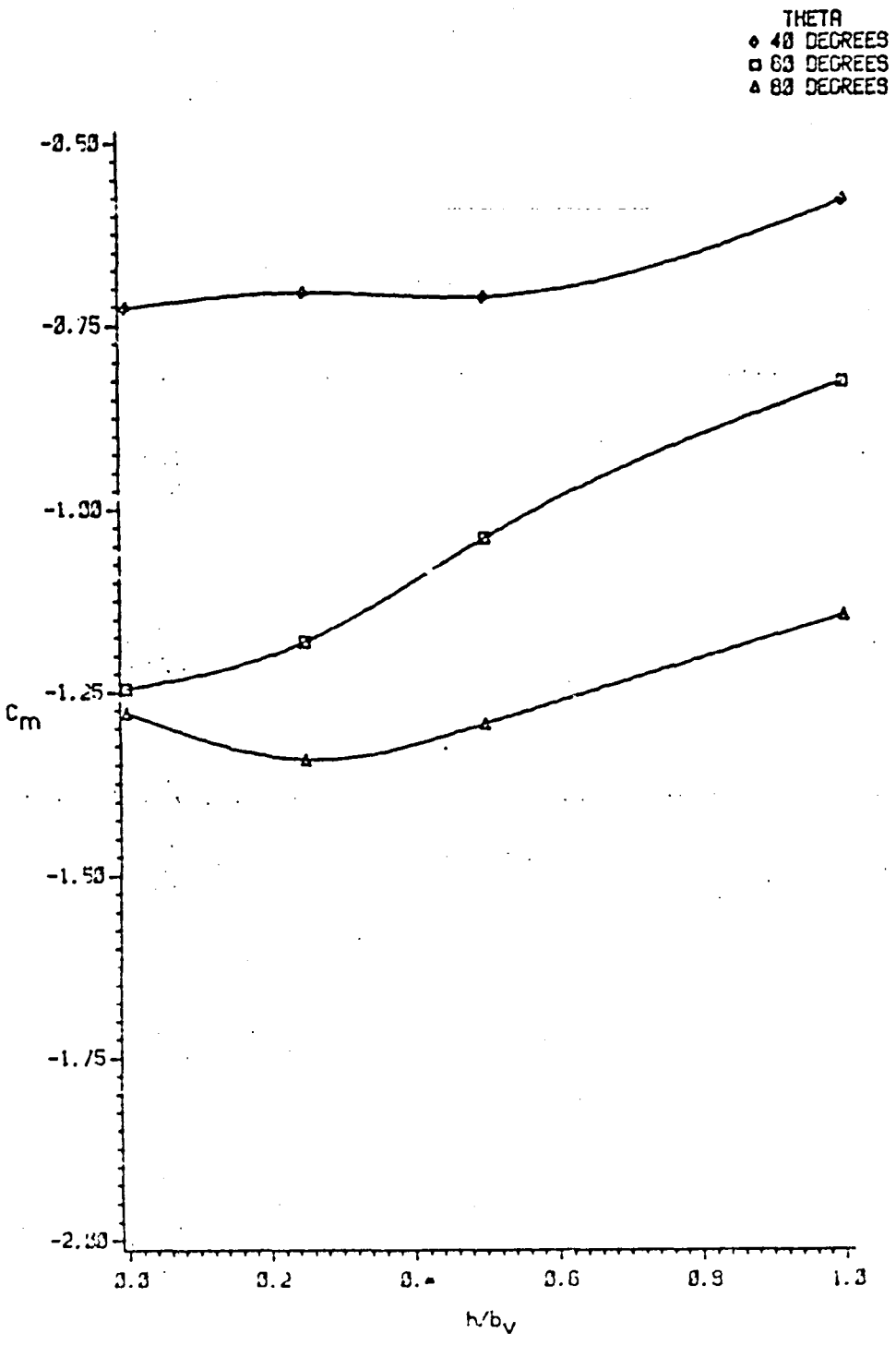

Figure 4-9. Pitching Moment as a Function of Vertical Position of Horizontal Tail, $\bar{\omega}$ = .7

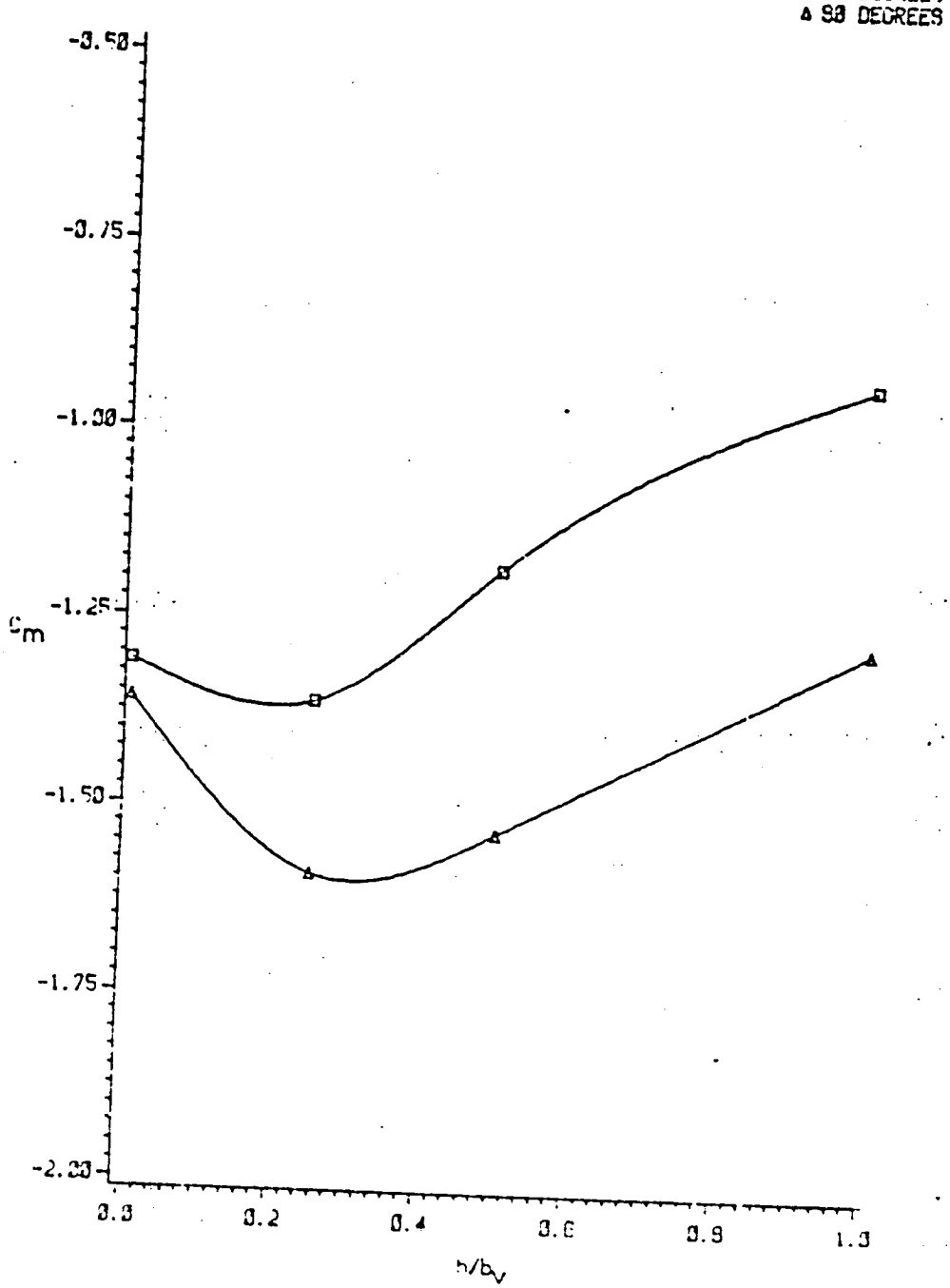

Figure 4-10. Pitching Moment as a Function of Vertical Position of Horizontal Tail, $\bar{\omega}$ = .9

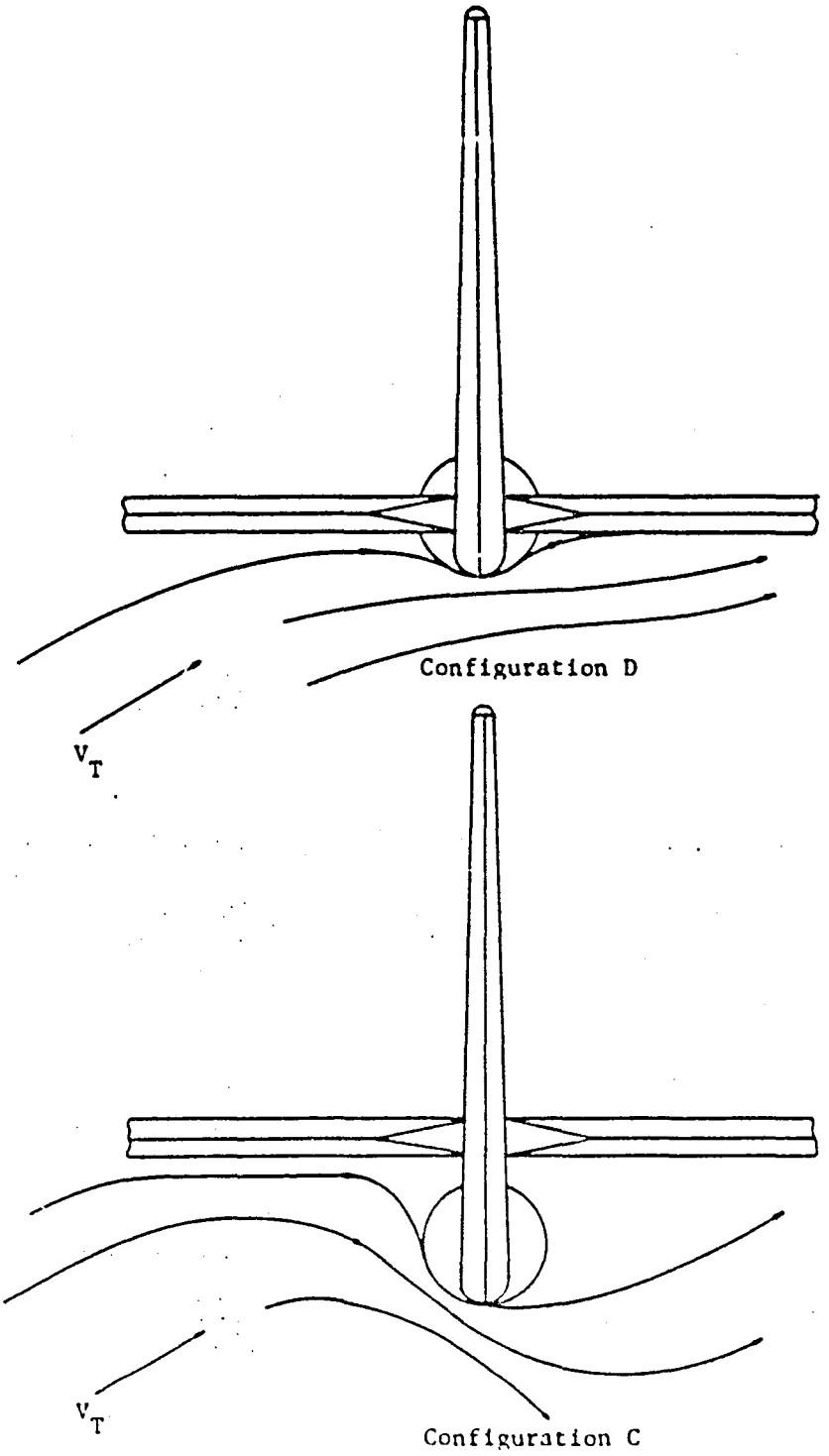

Figure 4-11. Flow About Configurations C and D at High Spin Rate

S-shaped curve at low spin rates. Horizontal tail blanketing effects described earlier result in a positive slope, and forward fuselage wake interaction lowers the overall pitching moment at an h/b_v value of 0.25. At higher values of h/b_v, the horizontal tail is clear of the fuselage wake.

Variation of h/b_v has a substantial effect on yawing moment, as indicated in Figures 4-12 through 4-15. The T-tail provides by far the greatest side forces in all cases, while at moderate spin rates, the autorotative effect of the horizontal tail actually provides a propelling yawing moment. Because of differences in horizontal tail planform and area, this effect is not seen in the NASA test data for the steep spin case (Figure 4-16). In fact, variation of horizontal tail height showed little effect on yawing moment in NASA steep spin data. It is suspected that lower aft fuselage shape has a substantial effect on the autorotative force created by the horizontal tail at low values of h/b_v. Further testing in this area would be helpful.

A flat spin yawing moment comparison is shown in Figure 4-17. Despite differing horizontal tail planforms, spin velocities, and fuselage effects, similar trends are indicated in both tests at lower pitch angles. Again, the autorotative component of side force is present, notably at a pitch angle of 60°. At low h/b_v and high values, however, the correlation breaks down. This may be caused by differing horizontal tail planforms; at high pitch angles, vertical tail blanketing is large for the low aspect ratio NASA horizontal tail. It must also be noted that fuselage effects were not subtracted out of the NASA data.

Analytical prediction of the effect of horizontal tail vertical

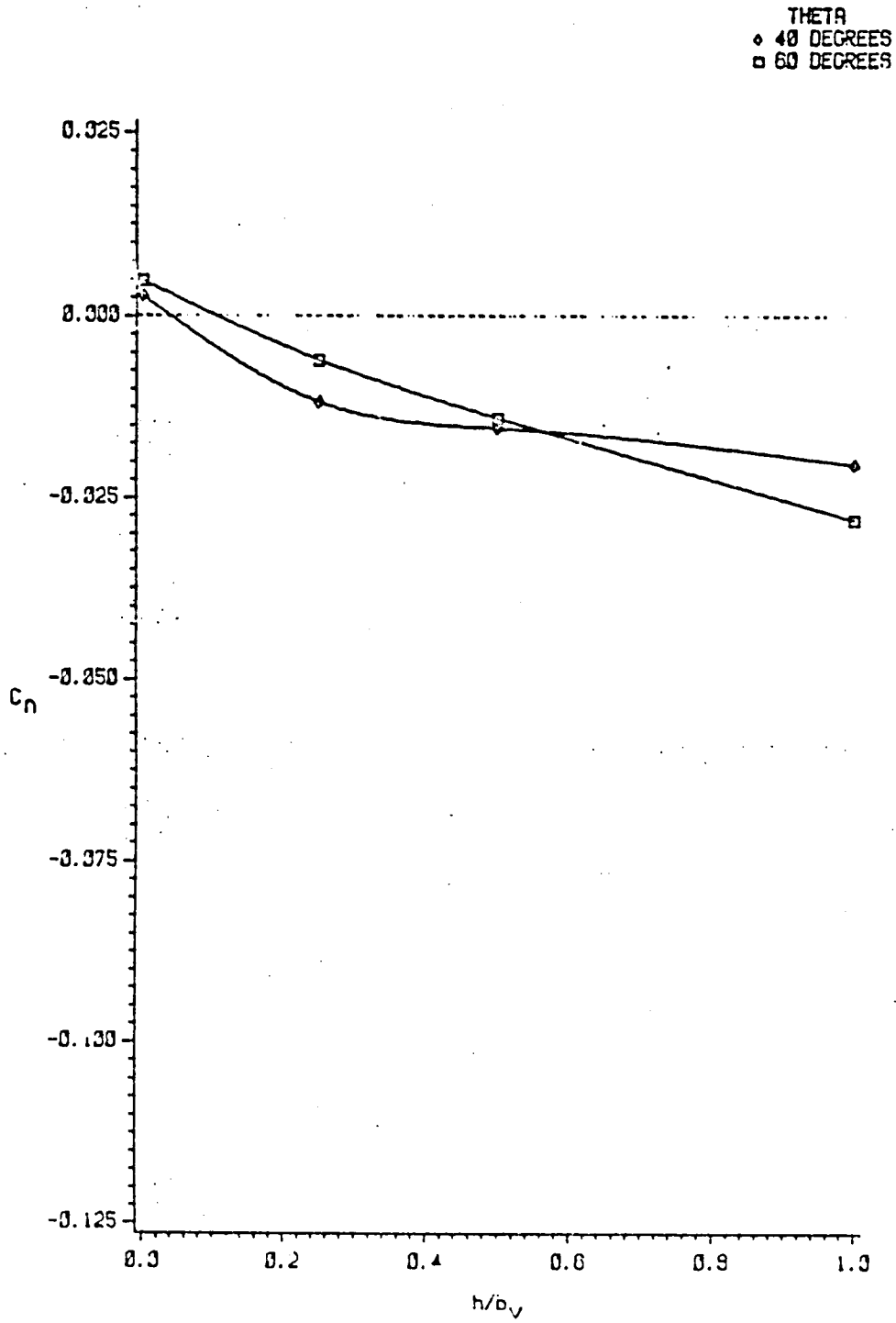

Figure 4-12. Yawing Moment as a Function of Vertical Position of Horizontal Tail, $\bar{\omega}$ = .3

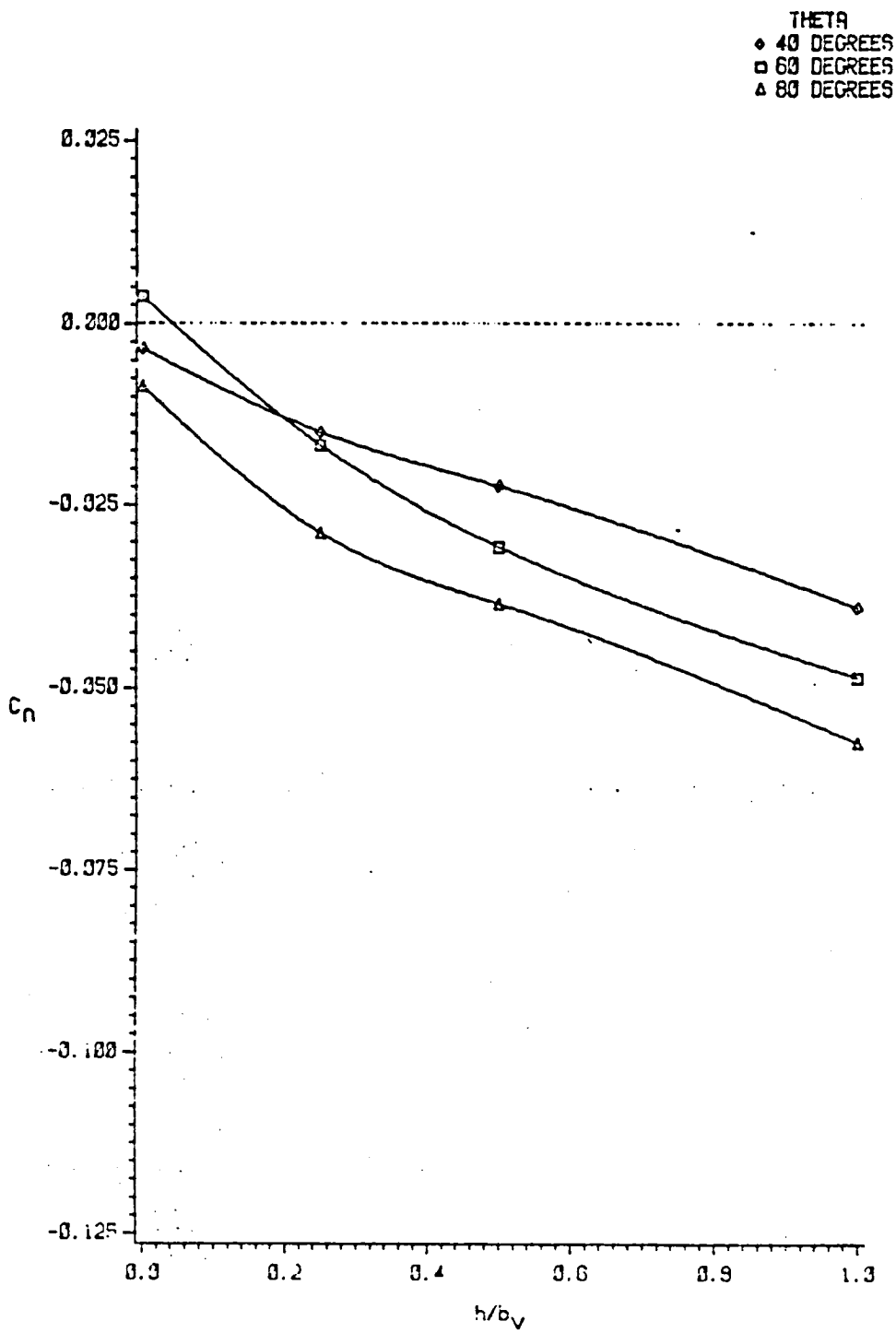

Figure 4-13. Yawing Moment as a Function of Vertical Position of Horizontal Tail, $\bar{\omega}$ = .5

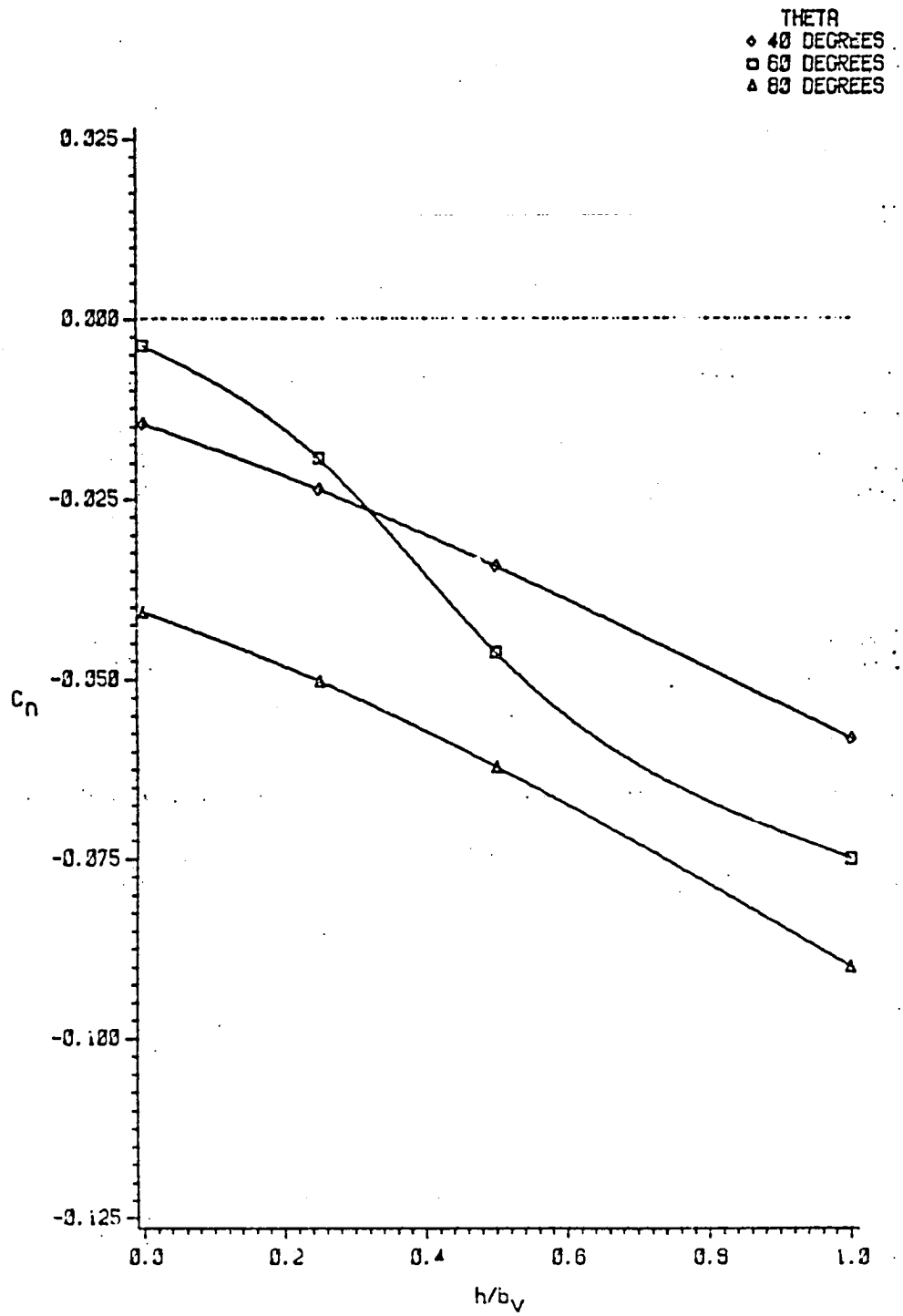

Figure 4-14. Yawing Moment as a Function of Vertical Position of Horizontal Tail, $\bar{\omega}$ = .7

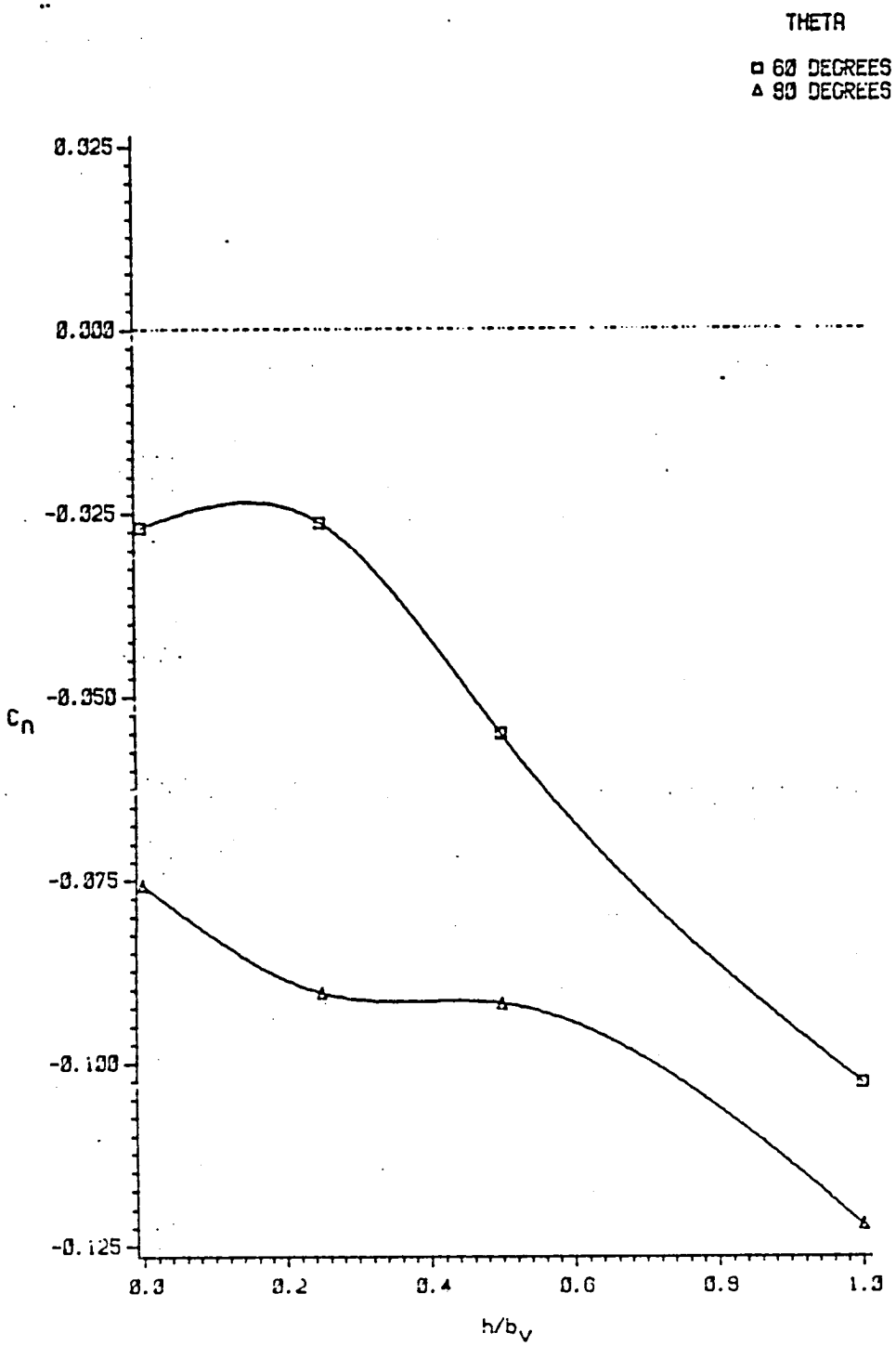

Figure 4-15. Yawing Moment as a Function of Vertical Position of Horizontal Tail, $\bar{\omega}$ = .9

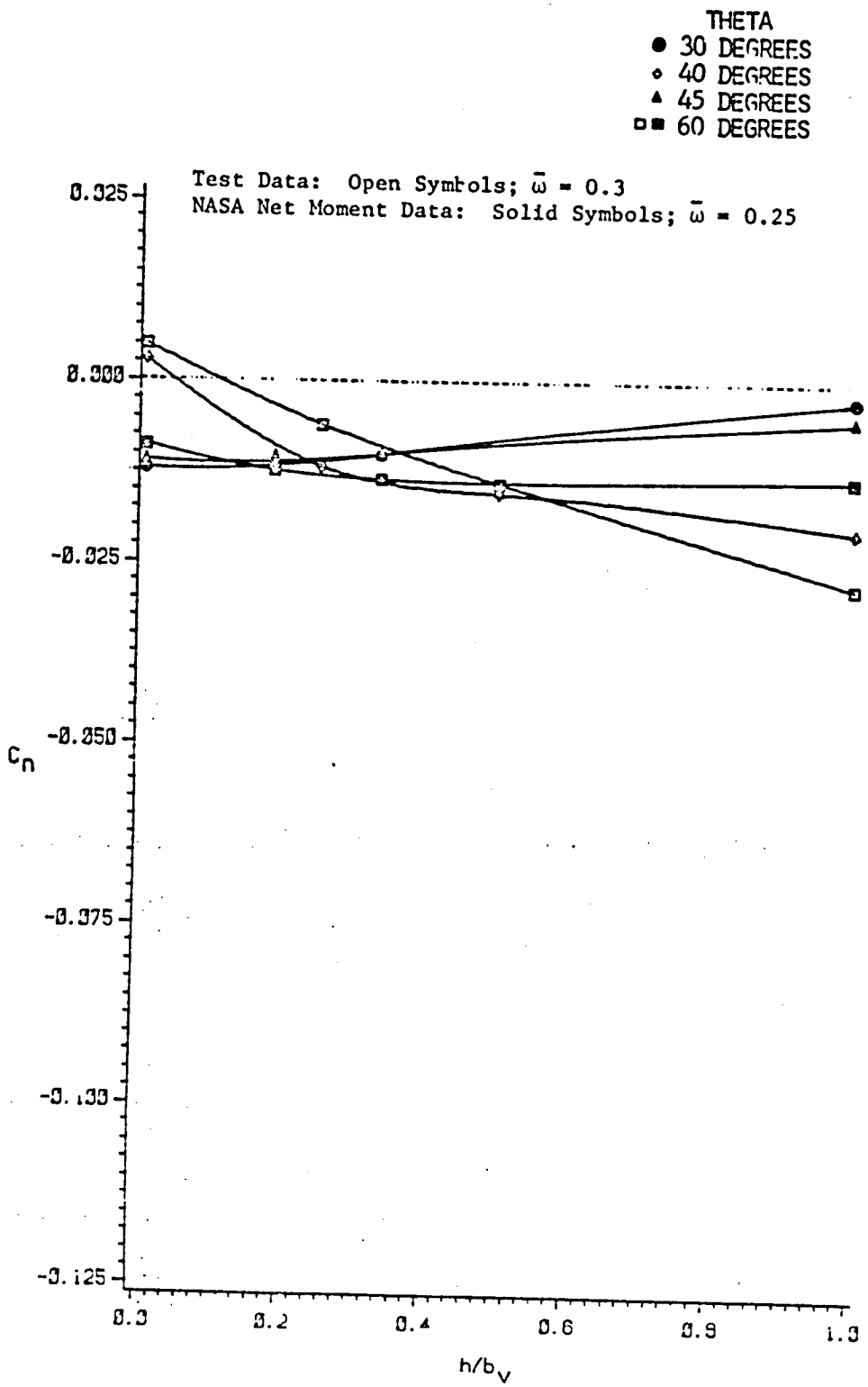

Figure 4-16. Yawing Moment as a Function of Horizontal Tail Vertical Position

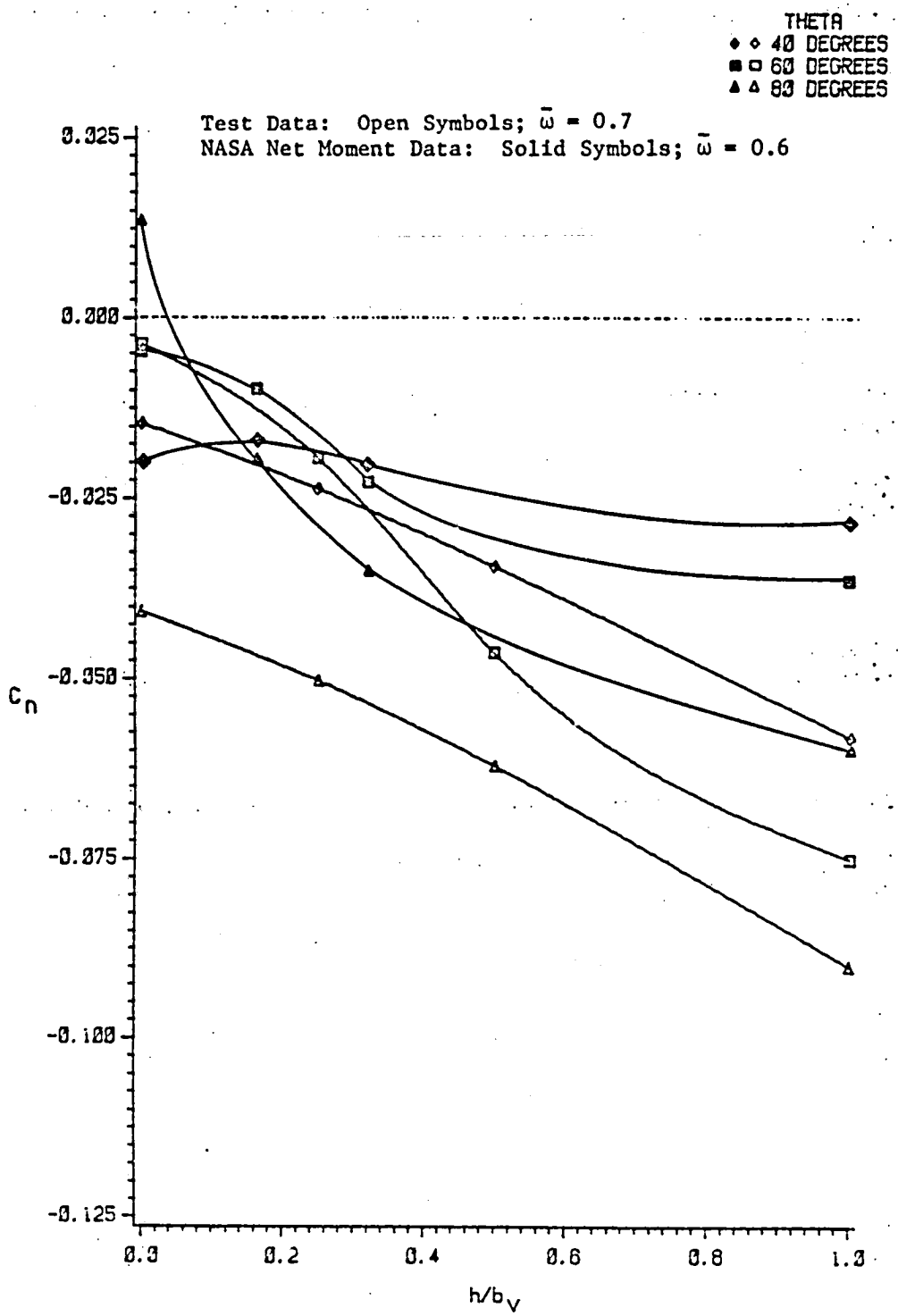

Figure 4-17. Yawing Moment as a Function of Horizontal Tail Vertical Position for a Flat Spin

position has not previously met with success because of the need for isolated tail side force data for comparison. McCormick (1979) investigated the simple relation presented below, which is further examined using side force data from the present testing.

If the local difference in pressure coefficient along the vertical tail is assumed to be a function of the distance down from the horizontal tail relative to h, then side force can be expressed as

$$F_s = \frac{1}{2} \rho V^2 \frac{S_v}{b_v} \int_o^h C_p \left(\frac{z}{h}\right) dz$$

where z is defined as the vertical distance from the given vertical tail location to the fuselage reference line. The above equation may be simplified to

$$F_s = \frac{1}{2} \rho V^2 S_v \left(\frac{h}{b_v}\right) \int_o^1 C_p (x) dx .$$

Ignoring interference and vertical tail planform effects, let

$$\int_o^1 C_p (x) dx = K$$

Since

$$C_{F_s} = \frac{F_s}{1/2 \rho V^2 S_h}$$

$$C_{F_s} = \frac{S_v}{S_h} \frac{h}{b_v} K$$

or

$$K = C_{F_s} \frac{S_h}{S_v} \frac{b_v}{h} .$$

A plot of K versus horizontal tail vertical position is shown in Figure 4-18 for $\bar{\omega}$ equal to 0.5. Curves for other spin rates displayed similar characteristics. The results show that K cannot be considered a constant for any position of the horizontal tail. In addition to interference effects from the fuselage, the horizontal tail may create a high dynamic pressure on the vertical tail area immediately below it. This high pressure region may be independent of horizontal tail vertical position, making K strongly dependent on both h/b_v and vertical tail planform.

It is evident from model and full-scale flight testing that the highest value of h/b_v possible is favorable for spin safety. In fact, test tail 5 (h/b_v equal to 1.0) did not have a flat spin mode. This suggests that increasing yaw damping to prevent equilibrium is more effective than increasing the nose-down pitching moment, and that the pitching penalty paid for increasing h/b_v is minor compared to the advantages of increased yaw damping.

Effects of Vertical Tail Aspect Ratio

The change in C_m with a change in vertical tail aspect ratio is small, as shown in Figures 4-19 through 4-22. The differences seen in some curves are believed to be the result of experimental scatter or minor interference effects.

Yawing moment effects are more noticeable. At $\bar{\omega}$ equal to 0.3

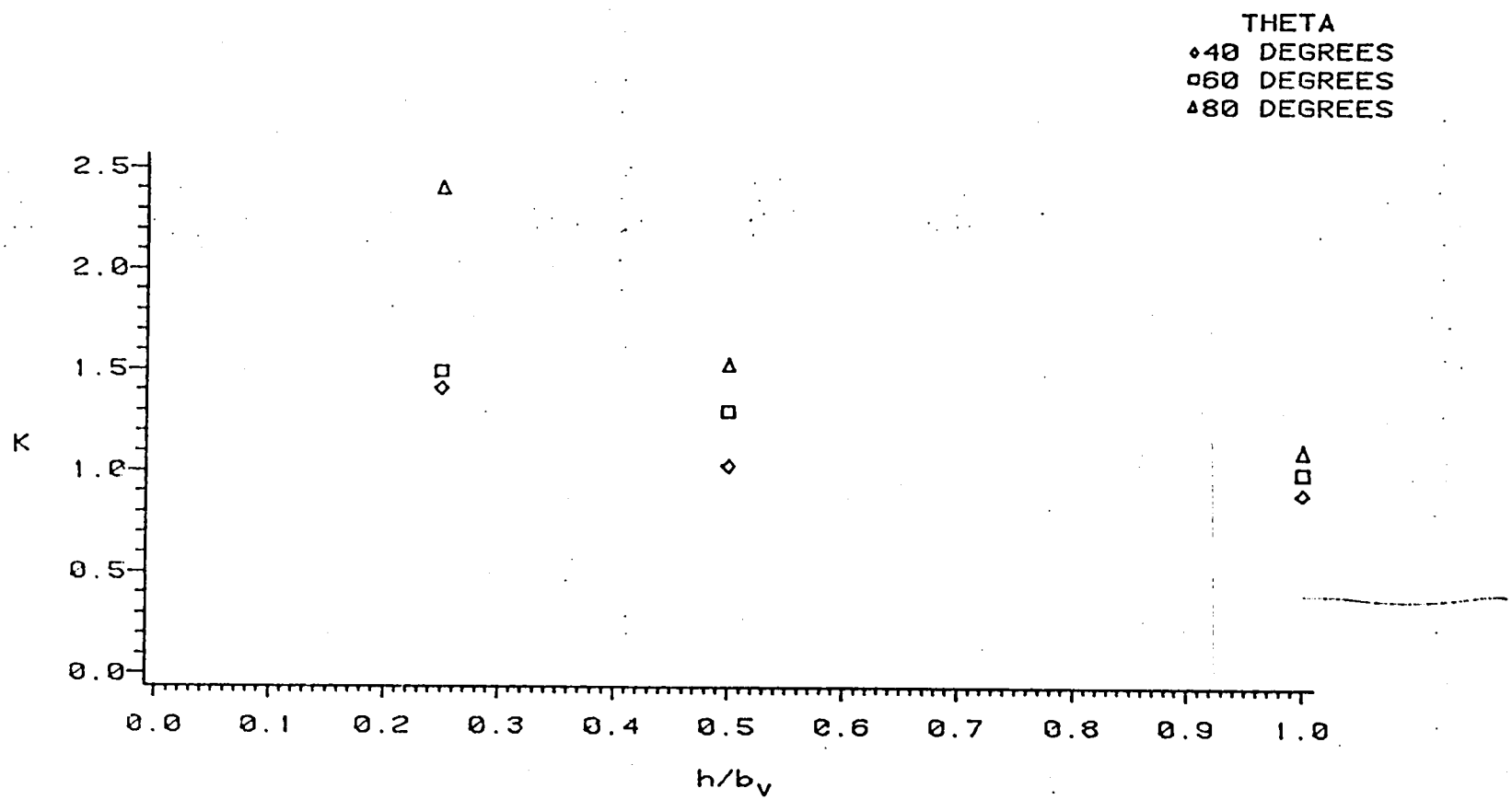

Figure 4-18. K as a Function of Vertical Position of Horizontal Tail, $\bar{\omega}$ = .5

(Figure 4-23), lines of constant θ are seen to cross at a value of AR_V equal to 1.45. Vertical tail area above the horizontal tail apparently causes larger yawing moments at the lower theta value. One possible explanation is that unblanketed area in this region decreases with increasing theta, rather than increasing, as it would at high spin rates when transverse flow becomes large (see Figure 4-27). Test results from the T-tail configuration, which does not show the effect, substantiate this conclusion. The yaw damping effectiveness of the vertical tail at low pitch angles is another possible factor. At low values of θ, the angle of attack as seen by the vertical tail is small. Because the two-dimensional normal force curve reaches a local maximum immediately before stall, such low angles of attack may produce a larger normal force on the exposed part of the vertical tail.

To investigate the phenomenon more closely, the body-fixed sideslip angle seen by the vertical tail, β_V, was determined for each orientation (see Figure 4-28). The vertical tail normal force was then plotted as a function of β_V for the baseline configuration as shown in Figure 4-29. Because of the lack of experimental data between β_V values of 0 and 17°, it is difficult to determine the influence of the unstalled part of the curve. The figure does indicate, however, that there is a strong pitch angle influence on yaw damping force, with lower pitch angles providing higher forces. This result suggests that tail geometry, and not stalling angle of attack, is the more influential factor. Note that lines of constant $\bar{\omega}$ are nearly linear, increasing in slope with increasing magnitude of spin rate. It can be seen that the curve corresponding to an $\bar{\omega}$ of 0.3 has a slightly negative slope, giving rise to the intersecting curves of Figure 4-23.

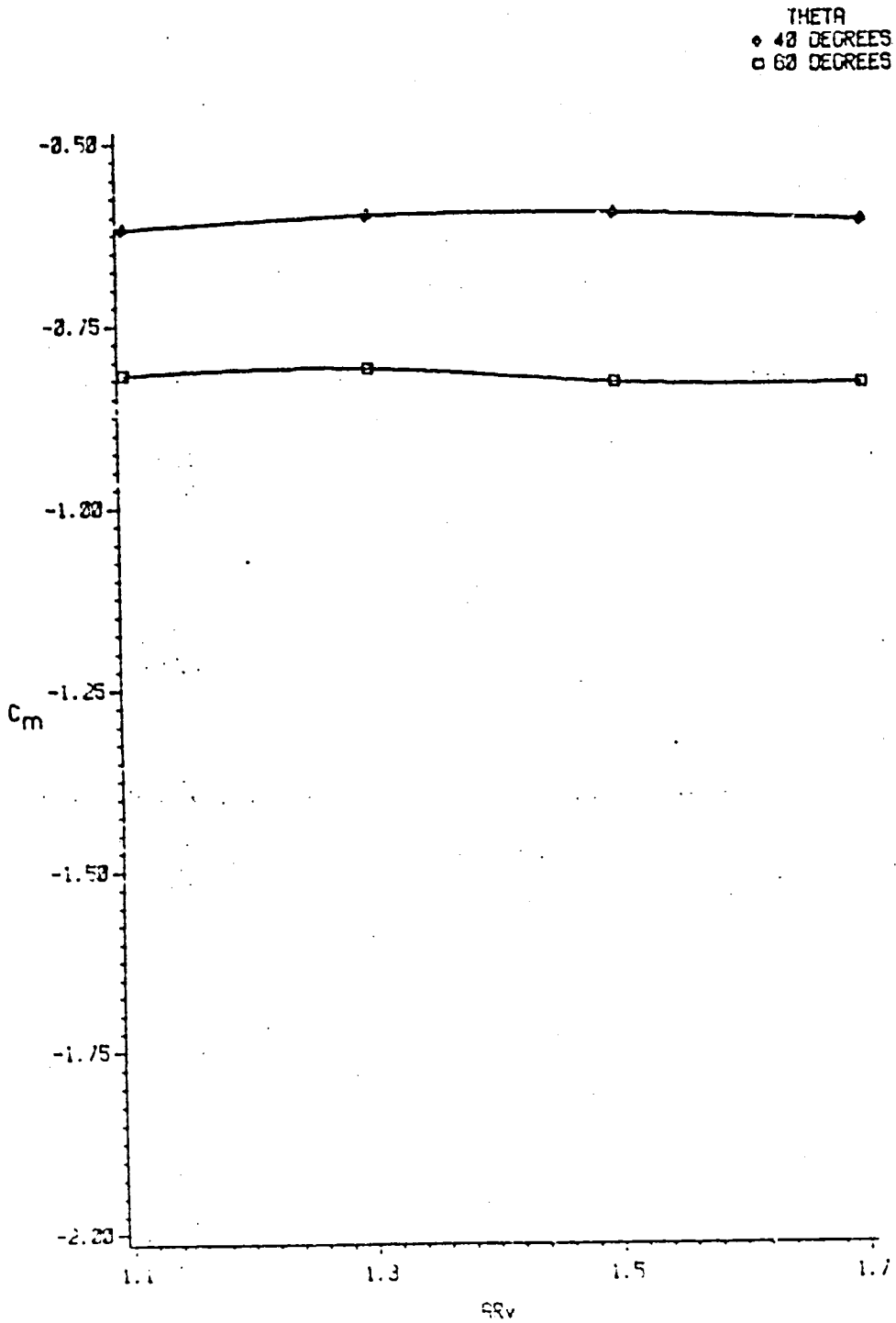

Figure 4-19. Pitching Moment as a Function of Vertical Tail Aspect Ratio, $\bar{a}$ = .3

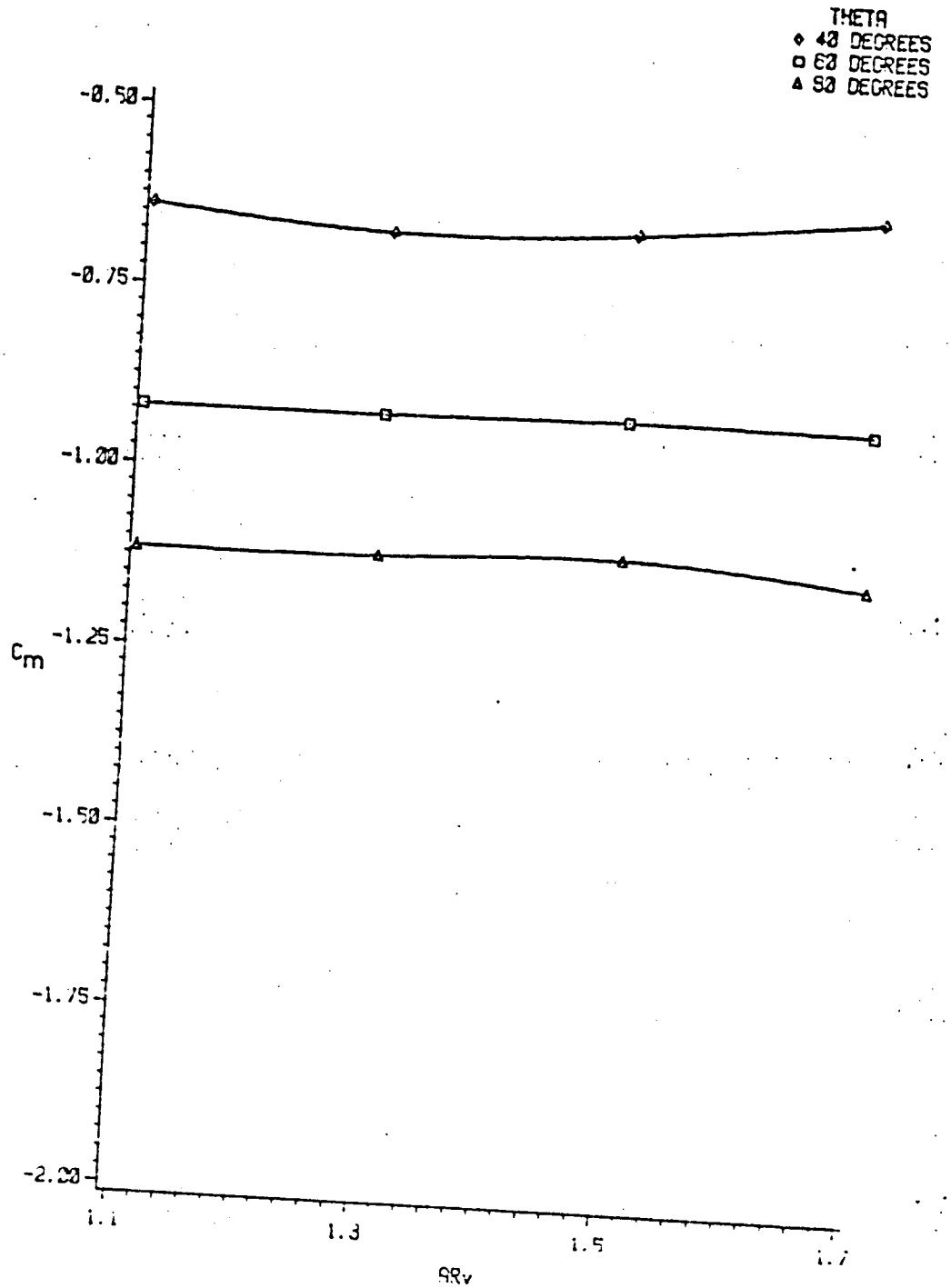

Figure 4-20. Pitching Moment as a Function of Vertical Tail Aspect Ratio, $\bar{\omega}$ = .5

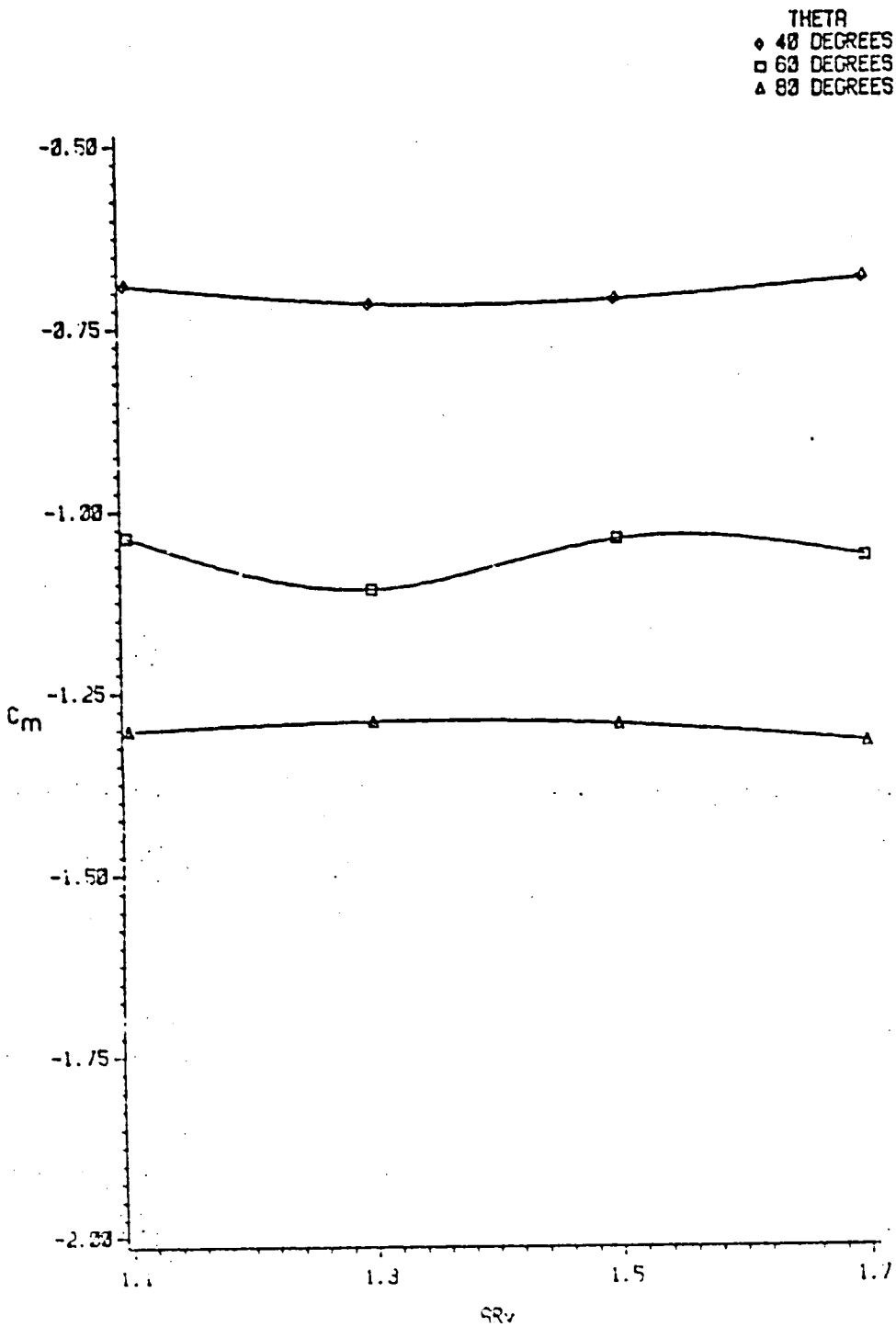

Figure 4-21. Pitching Moment as a Function of Vertical Tail Aspect Ratio, $\bar{\omega}$ = .7

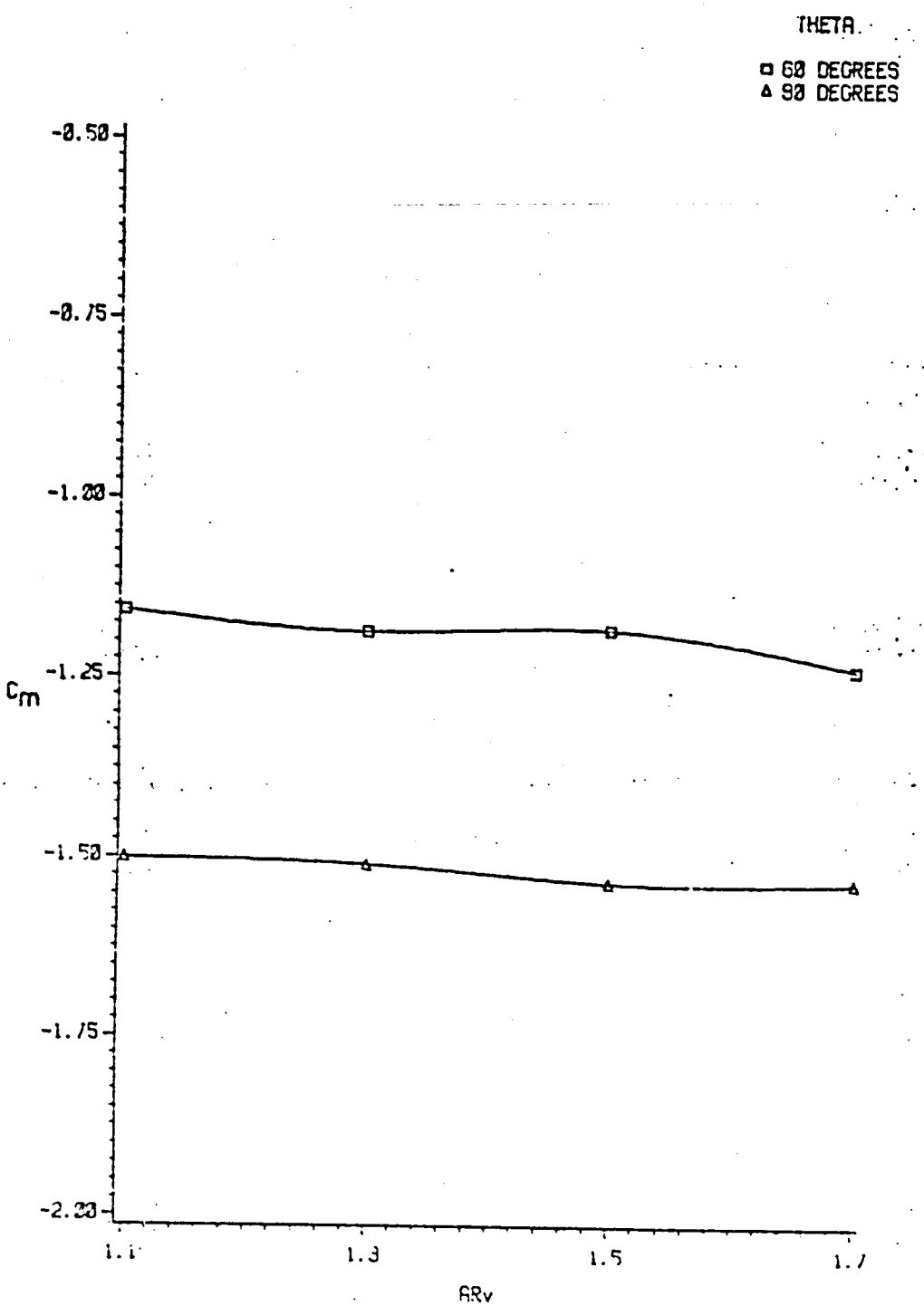

Figure 4-22. Pitching Moment as a Function of Vertical Tail Aspect Ratio, $\bar{\omega}$ = .9

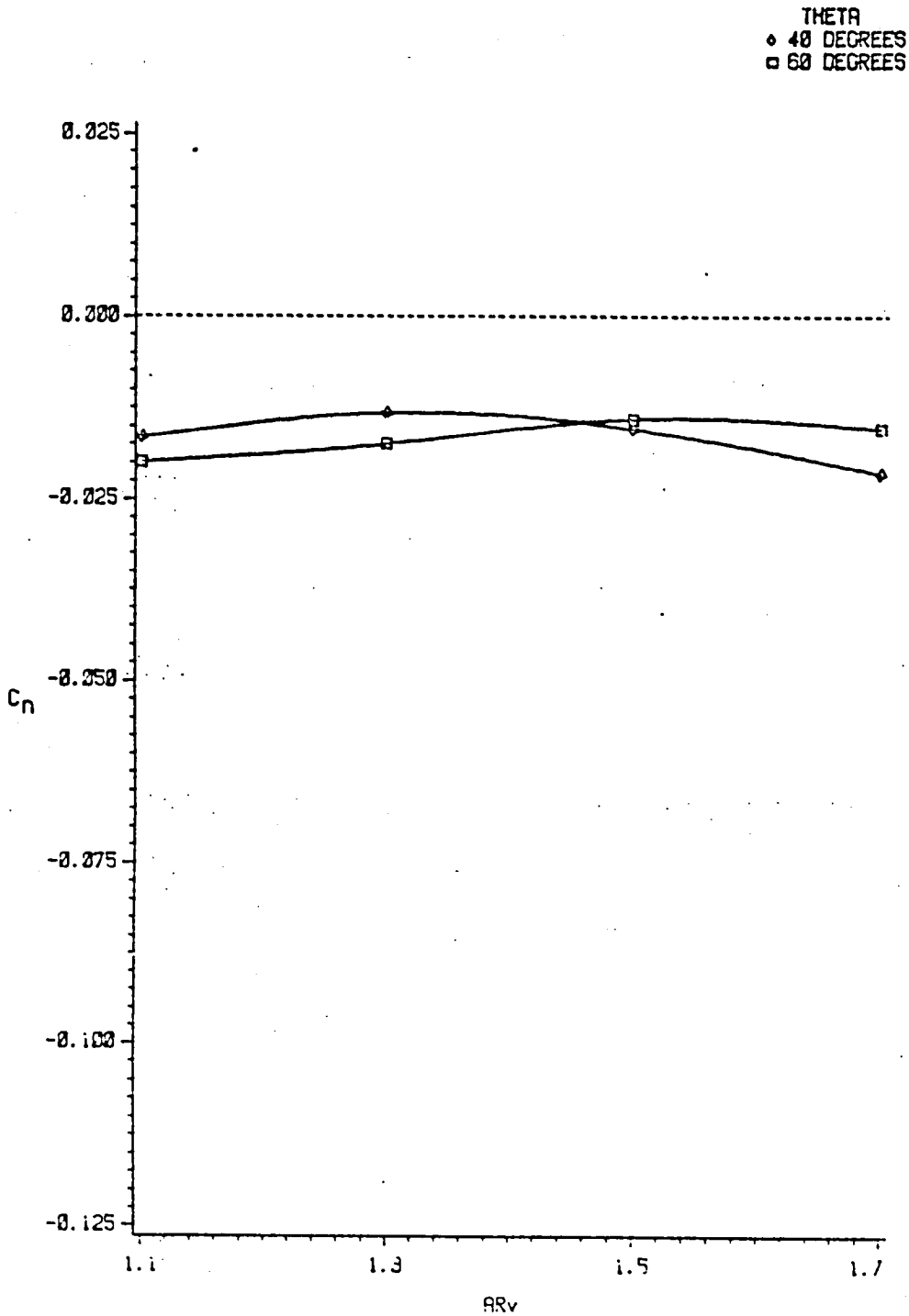

Figure 4-23. Yawing Moment as a Function of Vertical Tail Aspect Ratio, $\bar{\omega}$ = .3

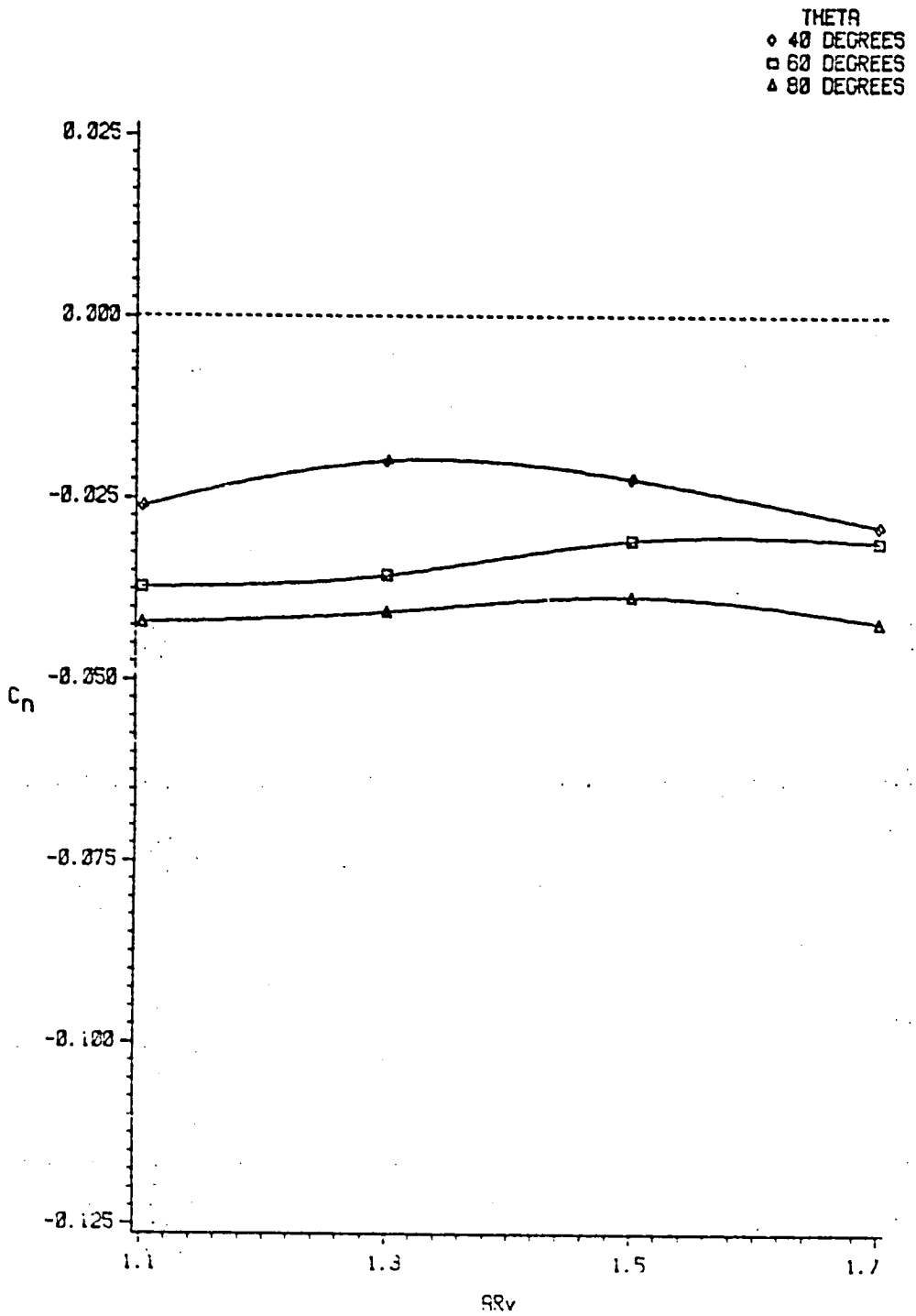

Figure 4-24. Yawing Moment as a Function of Vertical Tail Aspect Ratio, $\bar{\omega}$ = .5

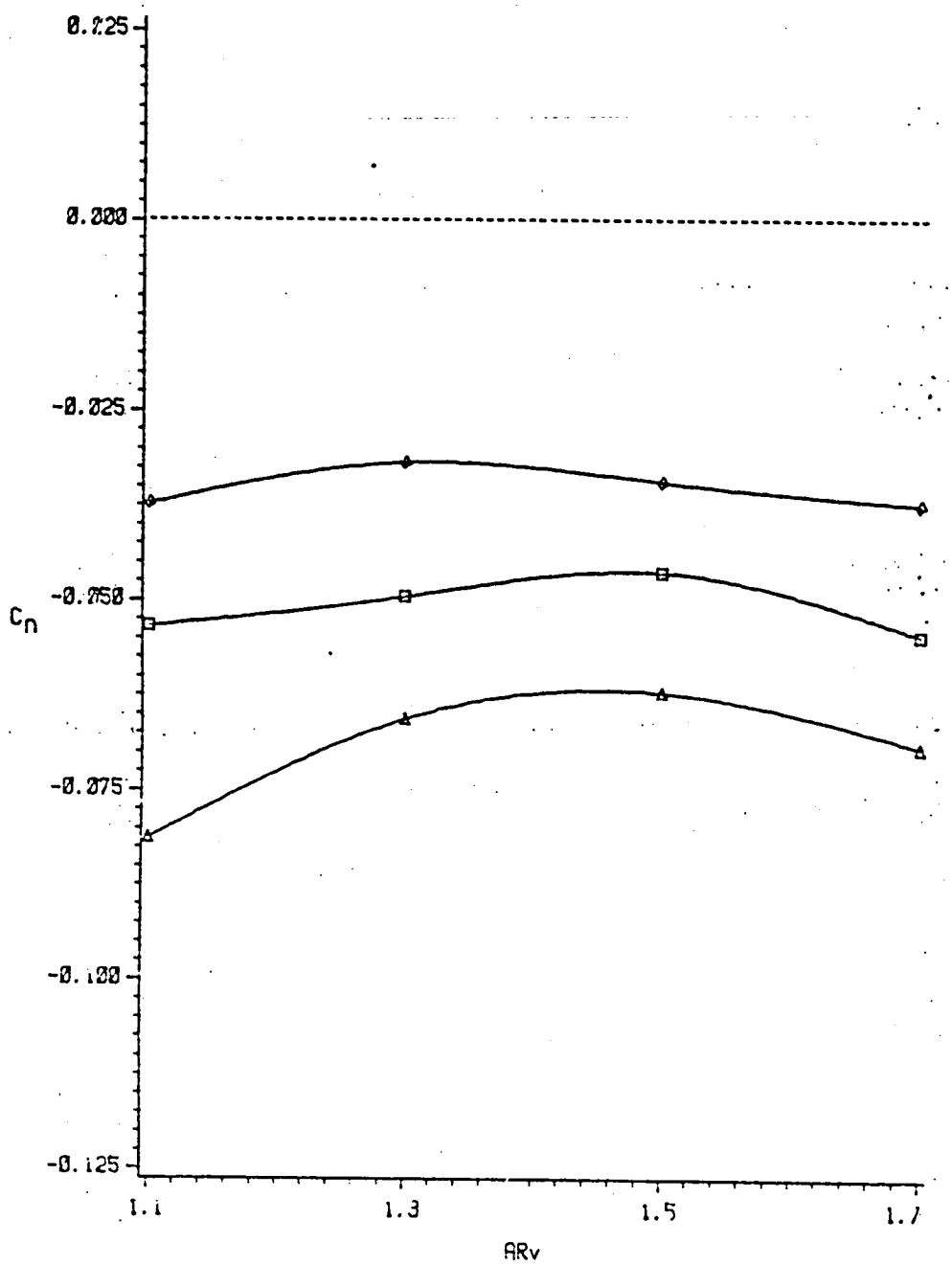

Figure 4-25. Yawing Moment as a Function of Vertical Tail Aspect Ratio, $\bar{\omega}$ = .7

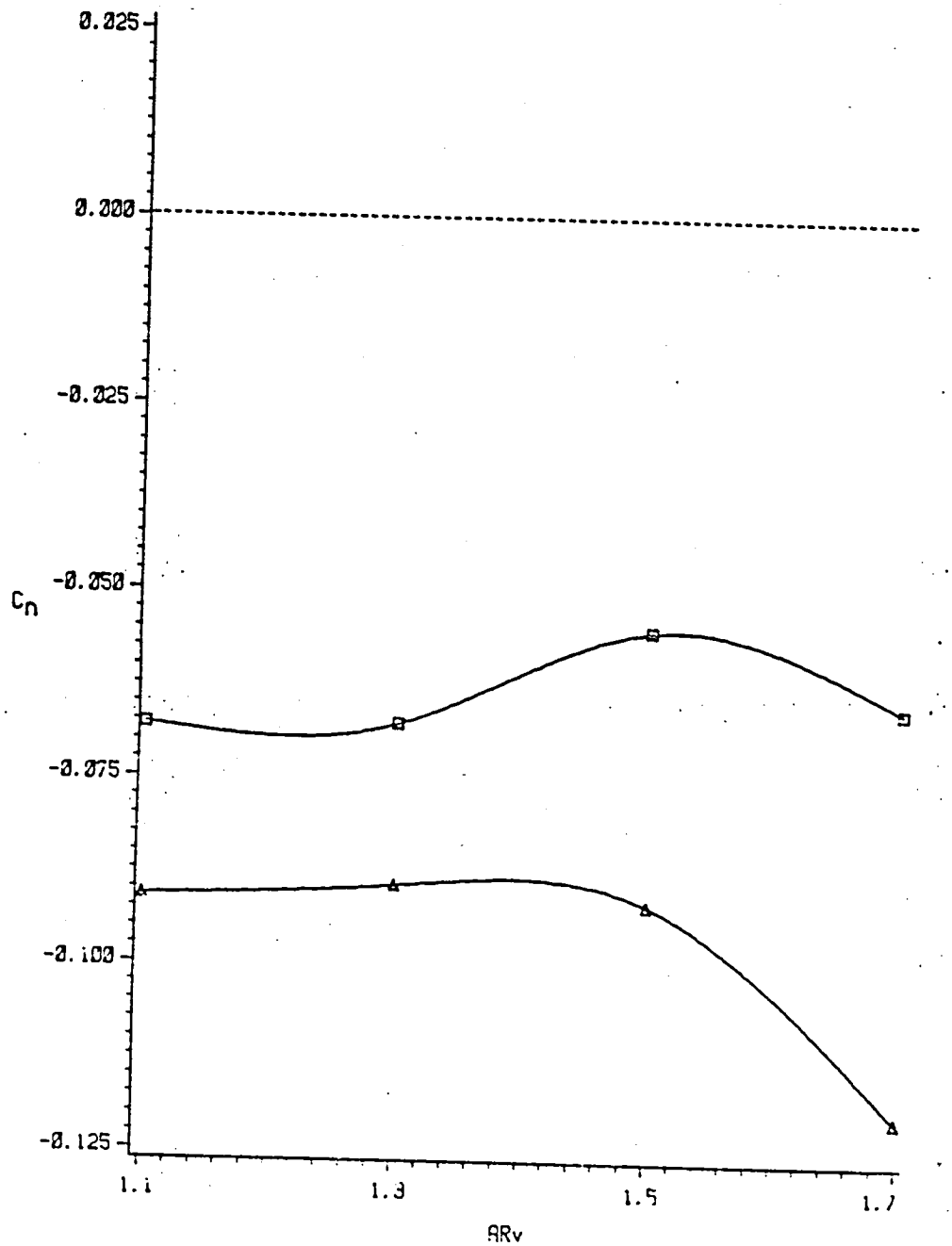

Figure 4-26. Yawing Moment as a Function of Vertical Tail Aspect Ratio, $\bar{\omega}$ = .9

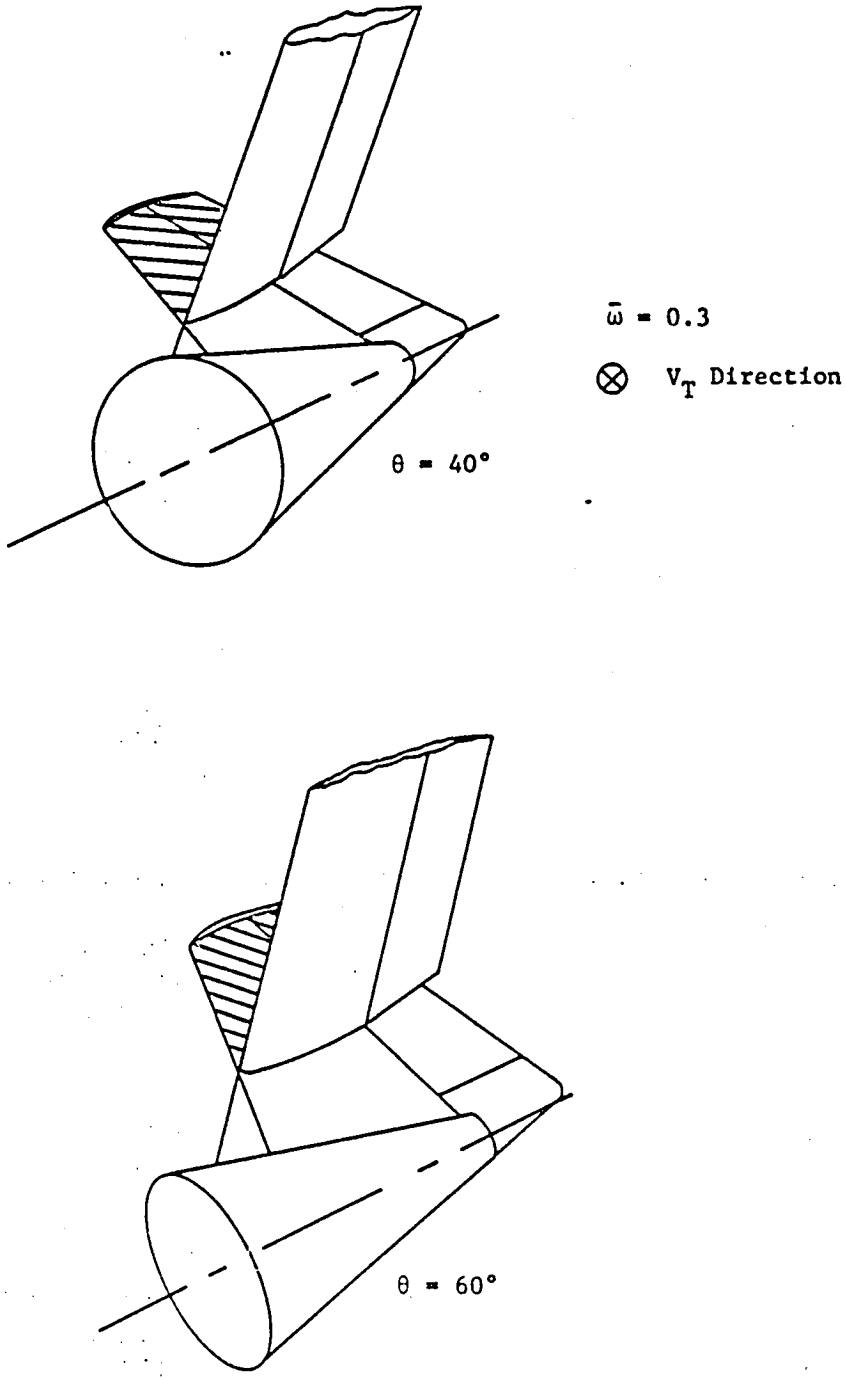

Figure 4-27. Effect of θ and α_v on Unblanketed Vertical Tail Area at Low Spin Rates

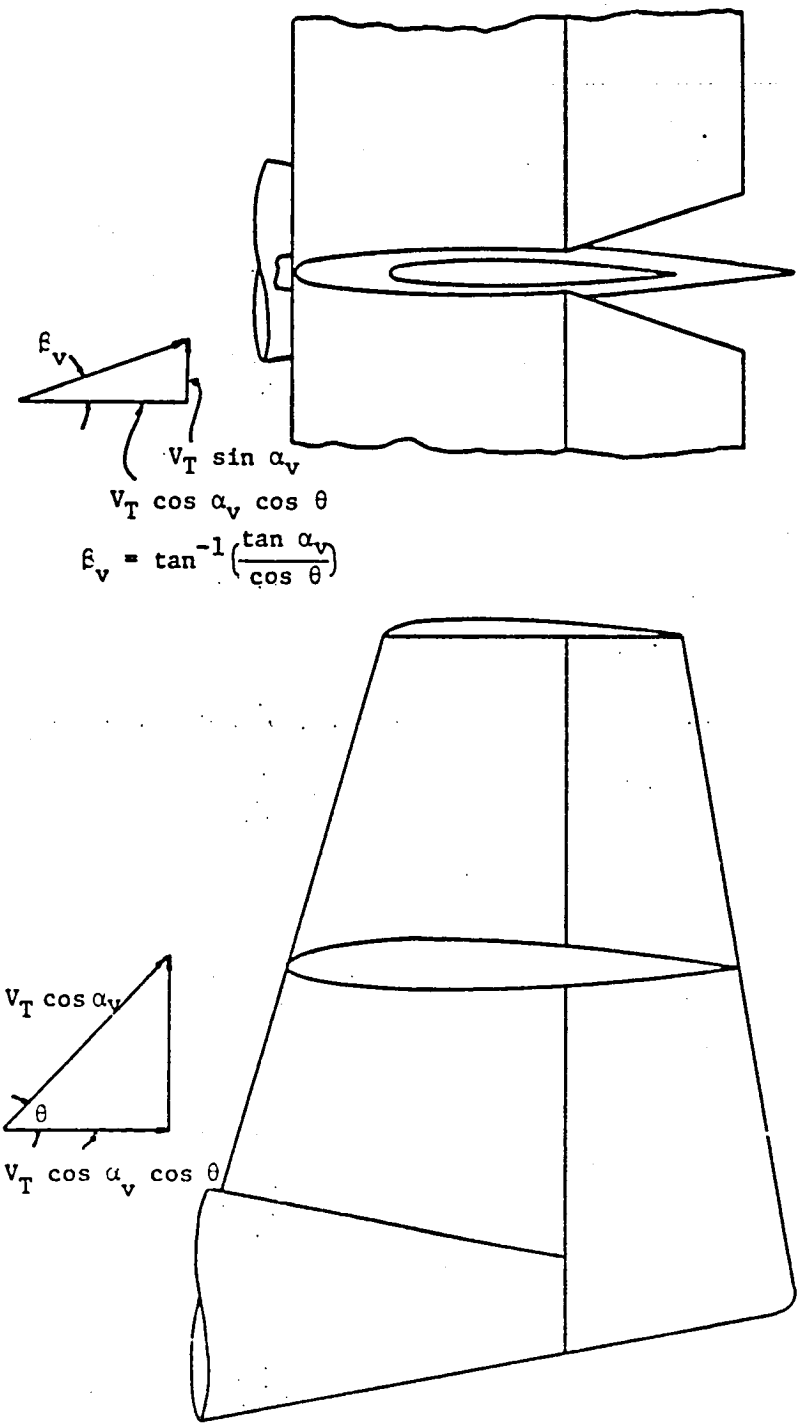

Figure 4-28. Definition of Sideslip Angle

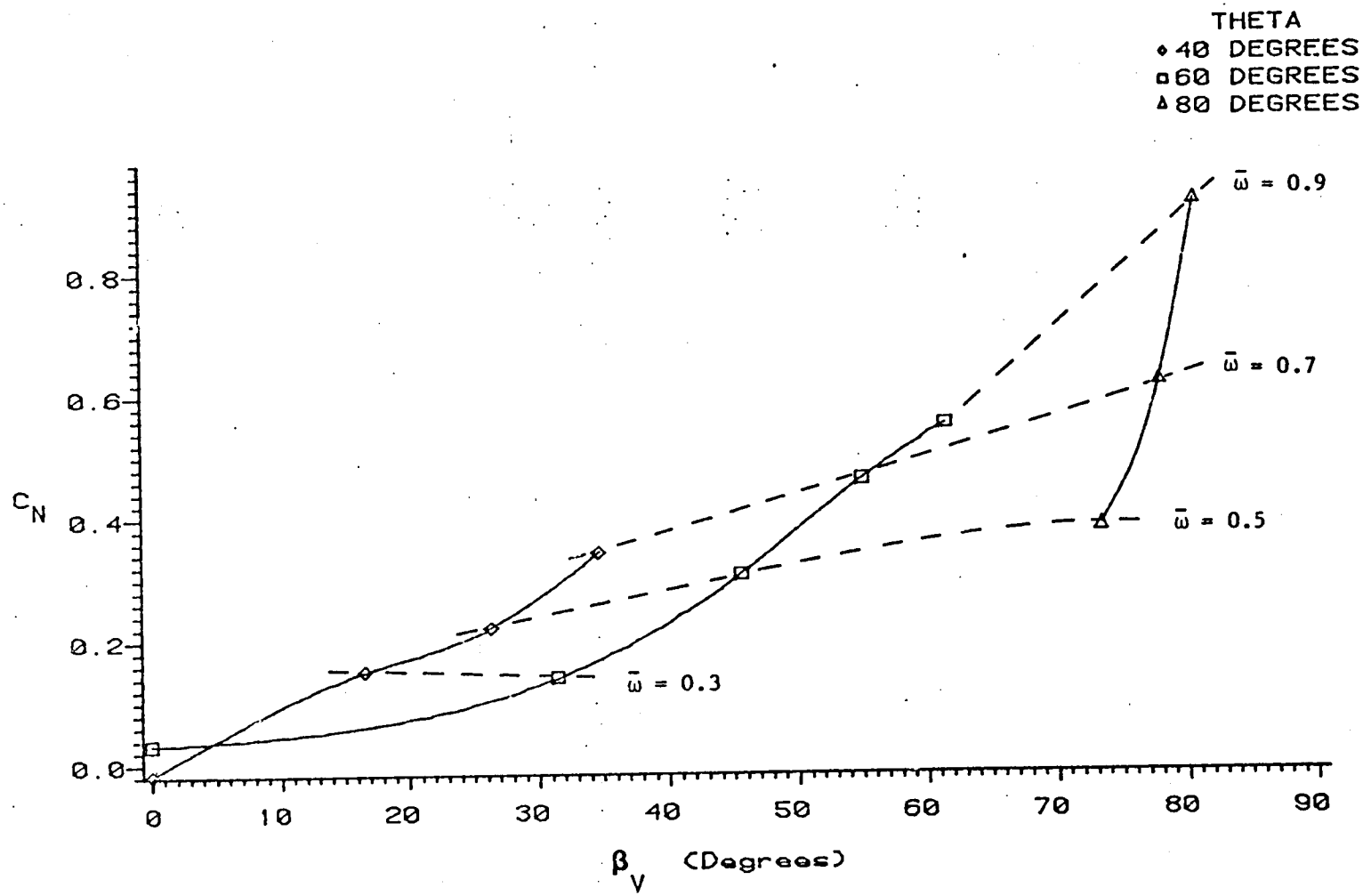

Figure 4-29. Vertical Tail Normal Force as a Function of Sideslip Angle, Configuration A

At larger values of $\bar{\omega}$, the low vertical tail aspect ratio surprisingly results in greater yawing moments than intermediate values of AR_v, as shown in Figures 4-24 through 4-26. For each vertical tail, the horizontal tail height above the fuselage centerline, h, was constant. This was done to prevent h/b_v effects from dominating the results. The configurations were nearly identical below the horizontal tail level. The unexpected result must therefore again be related to interference effects of the vertical tail area above the horizontal tail.

At high spin rates, the beneficial effect of a low aspect ratio disappears because the high aspect ratio vertical tails are not totally blanketed by the stalled air cavity above the horizontal tail. This phenomenon leaves the tail designer with the dilemma of choosing between satisfactory steep spin or flat spin characteristics. Fortunately, increasing exposed area under the horizontal stabilizer can provide satisfactory characteristics for both spin modes.

Effects of Horizontal Tail Aspect Ratio

The horizontal tail aspect ratio plays a small part in the overall pitching moment contribution of the tail. As seen in Figures 4-30 through 4-34, C_m is greatest in magnitude at the lowest aspect ratio, AR_h equal to 3.48, and it decreases with increasing AR_h. Although all horizontal tails tested were designed to possess identical lift effectiveness at small angles of attack, they obviously do not possess similar lift characteristics in stall. The results show that it benefits the designer to employ a lower aspect ratio, lower efficiency horizontal tail for spin safety. At high spin rates, however, fuselage

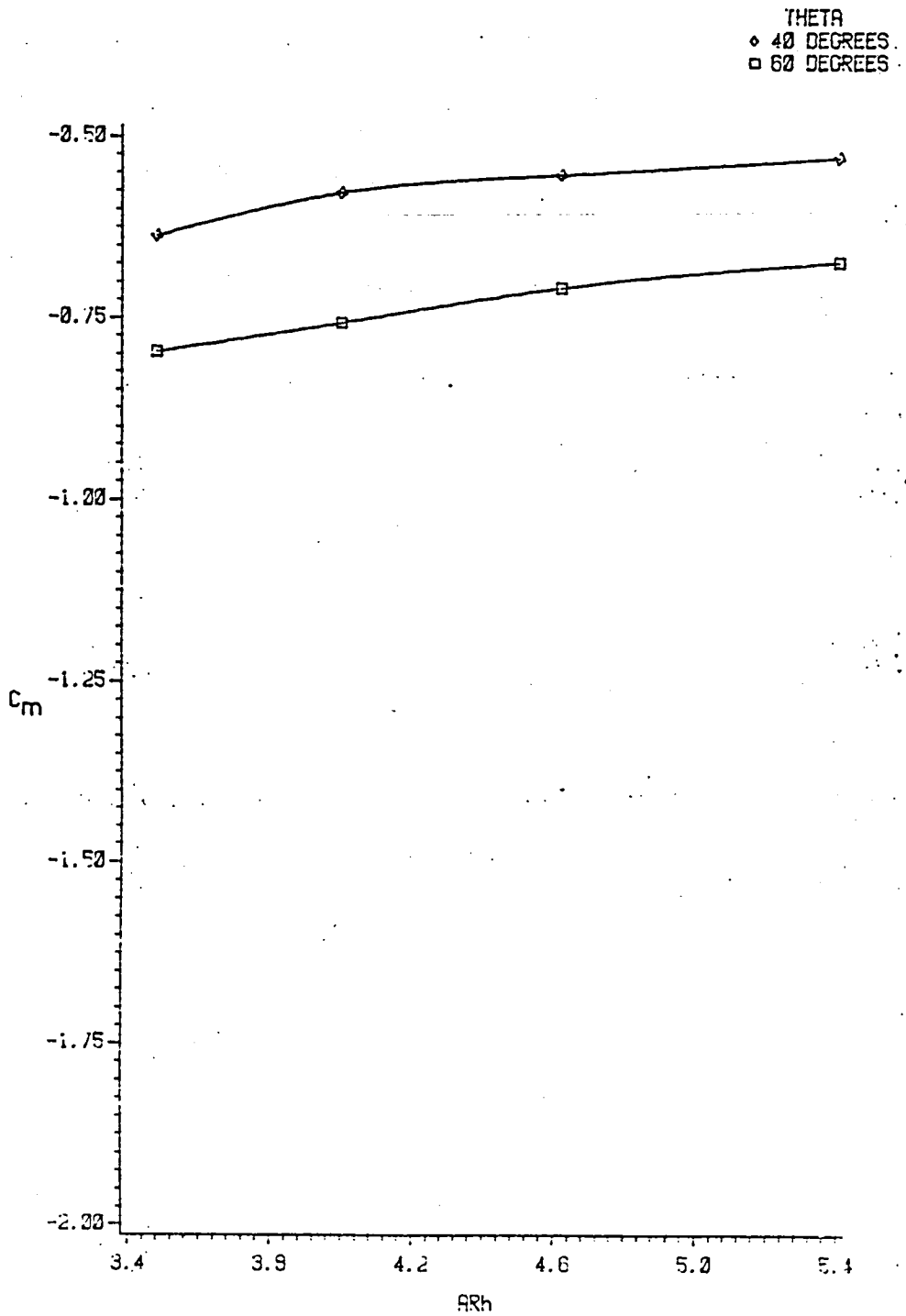

Figure 4-30. Pitching Moment as a Function of Horizontal Tail Aspect Ratio, $\bar{\omega} = 0$

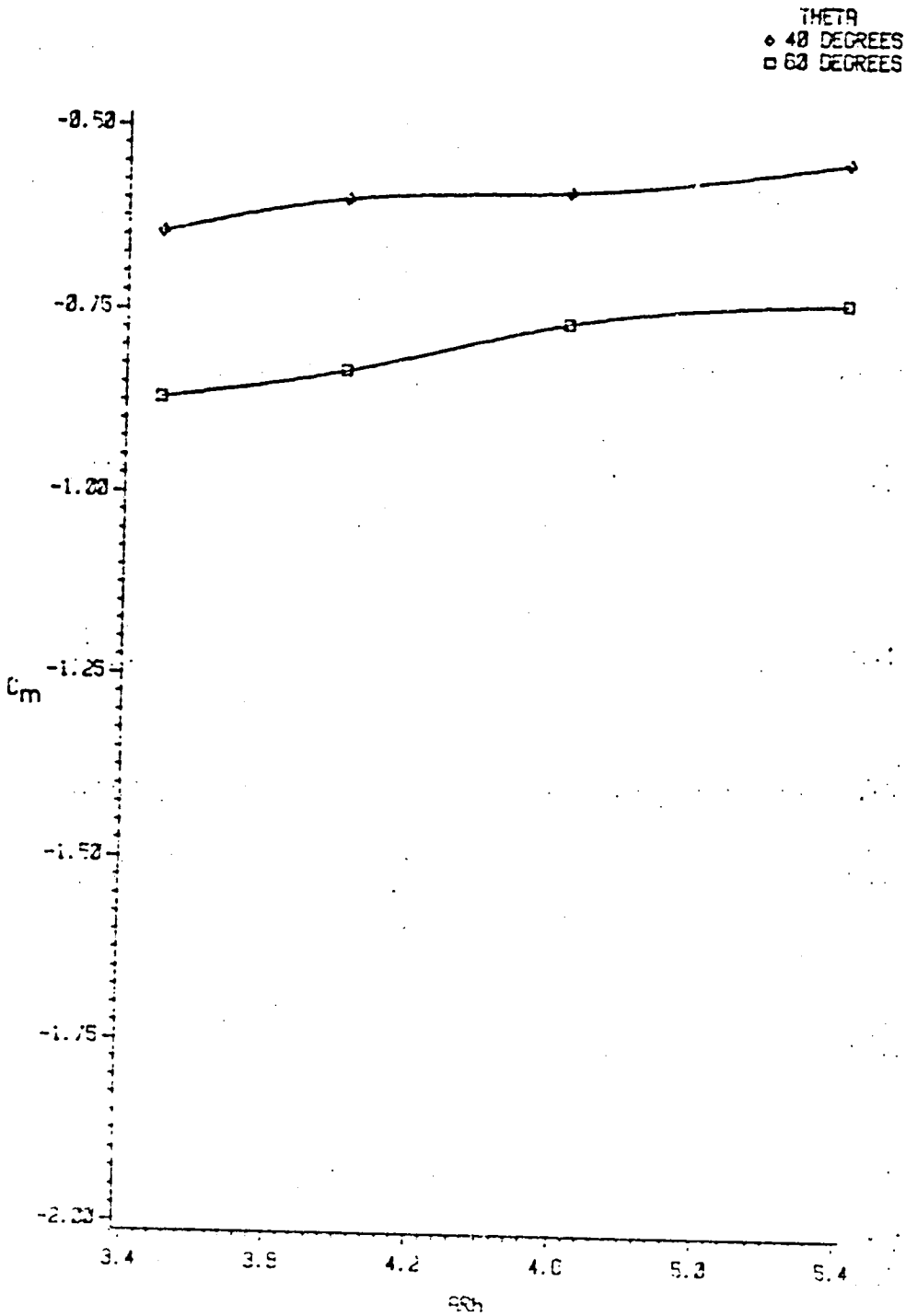

Figure 4-31. Pitching Moment as a Function of Horizontal Tail Aspect Ratio, $\bar{a}$ = .3

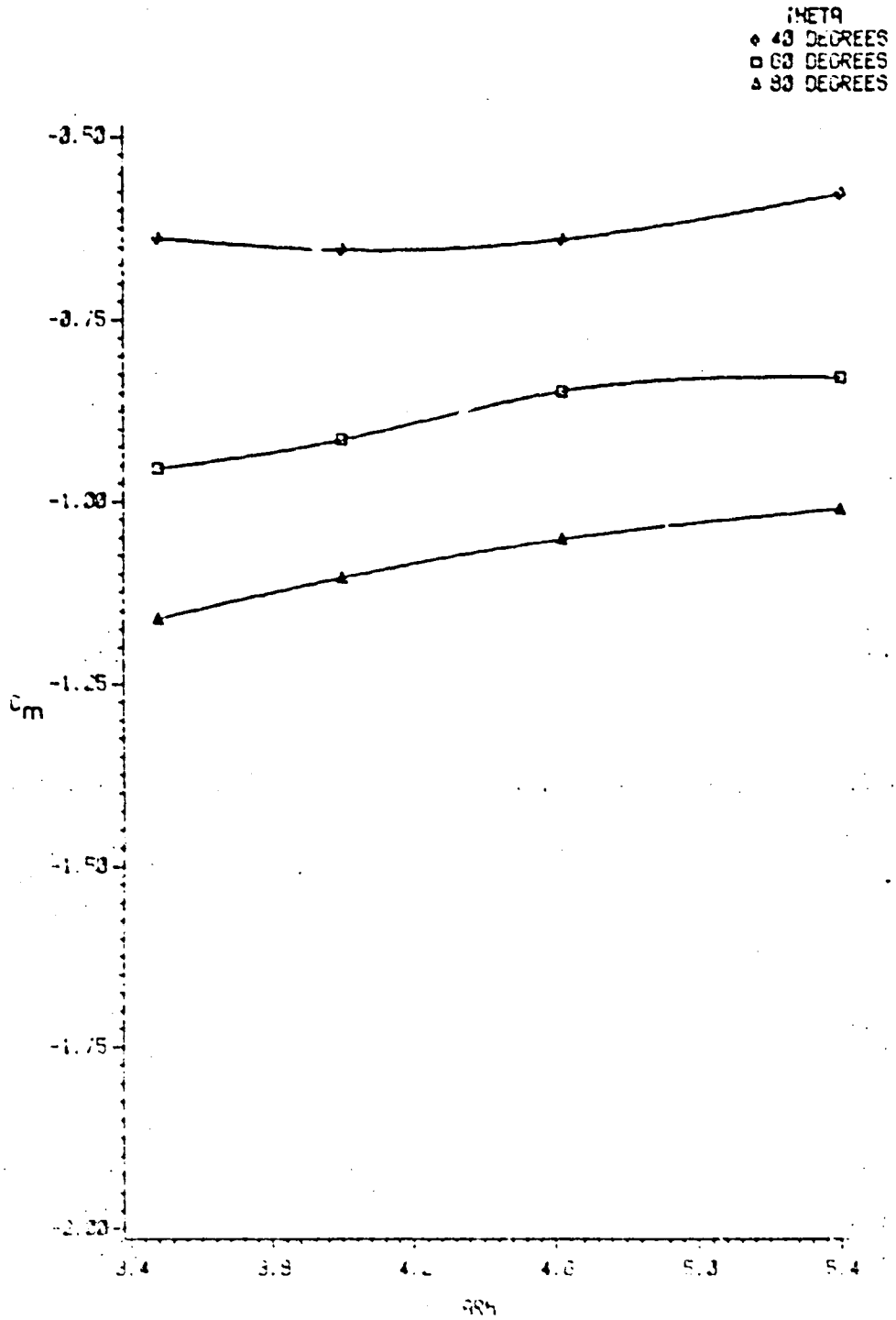

Figure 4-32. Pitching Moment as a Function of Horizontal Tail Aspect Ratio, $\bar{z} = .5$

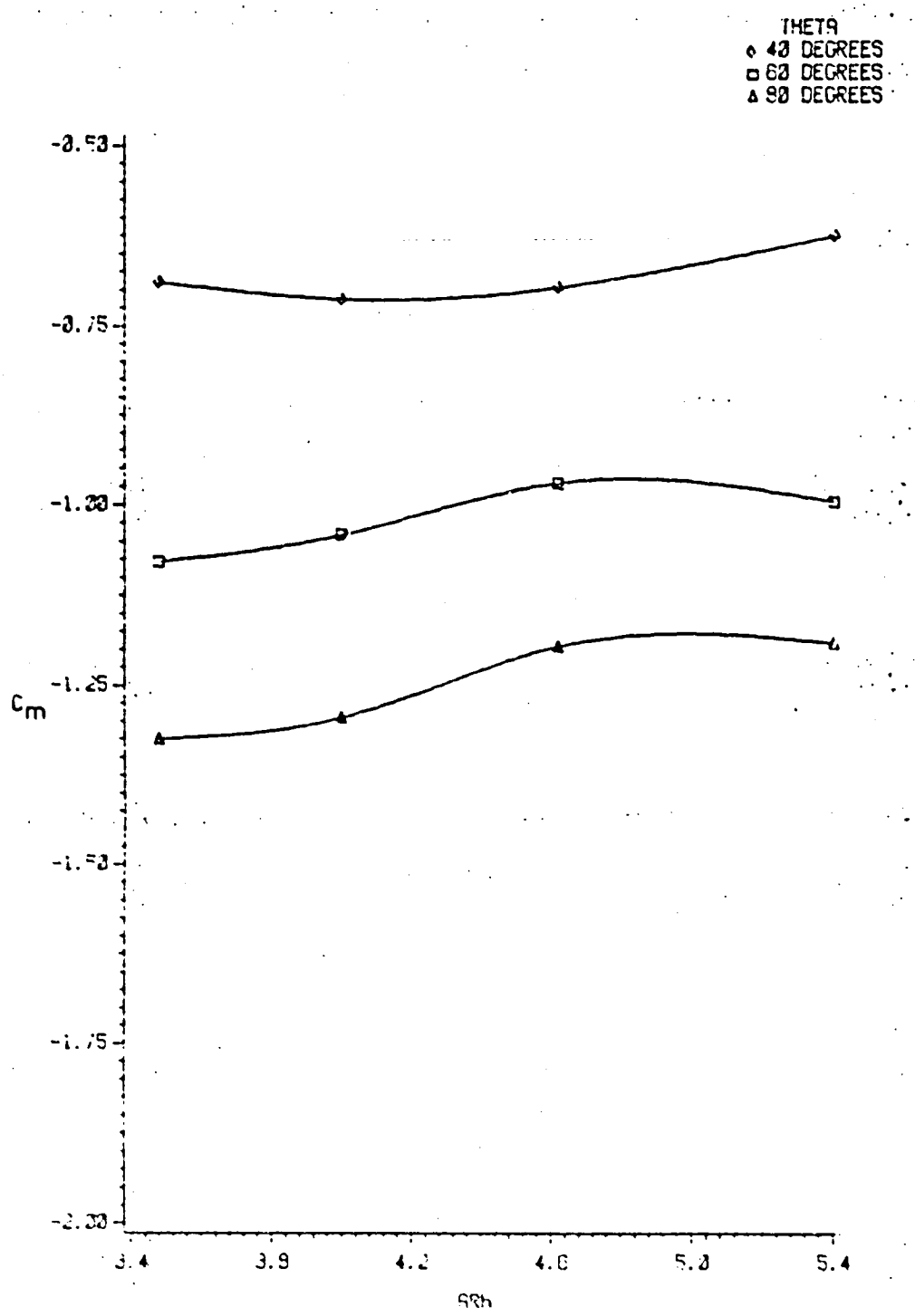

Figure 4-33. Pitching Moment as a Function of Horizontal Tail Aspect Ratio, $\bar{\omega}$ = .7

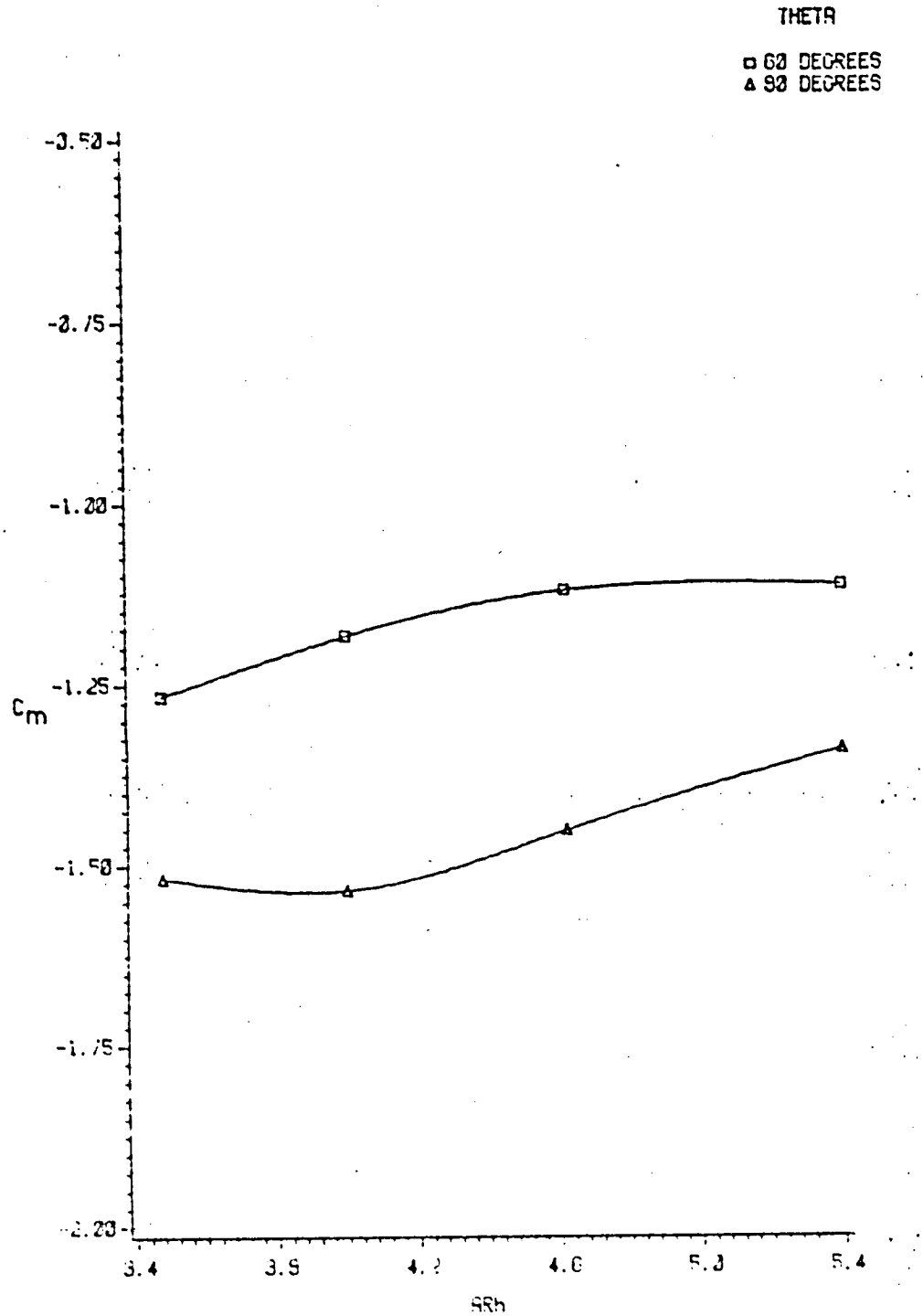

Figure 4-34. Pitching Moment as a Function of Horizontal Tail Aspect Ratio, $\bar{\omega}$ = .9

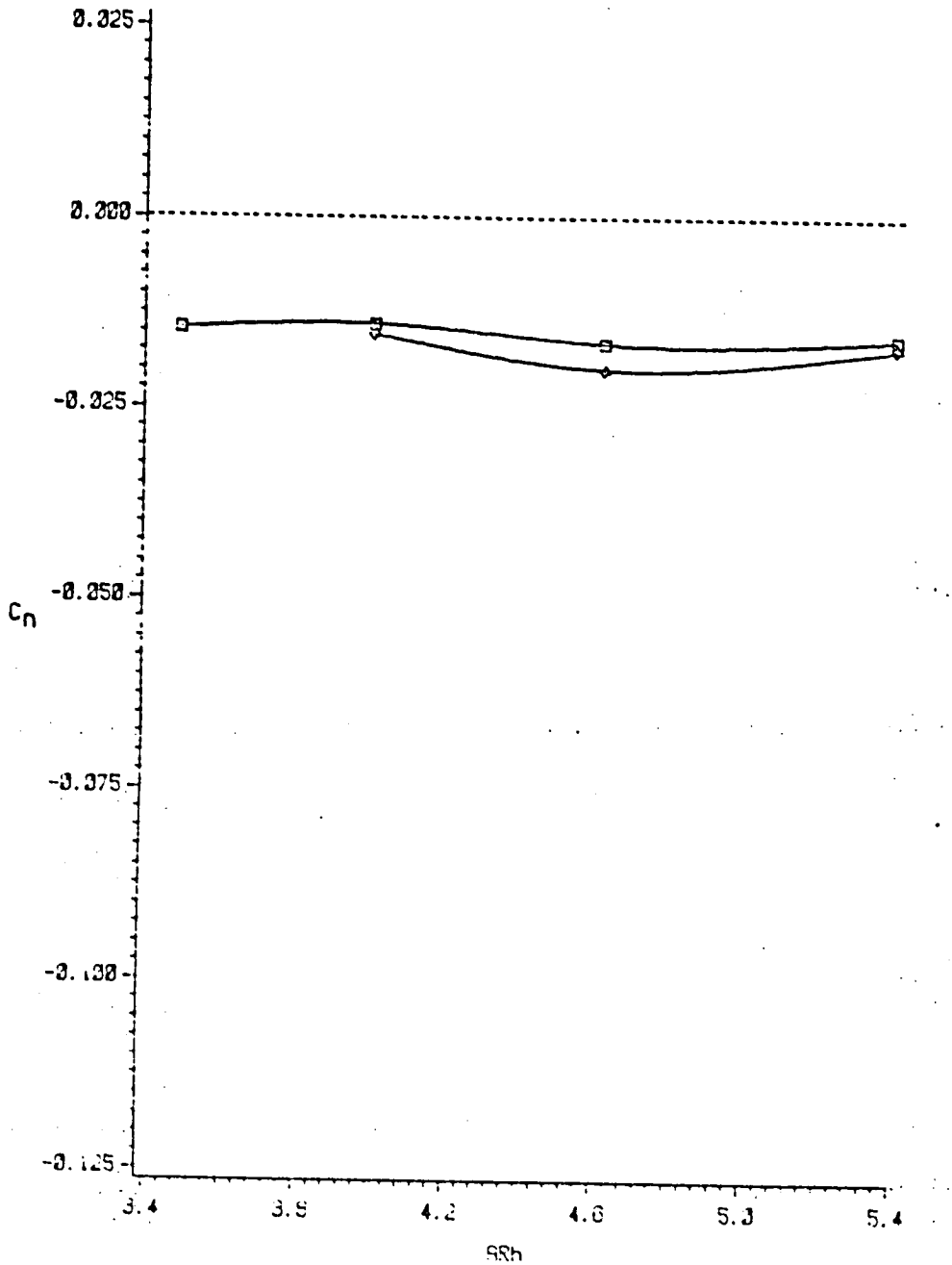

Figure 4-35. Yawing Moment as a Function of Horizontal Tail Aspect Ratio, $\bar{\omega}$ = .3

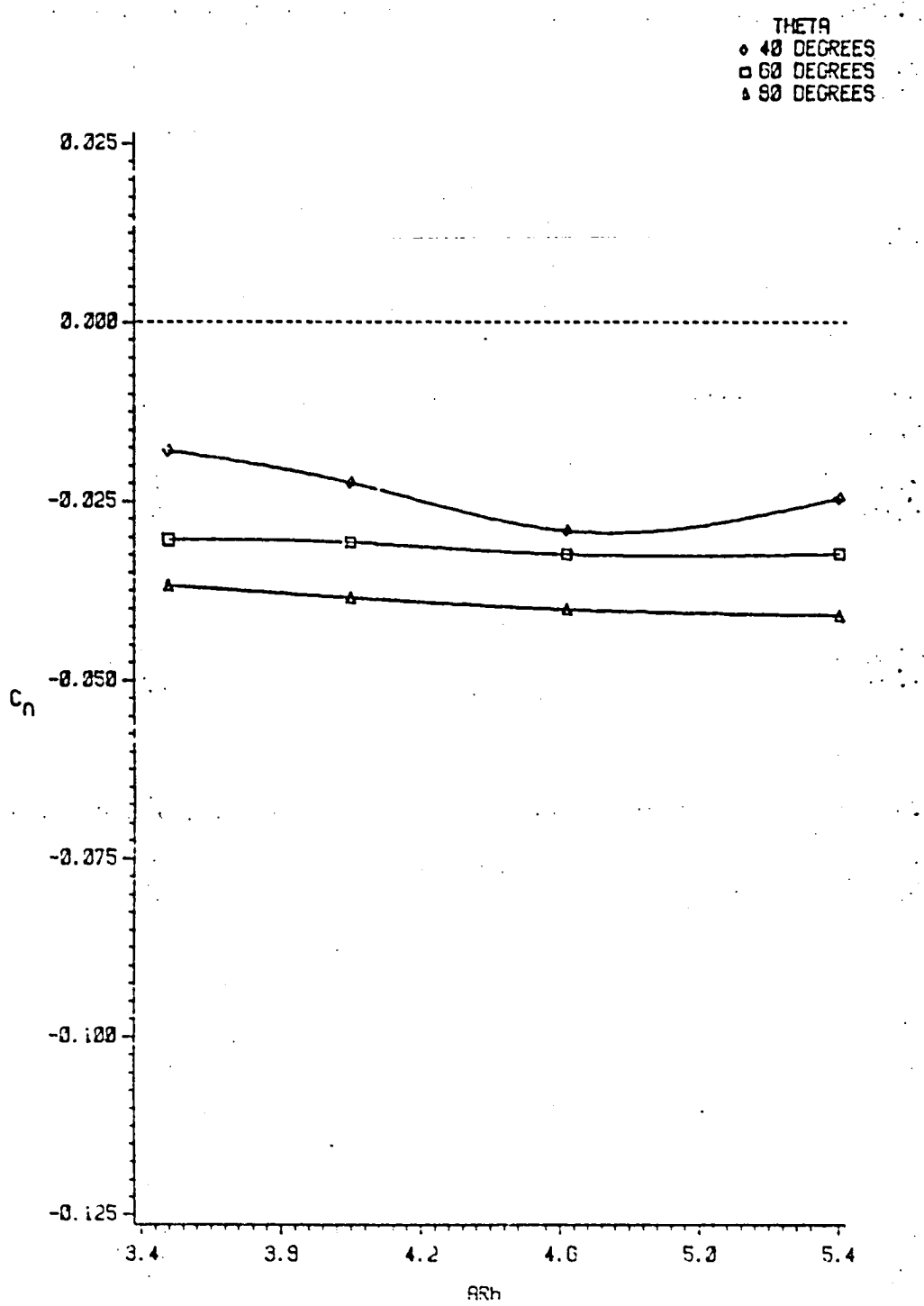

Figure 4-36. Yawing Moment as a Function of Horizontal Tail Aspect Ratio, $\bar{\omega}$ = .5

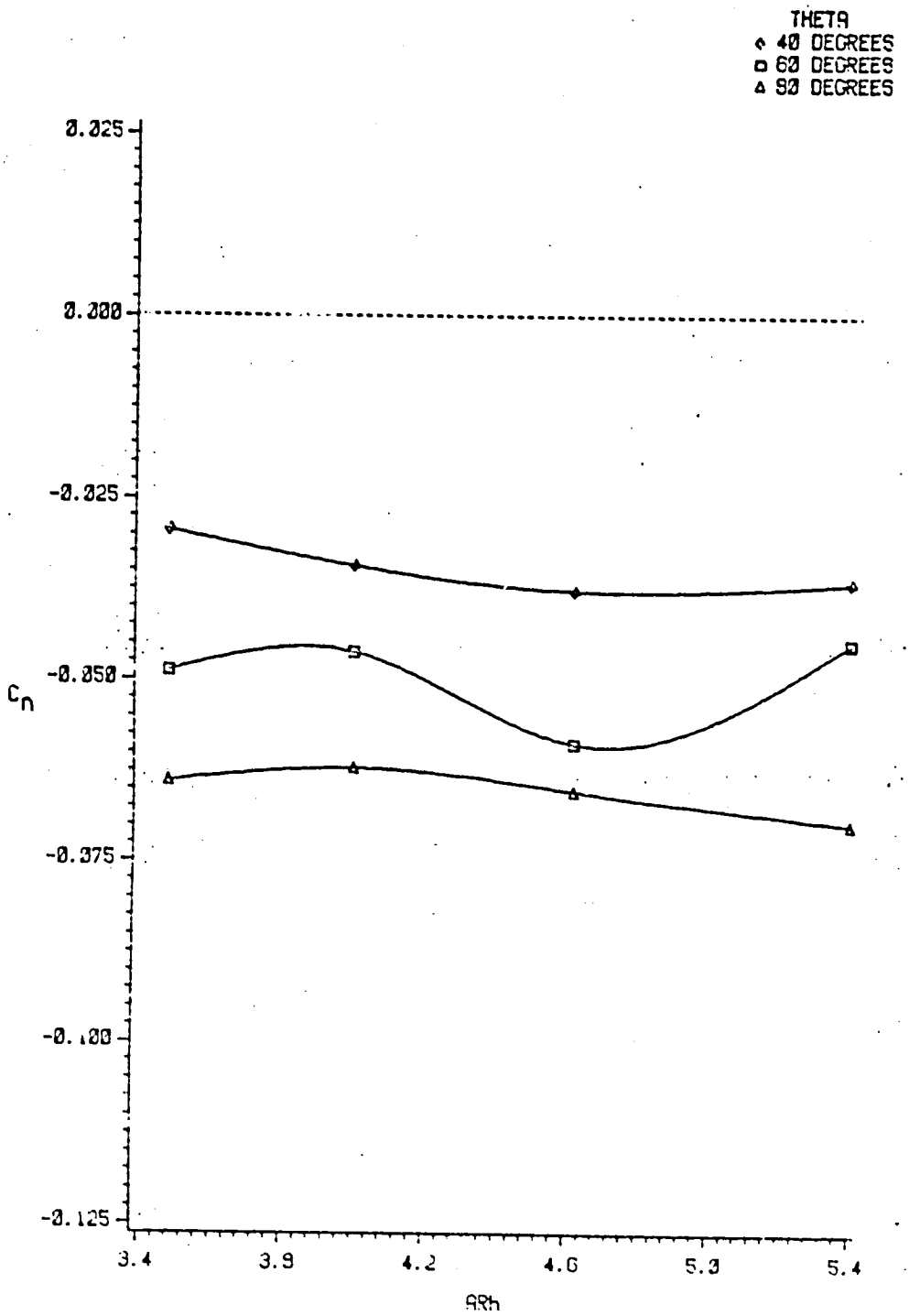

Figure 4-37. Yawing Moment as a Function of Horizontal Tail Aspect Ratio, $\bar{\omega}$ = .7

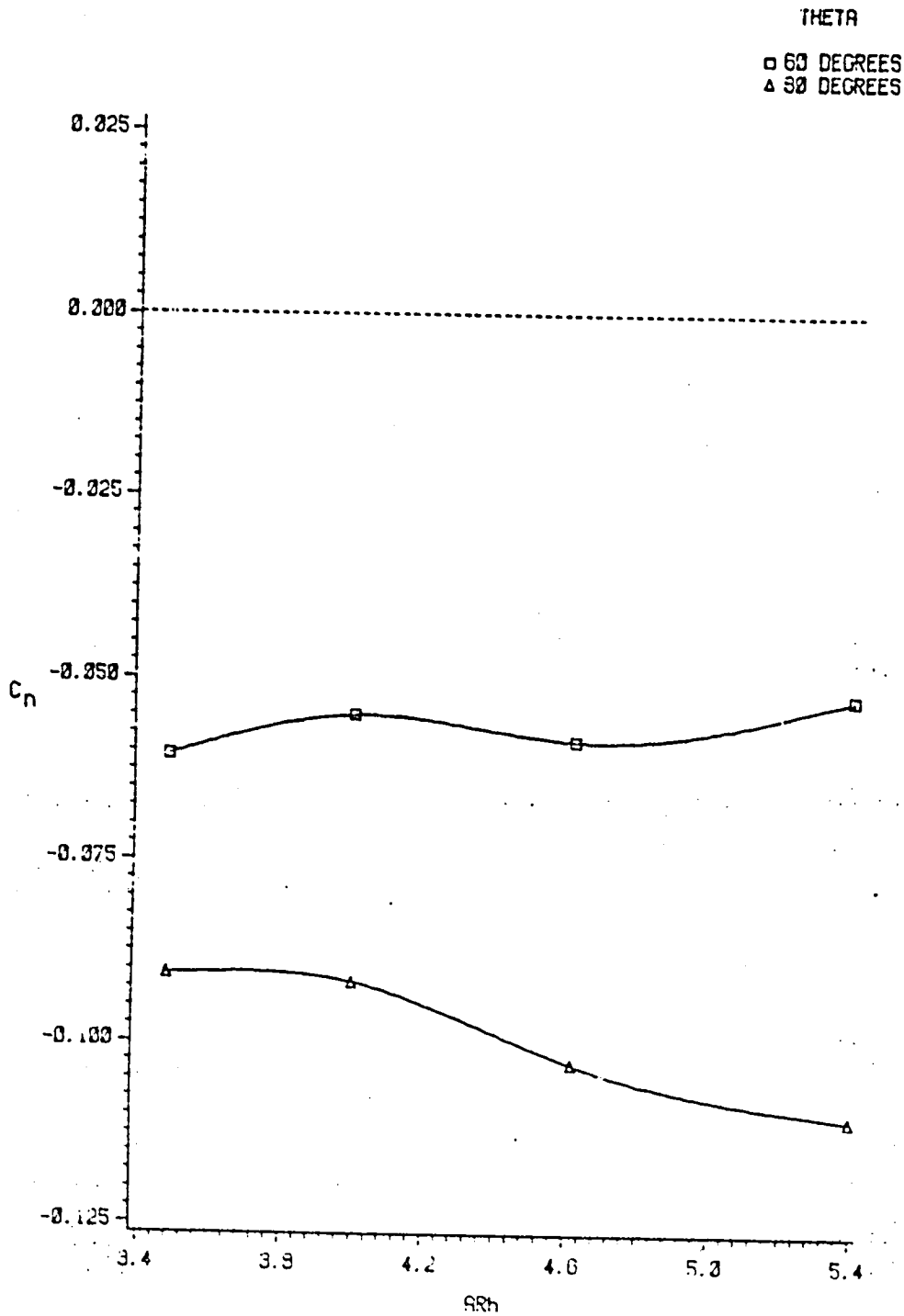

Figure 4-38. Yawing Moment as a Function of Horizontal Tail Aspect Ratio, $\bar{\omega}$ = .9

blanketing of the leeward tail can cause the higher aspect ratio, longer span horizontal tail to have a slight advantage (as seen in Figure 4-34). In most test cases, this interference effect is outweighed by the greater flat-plate drag of the lower aspect ratio tail surface.

Horizontal tail aspect ratio also has a relatively small effect on yawing moment (Figures 4-35 through 4-38). Complex effects from the altered chord and span of the horizontal tail surface make explanation of the results difficult. Nevertheless, definite trends can be noticed: under flat spin conditions, the higher aspect ratio tails provide stronger yawing moments; under steep spin conditions, a value of AR_h equal to 4.62 appears to be the optimum value for the configuration tested.

As stated previously, under zero-loading conditions, preventing or breaking equilibrium in yaw appears to be the dominant factor in spin safety. Therefore, a moderately high aspect ratio horizontal tail probably has a slight spin-damping advantage. Relative magnitudes of the effects are small, however, and AR_h should not be considered a primary design parameter to prevent spin.

Effects of the Horizontal Tail Chordwise Position

The horizontal position of the horizontal tail has a significant effect on the pitching moment of the aircraft, particularly at high spin rates. Figures 4-39 through 4-43 show that the aft position of the horizontal tail is most favorable for breaking pitch equilibrium. Note that the resultant curves are nearly linear in the intermediate spin range, probably caused by the increased moment arm associated with the aft position. The configuration tested, with h/b_v equal to 0.5, also

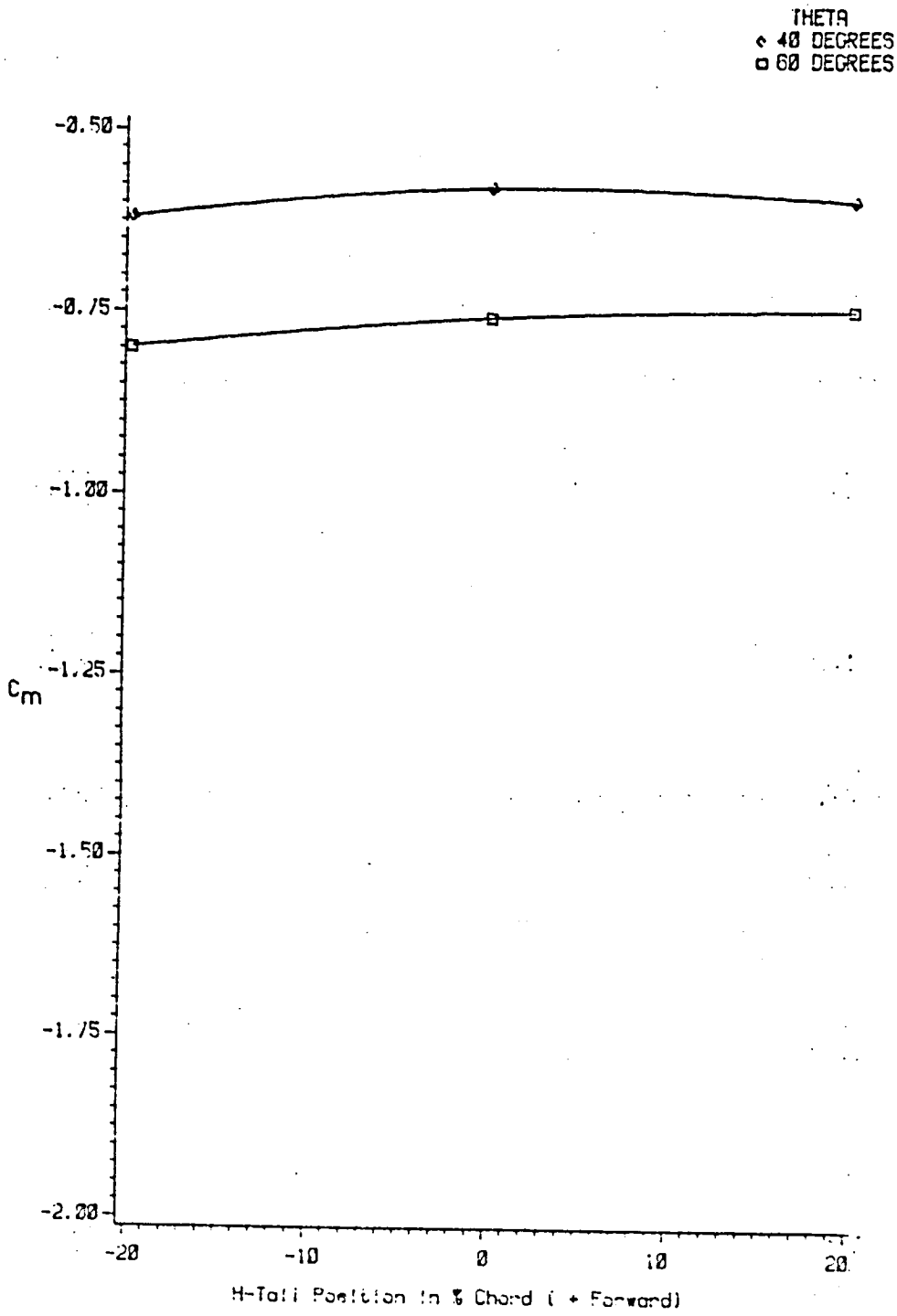

Figure 4-39. Pitching Moment as a Function of Horizontal Position of Horizontal Tail, $\bar{\omega} = 0$

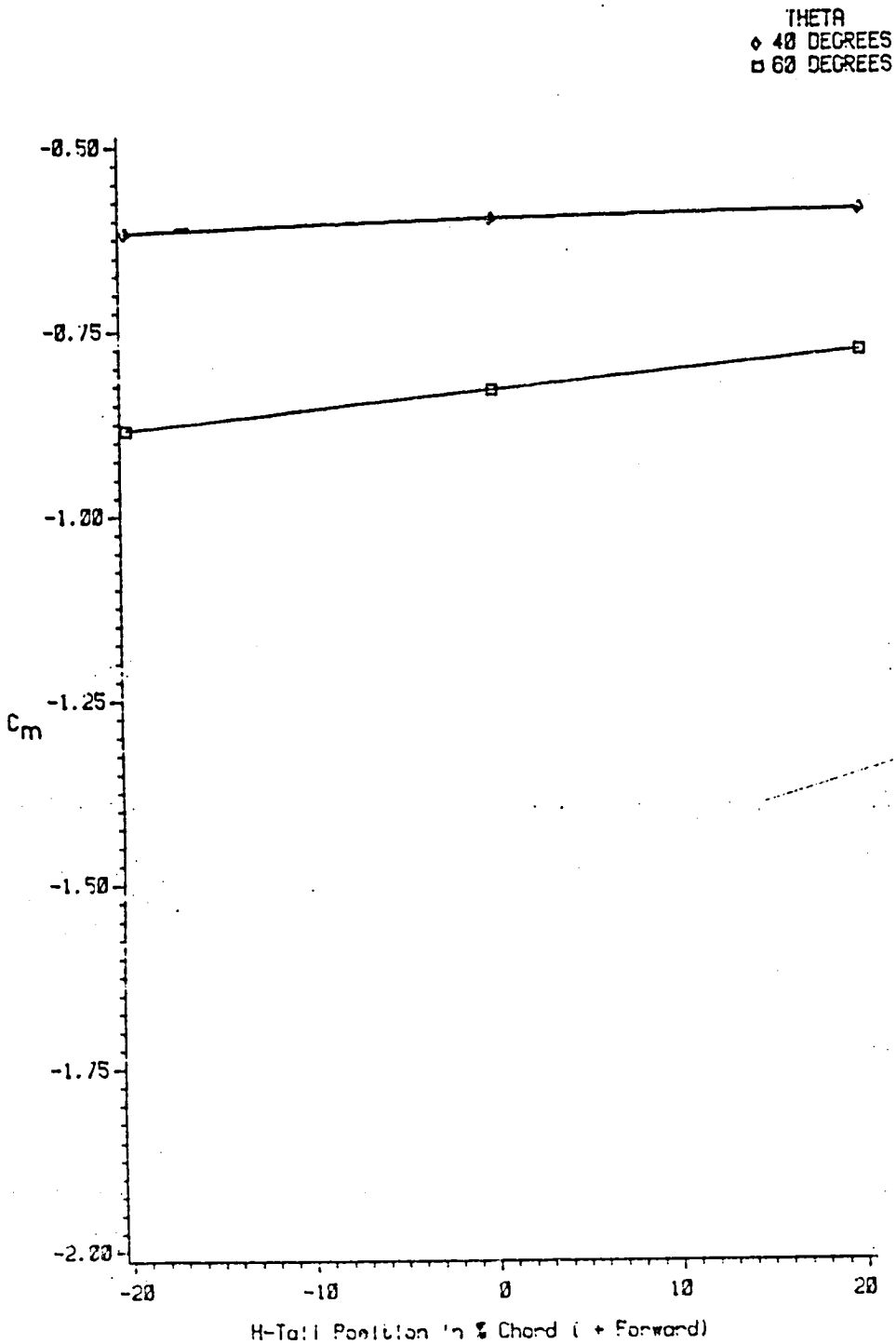

Figure 4-40. Pitching Moment as a Function of Horizontal Position of Horizontal Tail, $\bar{\omega}$ = .3

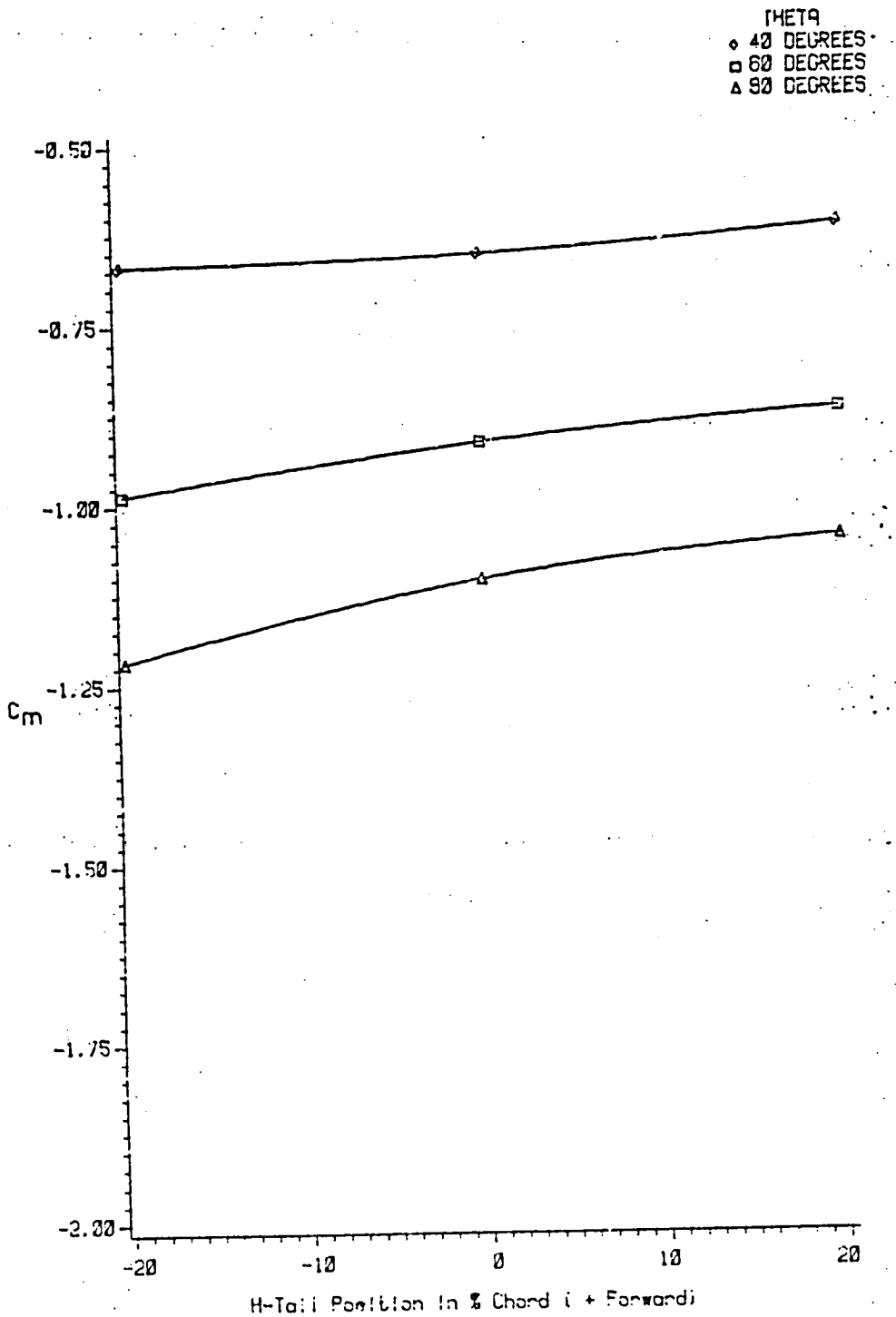

Figure 4-41. Pitching Moment as a Function of Horizontal Position of Horizontal Tail, $\bar{\omega}$ = .5

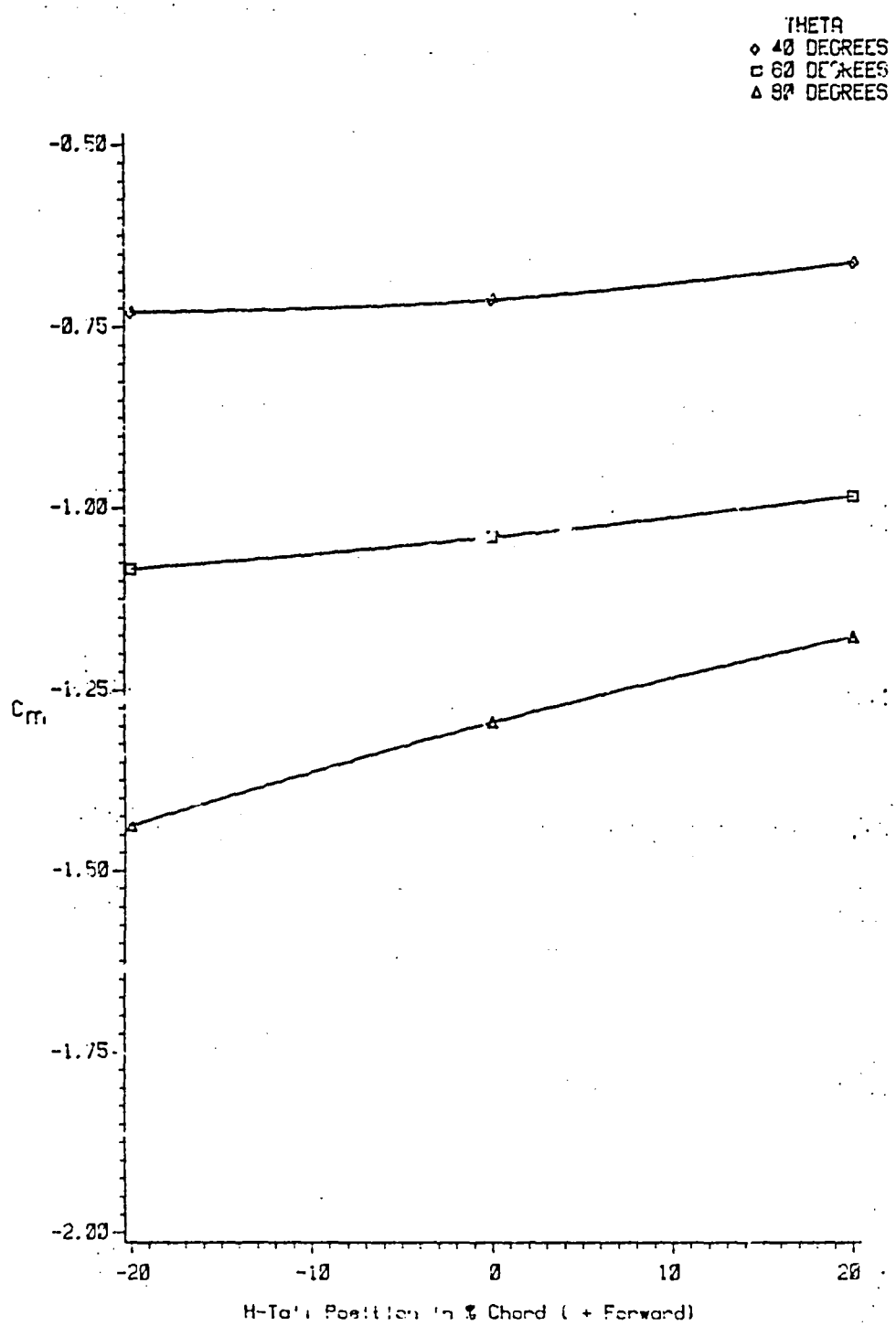

Figure 4-42. Pitching Moment as a Function of Horizontal Position of Horizontal Tail, $\bar{\omega}$ = .7

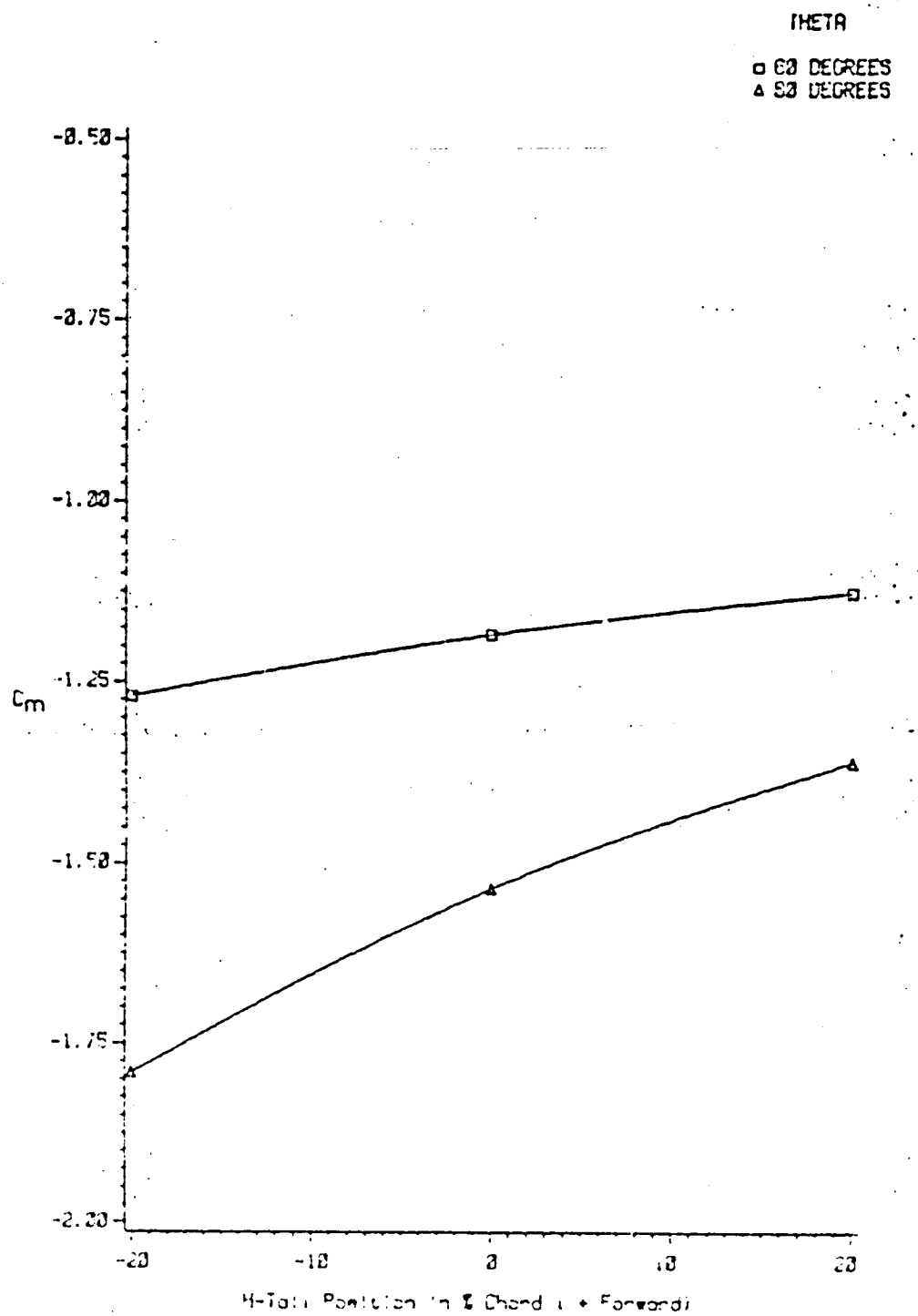

Figure 4-43. Pitching Moment as a Function of Horizontal Position of Horizontal Tail, $\bar{\omega}$ = .9

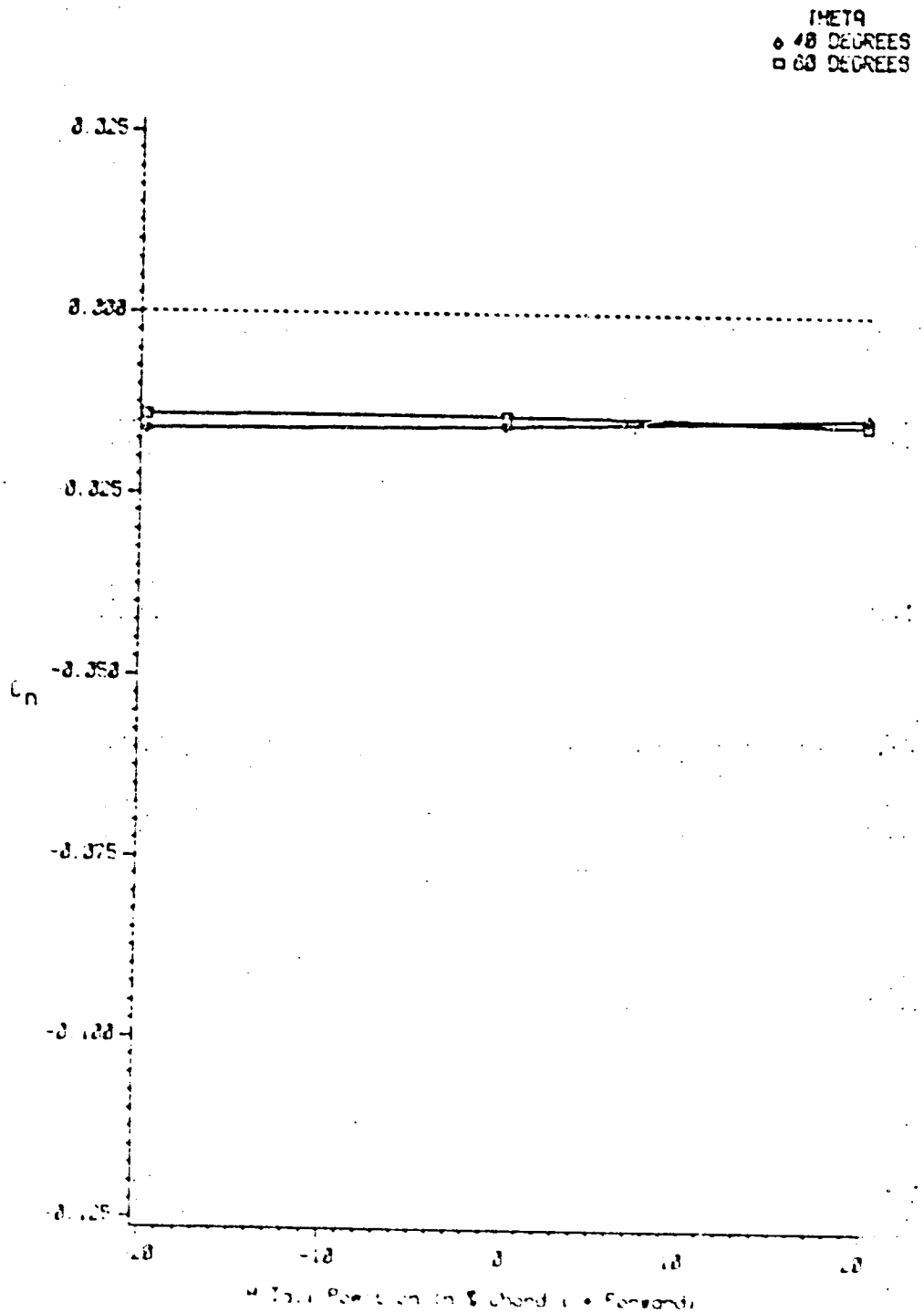

Figure [illegible]. Yawing Moment as a Function of Horizontal Position of Horizontal Tail, $\bar{z}$ = .1

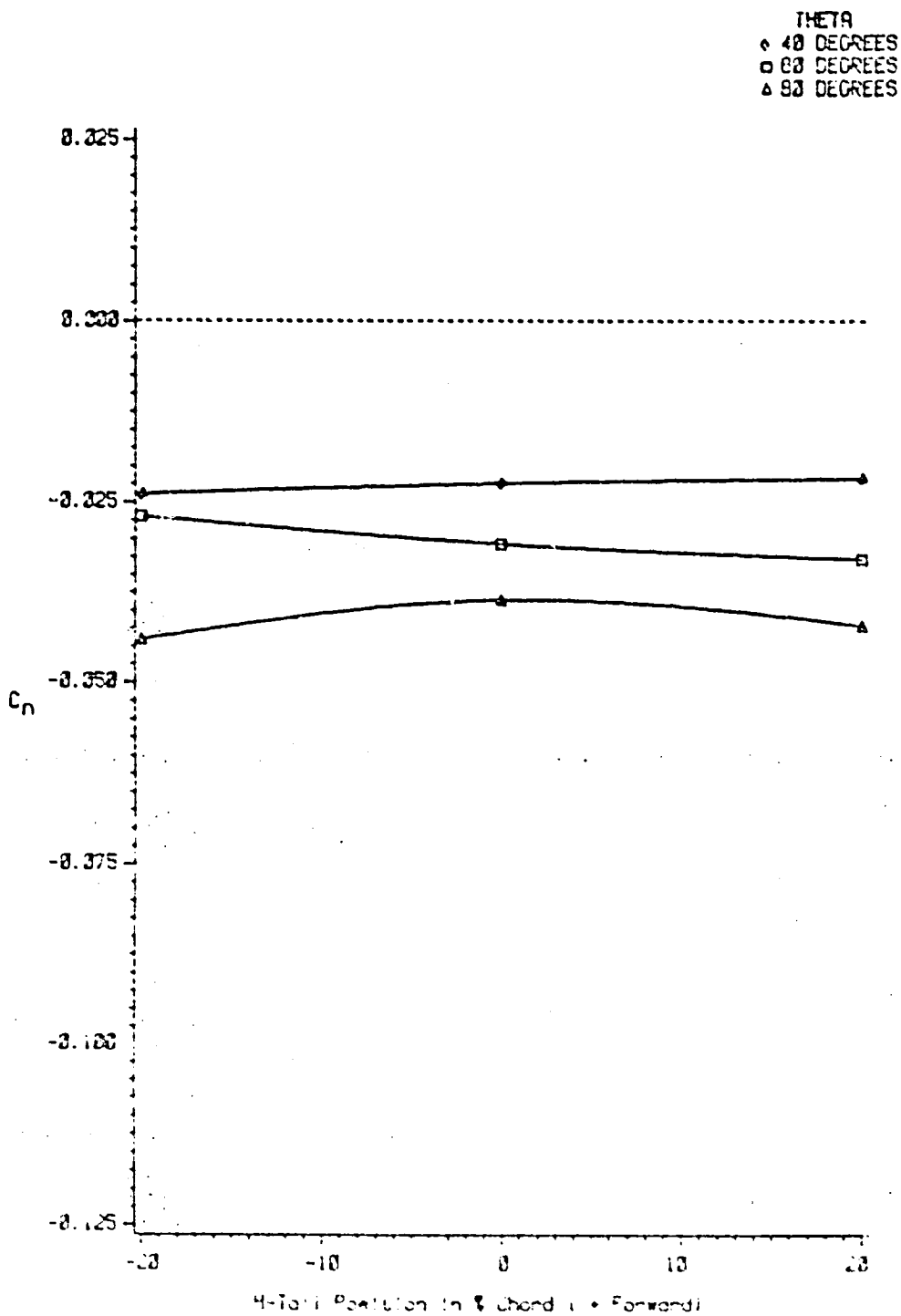

Figure 4-45. Yawing Moment as a Function of Horizontal Position of Horizontal Tail, $\bar{\omega} = .5$

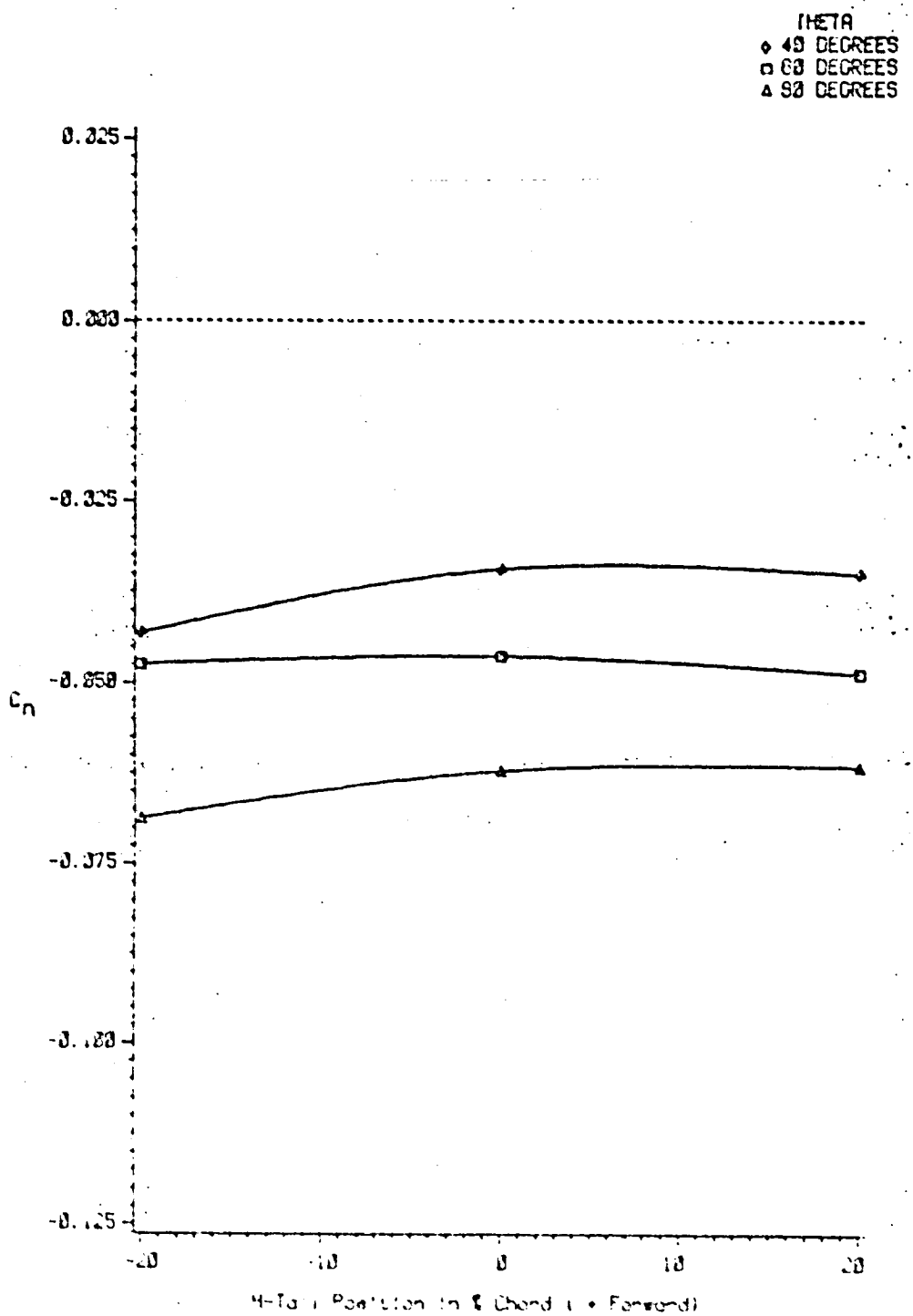

Figure 4-46. Yawing Moment as a Function of Horizontal Position of Horizontal Tail, $\bar{z}$ = .7

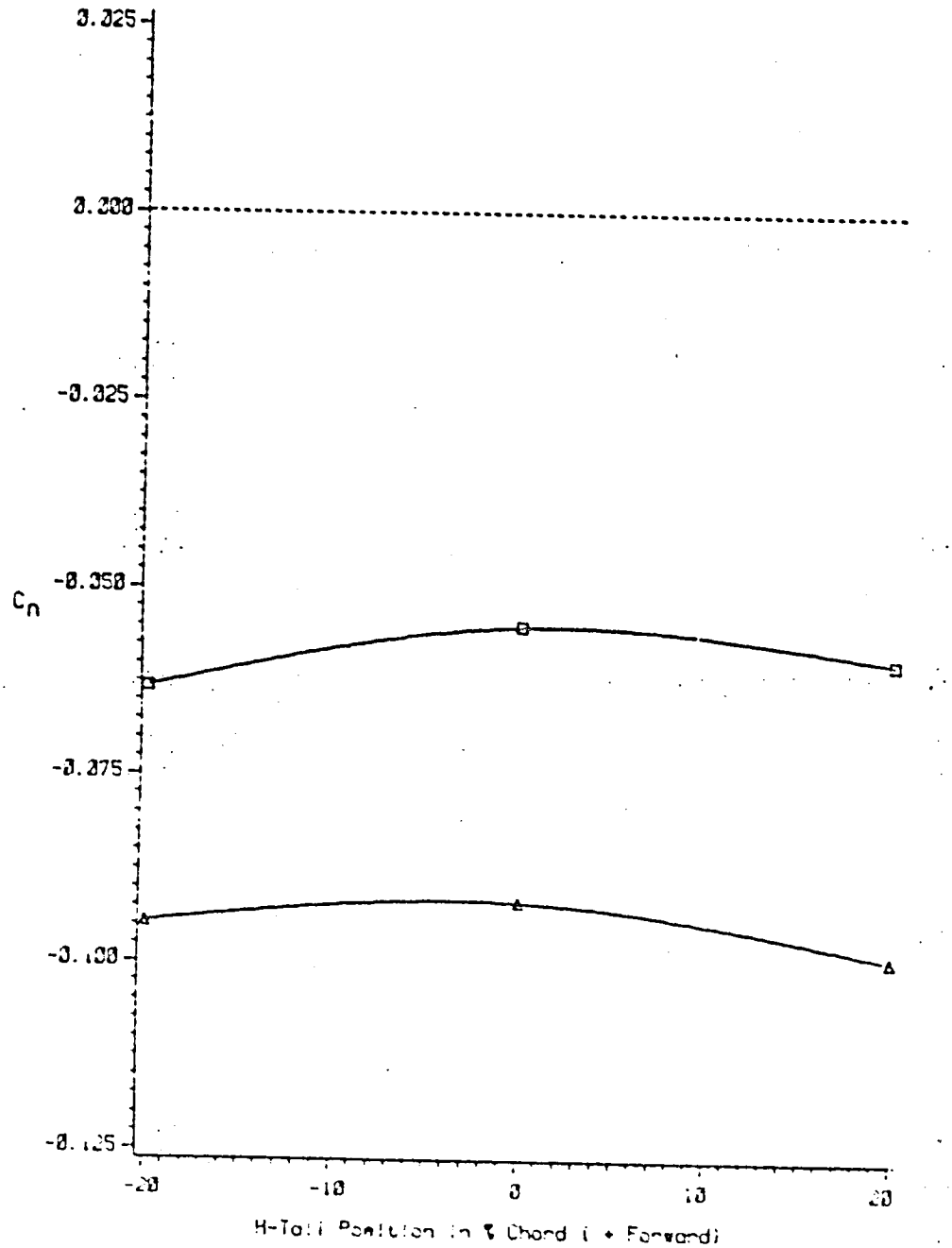

Figure 4-47. Yawing Moment as a Function of Horizontal Position of Horizontal Tail, $\bar{\omega}$ = .9

showed an increase in normal force with aft positioning, suggesting a fuselage blockage effect in the forward position.

Yawing results are affected greatly by $\bar{\omega}$. At low spin rates (Figure 4-44), constant θ curves intersect between the 0 and 20%-chord data points. The phenomenon causing greater yawing moments at steep spin values is evidently also related to chordwise horizontal tail location. Possibly the greater exposed vertical tail area in the horizontal tail-aft configuration tends to amplify the trends noted previously. At intermediate and high spin rates (Figures 4-45 through 4-47), a concave downward trend is seen, resulting in higher yawing moments for both forward and aft horizontal tail positions. In the forward position, more rudder area is exposed, and in the aft position, more forward vertical tail area is exposed.

NASA testing was limited to the low horizontal tail configuration, where forward positioning of the horizontal tail (NASA tail 1) resulted in a slightly flatter steep spin which required elevator deflection as well as rudder reversal for criterion spin recovery. Possibly rudder blanketing was a factor in the tests, and the small differences indicate that, despite large relative effects on pitching moment, chordwise horizontal tail location is not a primary parameter.

Effects of Control Deflections

All control effectiveness tests were performed at an intermediate spin rate of $\bar{\omega}$ equal to 0.5. Time considerations limited the tests to two theta angles, simulating a steep and a flat spin. All tests were performed with the baseline configuration. Elevator deflection alone induced small changes to pitch and yaw, as shown in Figures 4-48 and

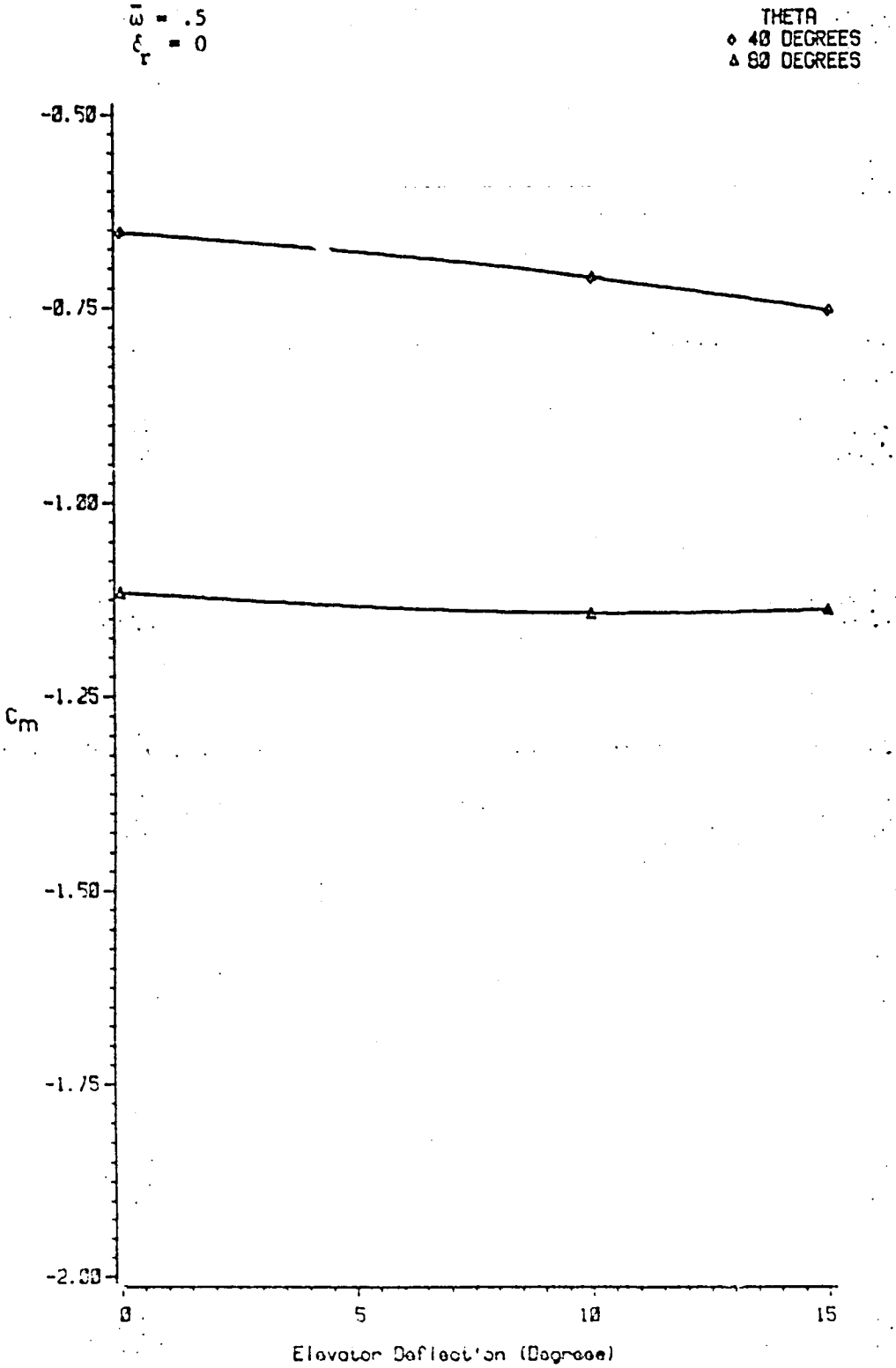

Figure 4-48. Pitching Moment as a Function of Elevator Deflection

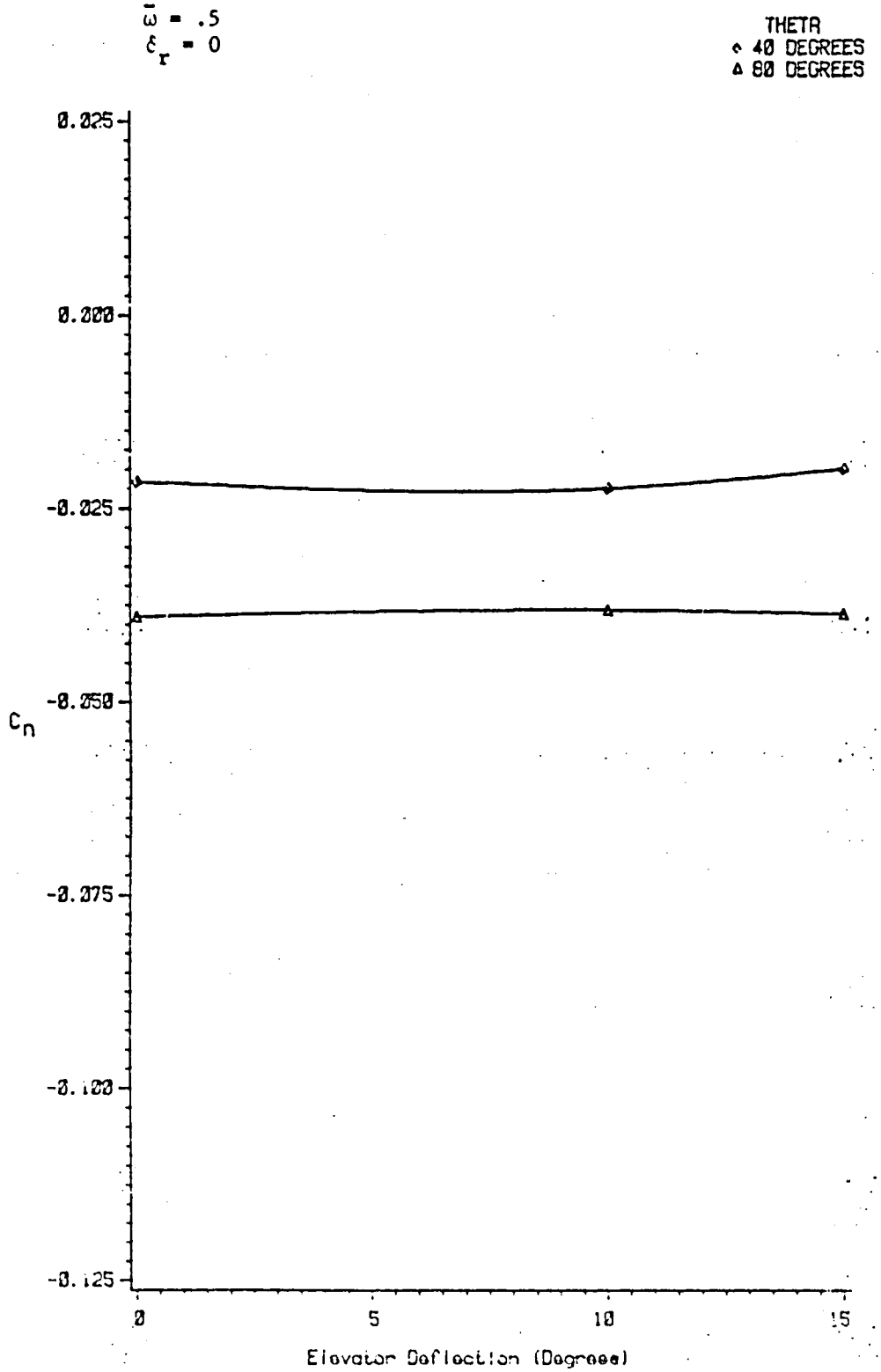

Figure 4-49. Yawing Moment as a Function of Elevator Deflection

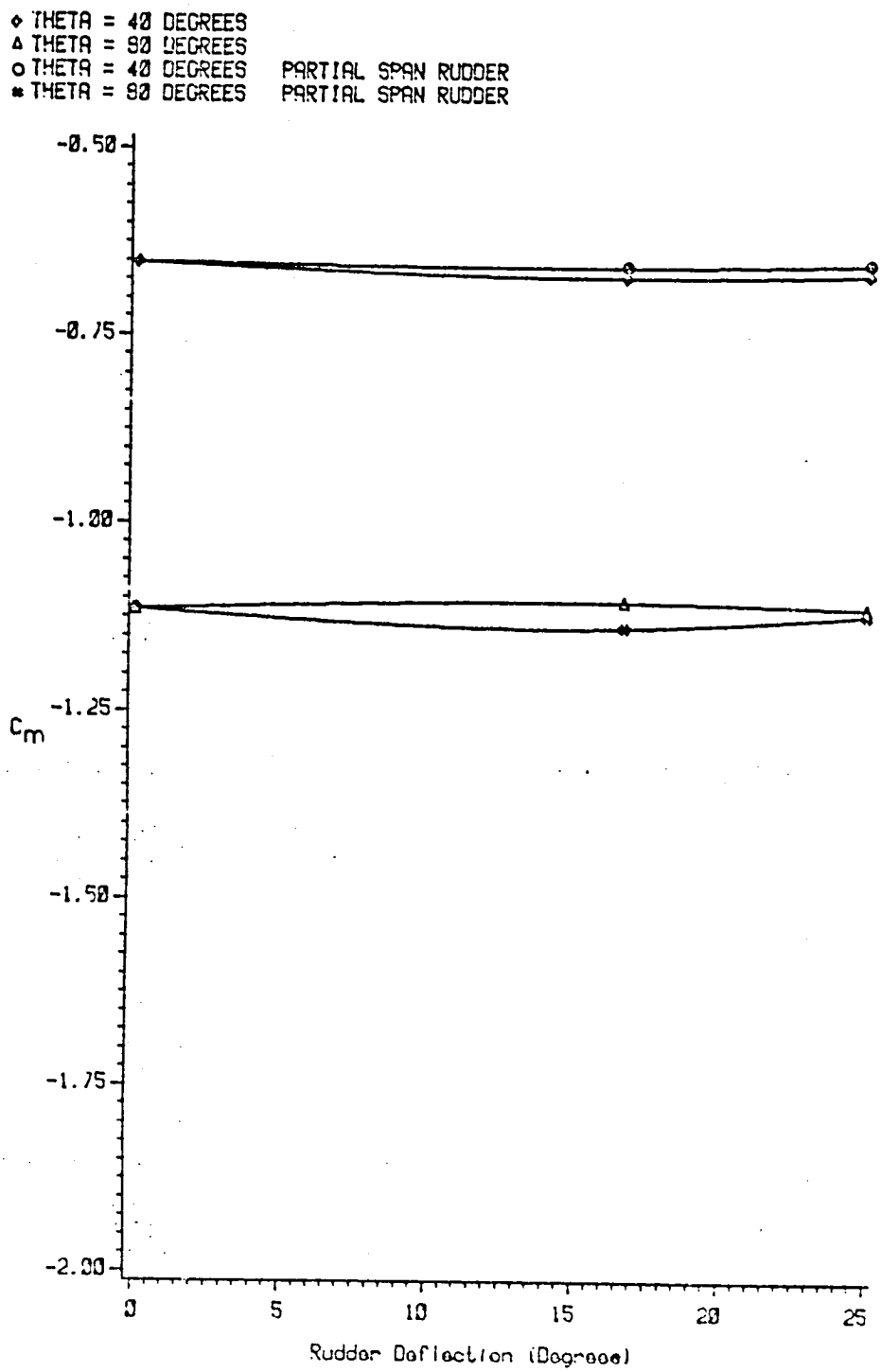

Figure 4-50. Pitching Moment as a Function of Rudder Deflection, $\bar{\omega}$ = .5

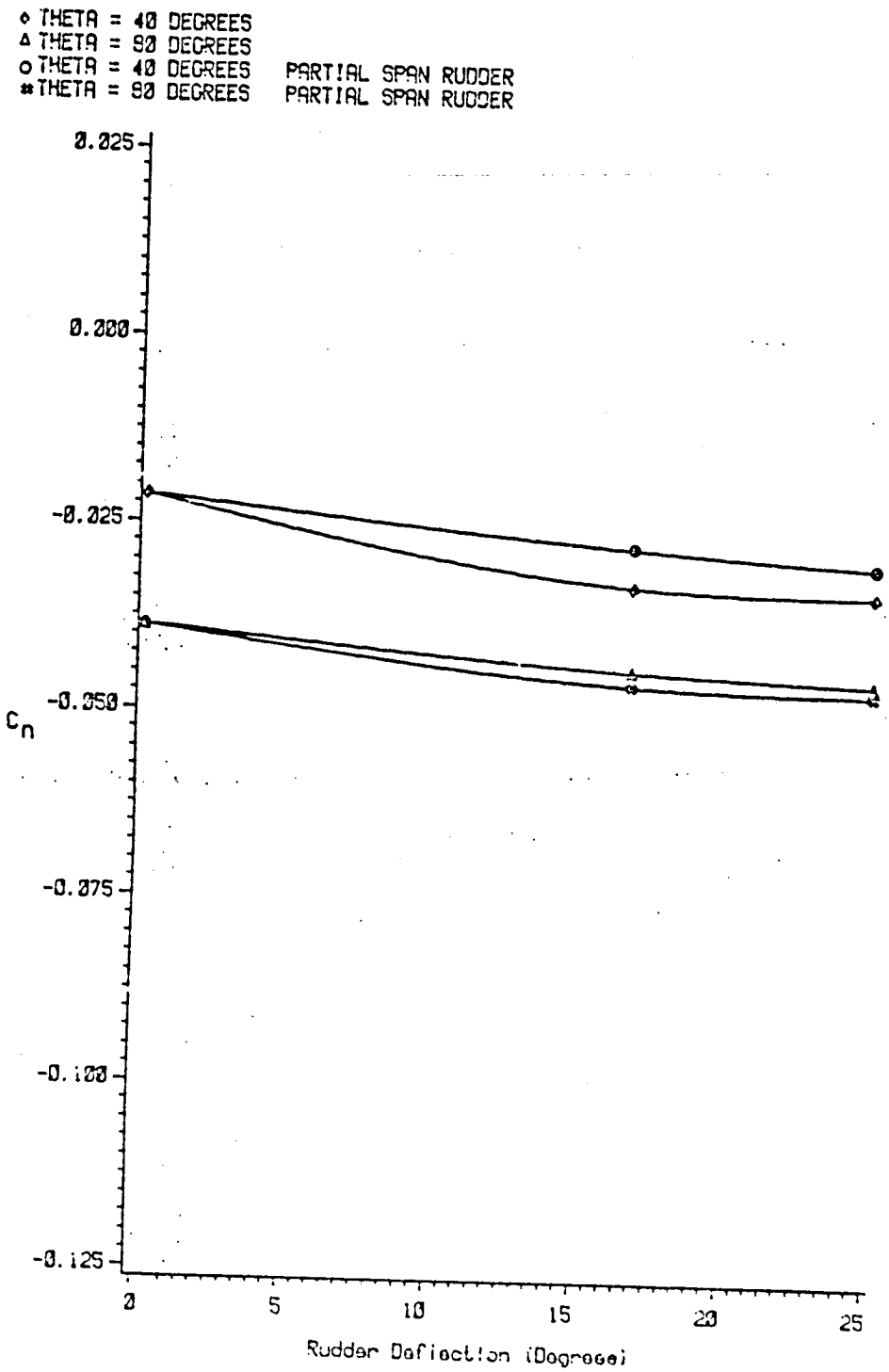

Figure 4-51. Yawing Moment as a Function of Rudder Deflection, $\bar{\omega}$ = .5

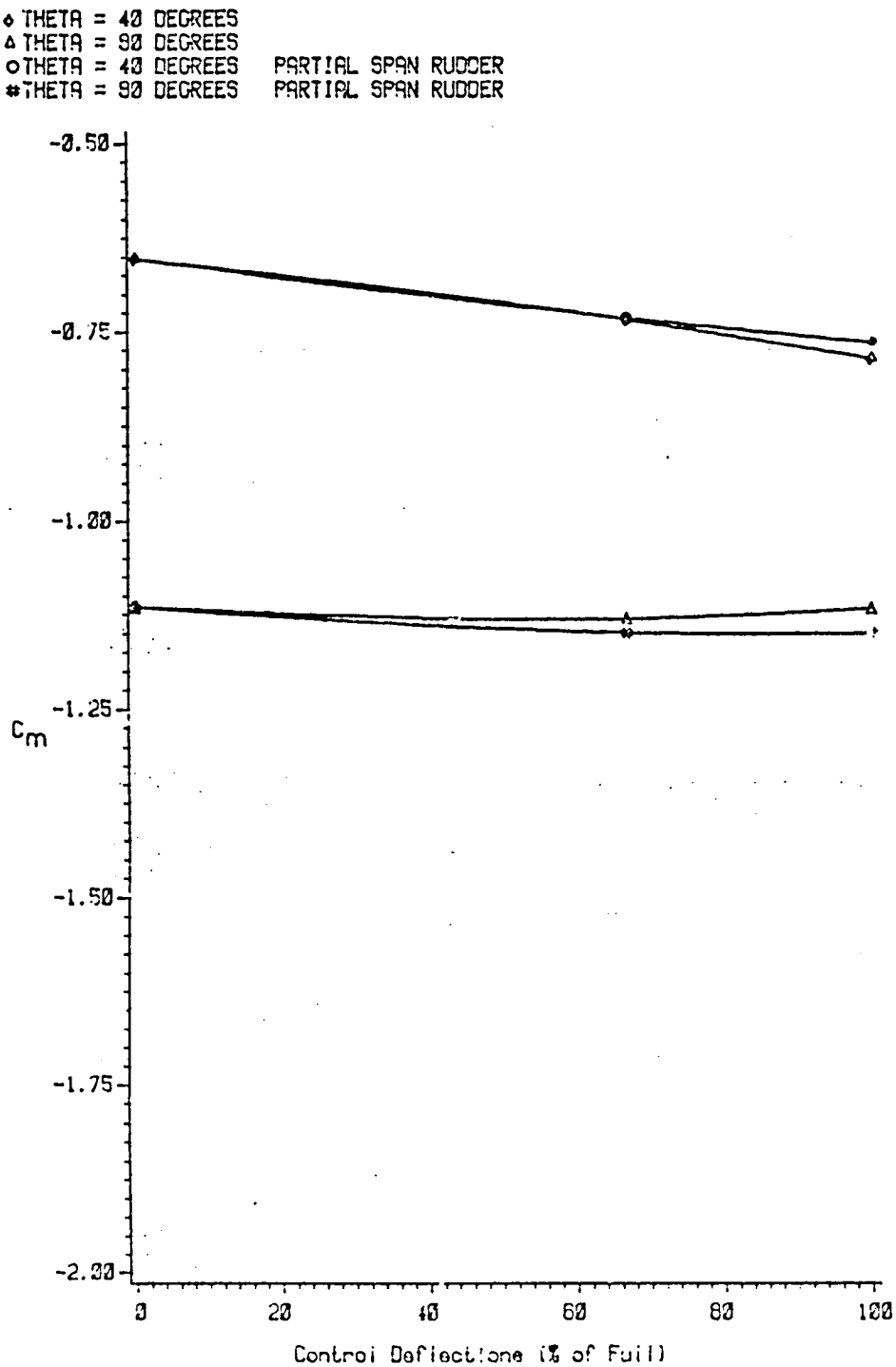

Figure 4-52. Pitching Moment as a Function of Combined Control Deflections, $\bar{\omega}$ = .5

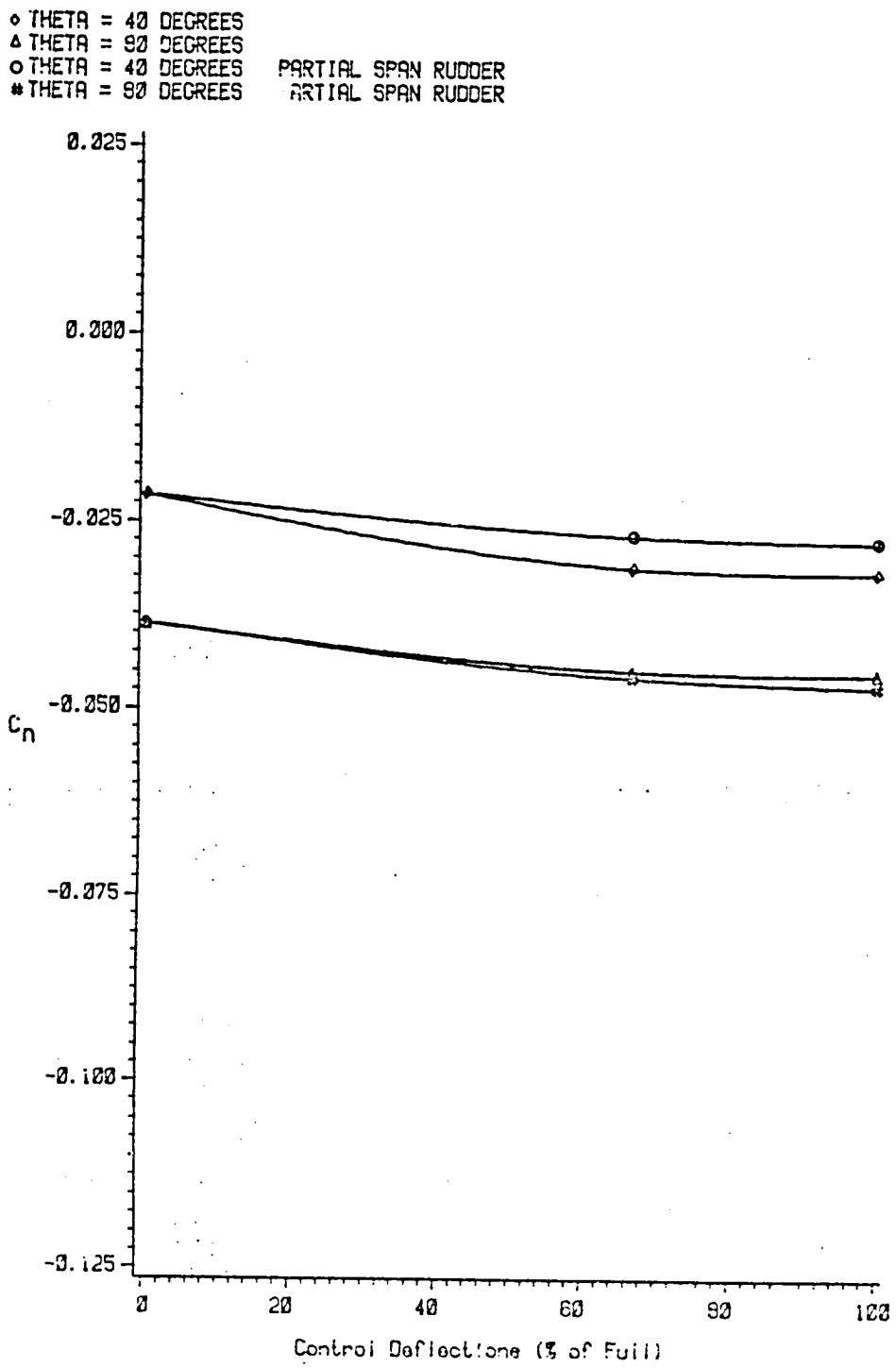

Figure 4-53. Yawing Moment as a Function of Combined Control Deflections, $\bar{\omega}$ = .5

4-49. At a pitch angle of 40°, elevator deflection resulted in a 14% increment to C_m at the maximum positive deflection of 15°. Yawing moment was also affected at a low pitch angle, probably by increased vertical tail blanketing. Flat spin elevator deflections resulted in minimal pitch and yaw effects. The results illustrate the danger in relying on the elevator for spin recovery. In some aircraft, however, high wing loadings make rudder reversal ineffective, leaving the elevator as the primary recovery control. Tail designs which maximize the nose-down pitching moment are necessary for such aircraft.

The effects of rudder deflection on pitch and yaw are shown in Figures 4-50 and 4-51. Effects on pitching moment are small, but yawing moment is strongly influenced by rudder reversal. Steep spin results indicate a 53% increment in yawing moment at the maximum rudder deflection of 25°. Note that rudder effectiveness decreases with increasing pitch. The high spin rates common at higher pitch angles would probably tend to minimize this loss of influence.

The partial-span rudder is much less effective than the full-span rudder under steep spin conditions. At a pitch angle of 80°, the differences are small, with the suggestion of reversal of the above trend: yawing moments produced by the partial-span rudder are slightly greater than those produced by the full-span rudder. This result is in agreement with NASA tests, where it was found that NASA tail 2, identical to tail 3 except for its partial-span rudder, did not have a flat spin mode, while tail 3 exhibited an unrecoverable flat spin mode as well as a moderately flat steep spin mode. Such a control configuration apparently prevents a spin in two ways: by reduced rudder effectiveness while deflected in a pro-spin direction, and by increased

yaw damping after rudder reversal. It is questionable whether this slight increase in flat spin C_n is worth the trade-off in lowered steep spin damping. NASA testing indicates that it is, at least by preventing high pro-spin yawing moments when the rudder is deflected in a pro-spin direction.

Simultaneous deflection of the elevator and rudder provides very little additional positive effect, aside from the fact that it sums the effects of each control surface. Overall control effectiveness is very poor under flat spin conditions. Under steep spin conditions, rudder effectiveness is actually lessened with the combined deflections because of increased rudder blanketing caused by the deflected elevator. For this reason, standard recovery procedure consists of rudder reversal followed by elevator deflection, applied before the spin becomes fully developed.

CHAPTER V

DEVELOPMENT OF A PREDICTIVE PARAMETER

As previous research has shown, the Tail Damping Power Factor and its associated general aviation aircraft design criterion have proven to be insufficient for prediction of satisfactory spin characteristics and recovery. This is due in part to the contributions of other airplane components. Nevertheless, a truly effective design criterion for general aviation tails would be useful to the designer. It must incorporate a measure of control effectiveness while accounting for effects of possible adverse aileron deflection (Burk et al. 1977). It must also be dependent on the aircraft density coefficient and pitch angle. In addition, because spin has been shown to be dependent on method of control reversal, the parameter must also account for incorrect or insufficient (criterion) control deflections.

A design criterion such as described above would be less than practical because of its complexity. Certainly it would involve extensive spin tunnel and radio controlled model tests. A more feasible alternative would be extensive wind tunnel studies of tail configurations, with tabulation of nondimensional force and moment coefficients for varying pitch, roll, and sideslip angles. Control derivatives could also be tabulated for spin conditions. With the use of one of the many nonlinear numerical simulation routines becoming available, the designer would then be able to study the spin characteristics of several configurations and choose the optimal one for his needs. Of course, full scale flight testing would still be necessary, but by increasing confidence in predictive methods, much

effort could be saved in other preliminary studies.

Adequacy of the Tail Damping Power Factor

The designer would also find useful a criterion which provides a rough indication of the spin characteristics of the tail. Such a criterion would be helpful during preliminary layout and sizing. The present tail design criterion for light general aviation aircraft is not acceptable, at least in its present form. Because of its conservative nature, several designs showing acceptable spin recovery are deemed unacceptable by the criterion (see Chapter 2).

A tail design criterion which would not be misleading must only concern the damping characteristics of the tail. Thus, it is necessary to develop a factor which approximately predicts pitching and yawing moments and indicates control effectiveness in terms of increased moments. Figure 5-1 is a plot of yawing moment as a function of the Tail Damping Power Factor for each configuration tested. Three typical spin conditions are shown. Correlation of the TDPF with yawing moment is poor, particularly under flat spin conditions.

There are several reasons for the inadequacy of the TDPF. Because it is made up of the product of two other criteria, the TRVC and the TDR, it cannot measure separate contributions to yawing moment of each factor; the rudder actually has the dual purpose of contributing to C_n in its undeflected position, and contributing a positive yawing increment while deflected. In addition, the Tail Damping Ratio was arbitrarily set up to include area only under the horizontal stabilizer. This rough approximation is perhaps too rough: increasing the chord of the horizontal tail slightly can have a dramatic effect on the TDR.

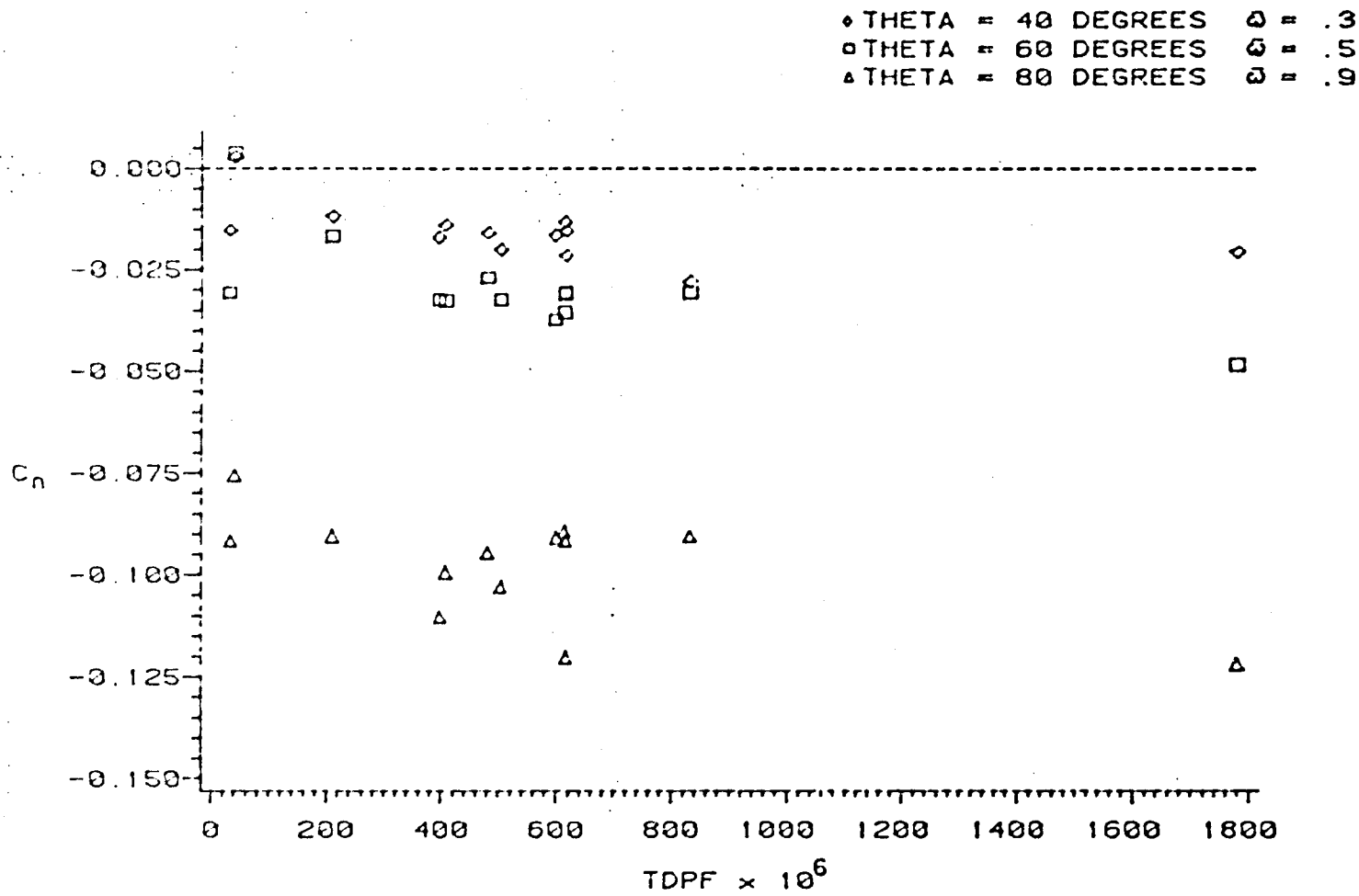

Figure 5-1. Yawing Moment as a Function of Tail Damping Power Factor

Spin angles used in the TDPF are set up arbitrarily. The aircraft is assumed to spin at a pitch angle of 45° if it uses a full-span rudder. If a partial-span rudder is used, it may spin at an attitude of 30° or 45°, depending on the value of the TDR. Finally, there is no estimation of the shape of the blanketed region on the vertical tail.

Moment Correlation with a Modified Anti-Spin Parameter

Perhaps the greatest utility of any criterion developed is in providing some measure of correlation with the many factors influencing tail forces. The TDPF has proven to be unsatisfactory; a true damping parameter must correlate with generated moments. This discussion is concerned with simple improvements based on tail geometry and shape of the air cavity in two dimensions, and it will therefore be approximate.

Testing has shown that for a zero-loaded aircraft, yawing velocity is the major contributor to inertial moments which perpetuate a spin. The vertical tail and rudder thus provide the largest tail contribution to spin damping. For this reason, a tail anti-spin parameter (referred to as TASP below) should be based primarily on unblanketed vertical tail area. Rudder contribution to yawing moment should be added as a separate factor, and only during separate comparison of rudder effectiveness:

$$\text{TASP} = \frac{\text{Unblanketed Area}}{S(b/2)} + K_2 \times \text{Rudder Volume Coefficient}$$

The constant K_1 is needed to prevent the first term from dominating the parameter, and must be determined through a study of the relative importance of each term.

The cavity which blankets part of the vertical tail is of the shape shown in Figure 5-2. McCormick, in an unpublished study, derived a numerical method for determining two-dimensional cavity shapes of flat plates at high angles of attack. Examination of the results shows that cavity width in the plane of the plate is relatively constant with respect to θ.

It is this research which forms the basis for the tail volume calculation as shown in Figure 5-3. The cavity has been simplified to form a blanketing area determined in size by lines l_1 and l_2, which are separated a distance of $2.28\bar{c}$ in the plane of the horizontal tail. The lines are parallel and at an angle of θ to the horizontal. Areas are defined below:

A_1 Area of the vertical tail not in the blanketed region or defined by other areas.

A_2 Triangular area forward of the leading edge of the horizontal tail; determined by a line extending forward from the leading edge at an angle of 45°.

A_3 Upper forward tip of the vertical tail; bounded by the line l_1.

A_4 Triangular area aft of the trailing edge of the horizontal tail; determined by a line extending aft from the leading edge at an angle of 45°.

A_5 High pressure region immediately below the horizontal tail and above the unblanketed lower area, A_1.

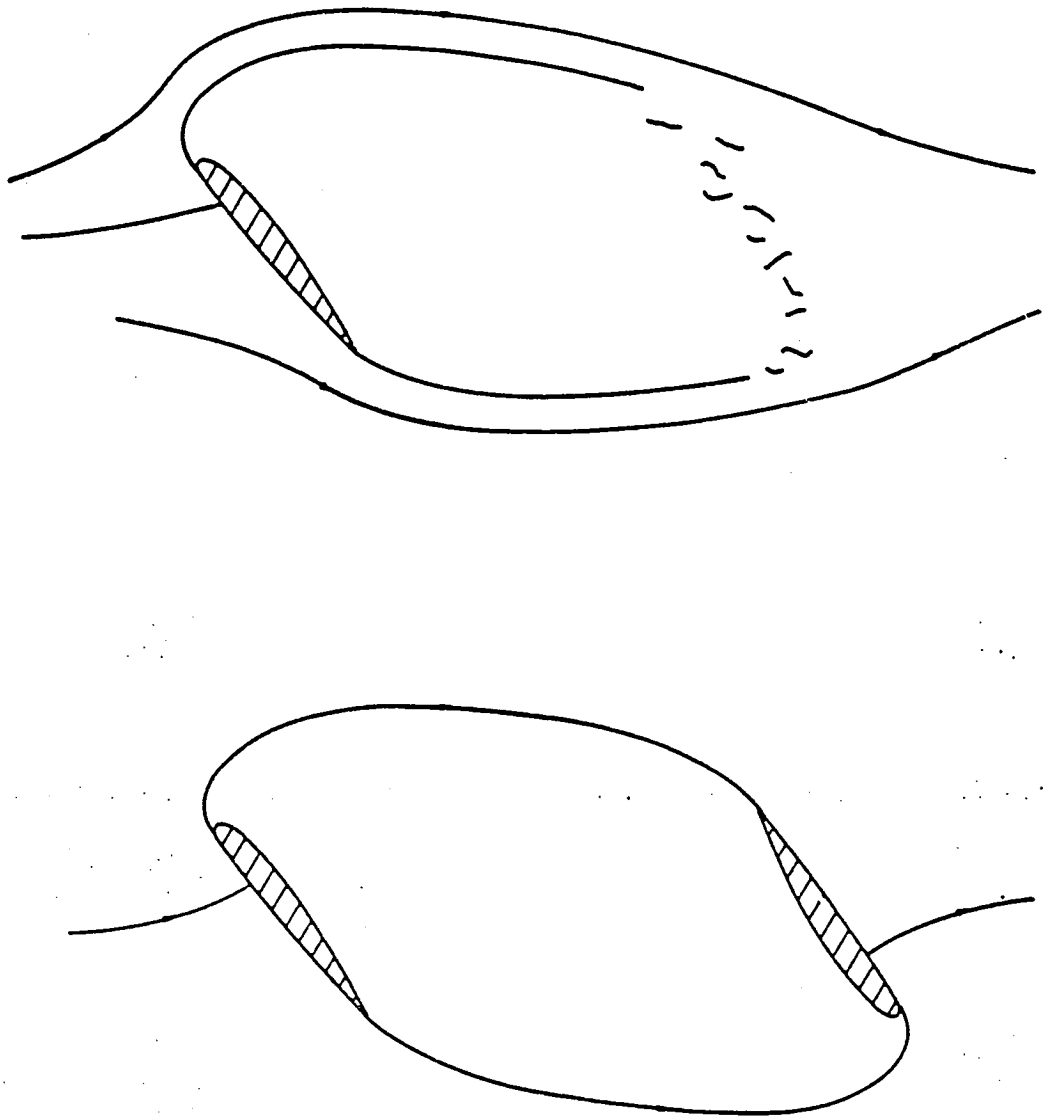

Figure 5-2. Actual Flow Around a Stalled Airfoil Compared with the McCormick Image Model

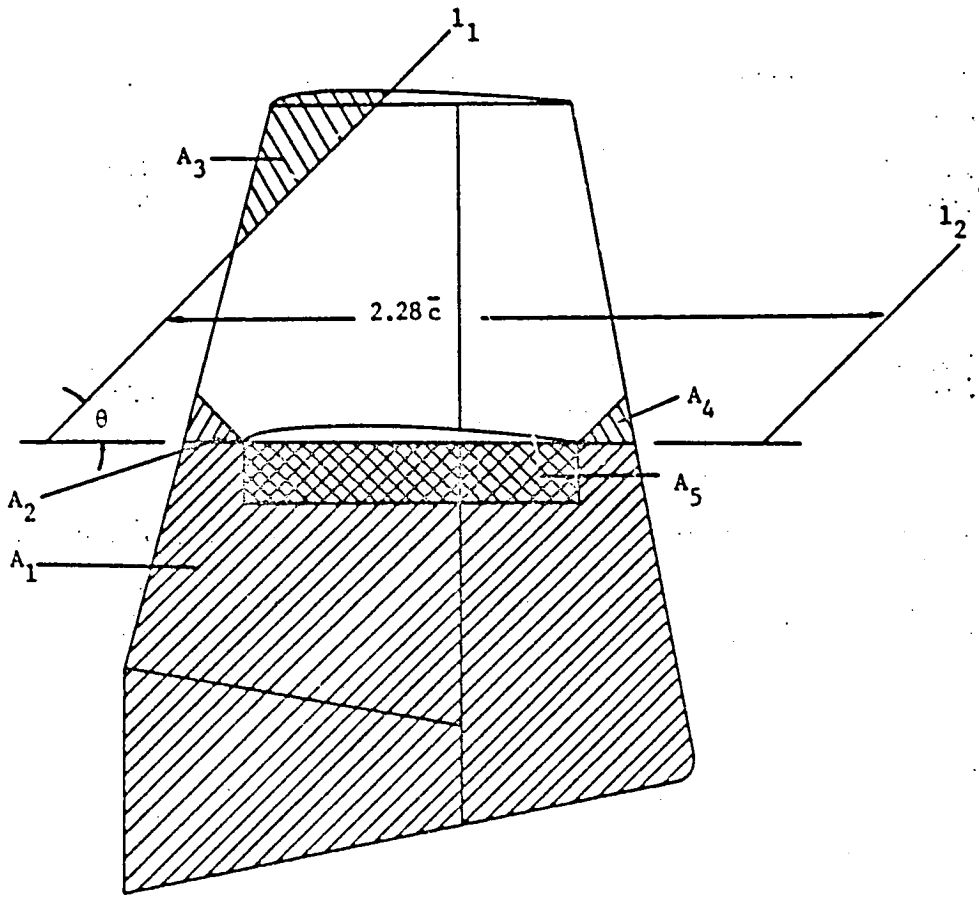

Figure 5-3. Approximation of Unblanketed Vertical Tail Area

The actual dimensions of the high pressure region should be determined experimentally. For the appoxi··ation presented, the height of A_5 was arbitrarily set at $0.1\bar{c}$, and the width was set equal to $\bar{c}$. The resulting coefficient becomes

$$TASP = \frac{A_1L_1 + A_2L_2 + A_3L_3 + A_4L_4 + K_2A_5L_5}{S(b/2)}$$

where L_1 through L_5 represent the distances from the aircraft c.g. to the centroid of each area. The variable K_2 represents the value q_{A_5}/q_{A_1} and must be determined experimentally. A value of 1.2 was used in the following analysis.

Results are presented in Figure 5-4. They show a fair correlation under steep spin conditions, but the relationship breaks down at high spin rates and pitch angles. The major cause for poor correlation is the highly three-dimensional flow which occurs at high spin rates, affecting the shape of the cavity. Results also indicate, even at low pitch angles, that blanketed area is being overestimated. Perhaps the rounded leading edge of the horizontal tail affects the forward shape of the cavity, creating a larger unblanketed vertical tail area. In addition, autorotative effects witnessed in the testing were not accounted for, and aft fuselage shape was not considered.

Better correlation may be obtained by applying some theory estimating the three-dimensional cavity shape formed by the horizontal tail. This would allow parameters AR_h and $S_{h\text{-}tail}$ as well as α_v to be taken into account.

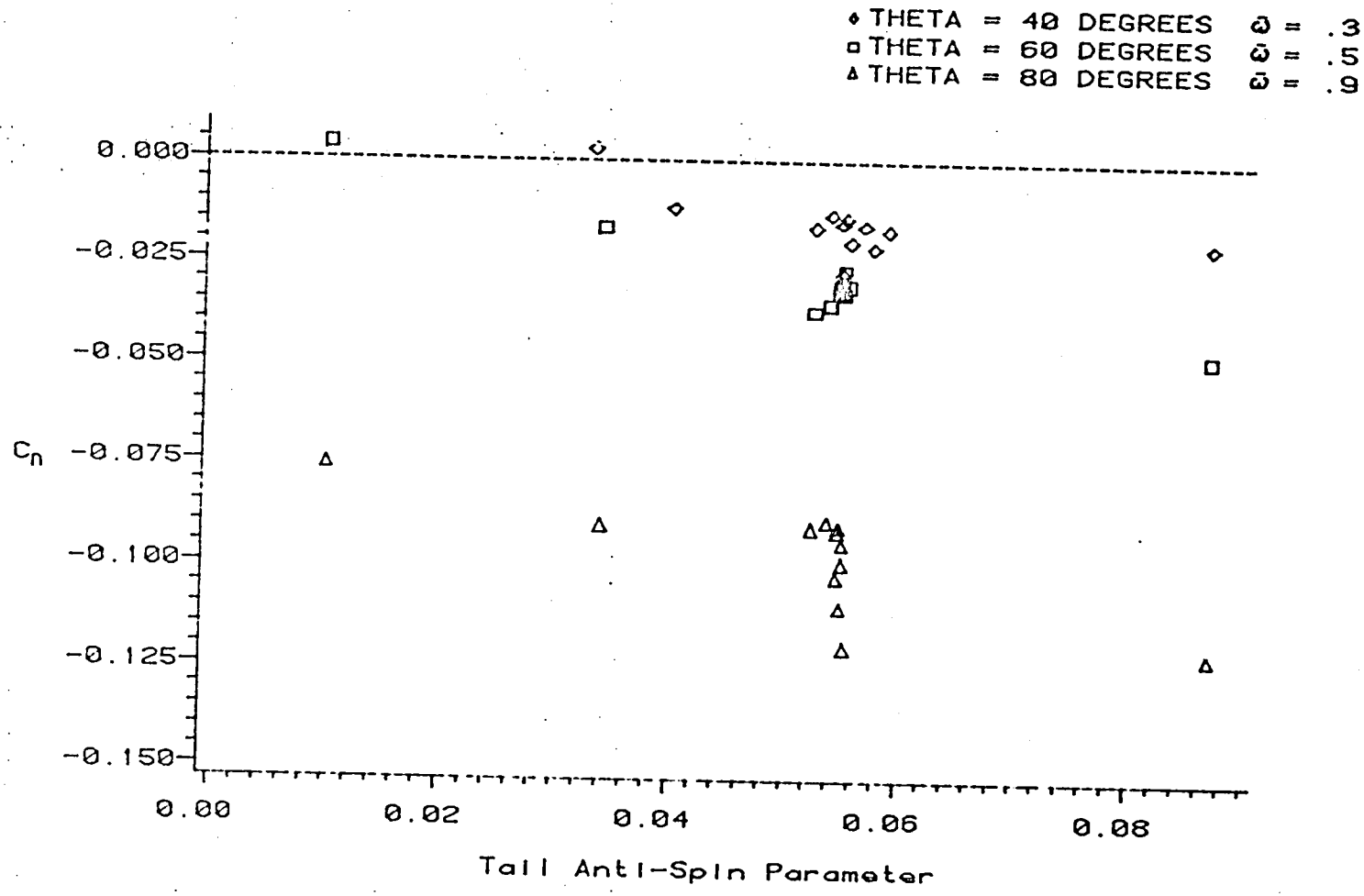

Figure 5-4. Yawing Moment as a Function of Tail Anti-Spin Parameter

CHAPTER VI

CONCLUSIONS AND RECOMMENDATIONS

The present tests have shown the possibility of using conventional wind tunnel testing to obtain information about aerodynamic moments produced by the tail of a spinning airplane. The tests enable tail parametric studies to be performed without influence from a main wing and body, and they allow for intensive studies of the causes of aerodynamic interference from the aft fuselage and horizontal tail. The major conclusions of the present study are summarized below.

1. The tests show satisfactory agreement with NASA rotary balance data, with discrepancies at low pitch angles and spin rates attributable to wing and body interference effects not modelled in the present studies. The influence of a rotational flow field on tail forces is considered to be minimal.

2. The primary parameter influencing spin damping is horizontal tail vertical position. Vertical tail aspect ratio can also have a large yawing effect for high values of AR_v.

3. Horizontal tail aspect ratio has a small effect on spin damping, with a moderately high AR_h inducing larger yawing moments because of reduced vertical tail blanketing.

4. Horizontal tail chordwise position has an appreciable effect on pitching moment, but a small effect on yaw damping. This parameter may be important to aircraft which must break pitch equilibrium for recovery.

5. The rudder is a more effective spin recovery control than the elevator under equilibrium conditions, incrementing yawing moment as much as 50% in some cases. The partial-span rudder configuration displays some advantage under flat spin conditions.

6. Some low horizontal tail configurations can actually produce pro-spin moments under steep spin conditions.

7. To be useful, any parameter developed to predict tail damping characteristics must account for all major interference effects of the horizontal tail, and it will be strongly dependent on the spin rate. A simple tail volume related factor will probably not be usable.

Additional testing of tail parameters to provide data for analytical studies and numerical simulations is highly recommended. Specifically, further study is needed to determine the effect of fuselage shape directly below the horizontal tail on the pro-spin forces encountered at low values of h/b_v. Control effectiveness should be determined for all configurations, with special study of the influence of h/b_v and chordwise position of the horizontal tail on rudder effectiveness. The effect of a partial-span rudder to increase yawing forces at high spin rates should also be thoroughly investigated.

For a satisfactory analytical model of tail forces to be developed, further testing would also be necessary. Tests should be performed which determine the pressure distribution over the vertical tail, particularly in the region below the horizontal tail. Flow measurement and visualization would also be helpful in the development of a three-dimensional cavity model, which is necessary to accurately predict the effect of tail configuration on yawing moment under flat spin conditions.

REFERENCES

1. Ballin, Mark G. and Zilliac, Gregory G., "Report on the Condition of the Low-Speed Wind Tunnel." (Interdepartmental report, Department of Aerospace Engineering, The Pennsylvania State University, 1980.)

2. Beaurain, L., "General Study of Light Plane Spin, Aft Fuselage Geometry, Part 1," NASA Technical Translation TTF-17,446. Washington, D.C.: Government Printing Office, 1977.

3. Bihrle, William, Jr., Hultberg, Randy S., and Mulcay, William, "Rotary Balance Data for a Typical Single-Engine, Low Wing General Aviation Design for an Angle-of-Attack Range of 30° to 90°," NASA Contractor Report 2972. Washington, D.C.: Government Printing Office, 1978.

4. Bihrle, William, Jr., and Barnhart, William, "Spin Prediction Techniques," AIAA Paper 80-1564. New York: American Institute of Aeronautics and Astronautics, 1980.

5. Bowman, James S., Jr., "Summary of Spin Technology as related to Light General-Aviation Airplanes," NASA Technical Note D-6575. Washington, D.C.: Government Printing Office, 1971.

6. Burk, Sanger M., Jr., Bowman, James S., Jr., and White, William L., "Spin-Tunnel Investigation of the Spinning Characteristics of Typical Single-Engine General Aviation Airplane Designs, I - Low-Wing Model A: Effects of Tail Configurations," NASA Technical Paper 1009. Washington, D.C.: Government Printing Office, 1977.

7. Burns, B.R.A., "Going for a Spin - Fighter Style." Flight International, April 8, 1978, pp. 985-989.

8. Chambers, Joseph R., "Overview of Stall/Spin Technology," AIAA Paper 80-1580. New York: American Institute of Aeronautics and Astronautics, 1980.

9. Grunwald, Kalman J., "Wall Effects and Scale Effects in V/STOL Model Testing." AIAA Aerodynamics Testing Conference, March 9-10, 1964. New York: American Institute of Aeronautics and Astronautics, 1964.

10. Heyson, Harry H., "Linearized Theory of Wind Tunnel Jet Boundary Corrections and Ground Effect for VTOL-STOL Aircraft," NASA Technical Report R-124. Washington, D.C.: Government Printing Office, 1962.

11. Heyson, Harry H., "Rapid Estimation of Wind Tunnel Corrections with Application to Wind Tunnel Model Design," NASA Technical Note D-6416. Washington, D.C.: Government Printing Office, 1971.

12. McCormick, Barnes W., Aerodynamics of V/STOL Flight. New York: Academic Press, 1967.

13. McCormick, Barnes W., Aerodynamics, Aeronautics, and Flight Mechanics. New York: John Wiley and Sons, 1979.

14. McCormick, Barnes W., "Equilibrium Spinning of a Typical Single-Engine Low-Wing Aircraft," AIAA Paper 81-4076. New York: American Institute of Aeronautics and Astronautics, 1981.

15. Neihouse, Anshal I., "Tail Design Requirements for Satisfactory Spin Recovery for Personal Owner Type Light Airplanes," NACA Technical Note 1329. Washington, D.C.: Government Printing Office, 1947.

16. Neihouse, Anshal I., Lichtenstein, Jacob H., and Pepoon, Philip W., "Tail Design Requirements for Satisfactory Spin Recovery," NACA Technical Note 1045. Washington, D.C.: Government Printing Office, 1946.

17. Neihouse, Anshal I., Klinar, Walter J., and Scher, Stanley H., "Status of Spin Research for Recent Airplane Designs," NASA Technical Report R-57. Washington, D.C.: Government Printing Office, 1960.

18. Polhamus, Edward C., "Effect of Flow Incidence and Reynolds Number on Low-Speed Aerodynamic Characteristics of Several Non-Circular Cylinders with Application to Directional Stability and Spinning," NASA Technical Note 4176. Washington, D.C.: Government Printing Office, 1958.

19. Pope, Alan, Wind Tunnel Testing, 2nd ed. New York: John Wiley and Sons, 1954.

20. Scher, Stanley H., "An Analytical Investigation of Airplane Spin-Recovery Motion by Use of Rotary Balance Aerodynamic Data," NACA Technical Note 3188. Washington, D.C.: Government Printing Office, 1954.

21. Stough, H.P., III, and Patton, J.M., Jr., "The Effects of Configuration Changes on Spin and Recovery Characteristics of a Low-Wing General Aviation Research Airplane," AIAA Paper 79-1786. New York: American Institute of Aeronautics and Astronautics, 1979.

22. Torenbeek, Egbert, Synthesis of Subsonic Airplane Design. Rotterdam: Delft University Press, 1976.

APPENDIX A
MODEL AND APPARATUS DIMENSIONS AND CONFIGURATIONS

Table A-1

Configuration Dimensions

Configuration	b_v (in)	b_h (in)	S_v (in^2)	S_h (in^2)	AR_v	AR_h	$\Lambda_{v_{L.E.}}$ (°)	Hinge Position, $\bar{z}_c$ Rudder	Hinge Position, $\bar{z}_c$ Elevator	h/b_v	Tailplane Chordwise Position
A	7.5	20	37.5	100	1.5	4.0	15.0	60	60	0.5	Neutral
B	7.5	20	37.5	100	1.5	4.0	15.0	60	60	1.0	Neutral
C	7.5	20	37.5	100	1.5	4.0	15.0	60	60	0.25	Neutral
D	7.5	20	37.5	100	1.5	4.0	15.0	60	60	0	Neutral
E	7.5	20	37.5	100	1.5	4.0	15.0	60	60	0.5	20% Forward
F	7.5	20	37.5	100	1.5	4.0	15.0	60	60	0.5	20% Aft
G	5.5	20	27.5	100	1.1	4.0	20.0	60	60	0.5	Neutral
H	6.5	20	32.5	100	1.3	4.0	17.0	60	60	0.5	Neutral
J	8.5	20	42.5	100	1.7	4.0	12.5	60	60	0.5	Neutral
K	7.5	19.3	37.5	107.1	1.5	3.48	15.0	60	60	0.5	Neutral
L	7.5	20.8	37.5	93.75	1.5	4.62	15.0	60	60	0.5	Neutral
M	7.5	21.8	37.5	88.23	1.5	5.40	15.0	60	60	0.5	Neutral

All Configurations - $\lambda_v = 0.5$, $\lambda_h = 1.0$, $t/c = .12$ for all surfaces, $\Lambda_{v(c/2)} = 0$, $\Lambda_h = 0$

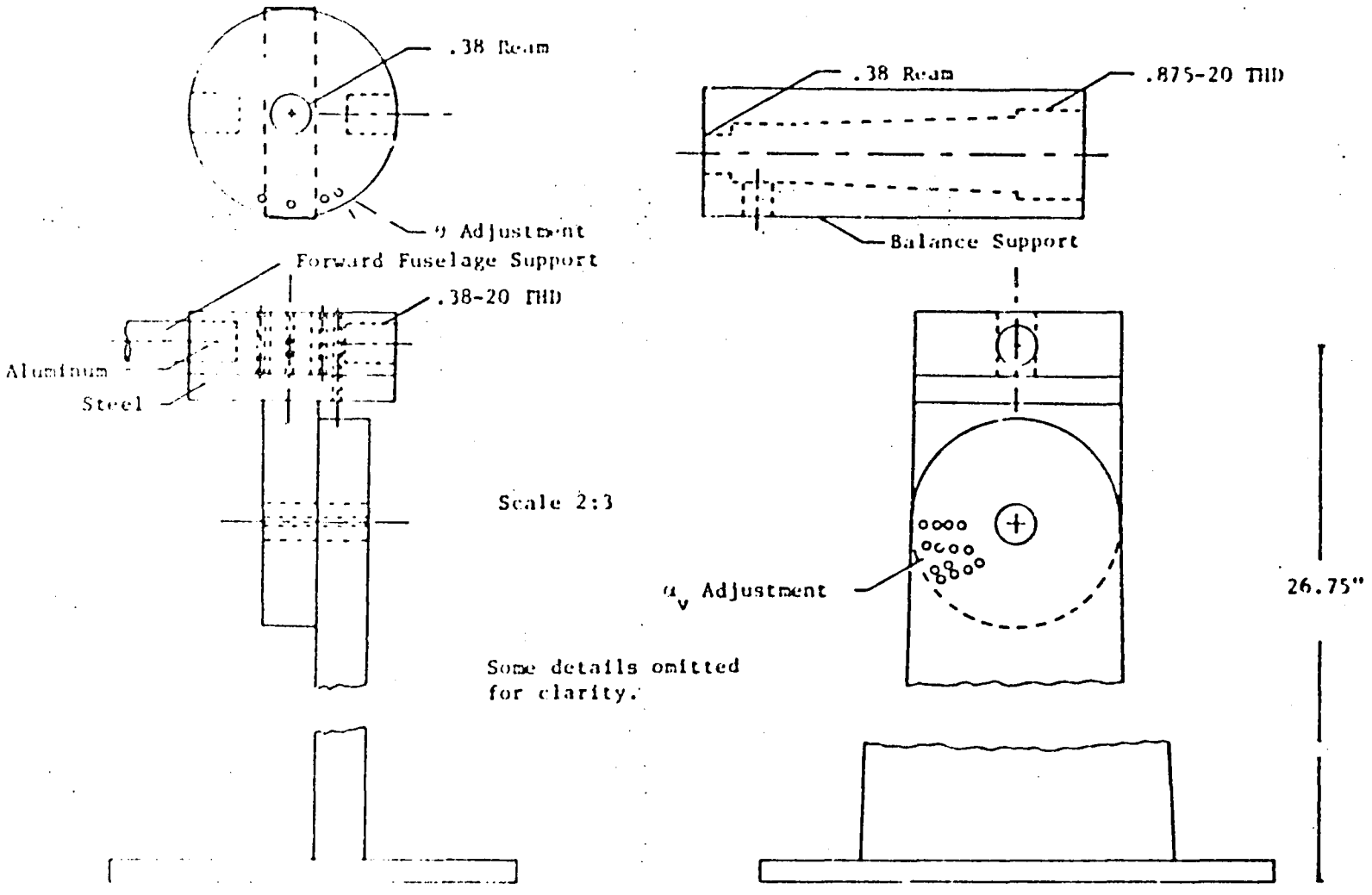

Figure A-1. Orienting Support and Strut

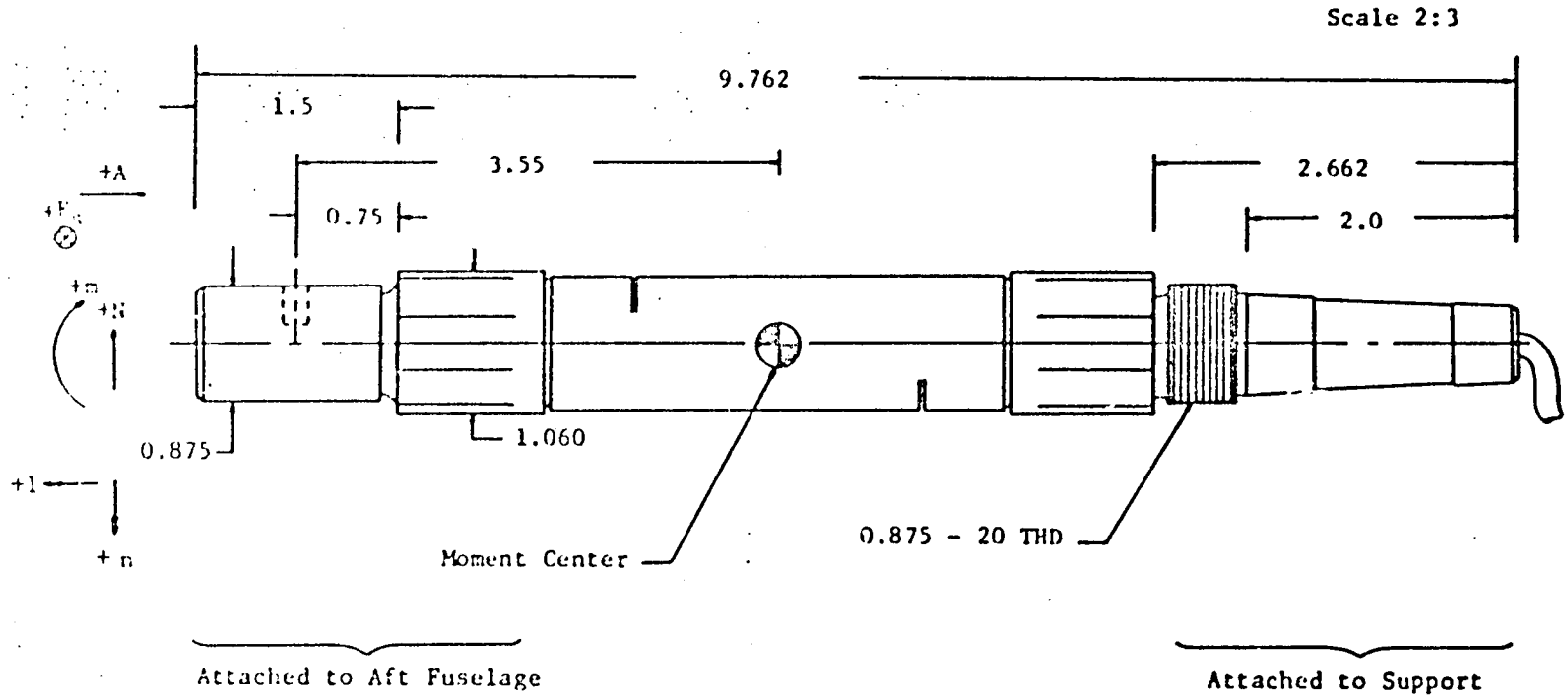

Figure A-2. NASA IR-21 Balance

Scale 2:3

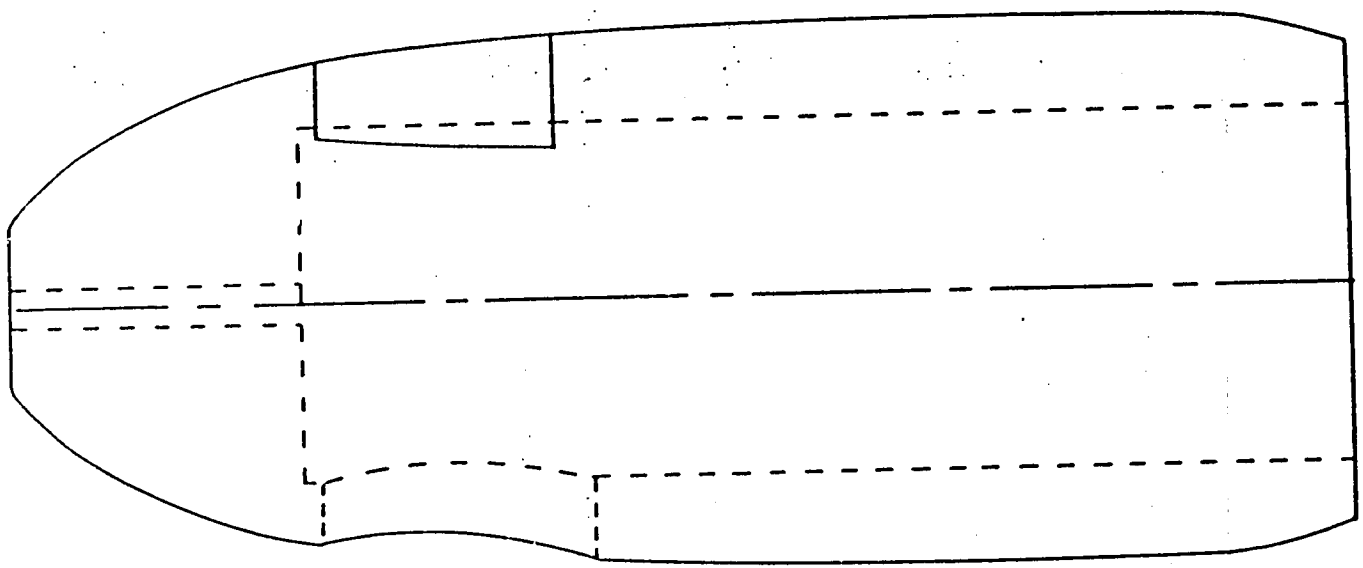

Figure A-3. Forward Body

APPENDIX B
AERODYNAMIC MOMENT COEFFICIENTS AS FUNCTIONS OF SPIN RATE

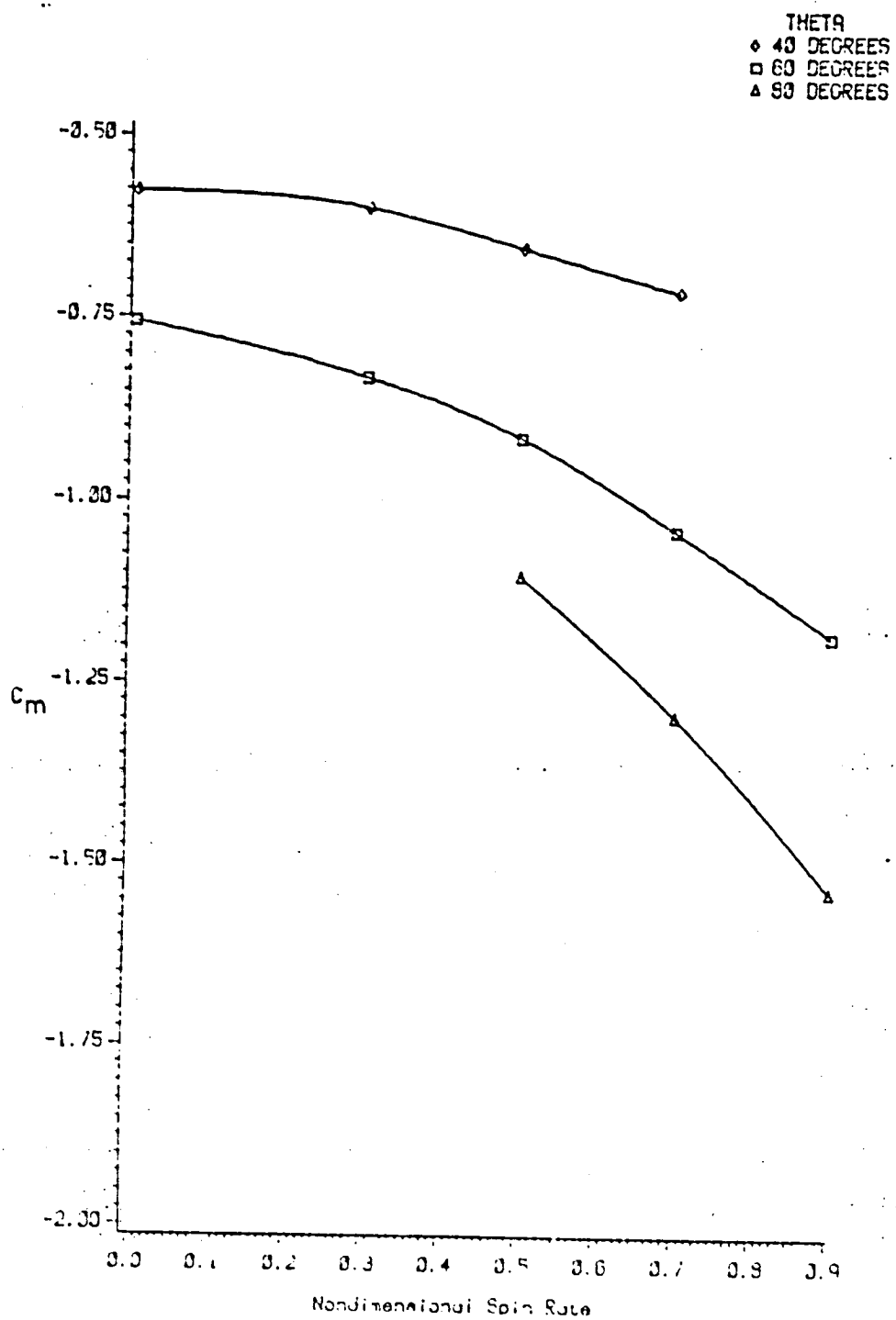

Figure B-1. Pitching Moment as a Function of θ and $\bar{\omega}$, Configuration A

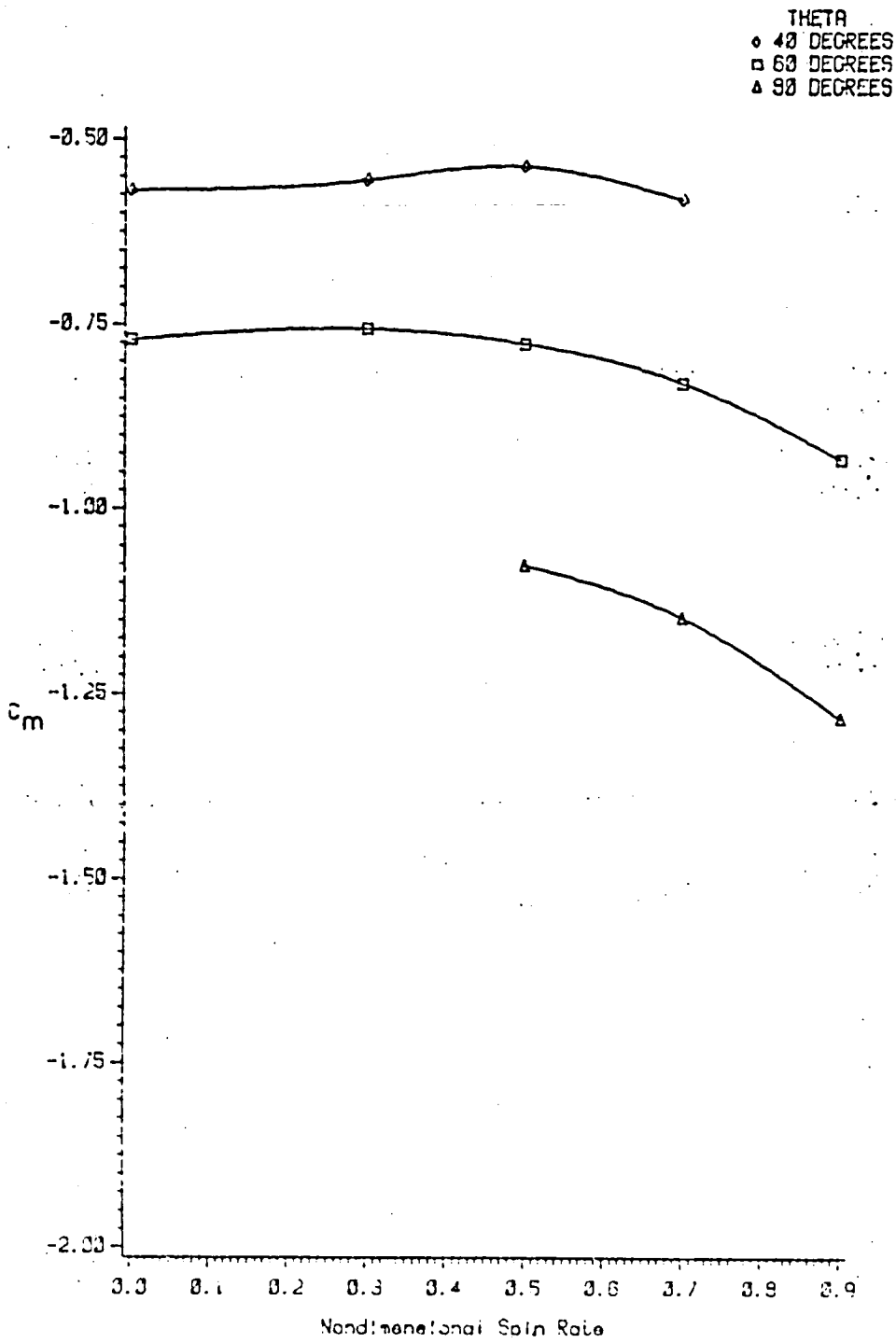

Figure B-2. Pitching Moment as a Function of θ and $\bar{\omega}$, Configuration B

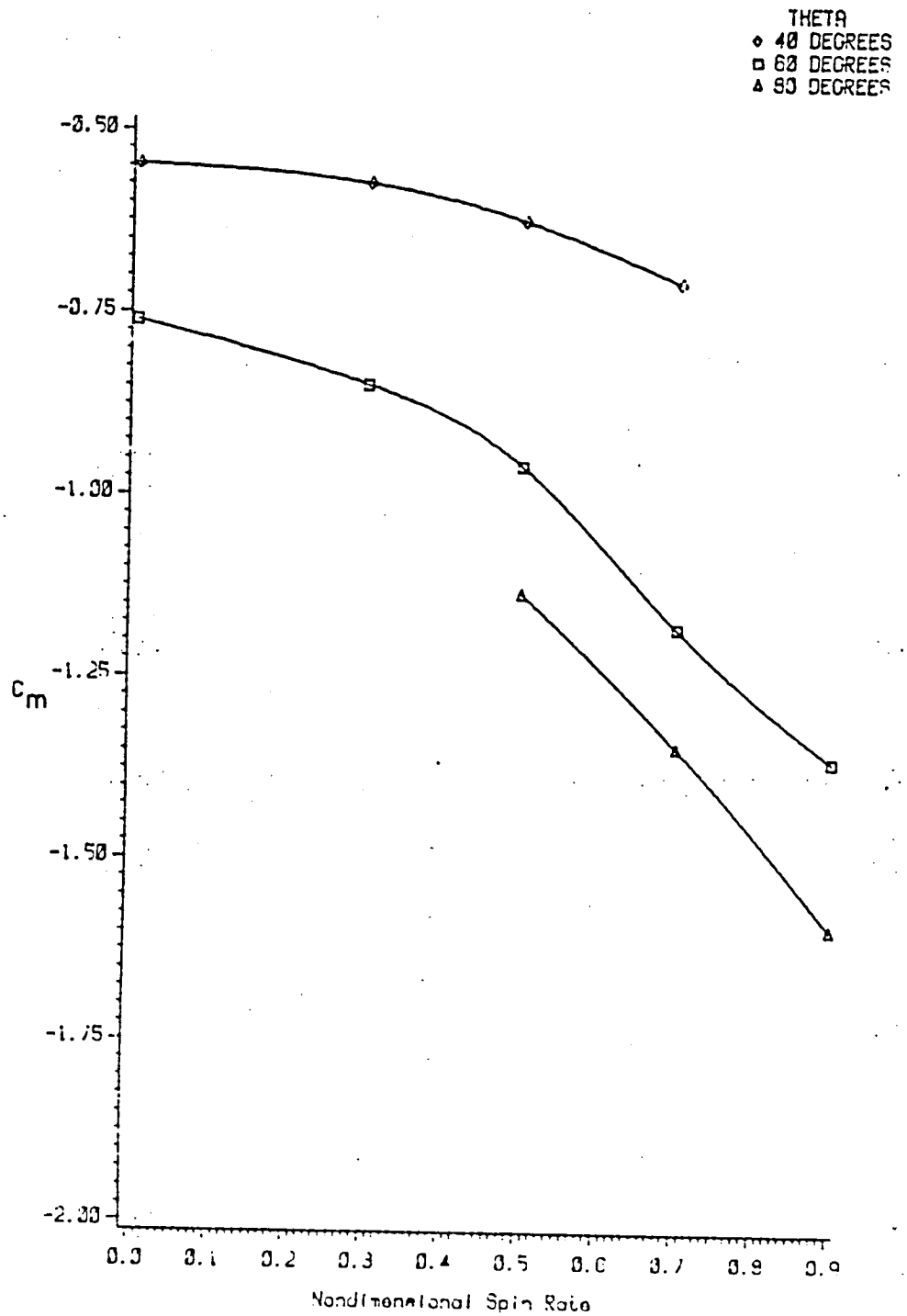

Figure B-3. Pitching Moment as a Function of θ and $\bar{\omega}$, Configuration C

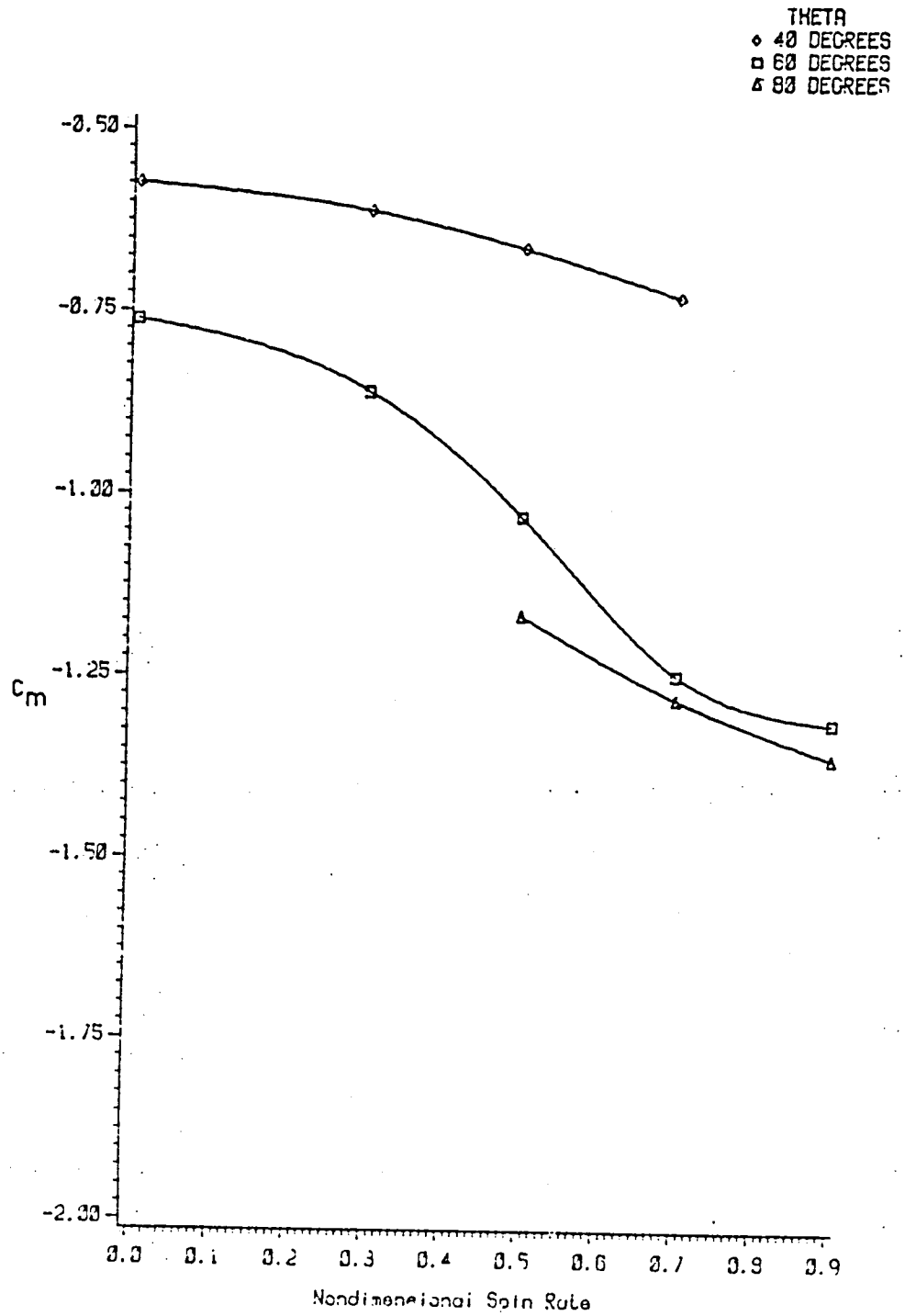

Figure B-4. Pitching Moment as a Function of θ and $\bar{\omega}$, Configuration D

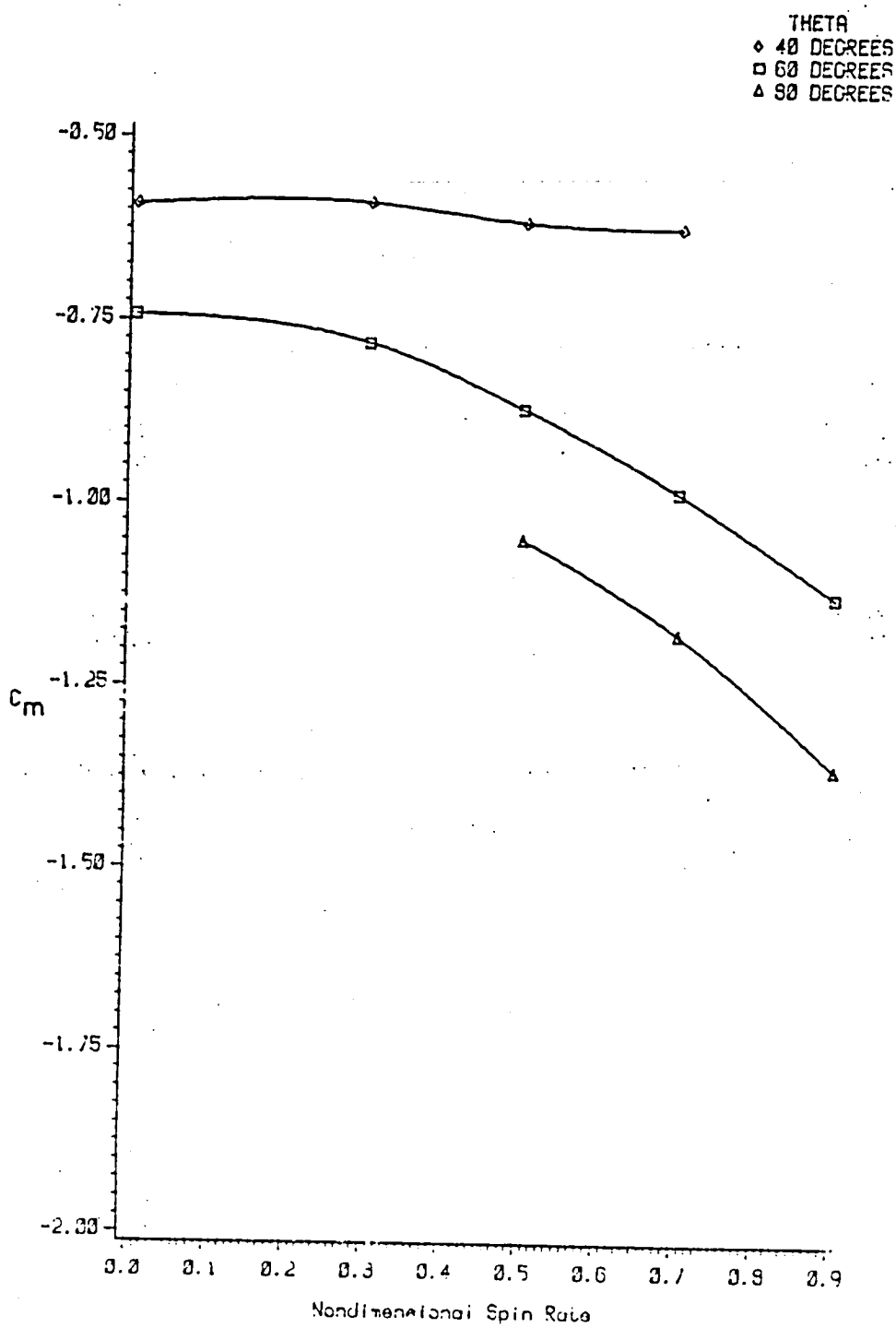

Figure B-5. Pitching Moment as a Function of θ and $\bar{\omega}$, Configuration E

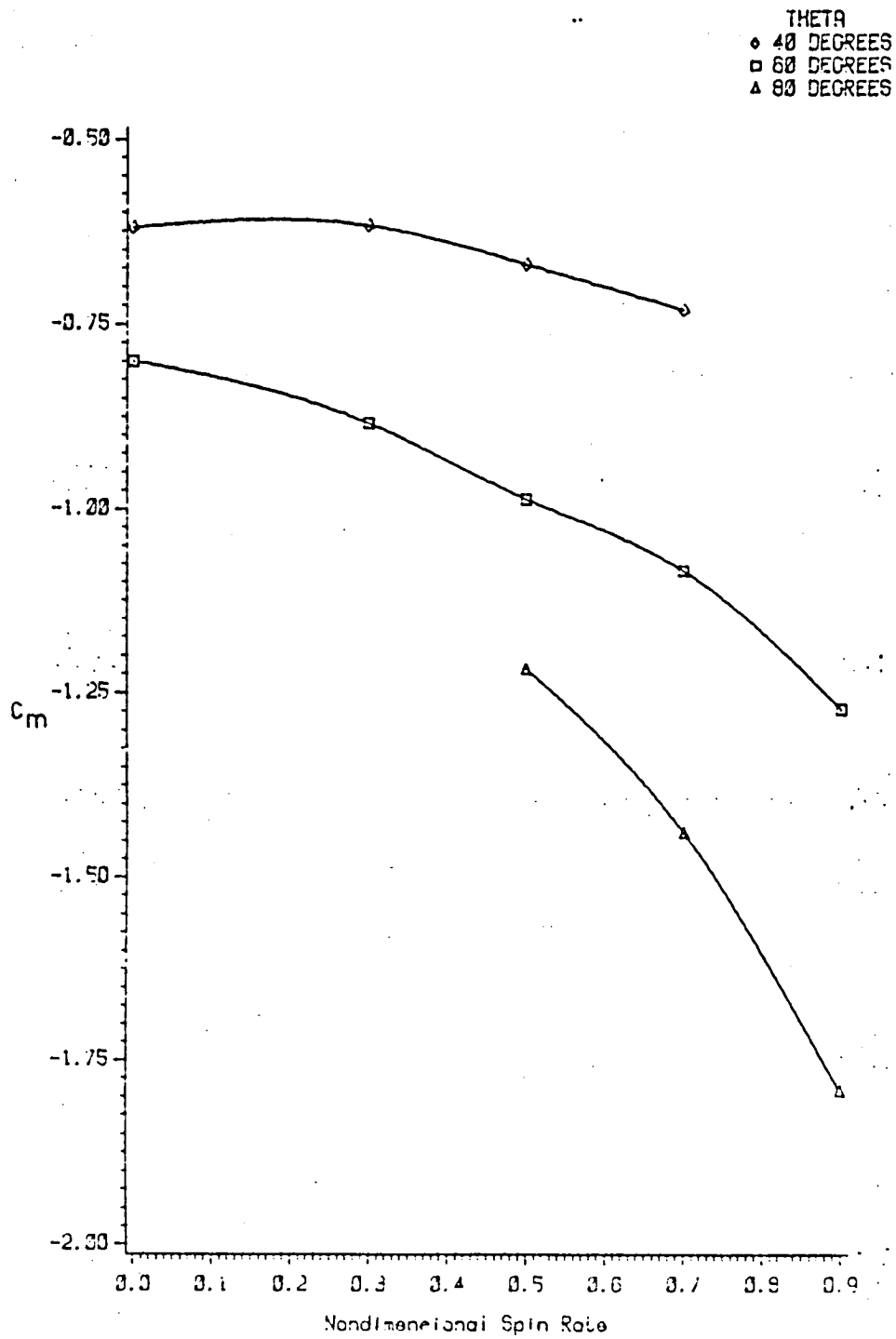

Figure B-6. Pitching Moment as a Function of θ and $\bar{\omega}$, Configuration F

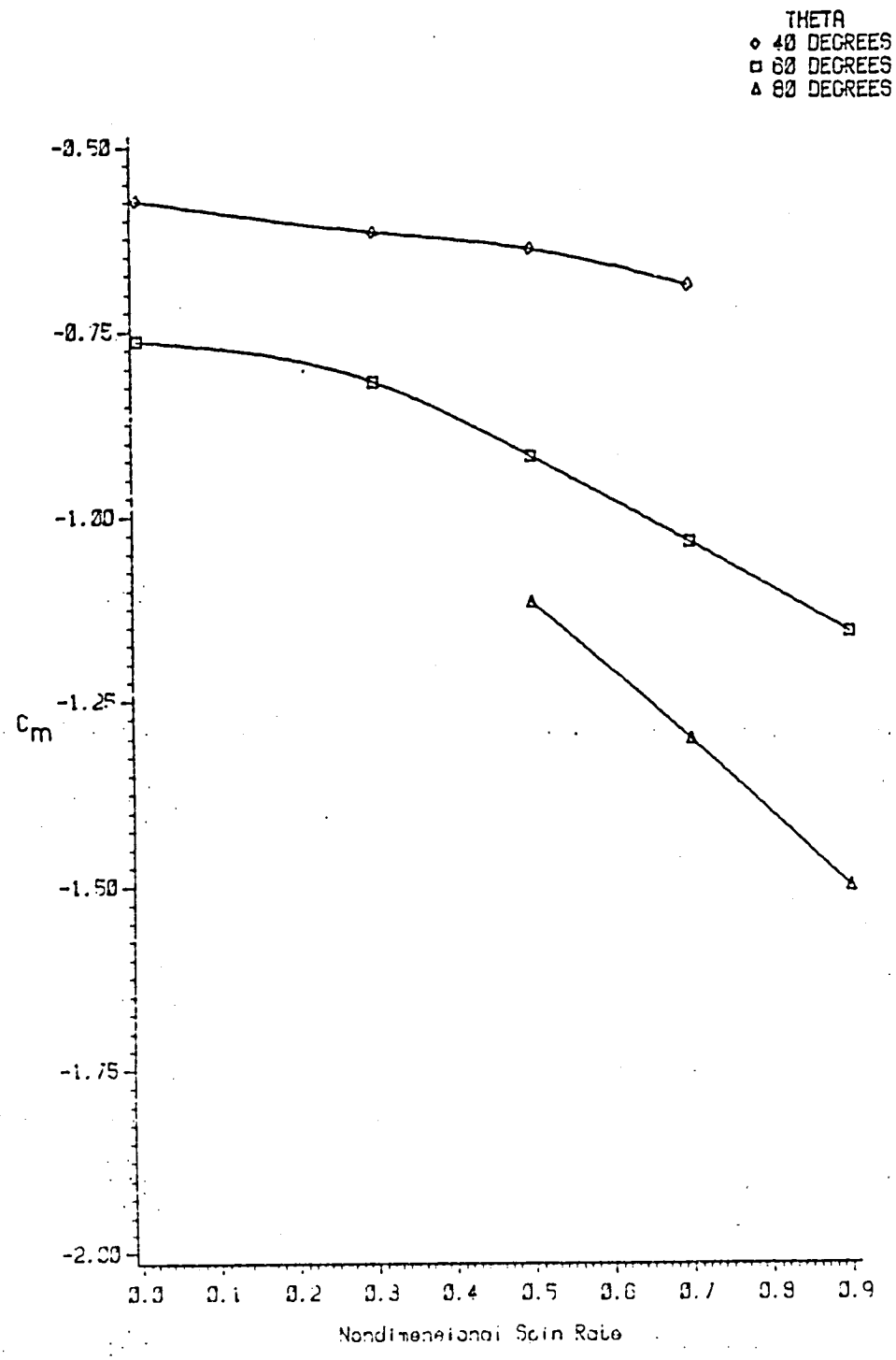

Figure B-7. Pitching Moment as a Function of θ and $\bar{\omega}$, Configuration G

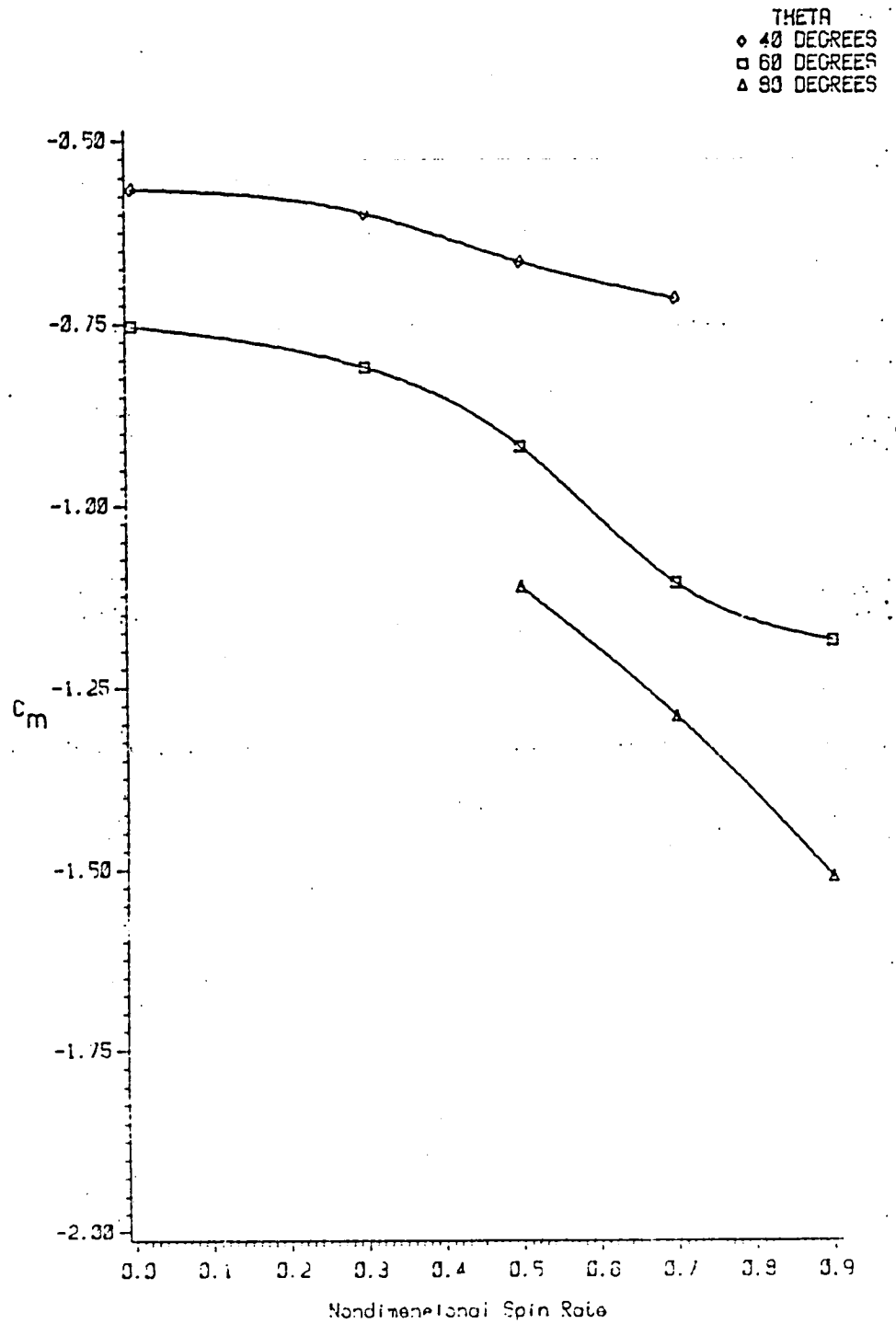

Figure B-8. Pitching Moment as a Function of θ and $\bar{\omega}$, Configuration H

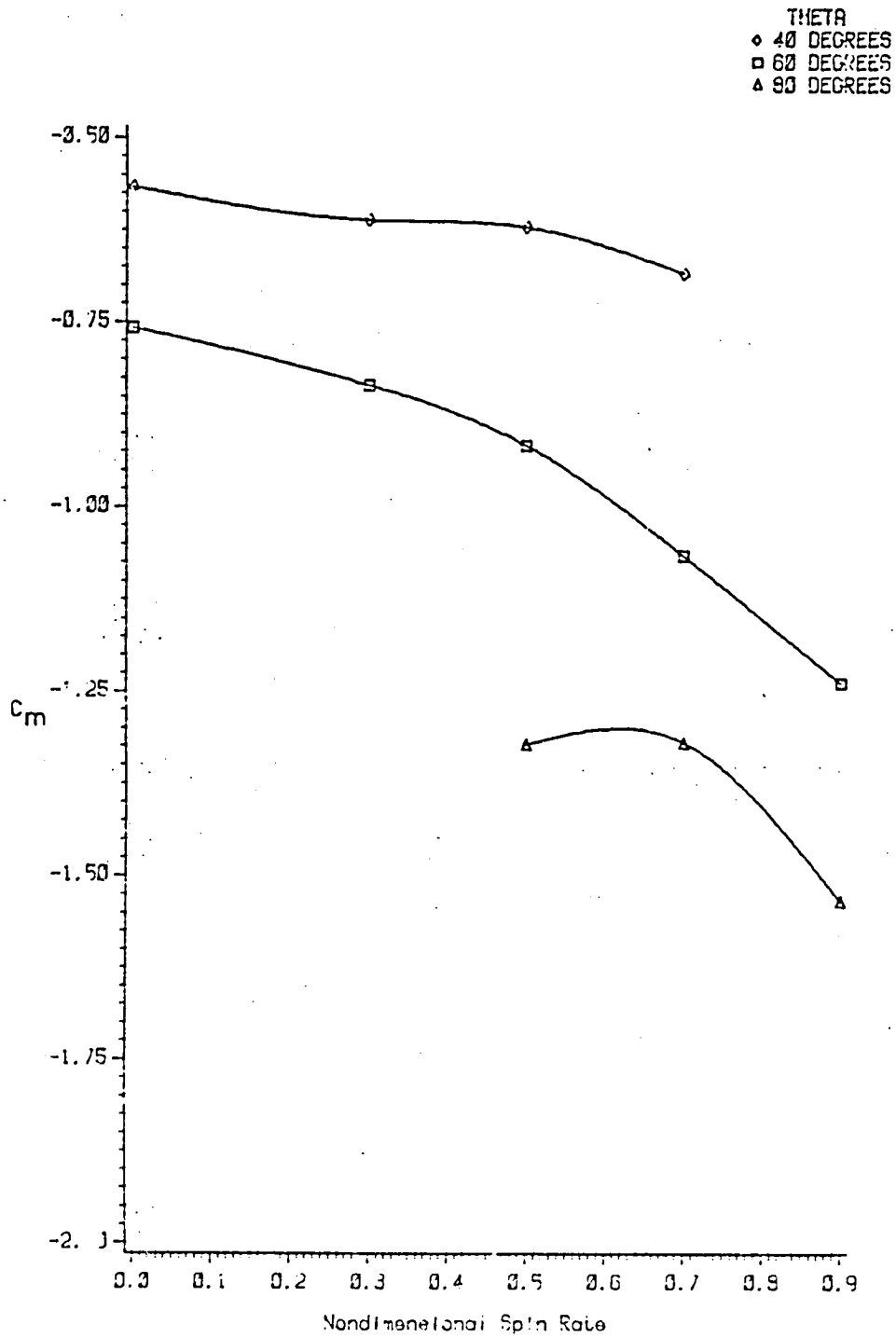

Figure B-9. Pitching Moment as a Function of θ and $\bar{\omega}$, Configuration J

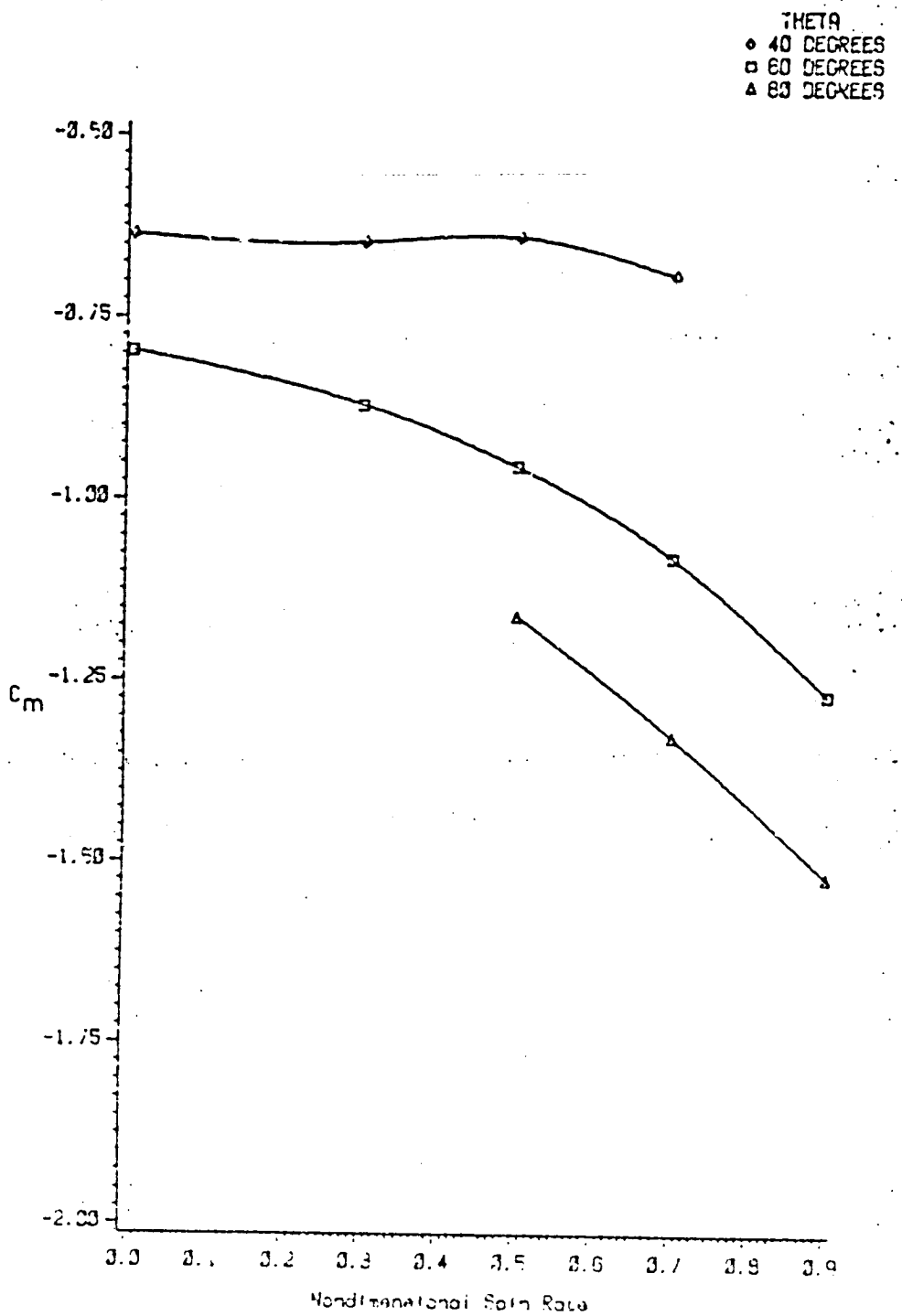

Figure B-10. Pitching Moment as a Function of θ and $\bar{\omega}$, Configuration K

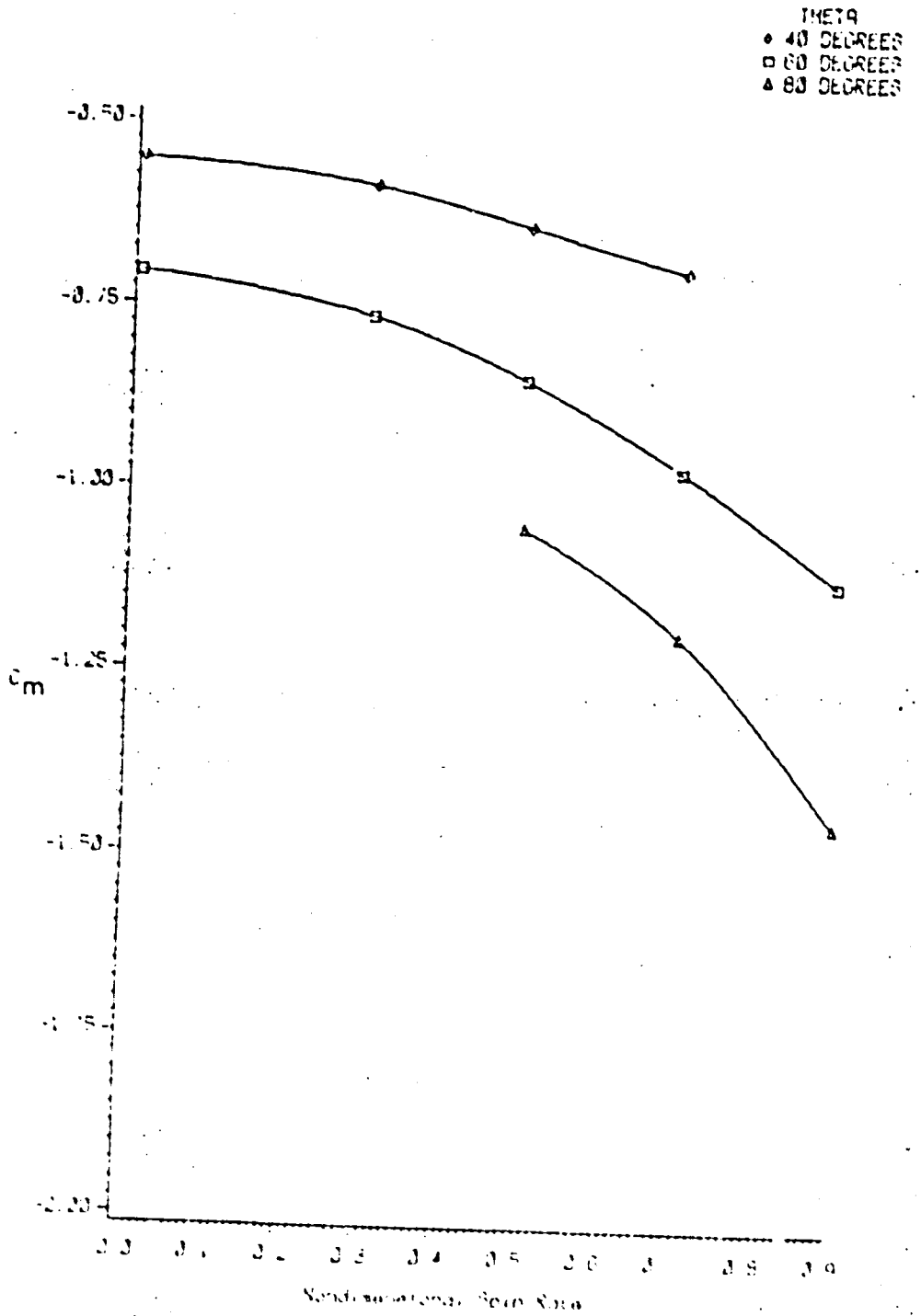

Figure 8-11. Pitching Moment as a Function of α and δ_e, Configuration 1.

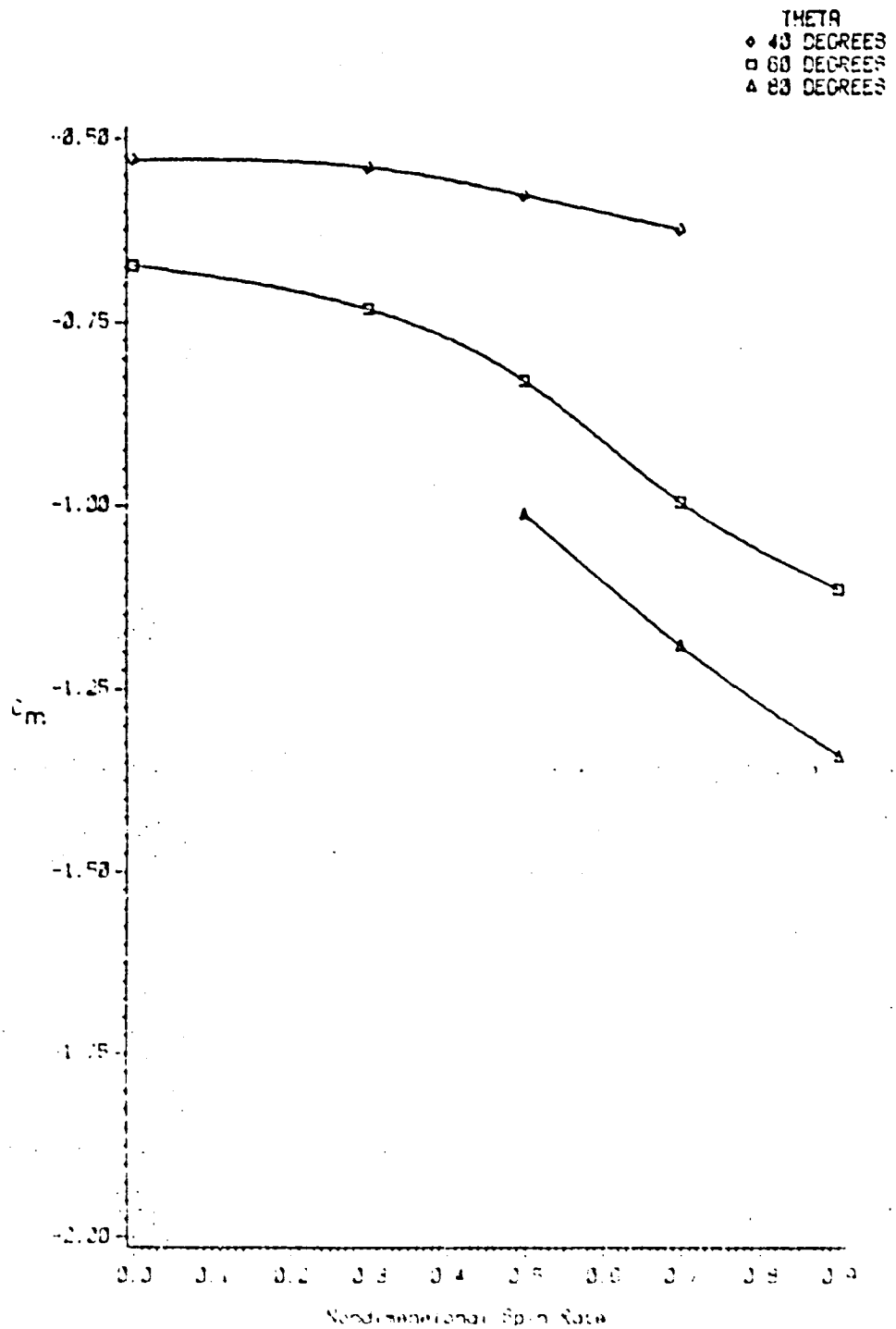

Figure B-12. Pitching Moment as a Function of θ and $\bar{\omega}$, Configuration M

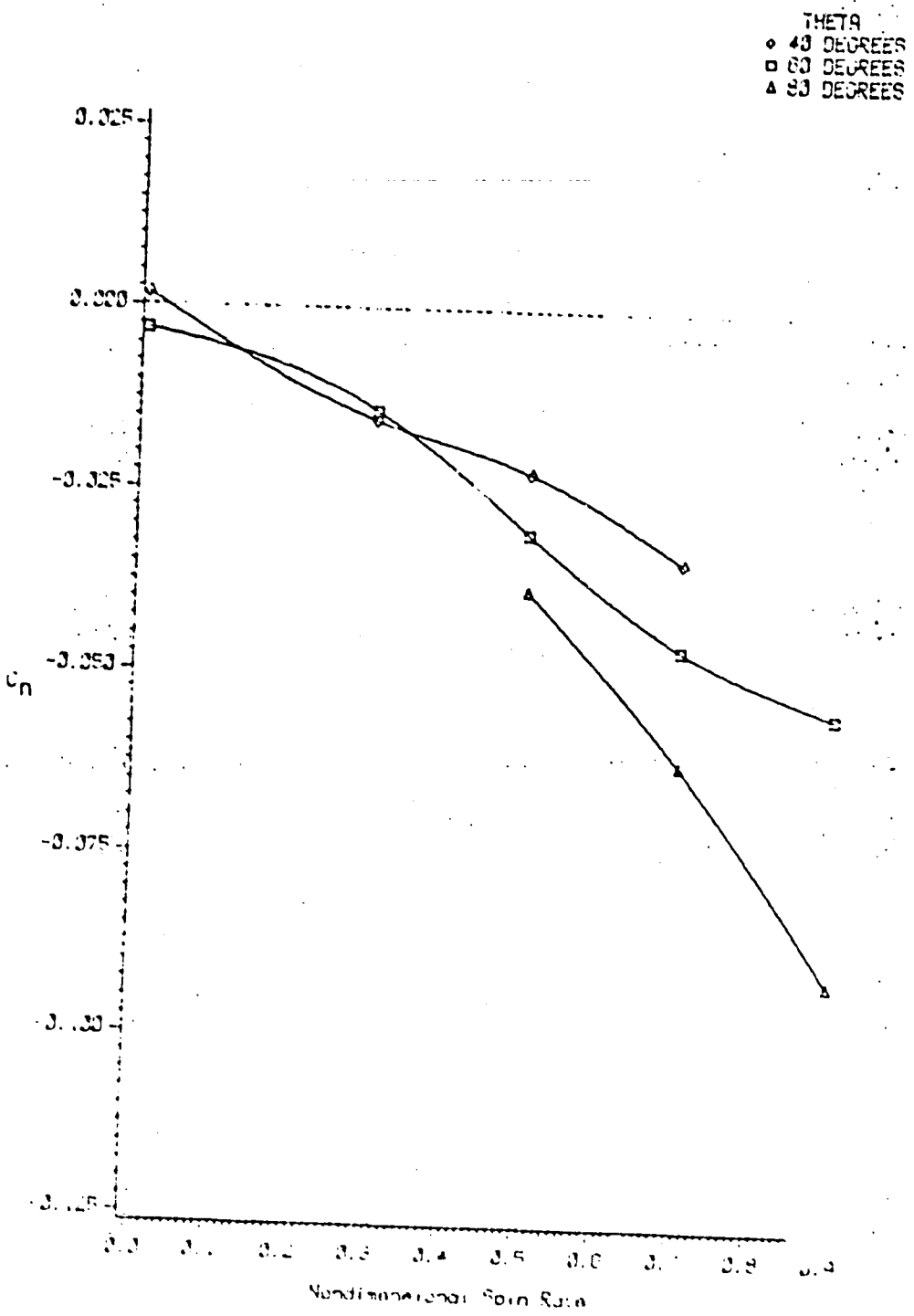

Figure B-13. Yawing Moment as a Function of θ and $\bar{\omega}$, Configuration A

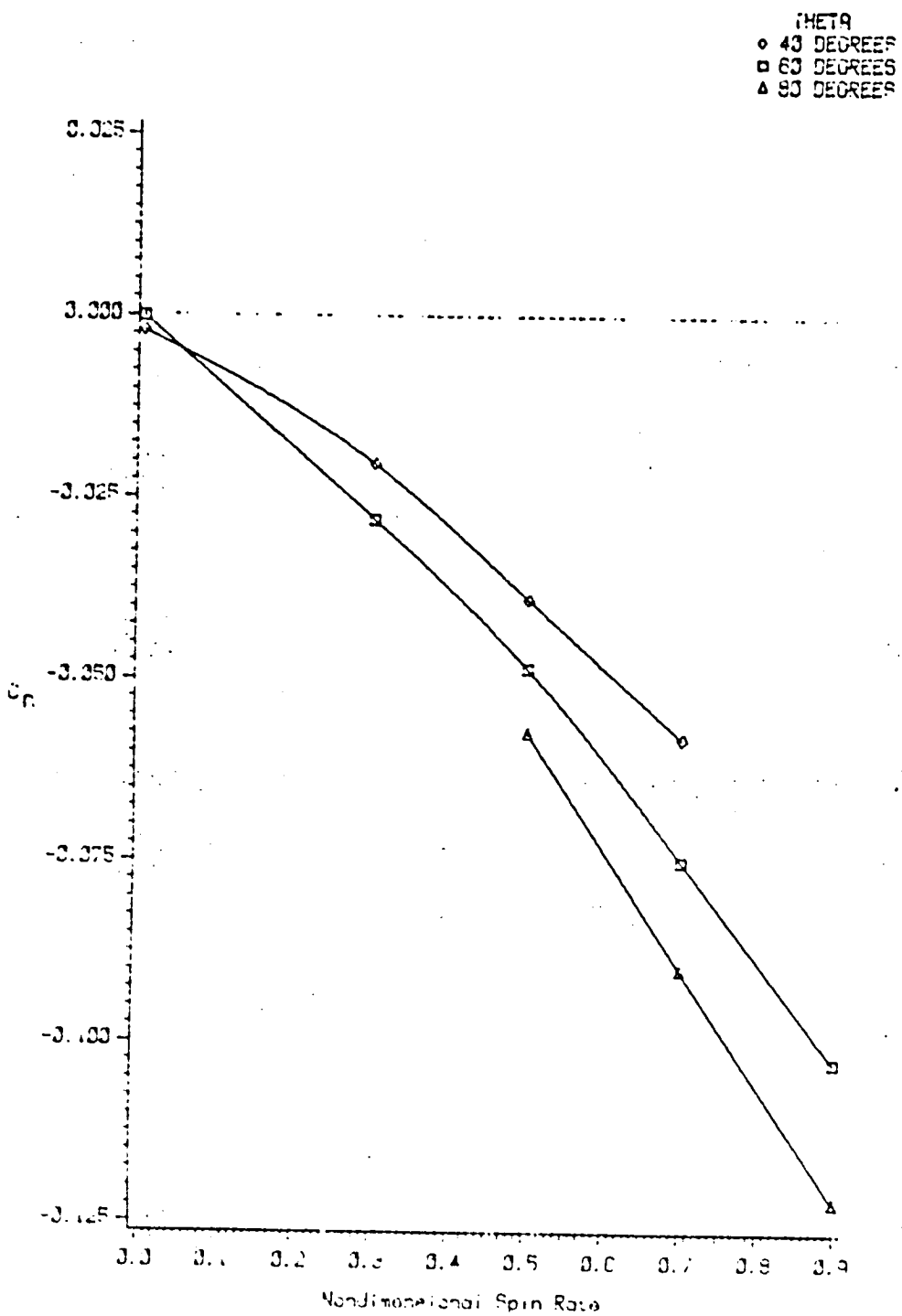

Figure B-14. Yawing Moment as a Function of θ and $\bar{\omega}$, Configuration B

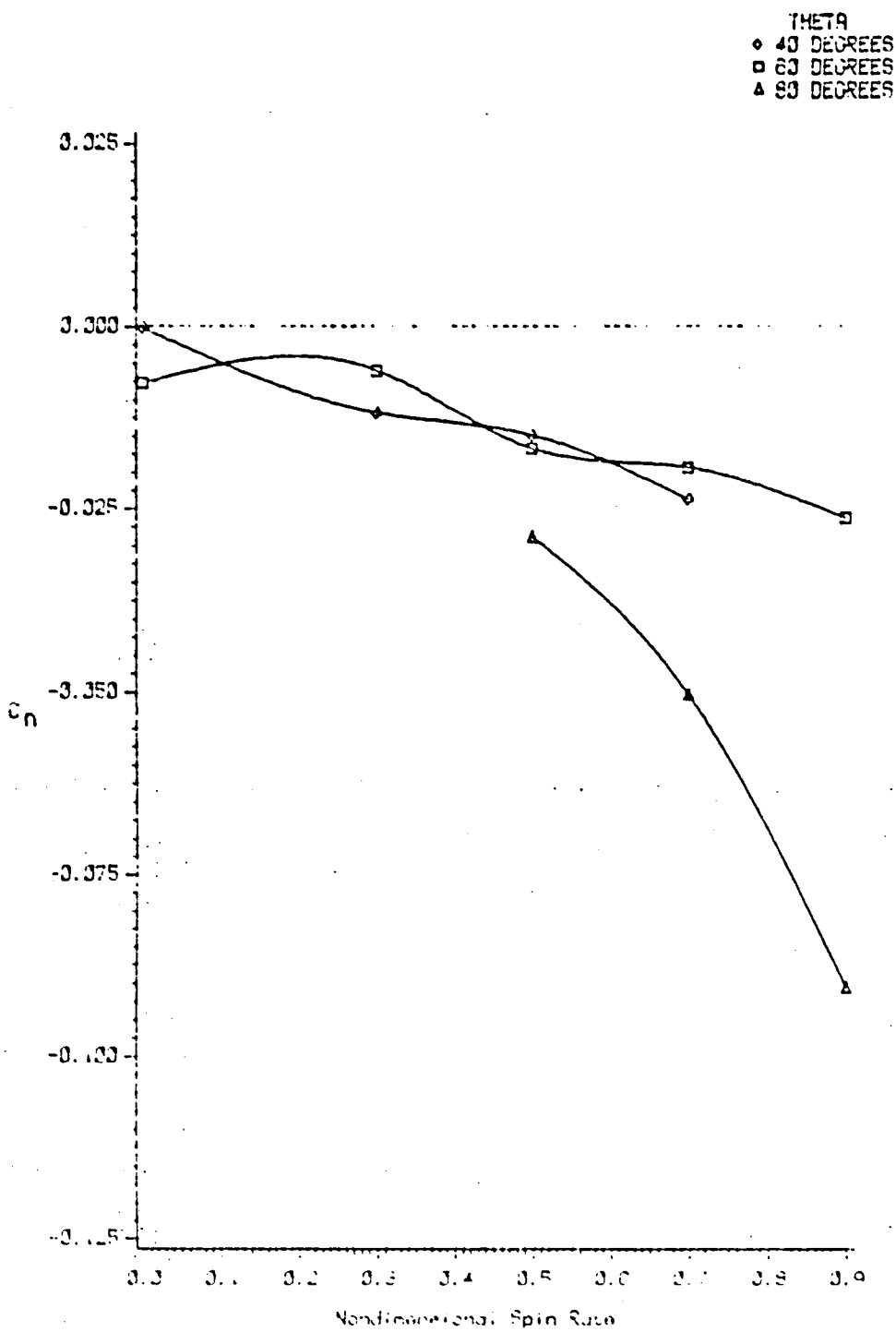

Figure B-15. Yawing Moment as a Function of θ and $\bar{\omega}$, Configuration C

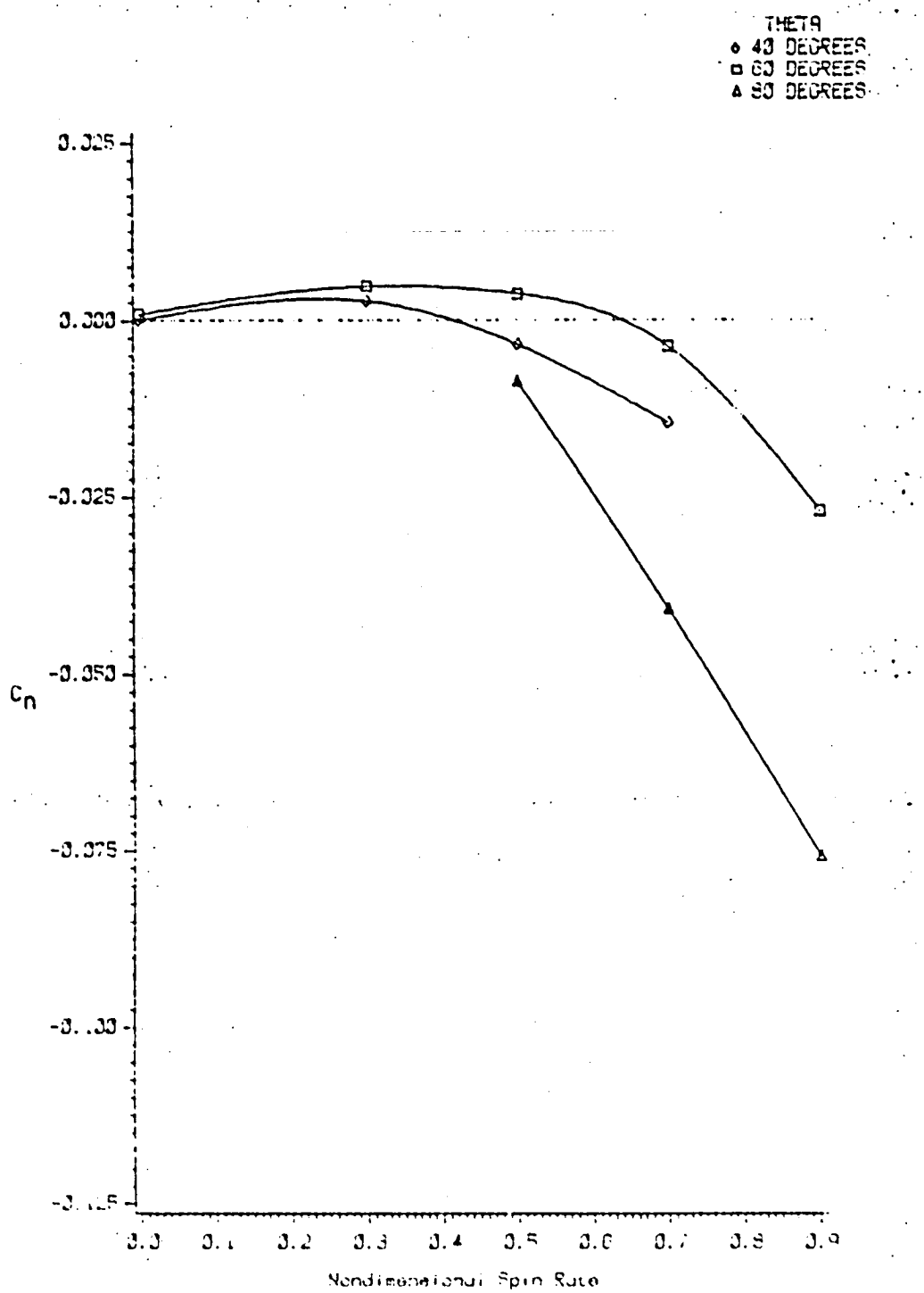

Figure B-1b. Yawing Moment as a Function of θ and $\bar{\omega}$, Configuration D

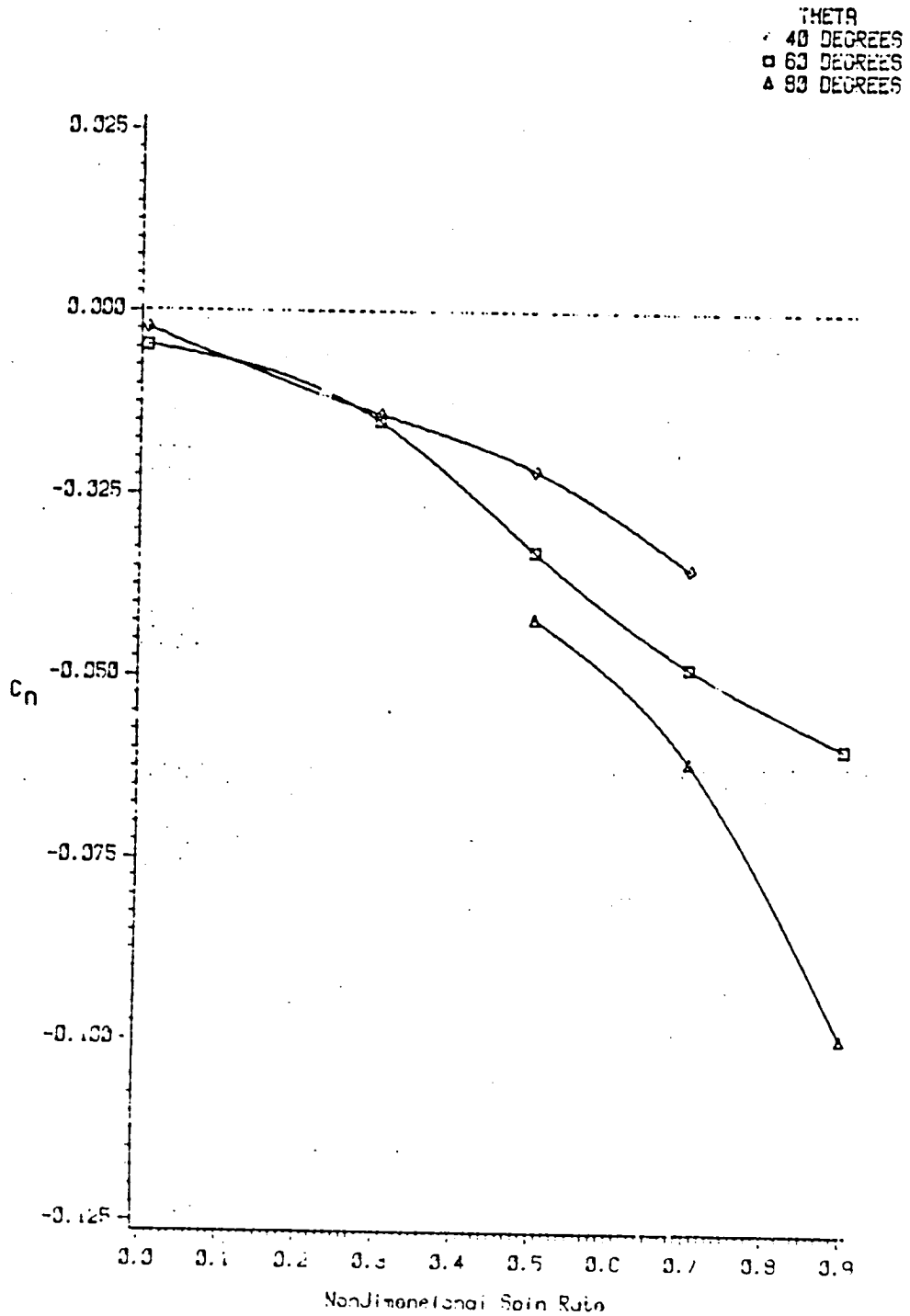

Figure B-17. Yawing Moment as a Function of θ and $\bar{\omega}$, Configuration E

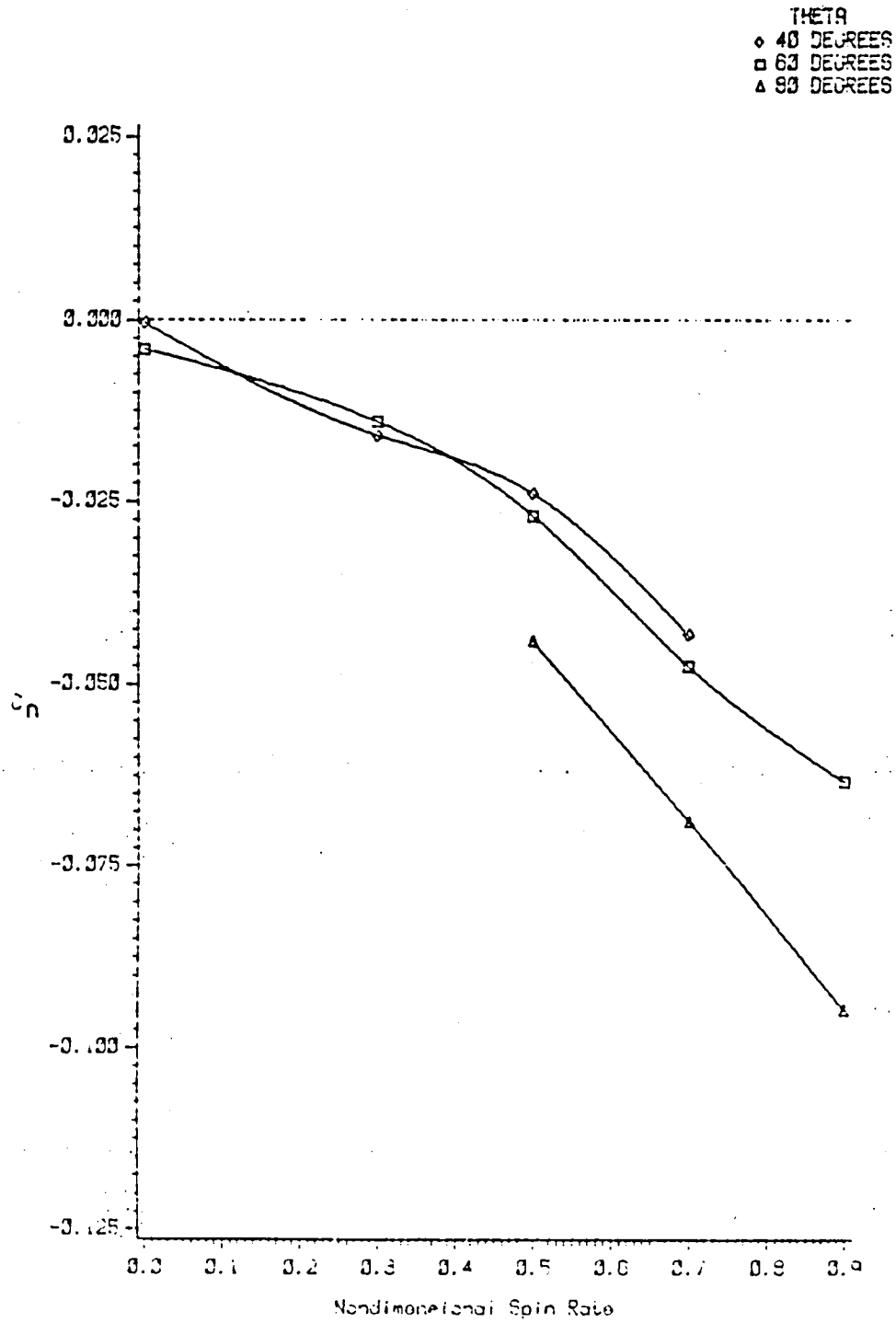

Figure B-18. Yawing Moment as a Function of θ and $\bar{\omega}$, Configuration F

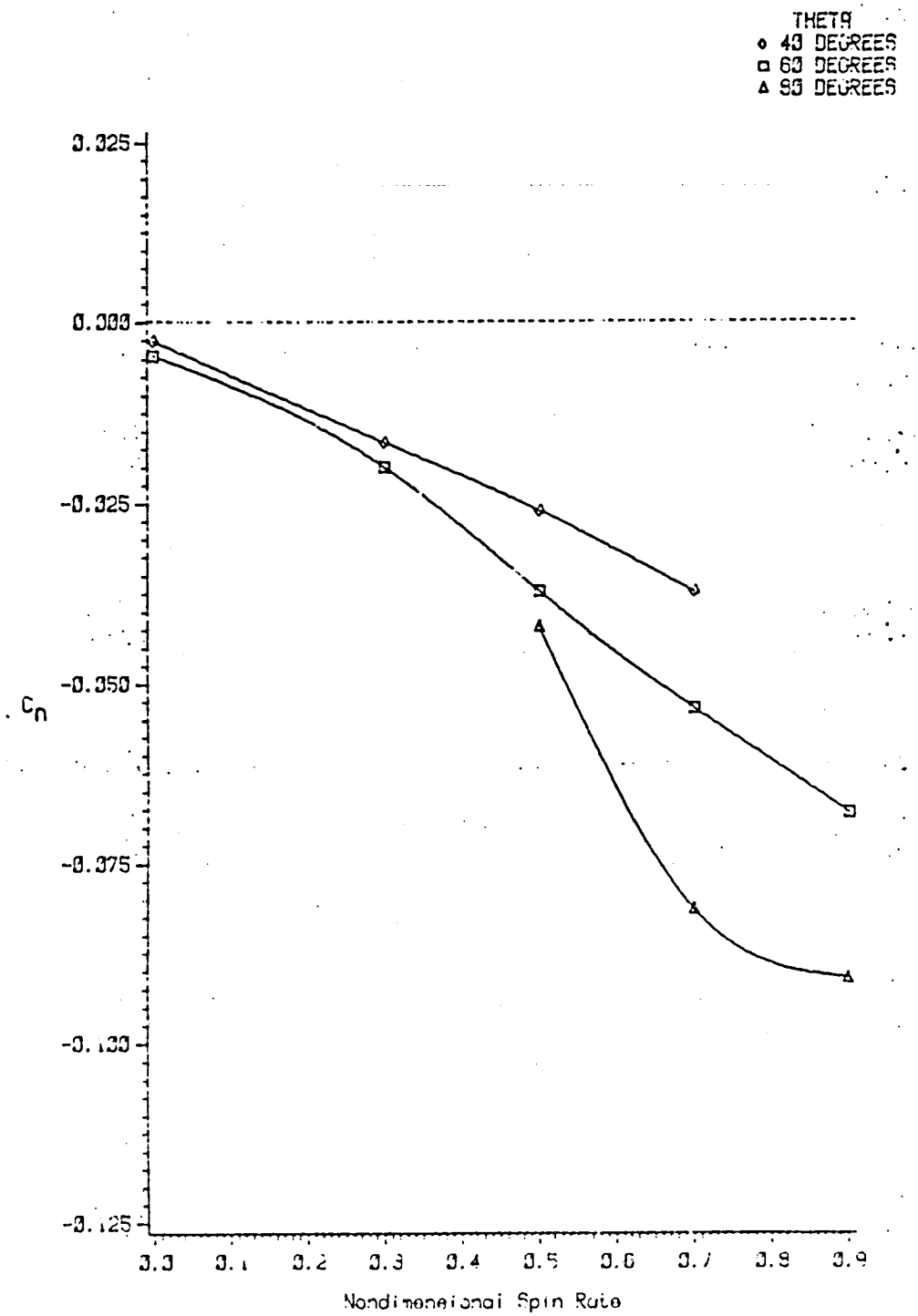

Figure B-19. Yawing Moment as a Function of ϑ and $\bar{\omega}$, Configuration G

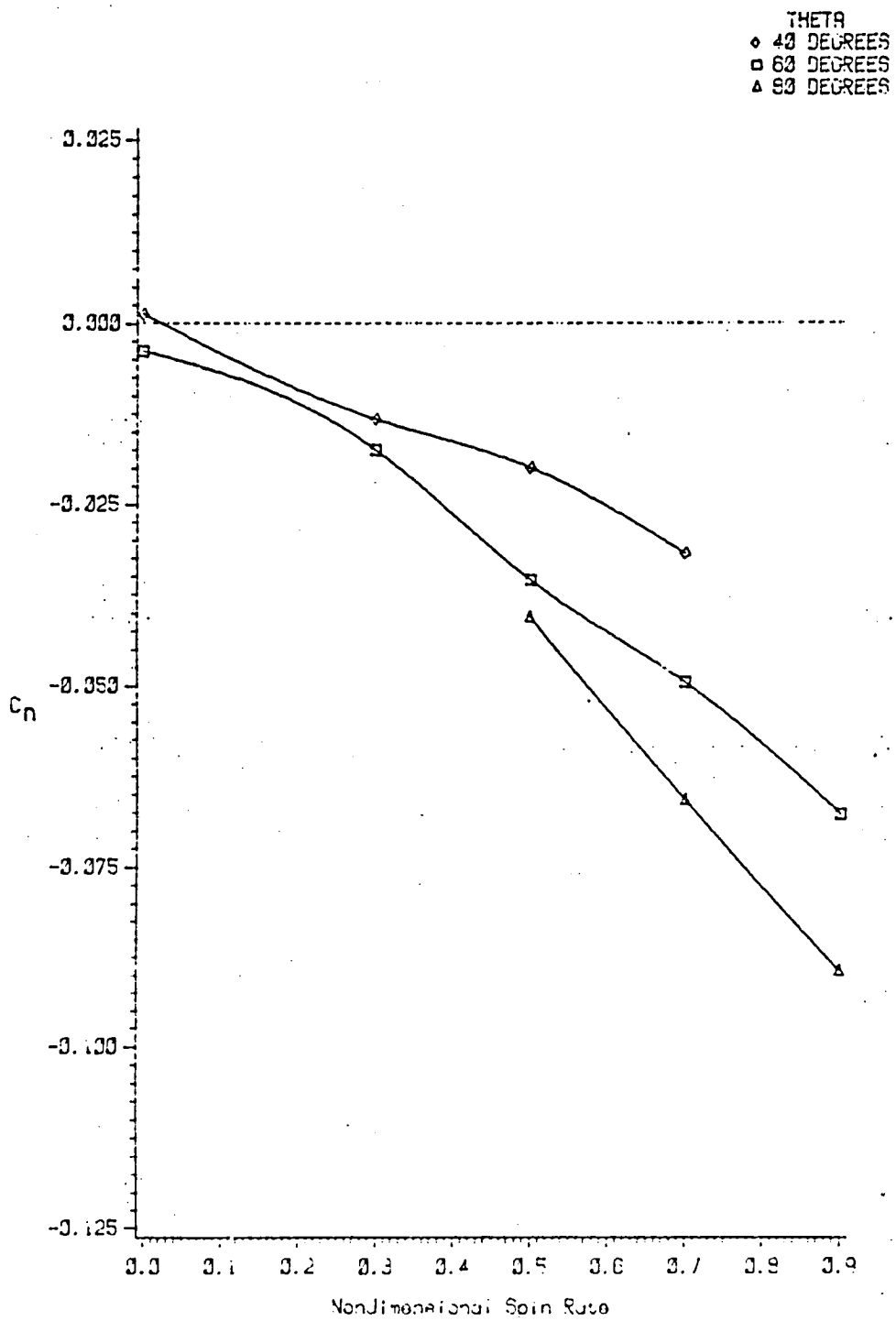

Figure B-20. Yawing Moment as a Function of θ and $\bar{\omega}$, Configuration H

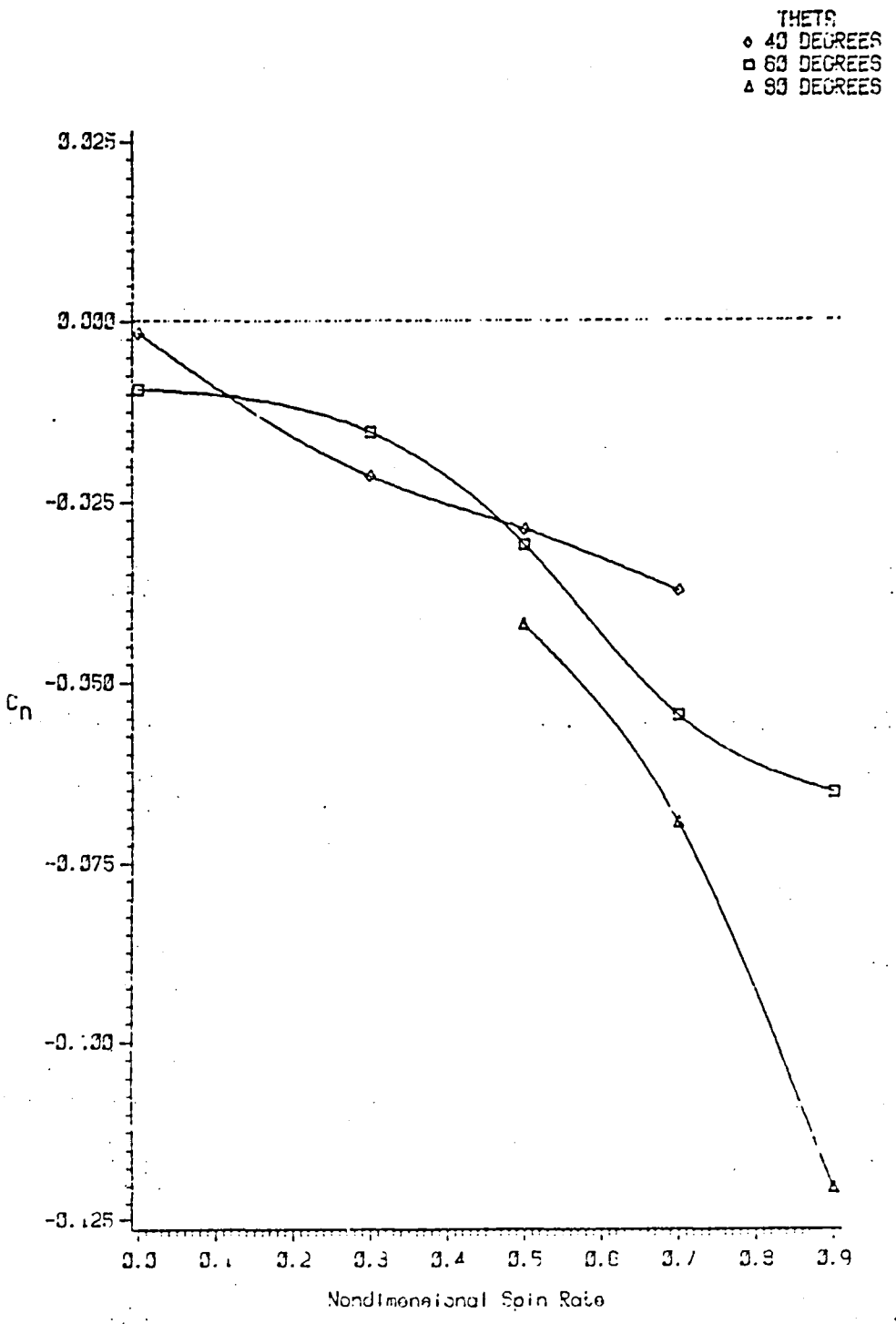

Figure B-21. Yawing Moment as a Function of θ and $\bar{\omega}$, Configuration J

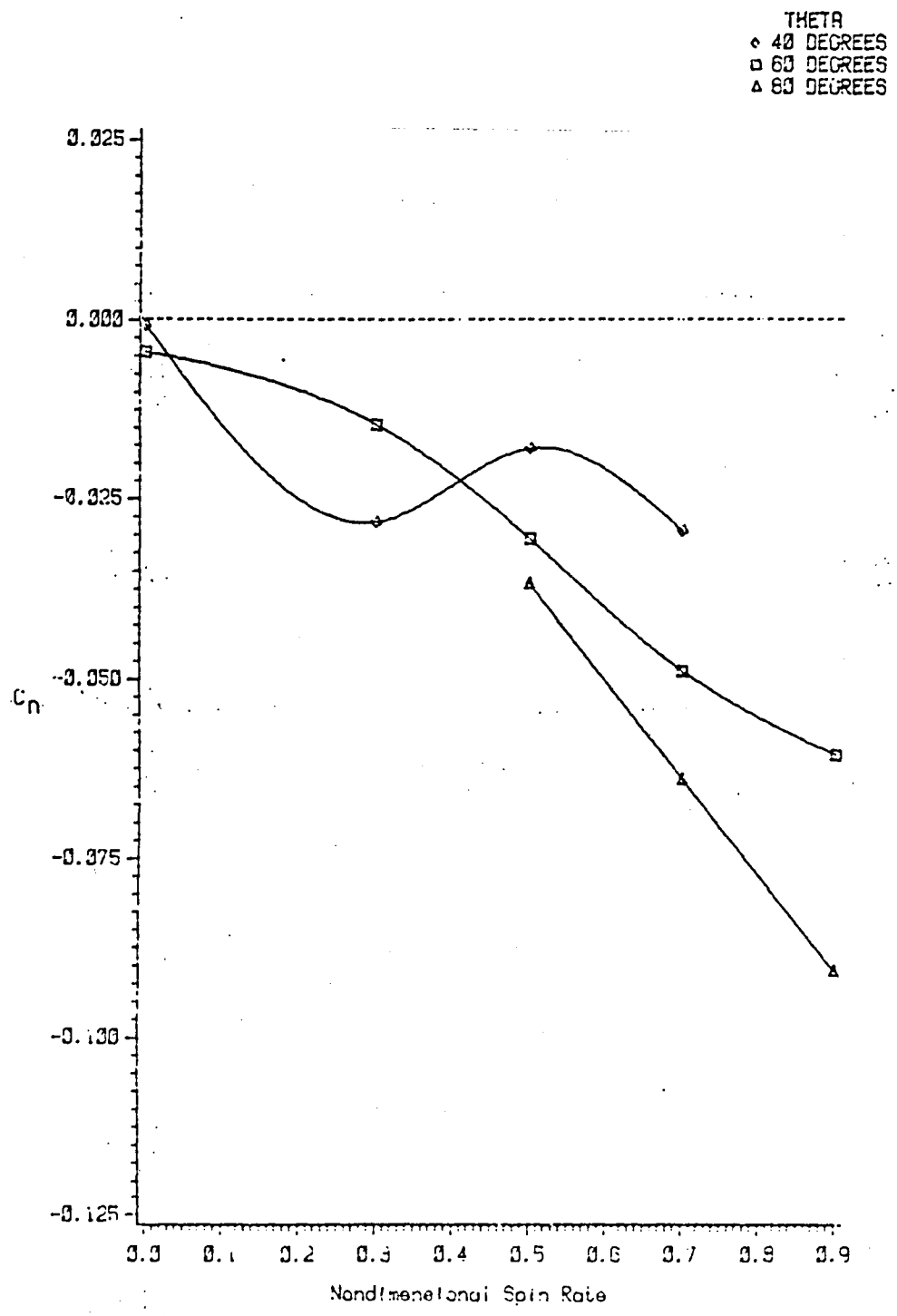

Figure B-22. Yawing Moment as a Function of θ and $\bar{\omega}$, Configuration K

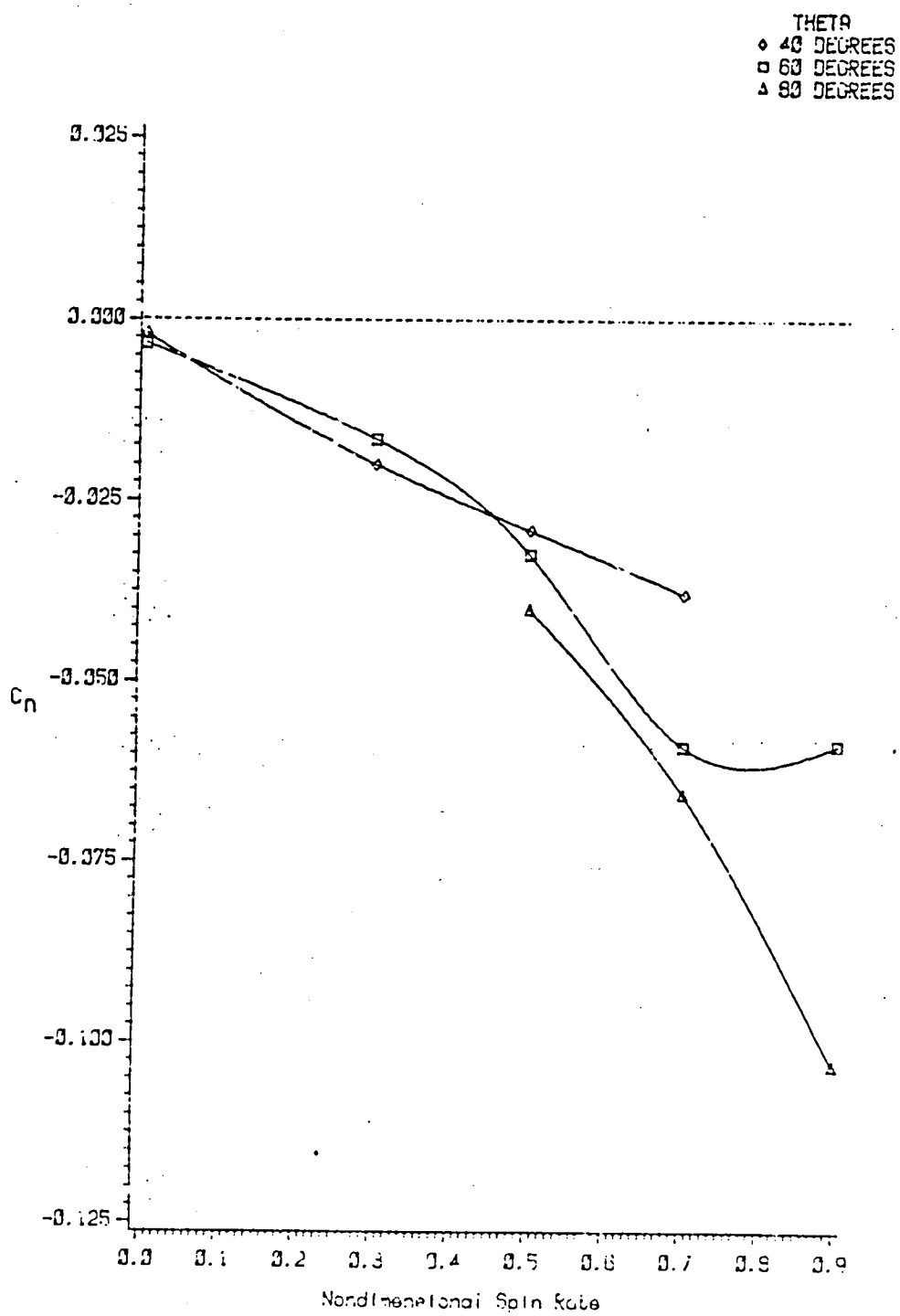

Figure B-23. Yawing Moment as a Function of θ and $\bar{\omega}$, Configuration L

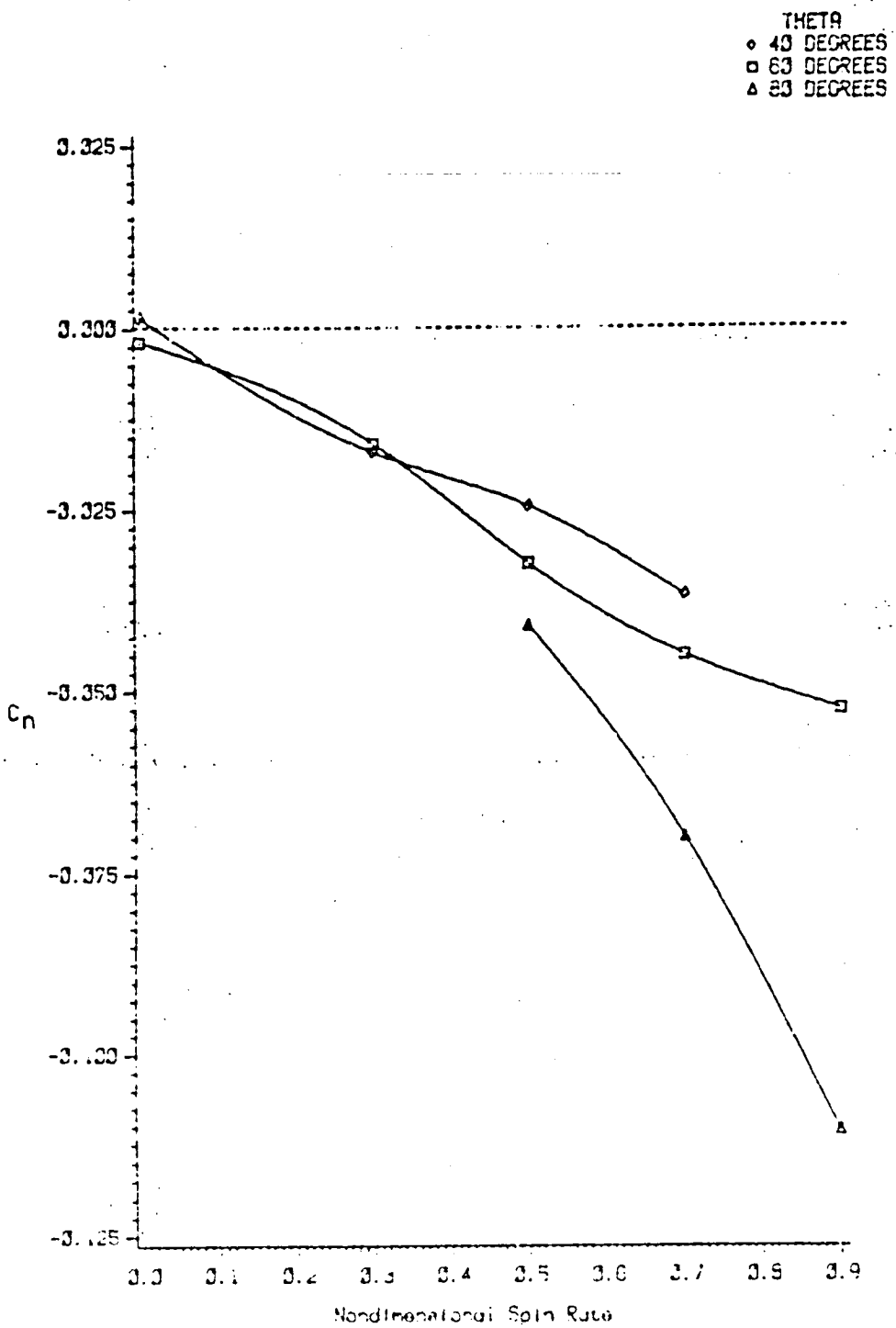

Figure B-24. Yawing Moment as a Function of ϑ and $\bar{\omega}$, Configuration M

APPENDIX C
TEST DATA

Table C-1

Configuration A Test Data*

δ	α_V	Density (slugs/ ft^3)	V_T (ft/sec)	V_d (ft/sec)	Normal Force (lb)	Axial Force (lb)	Pitching Moment (in-lb)	Rolling Moment (in-lb)	Yawing Moment (in-lb)	Side Force (lb)
80	46.20	0.00225	99.14	68.62	8.967	1.082	52.35	-18.02	-14.79	-3.351
80	39.04	0.00223	100.8	78.31	9.853	0.9789	55.78	-15.07	-13.00	-2.939
80	30.08	0.00223	100.7	87.14	10.34	0.9767	59.30	-11.71	-9.937	-2.246
60	42.52	0.00223	101.3	74.68	8.180	0.7844	46.42	-14.60	-9.827	-2.387
60	35.50	0.00222	101.2	82.43	8.758	0.7419	48.65	-12.28	-10.39	-2.421
60	27.00	0.00222	102.0	90.91	9.288	1.007	53.31	-9.444	-8.381	-1.951
60	17.00	0.00222	101.8	97.40	9.774	0.7440	53.13	-6.309	-4.615	-1.014
60	0	0.00221	101.8	101.8	9.677	0.4420	52.77	1.807	-1.040	-0.2517
40	27.89	0.00221	99.08	87.56	6.728	0.2325	36.99	-7.327	-8.936	-2.006
40	20.71	0.00221	101.2	94.62	7.222	0.3221	39.17	-3.631	-7.070	-1.513
40	12.78	0.00220	102.5	99.95	7.168	0.1501	39.73	-0.8351	-5.842	-1.147
40	0	0.00220	102.9	102.9	7.550	0.0055	40.09	4.155	0.4996	0.1269

* Moments resolved about balance center.

Table C-2

Configuration B Test Data

θ	α_v	Density (slugs/ ft^3)	V_T (ft/sec)	V_d (ft/sec)	Normal Force (lb)	Axial Force (lb)	Pitching Moment (in-lb)	Polling Moment (in-lb)	Yawing Moment (in-lb)	Side Force (lb)
80	46.20	0.00221	99.04	68.55	7.335	0.9574	43.43	-23.42	-21.13	-4.307
80	39.04	0.00220	97.93	76.00	8.009	0.997	48.59	-19.35	-19.54	-3.875
80	30.08	0.00220	99.55	86.13	9.659	1.074	57.37	-16.25	-16.79	-3.137
60	42.52	0.00219	98.54	72.65	5.946	0.7250	34.74	-25.54	-20.12	-4.020
60	35.50	0.00218	100.3	81.66	6.666	0.7515	38.70	-23.25	-19.03	-3.682
60	27.00	0.00218	99.05	88.25	7.295	0.7428	41.40	-15.10	-14.46	-2.768
60	17.00	0.00220	101.1	96.69	8.637	0.8780	48.68	-9.402	-10.647	-1.928
60	0	0.00219	100.4	100.4	9.471	0.5492	52.58	-0.8055	-0.3213	-0.0067
40	27.89	0.00219	99.50	87.93	5.471	0.1837	30.43	-20.27	-16.02	-3.358
40	20.71	0.00218	98.63	92.26	5.542	0.1776	30.79	-14.90	-12.07	-2.460
40	12.78	0.00218	102.6	100.1	6.769	0.1550	36.32	-9.851	-8.075	-1.493
40	0	0.00220	100.4	100.4	7.064	0.2103	37.85	2.13	-1.738	-0.1400

Table C-3

Configura'on C Test Data

θ	α_v	Density (slugs/ ft^3)	V_T (ft/sec)	V_d (ft/sec)	Normal Force (lb)	Axial Force (lb)	Pitching Moment (in-lb)	Rolling Moment (in-lb)	Yawing Moment (in-lb)	Side Force (lb)
80	46.20	0.00223	100.8	69.76	9.586	1.311	55.40	-23.53	-14.71	-3.401
80	39.04	0.00223	101.8	79.19	10.38	1.116	60.14	-17.68	-9.276	-2.468
80	30.08	0.00222	100.9	87.32	10.63	1.083	61.02	-10.55	-4.937	-1.761
60	42.52	0.00221	102.4	75.50	9.534	0.8713	54.21	-15.85	-2.730	-1.218
60	35.50	0.00221	102.8	83.71	10.20	0.7863	55.43	-12.38	-2.166	-1.114
60	27.00	0.00220	101.6	90.55	9.645	0.7070	52.77	-8.818	-2.470	-1.104
60	17.00	0.00221	101.6	97.14	9.888	0.7641	53.16	-6.022	0.1714	-0.4951
60	0	0.00221	102.6	102.6	9.901	0.7000	53.08	1.841	-3.526	-0.5929
40	27.89	0.00219	101.8	89.95	6.988	0.1612	38.27	-9.634	-5.061	-1.495
40	20.71	0.00218	101.2	94.68	6.839	0.1230	36.60	-6.870	-3.780	-1.028
40	12.78	0.00218	101.7	99.2	6.911	0.1418	36.50	-2.683	-3.878	-0.8700
40	0	0.00218	100.0	100.0	6.707	-0.0571	34.97	2.334	-0.6667	0.0014

Table C-4

Configuration D Test Data

ϕ	α_v	Density (slugs/ ft^3)	V_T (ft/sec)	V_d (ft/sec)	Normal Force (lb)	Axial Force (lb)	Pitching Moment (in-lb)	Rolling Moment (in-lb)	Yawing Moment (in-lb)	Side Force (lb)
80	46.20	0.00222	101.5	70.27	8.288	0.8700	46.60	-20.67	-13.15	-2.846
80	39.04	0.00221	101.9	79.22	9.891	0.933	55.25	-20.55	-8.436	-1.954
80	30.08	0.00220	101.8	88.12	11.10	0.8743	60.85	-15.61	-0.9707	-0.5459
60	42.52	0.00220	102.5	75.61	9.203	0.5290	50.02	-17.67	-4.803	-1.178
60	35.50	0.00219	101.0	82.23	10.35	0.5080	55.51	-16.02	1.163	-0 2536
60	27.00	0.00219	103.1	91.86	10.68	0.4840	56.55	-11.28	3.766	0.1490
60	17.00	0.00219	101.2	96.82	9.924	0.5080	51.81	-7.260	3.564	0.2731
60	0	0.00218	102.5	102.5	9.845	0.4346	50.73	1.059	-2.330	0.1570
40	27.89	0.00218	101.8	90.01	7.215	0.0825	37.59	-12.24	-2.838	-0.9210
40	20.71	0.00217	102.8	96.24	7.501	-0.0099	38.35	-9.708	-0.0154	-0.2726
40	12.78	0.00222	101.1	98.64	7.444	0.0128	37.75	-5.862	1.811	0.1715
40	0	0.00220	102.6	102.6	7.546	-0.1465	37.74	2.711	0.2775	0.0025

Table C-5

Configuration E Test Data

θ	α_v	Density (slugs/ ft^3)	V_T (ft/sec)	V_d (ft/sec)	Normal Force (lb)	Axial Force (lb)	Pitching Moment (in-lb)	Rolling Moment (in-lb)	Yawing Moment (in-lb)	Side Force (lb)
80	46.20	0.00222	99.82	69.09	8.250	0.6216	38.42	-21.10	-16.56	-3.624
80	39.04	0.00222	102.0	79.27	9.380	0.6394	43.66	-15.56	-13.74	-2.942
80	30.08	0.00221	100.1	86.60	9.933	0.7065	46.05	-11.56	-11.61	-2.373
60	42.52	0.00220	101.0	74.49	7.870	0.4904	36.03	-15.85	-10.80	-2.519
60	35.50	0.00220	100.4	81.72	8.285	0.5003	37.49	-13.18	-11.28	-2.453
60	27.00	0.00220	102.2	91.10	9.113	0.5000	40.80	-10.80	-9.784	-2.013
60	17.00	0.00219	100.4	95.99	9.053	0.4307	39.87	-7.271	-5.953	-1.010
60	0	0.00218	99.32	99.32	9.193	0.3500	41.38	0.6631	-0.4553	-0.3815
40	27.89	0.00219	102.0	90.12	6.774	0.0144	30.03	-10.54	-10.06	-2.140
40	20.71	0.00219	100.4	93.94	6.847	-0.0115	29.55	-6.423	-7.002	-1.424
40	12.78	0.00218	101.2	98.70	7.225	-0.0197	31.09	-2.674	-5.118	-1.015
40	0	0.00218	101.5	101.5	7.714	-0.2290	32.33	2.231	-0.847	-0.1833

Table C-6

Configuration F Test Data

θ	α_v	Density (slugs/ ft^3)	V_T (ft/sec)	V_d (ft/sec)	Normal Force (lb)	Axial Force (lb)	Pitching Moment (in-lb)	Rolling Moment (in-lb)	Yawing Moment (in-lb)	Side Force (lb)
80	46.20	0.00222	102.0	70.64	10.79	0.7426	69.43	-22.23	-17.23	-3.574
80	39.04	0.00221	101.5	78.85	10.75	0.6369	69.77	-16.80	-16.36	-3.201
80	30.08	0.00221	100.6	87.06	11.08	0.7081	71.41	-11.16	-12.84	-2.498
60	42.52	0.00221	101.9	75.1	8.591	0.4486	55.41	-14.72	-12.65	-2.695
60	35.50	0.00220	99.44	80.96	8.493	0.4080	55.07	-11.79	-11.06	-2.341
60	27.00	0.00220	100.2	89.28	9.421	0.3947	59.65	-9.105	-8.081	-1.593
60	17.00	0.00220	101.7	97.30	10.06	0.3769	63.30	-7.024	-5.626	-0.9724
60	0	0.00219	100.5	100.5	9.696	0.1924	60.32	2.153	-2.222	-0.2758
40	27.89	0.00220	100.9	89.22	6.943	-0.0547	44.43	-9.076	-11.20	-2.613
40	20.71	0.00219	101.2	94.74	7.195	-0.1580	45.03	-7.045	-7.359	-1.614
40	12.78	0.00219	101.8	99.36	7.285	-0.1727	45.03	-2.637	-5.768	-1.172
40	0	0.00219	101.2	101.2	7.633	-0.3056	45.96	2.453	-0.6820	-0.0151

Table C-7

Configuration G Test Data

θ	α_v	Density (slugs/ ft^3)	V_T (ft/sec)	V_d (ft/sec)	Normal Force (lb)	Axial Force (lb)	Pitching Moment (in-lb)	Rolling Moment (in-lb)	Yawing Moment (in-lb)	Side Force (lb)
80	46.20	0.00219	97.88	67.75	8.377	0.8273	43.11	-15.83	-14.35	-3.145
80	39.04	0.00219	96.10	74.68	8.826	0.8112	49.58	-13.77	-11.64	-3.529
80	30.08	0.00217	100.9	87.36	10.29	0.8861	57.95	-11.82	-12.03	-2.367
60	42.52	0.00217	98.47	72.60	7.362	0.5836	41.30	-13.12	-12.14	-2.667
60	35.50	0.00216	101.0	82.20	8.442	0.5930	46.73	-12.41	-12.63	-2.668
60	27.00	0.00216	100.1	89.23	8.798	0.6815	48.80	-9.136	-10.73	-2.174
60	17.00	0.00216	98.69	94.38	8.786	0.5966	48.07	-6.863	-7.019	-1.282
60	0	0.00215	97.39	97.39	8.705	0.3702	47.18	0.6196	-1.905	-0.3098
40	27.89	0.00215	101.0	89.26	6.592	0.2802	36.89	-7.591	-9.975	-2.196
40	20.71	0.00215	98.38	92.03	6.546	6.1999	34.75	-3.938	-7.322	-1.632
40	12.78	0.00215	101.6	99.05	7.3088	0.2153	38.19	-1.564	-6.002	-1.179
40	0	0.00215	101.6	101.6	7.146	0.0428	37.47	2.903	-1.386	-0.1860

Table C-8

Configuration H Test Data

θ	α_v	Density (slugs/ ft^3)	V_T (ft/sec)	V_d (ft/sec)	Normal Force (lb)	Axial Force (lb)	Pitching Moment (in-lb)	Rolling Moment (in-lb)	Yawing Moment (in-lb)	Side Force (lb)
80	46.20	0.00221	102.5	70.93	9.277	0.8919	54.32	-18.14	-15.15	-3.426
80	39.04	0.00220	100.8	78.35	9.645	0.9158	55.85	-15.11	-13.83	-3.052
80	30.08	0.00220	99.26	85.87	10.01	0.9780	57.07	-9.124	-10.50	-2.252
60	42.52	0.00220	98.82	72.86	7.706	0.5983	42.74	-13.09	-12.05	-2.720
60	35.50	0.00218	102.4	83.34	9.401	0.8688	49.55	-12.06	-12.54	-2.540
60	27.00	0.00219	99.29	88.47	8.775	0.5747	48.03	-9.338	-10.39	-2.058
60	17.00	0.00218	102.4	98.0	9.470	0.5422	52.13	-6.697	-6.578	-1.223
60	0	0.00217	102.0	102.0	9.518	0.4223	51.77	2.116	-1.530	-0.2918
40	27.89	0.00223	101.3	89.55	7.153	0.3169	39.62	-5.269	-9.325	-1.939
40	20.71	0.00222	102.4	95.83	7.609	0.3386	41.13	-3.517	-7.116	-1.370
40	12.78	0.00222	102.1	99.58	7.365	0.1661	40.01	-0.9997	-5.036	-0.9825
40	0	0.00221	102.8	102.8	7.409	-0.1185	38.89	4.122	0.1996	0.1122

Table C-9

Configuration J Test Data

θ	α_v	Density (slugs/ ft^3)	V_T (ft/sec)	V_d (ft/sec)	Normal Force (lb)	Axial Force (lb)	Pitching Moment (in-lb)	Rolling Moment (in-lb)	Yawing Moment (in-lb)	Side Force (lb)
80	46.20	0.00219	100.9	69.86	9.049	0.8401	52.65	-18.91	-16.46	-4.524
80	39.04	0.00219	99.98	77.70	9.656	0.8376	55.54	-13.48	-14.63	-13.14
80	30.08	0.00218	98.68	85.37	9.987	0.8899	56.76	-9.153	-11.08	-2.274
60	42.52	0.00217	102.2	75.35	8.502	0.5544	47.40	-14.06	-12.13	-2.785
60	35.50	0.00217	101.1	82.28	8.747	0.5906	47.73	-11.04	-11.82	-2.780
60	27.00	0.00222	102.4	91.24	9.450	0.6101	52.54	-8.052	-10.07	-1.926
60	17.00	0.00222	101.7	97.23	9.777	0.5460	52.88	-5.517	-5.553	-1.083
60	0	0.00220	101.9	101.9	9.669	0.3995	53.42	2.512	-3.991	-0.7147
40	27.89	0.00219	100.0	88.41	6.548	0.0481	36.32	-7.486	-10.67	-2.181
40	20.71	0.00219	101.2	94.68	6.816	0.1508	37.78	-3.700	-9.290	-1.930
40	12.78	0.00218	102.6	100.1	7.518	0.0715	39.29	-1.507	-8.108	-1.585
40	0	0.00218	101.3	101.3	7.124	-0.1159	37.58	3.274	-0.9248	-0.1179

Table C-10

Configuration K Test Data

θ	α_v	Density (slugs/ ft^3)	V_T (ft/sec)	V_d (ft/sec)	Normal Force (lb)	Axial Force (lb)	Pitching Moment (in-lb)	Rolling Moment (in-lb)	Yawing Moment (in-lb)	Side Force (lb)
80	46.20	0.00224	101.6	70.36	9.362	0.8510	51.89	-19.24	-15.74	-3.445
80	39.04	0.00222	101.8	79.15	10.26	0.8238	56.43	-16.42	-13.98	-3.048
80	30.08	0.00222	102.5	88.71	1. 0	0.9397	61.57	-12.76	-0.879	-2.210
60	42.52	0.00221	101.4	74.75	8.746	0.6441	46.91	-17.29	-11.11	-2.585
60	35.50	0.00221	101.0	82.20	8.998	0.6776	48.23	-13.43	-11.20	-2.504
60	27.00	0.00220	102.5	91.37	9.822	0.6691	51.92	-11.86	-9.370	-1.906
60	17.00	0.00221	102.4	97.92	10.39	0.6763	53.99	-8.957	-5.253	-1.049
60	0	0.00220	101.0	101.0	10.06	0.4040	52.67	1.6308	-2.069	-0.3340
40	27.89	0.00219	103.5	91.52	7.112	0.1223	37.24	-9.418	-9.564	-1.824
40	20.71	0.00219	102.1	95.54	7.169	0.1361	36.89	-5.920	-6.346	-1.202
40	12.78	0.00219	102.3	99.78	7.968	0.1556	39.34	-0.2904	-10.43	-2.092
40	0	0.00219	102.8	102.8	8.320	-0.0724	41.62	3.434	-0.9978	-0.0350

Table C-11

Configuration L Test Data

θ	α_v	Density (slugs/ ft^3)	V_T (ft/sec)	V_d (ft/sec)	Normal Force (lb)	Axial Force (lb)	Pitching Moment (in-lb)	Rolling Moment (in-lb)	Yawing Moment (in-lb)	Side Force (lb)
80	46.20	0.00223	100.3	69.46	8.658	0.9847	49.97	-22.66	-19.74	-3.736
80	39.04	0.00222	102.2	79.47	9.299	0.8981	53.24	-16.08	-16.00	-3.095
80	30.08	0.00222	101.4	87.75	10.02	0.9209	54.79	-12.51	-12.50	-2.290
60	42.52	0.00221	100.1	73.82	7.529	-1.717	42.01	-14.40	-11.83	-2.402
60	35.50	0.00221	102.1	83.14	8.236	0.6844	45.64	-13.70	-14.27	-3.071
60	27.00	0.00220	102.5	91.33	8.683	0.6752	47.64	-10.90	-11.13	-1.979
60	17.00	0.00220	101.7	97.22	8.861	0.6516	48.22	-8.175	-7.071	-1.125
60	0	0.00219	100.1	100.1	8.684	0.4754	47.61	0.7864	-3.372	-0.1832
40	27.89	0.00220	102.9	90.91	7.052	0.3476	39.57	-9.709	-11.83	-2.330
40	20.71	0.00220	101.0	94.44	7.015	0.3752	37.81	-2.130	-10.32	-1.911
40	12.78	0.00218	102.4	99.87	7.127	0.2025	38.69	-1.306	-8.054	-1.456
40	0	0.00218	100.9	100.9	6.858	0.0078	36.91	2.664	-1.877	-0.1218

Table C-12

Configuration M Test Data

θ	α_v	Density (slugs/ ft^3)	V_T (ft/sec)	V_d (ft/sec)	Normal Force (lb)	Axial Force (lb)	Pitching Moment (in-lb)	Rolling Moment (in-lb)	Yawing Moment (in-lb)	Side Force (lb)
80	46.20	0.00216	98.66	68.28	7.482	0.8048	42.85	-26.92	-18.52	-3.790
80	39.04	0.00216	100.1	77.77	8.691	0.6662	47.70	-18.81	-15.79	-3.089
80	30.08	0.00217	98.52	85.23	8.902	0.6197	47.76	-13.00	-11.37	-2.166
60	42.52	0.00217	98.77	72.82	7.162	0.4261	38.67	-14.01	-9.718	-2.064
60	35.50	0.00217	99.60	81.08	7.960	0.1446	42.62	-12.59	-10.69	-2.181
60	27.00	0.00218	100.6	89.68	8.129	0.4749	43.57	-10.43	-9.897	-1.907
60	17.00	0.00217	100.7	96.30	8.233	0.3553	43.89	-7.234	-5.994	-1.068
60	0	0.00217	99.31	99.31	8.077	0.1944	43.41	1.081	-1.002	-0.1263
40	27.89	0.00218	99.94	88.32	5.895	-0.0161	33.00	-8.631	-9.874	-2.128
40	20.71	0.00218	102.0	95.39	6.406	-0.0478	34.68	-5.777	-7.896	-1.665
40	12.78	0.00219	102.7	100.2	6.642	-0.0830	35.46	-1.853	-6.521	-1.268
40	0	0.00220	102.6	102.6	6.917	-0.2370	35.54	2.458	0.1934	0.1185

Table C-13

Control Deflection Test 1 Data, $\theta = 40.0°$, $\alpha_v = 20.71°$

δ_c (°)	δ_r (°)	Density (slugs/ft^3)	V_T (ft/sec)	V_d (ft/sec)	Normal Force (lb)	Axial Force (lb)	Pitching Moment (in-lb)	Rolling Moment (in-lb)	Yawing Moment (in-lb)	Side Force (lb)
0	0	0.00223	100.1	93.67	7.158	0.2473	38.48	-4.048	-6.833	-1.435
10	0	0.00222	101.1	94.58	7.874	0.0300	43.46	-4.856	-6.489	-1.531
15	0	0.00221	100.4	93.97	8.205	-0.1807	44.43	-5.645	-6.174	-1.318
0	15.7	0.00220	101.0	94.54	7.390	-0.0059	39.93	-6.796	-10.86	-2.197
0	25	0.00220	101.8	95.19	7.418	-0.0733	40.81	-7.322	-12.13	-2.257
15	25	0.00220	100.9	94.36	8.652	-0.4007	45.59	-7.050	-11.46	-2.095
10	16.7	0.00220	100.6	94.14	8.000	-0.2470	43.06	-7.763	-10.58	-2.061
0	16.7P*	0.00220	100.6	94.14	7.163	0.1940	38.98	-7.079	-9.200	-1.836
0	25P	0.00219	101.8	95.28	7.216	0.1208	40.38	-7.595	-10.26	-2.009
15	25P	0.00219	100.2	93.74	8.215	-0.2170	44.83	-7.239	-8.988	-1.818
10	16.7P	0.00219	99.49	93.07	7.750	-0.0627	42.15	-7.406	-8.514	-1.741

* Partial-span rudder.

Table C-14

Control Deflection Test 2 Data, $\theta = 80°$, $\alpha_v = 30.08°$

δ_c (°)	δ_r (°)	Density (slugs/ft^3)	V_T (ft/sec)	V_d (ft/sec)	Normal Force (lb)	Axial Force (lb)	Pitching Moment (in-lb)	Rolling Moment (in-lb)	Yawing Moment (in-lb)	Side Force (lb)
0	0	0.00224	102.2	83.43	10.86	1.060	61.55	-10.93	-10.67	-2.339
10	0	0.00222	100.3	86.77	10.68	0.4996	58.40	-10.97	-10.64	-2.162
15	0	0.00222	100.1	86.65	10.59	0.2023	57.45	-11.14	-10.98	-2.173
0	16.7	0.00221	100.8	87.21	10.32	0.8001	58.00	-11.28	-12.17	-2.543
0	25	0.00220	101.3	87.61	10.46	0.7079	58.59	-11.28	-12.56	-2.631
15	25	0.00220	101.6	87.94	10.59	-0.0394	58.04	-11.59	-13.25	-2.611
10	16.7	0.00220	100.7	87.13	10.51	0.3405	57.96	-11.43	-12.63	-2.546
0	16.7P*	0.00219	101.1	87.49	10.61	0.9559	59.04	-11.70	-12.67	-2.641
0	25P	0.00218	98.64	85.34	9.882	0.9032	56.16	-11.04	-12.25	-2.541
15	25P	0.00218	101.0	87.37	10.71	0.3027	58.19	-11.94	-13.23	-2.667
10	16.7P	0.00220	101.0	87.37	10.77	0.6336	59.67	-11.48	-12.76	-2.628

* Partial-span rudder.